THE UNIVERSITY
of EDINBURGH

Secure Optimal Operation and Control of Integrated AC/MTDC Meshed Grids

Faheem Akhter

Thesis submitted for the degree of Doctor of Philosophy (PhD)

The University of Edinburgh

2015

Abstract

Offshore wind energy is seen as the most promising source of electricity generation for achieving the European renewable energy targets. A number of wind farms are planned and under installation to collect the huge potential of wind energy at farther distances in the North Sea. The number of HVDC links in the North Sea is expected to increase with the development of offshore installations in Round 3 of the UK offshore windfarm programme. The increasing number of HVDC links and high power transfer control requirements leads to the formation of Multi-Terminal HVDC (MTDC) grid systems, which have become possible due to the technical advancements of VSC based HVDC systems. Additionally, a meshed MTDC grid structure can also provide interconnections for power trade across the Europe, which can help in better utilisation of power from offshore installations and can also support the AC network in tackling wind power variation issues.

However, the integration of the meshed MTDC grid with the existing AC grid has more challenges to overcome alongside the added advantages. One of the major challenge is to ensure the secure and optimal operation of the combined AC/MTDC grid considering stability requirements of the AC and DC grids in different operating conditions. The behaviour of the DC grid is governed by the fast acting controllers due to the high number of power electronic equipment unlike AC grid. In combined operation the response to a disturbance of two integrated grids can be different. The power balancing, co-ordination and dispatch requirements need to be identified, to implement appropriate controls and formulate a control structure for combined operation of two grids with different characteristics under normal and disturbance conditions.

Abstract

In this thesis, the basic principles of well-established three-layered AC grid control is employed to identify the power balancing, coordination and dispatch requirements of the DC grid. Appropriate control methods are proposed for primary, secondary and tertiary control layers in order to accomplish the identified requirements for the secure and optimal operation of combined AC/MTDC grids. Firstly, a comparison study is performed on different power balancing controls to find the most suitable control method for the primary control of the meshed DC grid. Secondly, the combined AC/DC grid power flow method is proposed to provide updated references of the VSC station in order to maintain coordinated power flow control under secondary control layers. Finally, security constraint optimization method for combined AC/DC grid is proposed for economic dispatch under the tertiary control layer of the three-layered hierarchal control. A number of case studies are performed to implement the proposed control methods on a combined AC/DC test case network. The performance of the proposed control methods is validated in a hierarchical control structure for secure and optimal operation integrated AC/MTDC grids.

Lay Summary

European Union has set the targets to get 27% of total energy generation from the renewable energy resources by 2030, mainly driven by the climate change and fast depletion of fossil fuels based resources. Offshore wind is one of most promising sources of renewable energy generation and North Sea has huge potential of wind energy resources. A number of wind farms are planned and under installation to collect these wind energy resources.

There are two major challenges in harvesting the offshore wind energy from the farther distances in offshore. First challenge is the transportation of bulk power from the offshore sites to the onshore grids. Second is the balancing of supply and demand in power system, with huge intermittent power from offshore wind farms.

To deal with these challenges, the proposals for a new undersea transmission network are under consideration, which is significantly different than existing onshore transmission network. In this thesis, the operation such a new undersea transmission network is studied and comparison of various control options is performed. The tools are developed to analyse possible influence of new transmission network on the existing onshore transmission network. Finally, a complete operational strategy for the combined operation and management of these two different transmission networks is proposed.

Declaration

I declare that this thesis has been completed by myself and that, the work herein is my own except where explicitly stated otherwise in the text.

Faheem Akhter

Acknowledgements

Firstly, I would like to thank my supervisor Dr. Ewen Macpherson for his invaluable support and guidance throughout the course of my research. His knowledge and experience along with encouragement and availability has greatly contributed towards this thesis.

Secondly, I would also like to acknowledge the financial support from Sukkur, Institute of Business Administration, for sponsoring my PhD study programme and being patient throughout the duration of my study leave.

I would like to thank all my colleagues in the Institute for Energy Systems (IES) for their friendly discussions and amazing time we spent together at Firbush trip. I would like to appreciate friendship and support of my colleagues in the Power lab, Douglas Carmichael, Juan Pablo, Ozan Keysan, Winnei Rong and others. I owe especial thanks to my best friends, Zaki Annuar and Nisar Ahmed for their support and fun we had together at the workplace.

I would also appreciate the support and facilitations provided by the University Chaplaincy team, in particular by, Ali Newell for being kind and understanding in all matters.

Finally, I would like to thank my whole family for their dedicated love, care and support in enabling me to get across to this stage.

List of Acronyms and Abbreviations

AC Alternating Current

C-PF Combined AC/DC Power Flow

C-OPF Combined AC/DC Optimal Power Flow

C-SCOPF Combined AC/DC Security Constrained Optimal Power Flow

DC Direct Current

EMTP Electromagnetic transient Programs

EWEA European Wind Energy Association

FOSG Friends of the Supergrid

HVDC High Voltage Direct Current

HVAC High Voltage Alternating Current

HF High Frequency

HVDC High Voltage Direct Current

ISO Independent System Operator

IGBT Insulated-Gate Bipolar Transistor

I-V Current Voltage

LCC Line Commutated Converter

LRSP Load Reference Set Point

MO Modulus Optimum

MTDC Multi-Terminal HVDC

MVA Mega Volt Ampere

MMC Modular Multi-level Converter

MAP Maximum Available Power

MPC Model Predictive Control

NSTG North Sea Transnational Grid

NR Newton Rapson

NLC Nearest Level Control

OWF Offshore Windfarm

OP Operation Point

PWM Pulse Width Modulation

PCC Point of Common Coupling

PLL Phase-lock Loop

PI proportional-integral

P-V Power Voltage

RTU Remote Terminal Units

RB-SCOPF Risk Based Security Constrained Optimal Power Flow

SCED Security Constrained Economic Dispatch

SCR Short Circuit Ratio

SHEM Selective Harmonic Elimination Methods

SPWM Sinusoidal Pulse Width Modulation

SO Symmetric Optimum

SM Sub-Modules

SHE Selective Harmonic Elimination

SCOPF Security Constrained Optimal Power Flow

SA Security Assessment

SSSA Steady State Security Assessment

TSO Transmission System Operator

VSC Voltage Source Converter

Table of Contents

List of Figures

List of Tables

CHAPTER 1

Introduction

1.1 Background

Offshore wind energy is seen as one of the most promising sources of electricity generation for achieving the European renewable energy targets. A number of wind farms are planned and under installation to collect the huge potential of wind energy at farther distances in the North Sea, and many more sites are expected with the development of offshore installations in Round 3 of the UK offshore windfarm programme as shown in **Figure 1:1**.

There are many challenges to overcome in order to harvest the offshore wind energy resources. One of the main challenges is the transmission of the power from Offshore Windfarms (OWF) located at a long distance offshore. Another major challenge is the balancing of the supply and demand in the power system, with the large amount of intermittent power from the Offshore Windfarms (OWF).

Due to the expected increase in the number of offshore installations, a meshed grid structure is seen as an attractive option to provide reliable operation of the system by efficient sharing of the offshore wind energy resources. Plans for the European offshore grid are under consideration to deal with the challenges of collecting the offshore wind energy and balanced power sharing among the interconnected countries such as, Netherlands, UK, Norway, Denmark and Germany. Several organisations, including the North Sea Transnational Grid (NSTG), the Friends of SuperGrid and the

European Wind Energy Association (EWEA), have started the initiative to look into the possibility and have provided their vision for the North Sea DC grid [1]–[5] as shown in **Figure 1:2**. Driven by these initiatives, there has been significant research looking into the technical and economical aspects with substantial achievements in the control and operation of a potential offshore DC grid. However, the possible influence of such a large DC offshore grid on the existing AC grid still needs careful investigation and understanding to develop a suitable operational strategy.

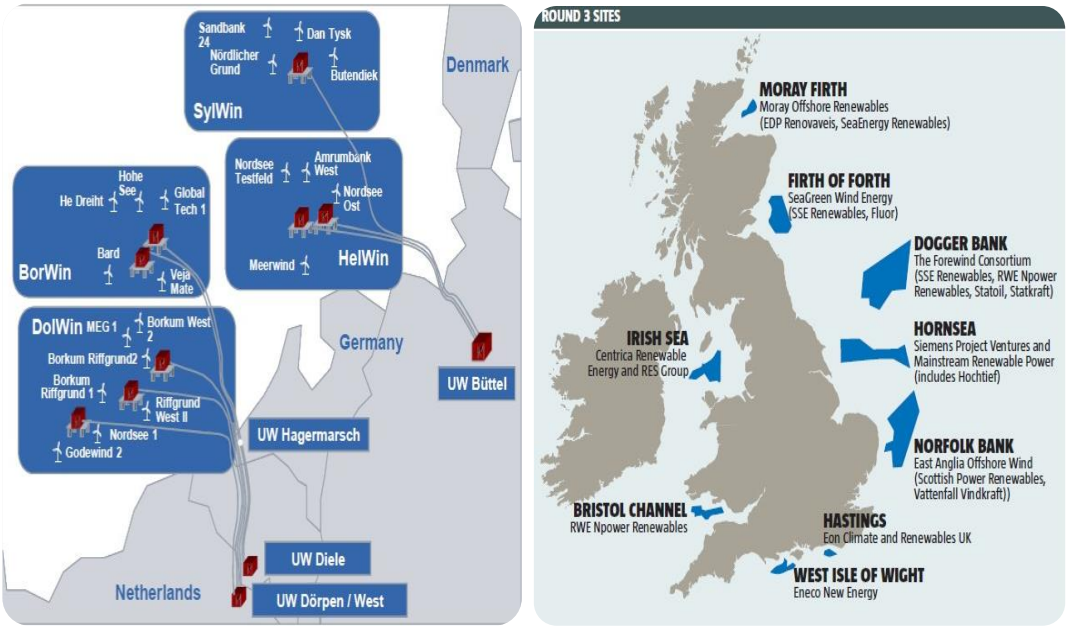

Figure 1:1 *The offshore windfarms installation and potential energy resources in the North Sea [6] [7]*

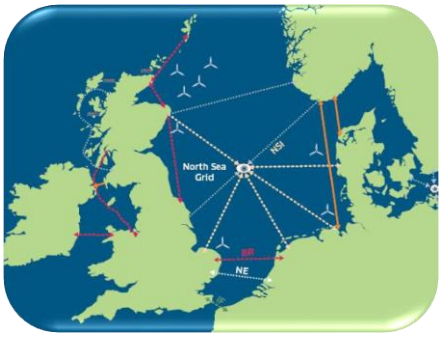

(a) Proposal endorsed by Scottish government [2]

(b)Proposal by Friends of SuperGrid [3]

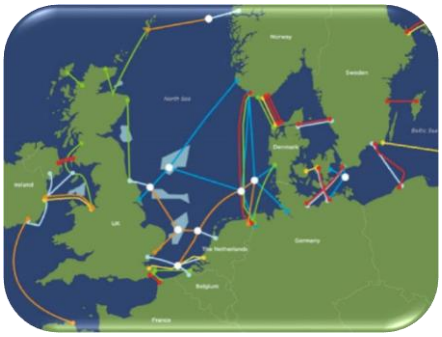

(c) Proposal by European Wind Energy Association [4]

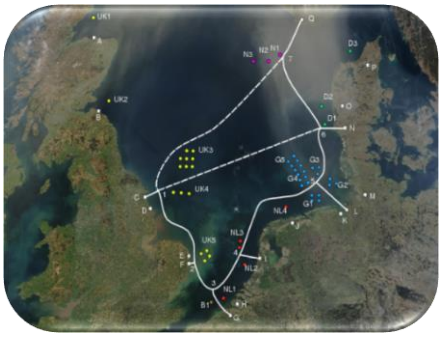

(d) Proposal by North Sea Transnational Grid *[1]*

Figure 1:2 *European offshore DC grid proposals*

The research work of this thesis started with the objective of obtaining a strategy for the secure and optimal operation of the integrated AC/MTDC meshed grids, citing the plans for a large offshore MTDC grid in the North Sea and the Scotland-Shetland offshore hub.

1.2 State of the Art of MTDC Systems

Following the historical "War of Currents" from 1880-1890 for the choice of Alternating Current (AC) or Direct Current (DC) technology for power systems, between Thomas Alva Edison and Nicola Tesla [8], AC technology emerged as the winner due to the efficient power transmission enabled by transformers, and subsequently dominated in all power systems. DC technology remained very limited

until the middle of the 20th century when it made its comeback into the power system for long distance cable transmission between mainland Sweden and Gotland Island, when AC technology appeared to be limited in its power capacity due to the high charging currents. The development in the converter technology (for AC to DC conversion and vice versa) from the mercury-arc switch to the semiconductor switch (thyristor) in the 1970s has enabled bulk power transfer through HVDC links. Both mercury-arc converters and thyristor switched converters are referred to as Current Source Converters (CSC) as on the DC side they behave as current sources, with energy stored in the inductors on the DC side. The thyristor switched converters are also referred to as Line Commutated Converters (LCC), as they can be turned ON but rely on polarity reversal of the line voltages of the AC system for commutation between the switches. Since then, HVDC transmission has been used for the point-to-point interconnection between asynchronous AC systems or long distance embedded links within an AC system, where HVDC transmission has significant technical and economic advantages over High Voltage Alternating Current (HVAC).

With growing maturity in the CSC technology in the 1980s, extension of the point-to-point HVDC links to MTDC systems looked promising, and much research was done into the control, stability and economic analysis of MTDC systems [9] [10][11]. The earliest MTDC systems were Sardinia–Corsica–Italy (SACOI) and Quebec-New England, which were commissioned as point-point HVDC links and later extended to MTDC systems. The SACOI scheme was a mercury arc converter based link, commissioned in 1967, to exchange power between Italy mainland and Sardinia via Corsica with capacity of 200MW at 200kV in a monopole configuration. Later, in 1988, a thyristor based Corsica station was added as a tap with 25% rating of the main

stations [10] with capability of bidirectional power flow. The location map is shown in **Figure 1:3** [10]. The main converter stations were replaced with thyristor switched converters in 1992 and the power capacity of each increased from 200MW to 300 MW.

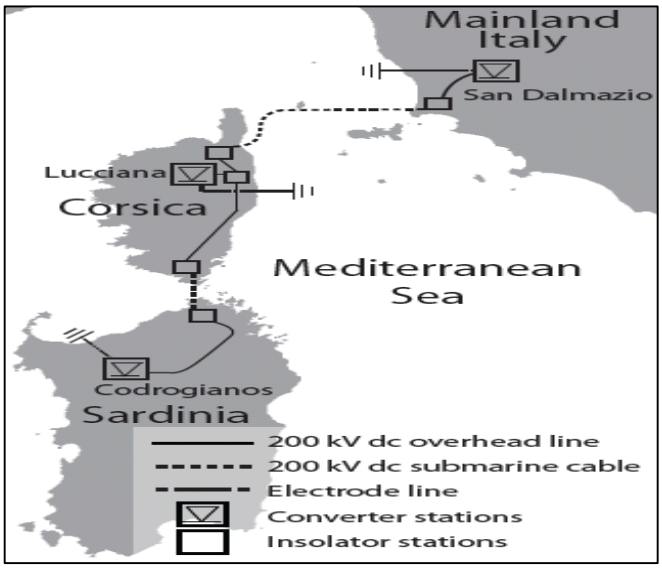

Figure 1:3 *Sardinia–Corsica–Italy (SACOI) scheme [10]*

The Quebec-New England scheme was the first large scale MTDC system involving more than three terminals. It was planned and constructed in two phases. During phase-I, a point-to-point HVDC link was commissioned between Quebec and New Hampshire in 1986, with power capacity of 690MW at ±450kV in bipolar configuration. During phase-II, three more converter stations were added; Radisson converter station in Quebec, Sandy Pond converter station in Boston, and Nicolet converter station near Montreal with respective power ratings of 2250MW, 2000MW and 2138MW [12]. **Figure 1:4** shows the location map of the five terminal layout of the Quebec-New England scheme. However, the operation of the scheme was restricted to three terminals soon after phase-II extension due to performance issues [11] and two converter stations installed in phase-I were decommissioned. The

Quebec-New England scheme is mostly operated as a two terminal link to transfer power from La Grande Hydro-electric power plant in Quebec to the Boston load centre.

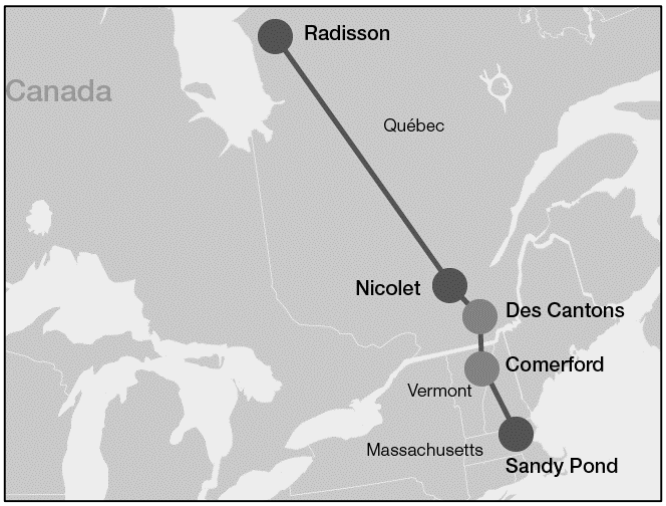

Figure 1:4 *Quebec-New England MTDC scheme [12]*

The Quebec-New England and SACOI schemes cannot be considered as true MTDC systems because power flow is restricted as unidirectional in the case of the Quebec-New England MTDC scheme and tapping operation in the SACOI scheme [13].

With the fast development in semiconductor technology in the 1990s, fully controlled switches with turn ON and OFF capability, called self-commutated devices such as the Gate Turn-off Thyristor (GTO) and the Insulated-Gate Bipolar Transistor (IGBT), became available commercially with high power ratings. The self-commutated switched converters are also referred to as Voltage Source Converter (VSC), as they behave as voltage sources, with energy stored in the capacitor on the DC side. The first VSC based HVDC point-to-point link was commissioned in 1999 between the Gotland Island and the mainland of Sweden. The applications of the VSC based HVDC links were initially limited to a few hundred MWs, in comparison to CSC

based HVDC links with power ratings of up to 8000MW [14]. VSC based HVDC has drawn much attention in recent years to capture the huge wind energy potential located at farther distances offshore, due to its black start capability, reactive power support and smaller area footprint [13]. However, the main advantage of VSC stations in the application of MTDC systems is the power reversal capability without shifting the DC voltage polarity, and independent control of active and reactive power flow, not possible in the CSC stations. A brief overview comparing the characteristics of CSC HVDC and VSC HVDC is given in **Table 1-1**.

Table 1-1 *Characteristic comparison of CSC HVDC and VSC HVDC [15]*

Characteristics	***CSC HVDC***	***VSC HVDC***
Converter type	Line-commutated current-source	Self-commutated voltage-source
Switch	Thyristor: turn on capability	IGBT: turn ON & OFF
Power ratings	Up to 8000MW	Up to 1800MW
Voltage ratings	Up to ± 800kV	Up to ±500kV
Control	Always consumes reactive power (2-quadrant operation)	Independent P & Q control (4-quadrant operation)
Losses	0.7% rated power	1-1.5% rated power
Launched	Old: 1st commercial project 1954	New: 1st commercial project 1999
Running projects	146	17
Multi-terminal operation	Difficult: power flow reversal requires polarity change	Easier: power flow reversal does not require polarity change

The first Voltage Source Converter (VSC) based MTDC system was installed in Japan in 1999 at Shin-Shinano substation in a low power back-to-back configuration for interconnecting the 50Hz and 60Hz AC grid [16]. However, the prospective MTDC

system proposed in recent years is considered to have three or more VSC stations connected by a common DC network allowing full, flexible, multi-direction power flows. With fast development in the VSC based HVDC technology, the power rating has also significantly improved and around seventeen VSC based transmission schemes are operational [17]. Three leading suppliers, ABB, Siemens and Alstom with the brand names of HVDC light™, HVDC Plus™ and HVDC MaxSine™, commercially supply VSC converter solutions. As in 2015, the highest commercially available power capacity of a VSC converter station is up to 1800MW at ±500kV, claimed by ABB [18].

In 2013, the MTDC grid eventually became reality when the first VSC based three-terminal Nan'ao VSC-MTDC project became operational in China, with a designed capacity of 200MW and the DC voltage level of ±160kV. The Nan'ao VSC-MTDC project was commissioned in two stages. In stage-I, two windfarms were interconnected through the Jinniu converter station, rated at 100MW, and Qing'ao converter station, rated at 50MW, to the Shantou Power Grid through the Sucheng converter station of 200MW capacity. In stage II, the offshore wind farm Tayu was connected to the system as the fourth terminal [19]. **Figure 1:5** shows the location map of the Nan'ao VSC-MTDC project.

Figure 1:5 *Nan'ao three-terminal HVDC project [20]*

Soon after, in 2014, the five-terminal Zhoushan VSC-MTDC project was launched into operation in China, with 1000MW capacity at ±200kV DC voltage [21]. The Zhoushan MTDC scheme has been planned to harvest the distributed wind power resources of the Zhoushan islands to meet the increasing demand of the Zhoushan regions. The five-terminal MTDC scheme interconnects the substations on the islands of Dinghai, Daishan, Qushan, Yangshan and Sijiao with power ratings given in **Table 1-2**. The location map of the five-terminal Zhoushan VSC-HVDC project is shown is **Figure 1:6**.

Table 1-2 *Technical details of the five-terminal Zhoushan VSC-HVDC project[22]*

Terminals	**Power ratings**	**DC voltage level**	**Cable length**
Dinghai converter station	400MW	±200 kV	129km-submarine cable
Daishan converter station	300MW		
Qushan converter station	100MW		
Yangshan converter station	100MW		
Sijiao converter station	100MW		

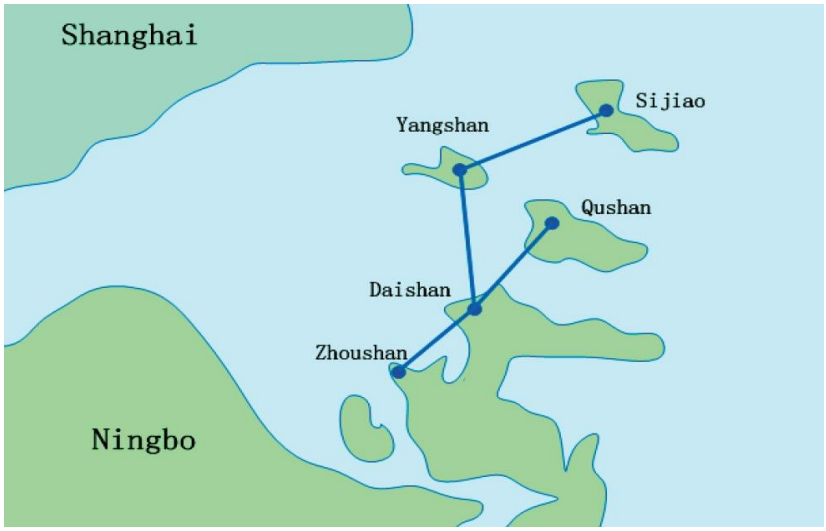

Figure 1:6 *Location map of the Zhoushan VSC-HVDC project [22]*

There are now many more MTDC systems in the planning stages, including the Unified Smartgrid in US, the EU Supergrid for Europe, DESERTEC for Europe, Middle East and North Africa, and SARRC for South Asian countries [5], [23]. It has become obvious from the planned MTDC systems that technology has become more mature for large-scale operations, but there are new challenges with regard to the integration of such MTDC grids with existing AC grids. The interaction of two different grids still requires more investigation and understanding to predict the behaviour of combined AC/MTDC grid operation.

1.3 Problem Statement

The integration of a meshed MTDC grid with the existing AC grid has significant challenges to overcome before the advantages of MTDC systems can be fully achieved. One of the major challenges is to ensure the secure and optimal operation of the combined AC/MTDC grid considering the stability requirements of the AC and DC grids under various operating conditions. The behaviour of an MTDC grid is different from that of a conventional AC grid, partly due to the large number of fast

acting power electronic equipment. Integration of an MTDC grid with an existing traditional AC grid introduces new operational and controllability issues for the combined system. In combined operation the response of two integrated grids to a disturbance can be different. The steady state interactions between the AC and MTDC grid is an area that still needs to be explored, with the following questions not well understood:

- How will the combined AC/MTDC system respond/behave under various operating conditions?
- What will be the operating strategy for power flow control in the combined AC/MTDC system?

Previous work has mainly focussed on the control dynamics of the MTDC grid largely without considering the behaviour of the AC grid. Several control configurations have been suggested in [24]–[29], with the majority of them focusing on different modifications of the droop control. Many of the studies in [30]–[33] have suggested the power flow solution of the MTDC grid without considering MTDC control configurations. Some of the studies have also focused on detailed modelling of the combined AC/DC systems in [34]–[37]. However, the control configurations considered are either not taken into account in these studies are considered for a specific control configuration. In a more recent work [38], the issue of non-linear droop implementation in MTDC grid power flows is addressed. It also proposes a method to specify mean voltage instead of the voltage of a single slack bus in the MTDC grid and the AC/DC grids are solved separately. There also has been some research in optimised operation of the combined AC/MTDC grid in [39]–[42] and a few papers cover the security constraints for combined optimisation with a linearised

power flow equation to avoid computation complexity. These studies have presented detailed behaviour concentrating on a single aspect of the combined system operation. A complete operating strategy including primary, secondary and tertiary control of the combined system is not fully covered. The following goals were identified to provide a complete operating strategy for the secure and optimal operation of the combined AC/MTDC system:

- To identify the power balancing, co-ordination and dispatch requirements and assign the appropriate control method for each stage of the combined operation of two grids under primary, secondary and tertiary control.
- To identify the most generic control configuration by the comparison of various DC voltage control methods of the MTDC grid, which can adopt all other control configurations.
- To develop models of combined AC/MTDC grids with the generic control in order to evaluate the combined AC/MTDC grid behaviour under various operating conditions.
- To develop a simplified method of optimisation based security assessment to obtain the Security Constrained Economic Dispatch (SCED) for the combined AC/MTDC grid.

1.4 Contribution of the Research Work

The contribution of this thesis covers three areas, (a) MTDC grid control, (b) AC/MTDC grids modelling and (c) AC/MTDC grids operation.

a) MTDC grid control

A generic tri-band droop control method is proposed, having three bands that can indicate the operation and response of the VSC units categorised into normal, upper and lower bands during the power balancing. The normal band indicates the allowed voltage and power regulation for normal operation of the VSC station. The upper band indicates the operation and response of the VSC station during an imbalance due to excessive power in the MTDC grid. The lower band indicates the operation and response of the VSC station during an imbalance due to a shortage of power in the MTDC grid. The main advantage of this generic control is that two separate droops can be assigned for balancing the power shortage and excess in the MTDC grid. It also enables the Independent System Operator (ISO) or Transmission System Operator (TSO) to choose the percentage of the voltage and power regulation setting the normal operation. The settings of each individual VSC unit can be modified during rescheduling by the co-ordinated control, including its droop gain, higher and lower voltage limits for the normal band, and separate droop gains for the upper and lower bands.

b) AC/MTDC grids modelling

A combined AC/DC Power Flow (C-PF) algorithm is proposed with generic tri-band droop implementation for re-scheduling in the co-ordinated control that enables the

computation of the steady state operating points of the combined system under various MTDC grid control configurations during different conditions.

A combined AC/DC Optimal Power Flow (C-OPF) algorithm along with security assessment method is proposed that enables the computation of the SCED for the VSC stations and generator units of the combined system in the tertiary control.

c) AC/MTDC grids operation

An implementation of a complete three-layered operational control strategy for the power flow control of the combined AC/MTDC grids is suggested, comprising primary, secondary and tertiary control. Primary control is assigned to ensure the balanced operation of the MTDC grid during various operating conditions. Secondary control is assigned with the co-ordination task. It receives the updated information of the current operating state of the combined system and estimates the operating set points (updated references) through the C-PF for the re-scheduling of VSC units in order to either re-store the post-disturbance condition, or ensure the planned operation. Tertiary control is identified to provide SCED for the combined AC/MTDC grid. It provides the secure and optimal references for the scheduling of the VSC and generator units to ensure secure optimal operation of the combined system.

The proposed systemised control can response to various disturbances. In this thesis all short-term transients due to faults and control are assumed to clear and disturbances are categorised into small and large disturbances. The incremental uncontrolled changes in load and generation are considered to be small disturbances. While, the complete loss of generation and load are considered as large disturbances. In the event of disturbance the three layer of systemised control response as:

Primary control: The primary control is integrated to the outer control of each VSC station and responses automatically to ensure the power balancing in the MTDC grid in accordance to chosen control configuration. For example, if tri-band droop control is implemented, its responses to the power disturbances with three different droops in three bands of operation.

Secondary control: The secondary control is proposed to be implemented from a centralised control station that receives the operating status from Remote Terminal Units (RTU) and estimates the updated references by C-PF to re-schedule reference set points to all the VSC stations and generator units of the combined AC/MTDC grid. It can response in a few seconds to a large disturbances and in cyclic pattern of few minutes to maintain the planned operation.

Tertiary control: The tertiary control is also implemented in centralised control that receives the Day ahead market demand through bidding information and perform optimisation along with security assessments for required power flow by C-OPF and schedules all the VSC stations and generations units to secure and optimum operation points. It responses in 20-30 minutes times.

1.5 Outline of the Thesis

In Chapter 2, three-layered hierarchical control is explained with the power balancing, coordination and dispatch requirements of the combined AC/MTDC grid operation. The fundamental principle of operation and control of the VSC station in explained in detail in order to obtain the overall system behaviour of a MTDC grid within a large system. Chapter 3 presents a comparison study performed on different power

balancing controls to find the most suitable control method for the primary control of the meshed DC grid. In Chapter 4, the combined AC/DC grid power flow method is proposed to provide updated references for the VSC station in order to maintain coordinated power flow control under secondary control layers. In Chapter 5, a security constraint optimisation method for the combined AC/DC grid is proposed for economic dispatch under the tertiary control layer of the three-layered hierarchal control. A number of case studies are performed to implement the proposed control methods on a combined AC/DC test case network. The performance of the proposed control methods is validated in a hierarchical control structure for the secure and optimal operation of integrated AC/MTDC grids. This is followed by the conclusion and future work in Chapter 6. The brief layout of this thesis is given in **Table 1-3**.

Table 1-3 *Brief layout of the thesis*

Chapter 2 **VSC Unit control**	Operation and control of VSC station
Chapter 3 **Primary Control**	Power balancing and DC node voltage control in the MTDC grid
Chapter 4 **Secondary Control**	Power flow control with re-scheduling of update power and voltage references following disturbances
Chapter 5 **Tertiary control**	Secure and optimal integrated AC/MTDC grid operation Security Constrained Economic Dispatch (SCED)

1.6 List of Publications

Papers published in journals/ Conference proceedings:

F. Akhter, D. E. Macpherson, and G. P. Harrison, "Enhanced multi-terminal HVDC grid management for reliable AC network integration," *7th IET Int. Conf. Power Electron. Mach. Drives (PEMD 2014)*, pp. 0495–0495, 2014.

F. Akhter, D. E. Macpherson, G. P. Harrison, and W. A. Bukhsh, "DC Voltage Droop Control Implementation in the AC / DC Power Flow Algorithm : Combinational Approach," in *IET 11th International Conference on AC and DC Power transmission*, 2015, pp. 1–6.

F. Akhter, D. E. Macpherson, and N. Shahzad, "Impact of Wind Integration on National Transmission Network," *Commun. Technol. Inf. Secur. Sustain. Dev.*, vol. 414, pp. 13–23, 2014.

Papers under review:

F. Akhter, D. E. Macpherson, G. P. H. W. A. Bukhsh, and M. A.A, "Power Balancing in the Proposed Supergrid Model for National Transmission Network of Pakistan," in *IET 12th International Conference on AC and DC Power transmission*, 2016.

F. Akhter, D. E. Macpherson, G. P. H. W. A. Bukhsh, and A.M.Soomro, "Proposal for VSC based Multi-Terminal HVDC transmission for Tajikistan, Afghanistan and Pakistan (CASA-1000) project against the planned LCC based Multi-Terminal HVDC," in *IET 12th International Conference on AC and DC Power transmission*, 2016.

CHAPTER 2

Operation and Control of VSC Station

2.1 Introduction

The VSC station is the basic building block of the Multi-Terminal HVDC (MTDC) grid, as the DC grid evolves from the combination of three or more VSC stations connected by a common DC network. It is necessary to understand the fundamental principle of operation and control of the VSC station in order to obtain the overall system behaviour of a MTDC grid within a large system. The future MTDC grid is expected to be connected to a number of AC grids under different conditions.

The objective of this chapter is to present the systemic three-layered control structure of the integrated AC/MDTC grids operation and to explore the operating characteristics and control behaviour of the VSC stations under different types of AC grid integrations i.e. passive or active, weak or stiff. In this chapter the first Section discusses the fundamental operation of the VSC station including an overview of different configurations of the VSC converter and its terminal voltage and power control. The second Section discusses the detailed control of the VSC station connected to different AC grids, which is followed by an overview of the modelling techniques of VSC transmission. Finally, the PV characteristics and safe operating limits are discussed along with a capability chart of the VSC station.

2.2 Three-layered Control for the Integrated AC/MTDC Grid Operation

The main purpose of the operational control strategy is to obtain the secure and optimal power flows from the MTDC grid, while maintaining the DC node voltages stable within the operating limits. The power balancing in the MTDC grid can be obtained mainly two control methods i.e. centralised or distributed control. In the case of centralised control when a disturbance or outage occurs in the MTDC grid and more than one VSC station controlling the DC node voltage, the new operating point depends on the power level of the MTDC grid. If there is shortage of power in the MTDC grid, then the VSC station with the lowest constrained limits takes over as master control and if there is excess of power in the MTDC grid then, the VSC station with highest constrained limit takes over as master control. Whereas, in the case of distributed control, the response of the MTDC grid to a disturbance or outage is according to the characteristics of the distributed control of the participating VSC stations.

The systemised control structure of the MTDC grid can be divided into high and low level as shown in **Figure 2:1**. High level control comprises of primary, secondary and tertiary control similar to an AC system [43], [44]; whereas, lower level control comprises of the basic inner current and firing control of the VSC stations. The responsibility of managing the DC node voltage regulation can be regarded as primary control, similar to the primary control in an AC system with frequency regulation. Secondary control can be implemented to adjust the power exchanges from the MTDC grid in order to restore the pre-disturbance conditions in the grid. Further, tertiary

control can be implemented in order to obtain the optimised reference set-points for the primary and secondary control.

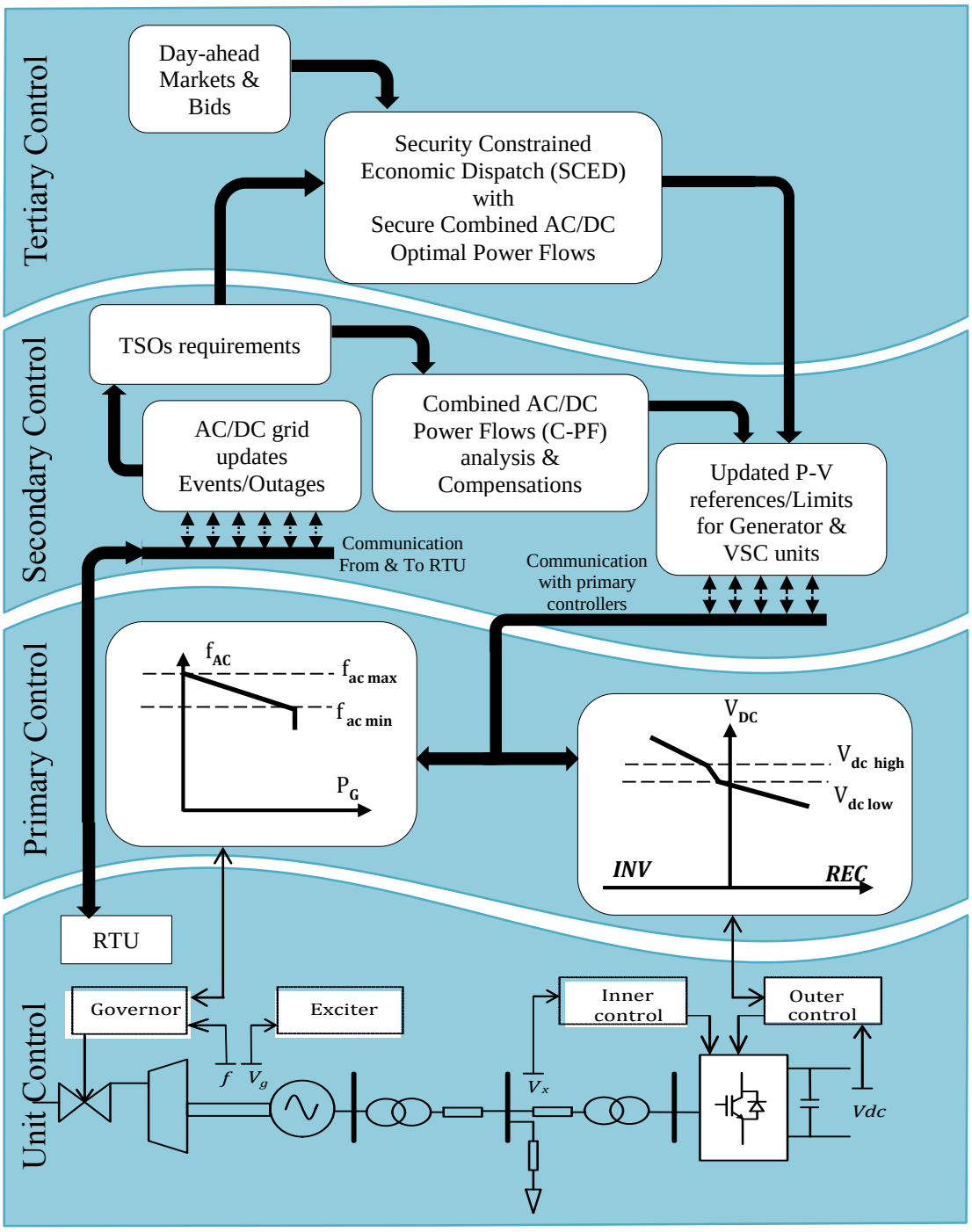

Figure 2:1 *Systemised control and operational strategy for the AC/MTDC grid*

The power-DC voltage characteristics in an MTDC grid are similar to the power-frequency characteristics of an AC system. However, frequency is a universal

parameter in an AC system, whereas DC node voltage varies at each VSC station according to the actual power flow and voltage drop in the MTDC grid. Secondly, the stored energy in the MTDC grid is very limited, only in capacitors and cables, as compared to inertia and kinetic energy in the rotating machine in an AC system. This makes the power-DC voltage characteristic more sensitive than the power-frequency characteristic of an AC system. Hence, the response of the controller in the MTDC grid is faster, which leads to smaller time constants for the high level controls of the MTDC grids. The response time discussed in [45][46] shows that, the primary control of the MTDC grid is activated in a few milliseconds in contrast to the time constant of up to 15-20 seconds for the AC system's primary control. The secondary control activates in the range of few seconds, while the tertiary control reacts in between 20 minutes and 30 minutes.

2.3 Operating Principle of Voltage Source Converter (VSC) Station

The name Voltage Source Converter (VSC) refers to an approximation of a voltage source which maintains a prescribed voltage across the DC side terminals regardless of the magnitude and polarity of the current flowing through it. The capacitor used on the DC side of the converter can be considered as a DC voltage source for short time transients to maintain the required voltage level. An inductor is used on the AC side of the converter to smooth the AC current. The array of fully controlled switches (e.g. IGBTs) with anti-parallel diodes forms a connection between the AC and DC terminals. A coupling transformer matches the VSC AC output voltage to the AC system standard voltage. The phase reactor in combination with a low pass filter forms a high frequency (HF) blocking filter to eliminate the HF stress on the coupling

transformer for the PWM operated converter [47]. A simplified single line diagram of the VSC station with its major components is shown in **Figure 2:2**.

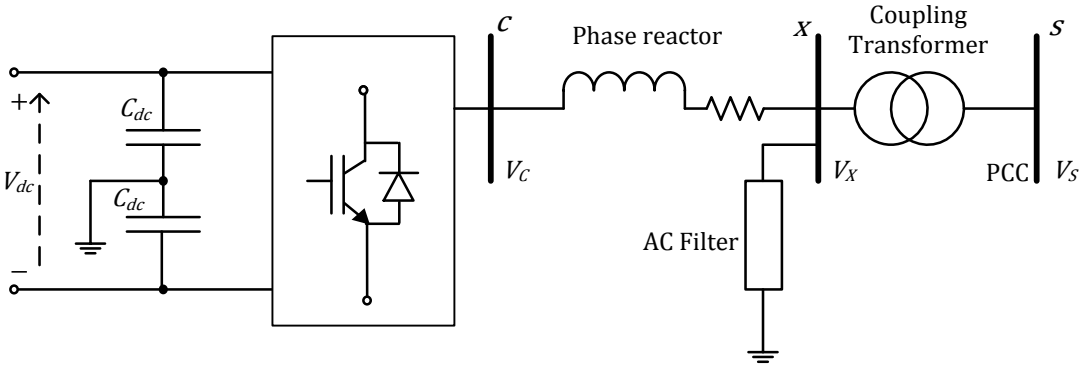

Figure 2:2 *Simplified single line diagram of the VSC station*

The self-commutated solid state devices turn ON and OFF in time sequence to generate high frequency square output waveforms without reliance on the AC grid voltage. Each IGBT is connected to an anti-parallel diode to form a basic VSC station unit called a VSC valve. The anti-parallel diodes are designed to withstand the short circuit currents as they function as uncontrolled bridges when the IGBTs are blocking. The switching controls the active and reactive power from the converter by controlling the phase angle and voltage magnitude of the VSC output voltage in relation to the AC grid voltage.

2.3.1 Configuration of the Voltage Source Converter (VSC) Station

There are many possible different topologies and control configurations of the VSC station. They are mainly categorised as:

(a) Basic 2-level three phase fundamental frequency operation,

(b) High frequency Pulse Width Modulation (PWM) switching control operation,

(c) Multi-level configuration operations [47], [48].

All the different operations and configurations of the VSC station have two main objectives:

- The conversion of the constant DC voltage into a controllable AC voltage, while producing output waveforms that are close to sinusoidal.
- Maintain independent control of the active and reactive power.

The PWM based 2-level three phase operation has restrictions on its power rating due to the inability of semiconductor switches to handle bulk power. The Multi-level configurations have been introduced to increase the power rating of the VSC station for future practical requirements. The various topologies includes diode-clamped, flying capacitor, cascaded H-bridge and modular multi-level converters (MMC) [49]–[51].

The Modular Multilevel Converter (MMC) topology has been widely adopted by the manufacturing industry due to its flexibility and fast control response with low harmonic content [52]. The converter arm acts as a controllable voltage source, with voltage steps to synthesise the sinewave form as shown in **Figure 2:3** (b). There are no common DC capacitors required, as the converter arm is built-up of cascaded sub-modules (SM) as shown in the main circuit configuration of an MMC in **Figure 2:3** (c). DC capacitors are distributed in the sub-modules as shown in **Figure 2:3** (a). In the MMC configuration, the voltage stress on each switch of the VSC station is reduced by reducing the voltage step size to different intermediate levels. Further, the harmonics in the AC voltage output of the VSC station are also reduced due to the

increase in the number of voltage levels without necessarily using the PWM technique. All competing manufacturers have opted for the Modular Multilevel Converter (MMC) due to its advantages over other multi-level configurations.

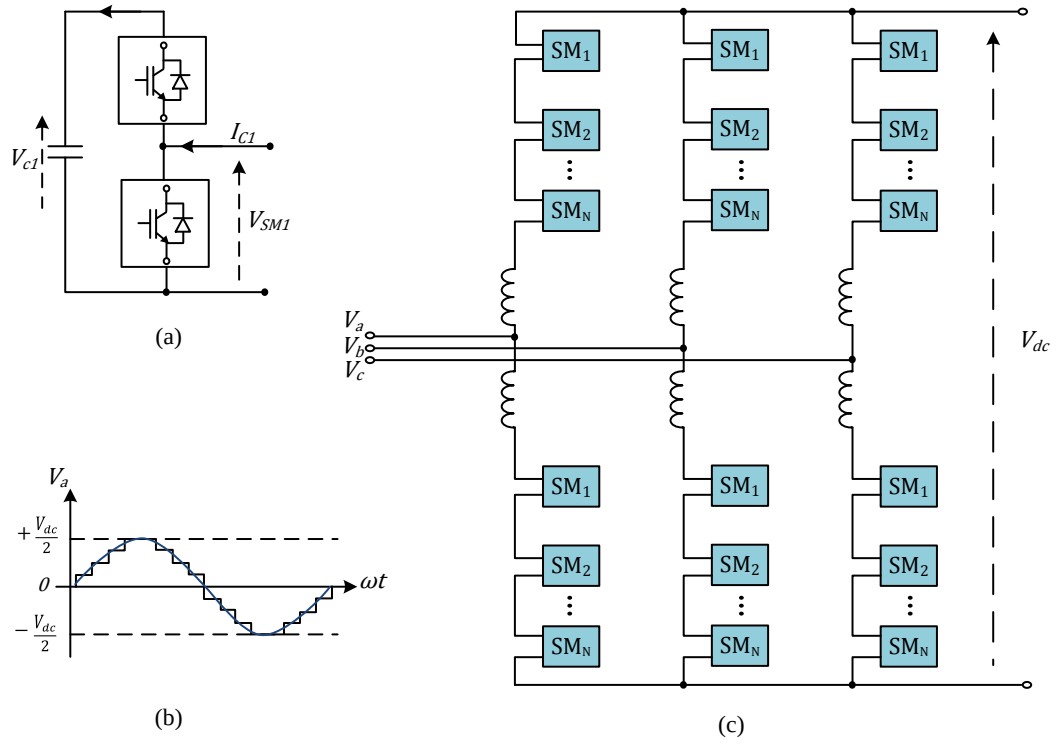

Figure 2:3 *Modular Multi-level Converter* (a) *Sub Module of MMC* (b) *Sine wave output of MMC* (c) *Circuit configuration of Modular Multi-level Converter*

However, the focus of this thesis is to obtain the behaviour of more than two VSC stations in a multi-terminal DC (MTDC) grid and their interaction with the connected AC grids. The converter topology will not much affect the system behaviour as long as a nearly sinusoidal wave is obtained at the AC side of the VSC station. In this thesis, a 2-level configuration with average models has been used, which will be discussed in detail in Section 2.4.

2.3.2 VSC Terminal AC Voltage Formulation

The AC output voltage of the VSC station needs to be controlled for most of its applications. The basic arrangement of the VSC valves for the 2-level three phase bridge is shown in **Figure 2:4**. The square wave operation is not practical due to the dependency of the VSC station's AC voltage on the DC node voltage and the very high level of harmonics in the AC output waveforms. The magnitude of the AC voltage can only be controlled by varying the DC node voltage. However, this will affect the AC voltage magnitude of the other VSC stations connected in the same MTDC grid.

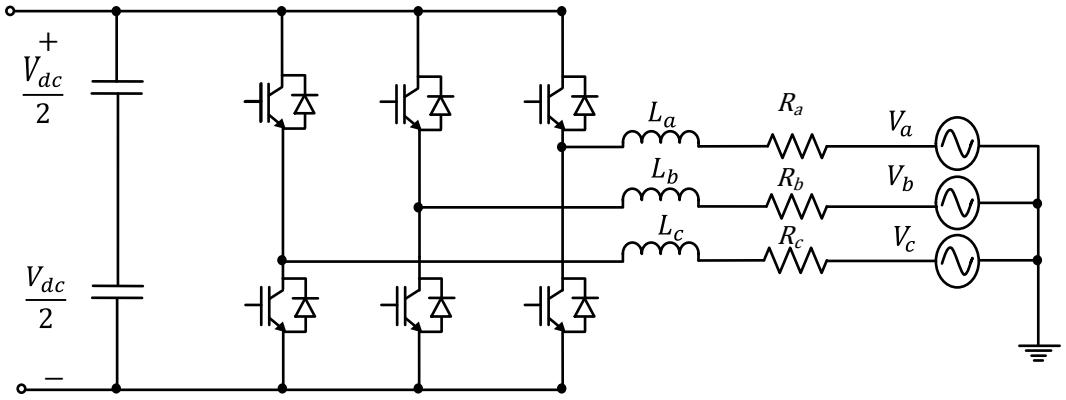

Figure 2:4 *Basic 2-level three phase configuration*

The PWM technique uses high frequency switching, usually around 1-2 kHz, to reduce the low order harmonics. It provides very fast control of the VSC station's AC voltage along with keeping the DC node voltage constant. The quality of output waveform can be improved by increasing the switching frequency. However, increasing the switching frequency increases power losses. There are various Selective Harmonic Elimination Methods (SHEM) that can be applied to obtain harmonic cancellation [53], [54]. A compromise is required in the selection of switching

frequency to achieve a balance between the harmonic elimination and the amount of switching losses in the VSC station.

The sinusoidal pulse width modulation (SPWM) is mostly used for low-order harmonic reduction in low powered converters [16]. There fundamental component of the VSC converter output voltage (V_c) can be given as:

$$v_c(t) = m.\frac{V_{dc}}{2}\sin(\omega t + \delta_c) \qquad (2.1)$$

where,

m is the modulation index,

δ_C is the phase angle of V_C with respect to V_S,

V_{dc} is the DC link voltage,

ω is the fundamental angular frequency.

The amplitude of the VSC converter output voltage (V_C) can be controlled by varying the modulation index (m) and the phase angle between the V_C and V_S can be controlled by δ_C. This principle applies to other converter modulation strategies as well. The modern MMC is most commonly used converter topology and its generated voltage is close to the reference voltage. The modulation technique used for the MMC can categorised as the PWM multicarrier based or Sort and Select based. The multicarrier based methods have some drawbacks such as unequal ripple distribution in the capacitors and large circulating currents [55]. Whereas, in case of sort and select methods, the SMs are first sorted on the basis of their capacitor voltages and then a selection methods such as Nearest Level Control (NLC), Selective Harmonic Elimination (SHE) and Model Predictive Control (MPC) are applied to select the number SMs for each arm [56].

2.3.3 Active and Reactive Power Flow

The active and reactive power flow control principle for the VSC station is the same as power flow between two nodes of an AC system, regardless of the topology of the VSC station. Two AC nodes are connected by the equivalent reactance of the phase reactor and the transformer shown in **Figure 2:5**, where X_T and r_T represent the combined reactance and resistance of the phase reactor and transformer respectively. V_C and V_S are the voltages at node C and node S respectively, with δ_C as the phase difference between the two node voltages.

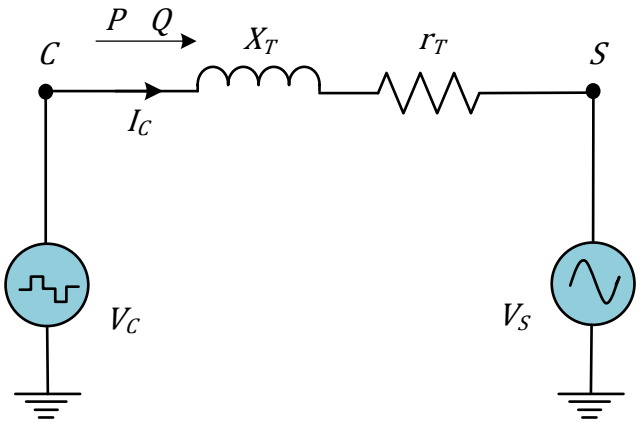

Figure 2:5 *Simplified AC equivalent representation of the VSC terminal*

The expression for the active power flow with and without taking resistance into account can be written as:

$$P = \frac{V_c\, V_s\, \sin\delta_c - r_T X_T}{X_T} \tag{2.2}$$

$$P = \frac{V_c\, V_s\, \sin\delta_c}{X_T} \tag{2.3}$$

And the expression for the active power flow with and without taking resistance into account can be written as:

$$Q = \frac{V_c V_s}{X_T}\cos\delta_c - \frac{V_s^2}{X_T} - \frac{r_T P}{X_T} \tag{2.4}$$

$$Q = \frac{V_c V_s}{X_T}\cos\delta_c - \frac{V_s^2}{X_T} \tag{2.5}$$

The active power flow through the VSC can be controlled by controlling the phase angle δ_C. When the VSC output voltage V_C leads the AC grid voltage V_S, the VSC injects active power into the AC grid and operates as an inverter. Whereas, the VSC operates as a rectifier when the VSC output voltage lags the AC grid voltage and absorbs active power from the AC grid. Similarly, when the amplitude of the VSC output voltage is kept higher than AC grid voltage through modulation index (m), the VSC most often operates in capacitive mode and injects reactive power into the AC grid. Conversely, if the amplitude of the VSC output waveform is kept lower than that of the AC grid then the VSC operates in inductive mode and reactive power is absorbed by the VSC station. The P-Q diagram in **Figure 2:6** shows the four quadrant operation capability and independent control of active and reactive power through the phasor diagrams. Due to these operating features VSC transmission can provide additional support to the integrated AC system [47], [57], [58].

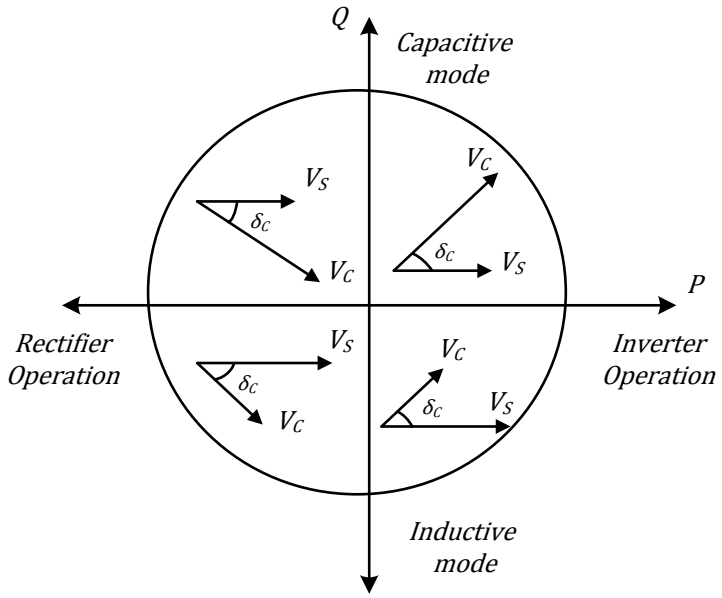

Figure 2:6 *PQ diagram with four quadrant operation*

2.4 Modelling of the Voltage Source Converter (VSC) Station

The modelling approach of the VSC varies in accordance with the requirements of the study undertaken. The detailed model includes all the semiconductor components with their arrangements to represent the different topologies of the VSC (i.e. 2-level or multi-level) along with their detailed switching control patterns. The detailed model simulation can be used in electromagnetic transient programs (EMTP-type) to perform high frequency harmonic analysis, switching loss calculations and DC fault studies. The detailed model simulation can be performed easily for point to point or for the study that involves just a few VSC stations. However, when a MTDC grid has several VSC stations, the complexity of the system study increases significantly. The detailed modelling of the VSC stations with full converter switching dynamics and with control design heavily reduces the speed of simulations for a large MTDC grid. The focus of this study is to develop an operational strategy of the integrated AC MTDC

grids and analyse the AC/DC network interactions in steady state. So, an average equivalent modelling technique is used in this thesis.

The average equivalent model is built using equivalent equations of the high power circuit of the VSC in order to avoid the inner VSC switching units. It presents the fundamental frequency equivalent output of the detailed VSC model: this is sufficient to study all the phenomena of the fundamental frequency voltage and current components of the VSC. The outer VSC components (inductors, cables) and control system dynamics can be fully modelled. The AC side of the VSC is represented as a controllable three phase AC voltage source and the DC side of the VSC is represented as a controllable current source[59]–[61], as shown in **Figure 2:7**. The switching and conduction losses of the VSC station are neglected. The equivalent mathematical equation for each single phase controllable AC voltage source of a typical 2-level three phase VSC station can be represented as:

$$V_a = \frac{1}{2} V_{dc}\, m_a, \quad V_b = \frac{1}{2} V_{dc}\, m_b\,, \quad V_c = \frac{1}{2} V_{dc}\, m_c \tag{2.6}$$

Similarly, the equivalent equation for the current source is given as:

$$I_o = \frac{1}{2}(i_a m_a + i_b m_b + i_c m_c) \tag{2.7}$$

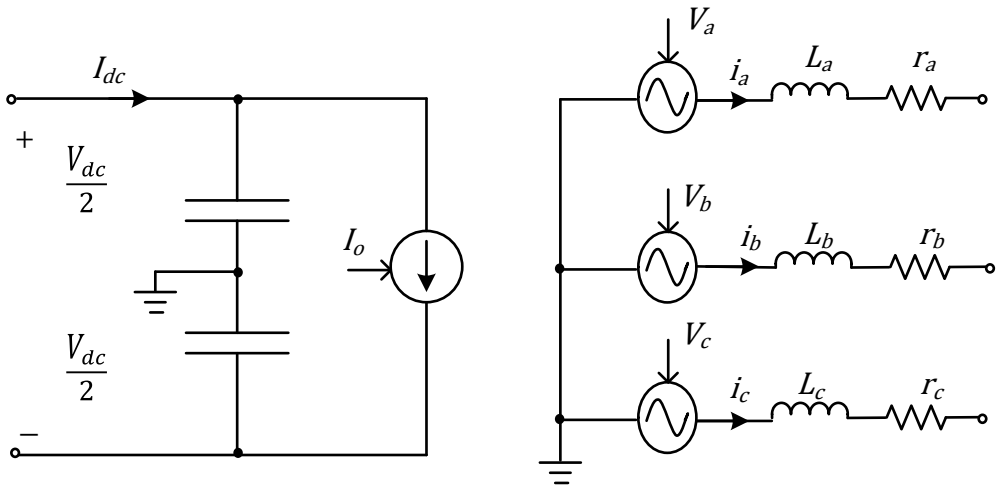

Figure 2:7 *Average model of VSC station*

where, m_a, m_b and m_c are the modulation indices that control the AC voltage sources V_a, V_b and V_c, while i_a, i_b and i_c are the resulting respective phase currents flowing into the AC grid. The neutral point of the controlled three phase voltage source is grounded for the actual representation of three phase current flow in the case of an unbalanced condition. The average VSC model has a significant advantage in the simulation studies, where the outer control and dynamics of the system is the main focus of this study. It enables the use of large time steps by avoiding the switching components and high frequency phenomena, which in turns reduces the size of the memory required to run the simulation. These advantages become more obvious when a large MTDC system is simulated with several VSC stations. Keeping in view the afore-mentioned advantages, the average VSC model has been used for the implementation and verification of the outer dynamics and control design of the VSC stations for the time domain studies of this thesis. The modulation index is taken at the output of the inner current by converting dq-axis voltage into three phase frame (*abc*) and it is not utilised in outer control. The single line equivalent diagram of **Figure 2:2** is shown in **Figure 2:8**.

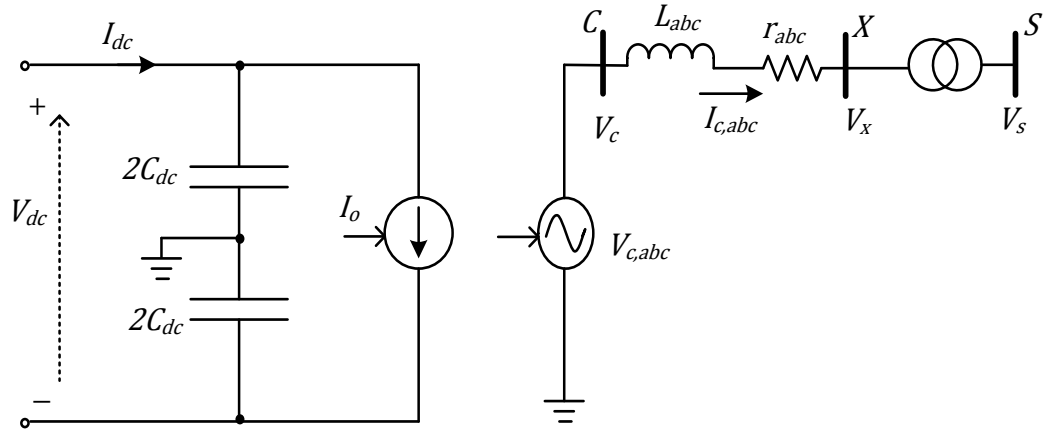

Figure 2:8 *Controlled voltage and controlled current based single line average model*

2.5 Control of the VSC station

The control requirements of the VSC station depends on the type of AC grid it is connected to. If it is connected to a passive grid (being the only source in the AC grid) then the VSC station is responsible for maintaining the fixed AC voltage magnitude and frequency at node *S*, the point of common coupling (PCC) of the AC grid. The primary objective of this VSC station is to control the AC voltage, which can be achieved by the implementation of a simple AC voltage controller shown in **Figure 2:9**(a). **Figure 2:9**(b) shows the per-phase AC side equivalent circuit of the VSC station with L_T and r_T representing per phase equivalent inductance and resistance of the phase reactor and transformer.

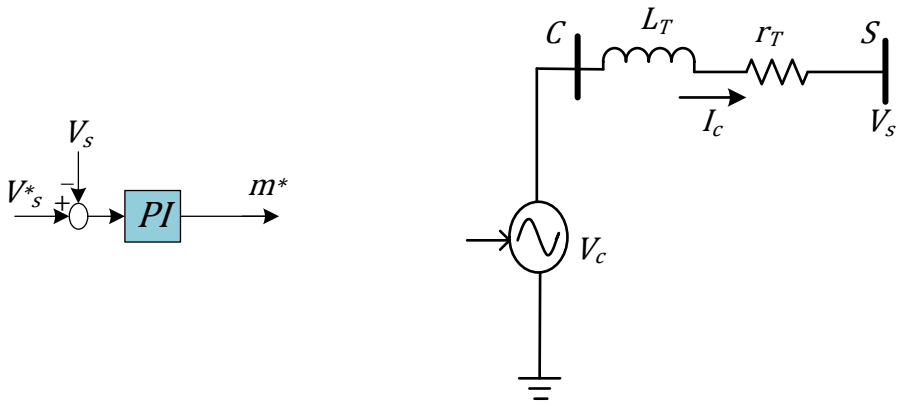

Figure 2:9 *AC voltage controller for passive grid* (a) *Control block diagram* (b) *per-phase AC side equivalent of VSC*

A VSC station connected to an active AC grid (with other sources, such as synchronous generators) requires more complex control, in order to maintain independent control of active and reactive power and synchronised operation. The frequency of the VSC station output has to be synchronised with the AC grid frequency and the currents need to be controlled to control the power, when connected to an active AC grid. The control of an active AC grid connected VSC comprises an inner and outer controller. The inner controller is fast acting, as it controls the switching (at carrier frequency in the case of PWM switching control) of the semiconductor devices (IGBTs). It also has a phase lock loop (PLL) to detect the phase angle and frequency of the AC grid. The active and reactive power is controlled in the outer controller by controlling the phase angle and voltage magnitude of the VSC station output voltage, respectively as mentioned in Section 2.3.

2.5.1 Inner Current Controller of the VSC Station

The inner controller of the VSC station can be implemented by two different methods, direct control and vector (d-q decoupled) control.

2.5.1.1 Direct Control

In the case of direct control, as discussed in Section 2.3.2, the voltage magnitude and phase angle are directly controlled by adjusting the modulation index *m* and phase shift δ_C respectively, in response to the comparison of the controlled parameters with the reference parameters. The direct voltage control requires the voltage and current phasor measurements from the PCC.

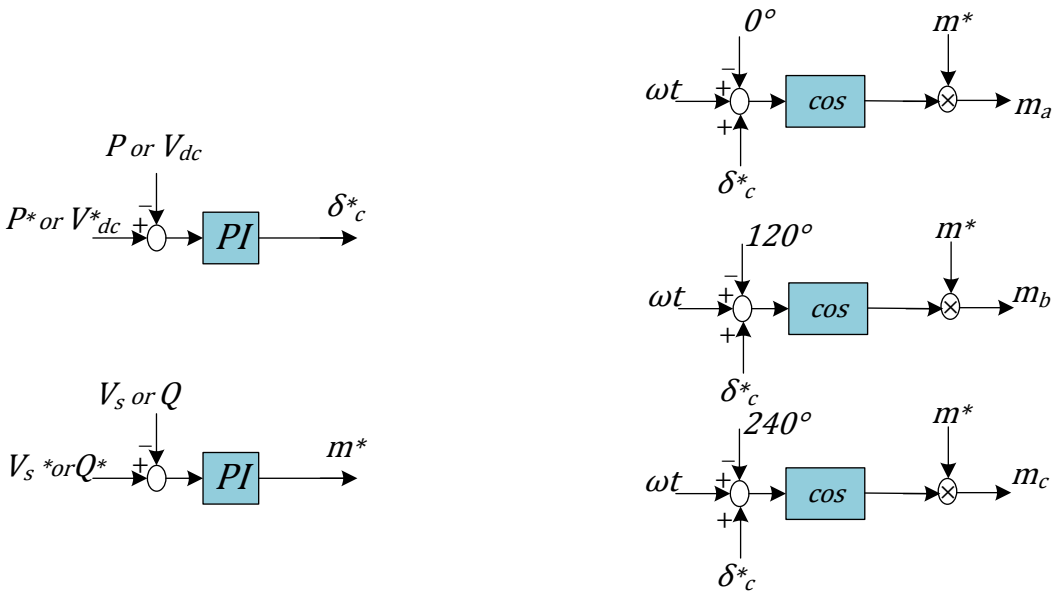

(a) (b)

Figure 2:10 *Direct control for active AC grid* (a) *Control block digram of Outer control* (b) *Control block diagram of Inner control*

The controlled parameters can be the real power, reactive power, DC node voltage or AC voltage of the VSC station as shown in **Figure 2:10**(a & b). However, the two parameters are not isolated completely, because change in phase shift not only changes the active power, but also affects the reactive power of the VSC station and vice versa.

2.5.1.2 Vector Control

In the case of vector control, also known as d-q decoupled control, the active and reactive power can be controlled independently by using the d-q current control strategy which can inherently limit the overloading of switches. Other methods are also suggested for the VSC control in low and medium power applications [62], [63]. However, decoupled control is mostly used in the practical application of the VSC stations in the power industry and it is used for the inner current controller of the VSC station in this thesis. The control configuration of the VSC station based on decoupled control comprises of cascaded control, with a faster inner controller and an outer controller to reference parameters to the inner controller. The complete diagram of the decoupled control configuration is shown in **Figure 2:11**.

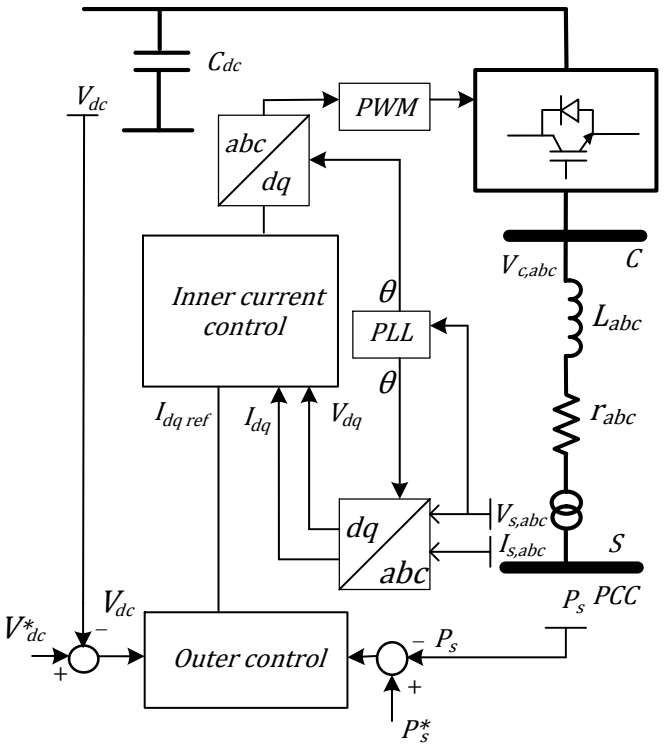

Figure 2:11 *Complete diagram of dq axis Vector control*

Basically, vector control uses the synchronously rotating d-q reference frame to transform three phase ac quantities (balanced voltage or current) into equivalent two phase quantities having the same resultant space vector [64] to synchronise with the AC grid through a PLL. It requires two transformations:

(a) One from the stationary three phase reference frame (*abc*) to the stationary two phase frame ($\alpha\beta$) through the Clarke transformation given by eq: (2.8).

(b) The second transformation involved is from the stationary two phase frame ($\alpha\beta$) to another two phase frame through Park transformation given by eq: (2.9). This frame rotates in synchronism with AC grid voltage phasor to obtain phase shift of θ.

$$\begin{bmatrix} v_\alpha \\ v_\beta \end{bmatrix} = K \begin{bmatrix} 1 & -\frac{1}{2} & -\frac{1}{2} \\ 0 & \frac{\sqrt{3}}{2} & -\frac{\sqrt{3}}{2} \end{bmatrix} \begin{bmatrix} V_a \\ V_b \\ V_c \end{bmatrix} \tag{2.8}$$

where, *K* is the multiplying factor for different conversions, and is equal to 3/2 for the magnitude invariant transformation used here.

$$\begin{bmatrix} v_d \\ v_q \end{bmatrix} = \begin{bmatrix} \cos\theta & \sin\theta \\ -\sin\theta & \cos\theta \end{bmatrix} \begin{bmatrix} v_\alpha \\ v_\beta \end{bmatrix} \tag{2.9}$$

Similarly, a transformation can be obtained for three phase current quantities.

From **Figure 2:9** the voltage through the equivalent inductance of the VSC station can be given as:

$$L\frac{di_{abc}}{dt} = V_{s,abc} - V_{c,abc} - ri_{abc} \tag{2.10}$$

Applying the magnitude invariant Clarke transformation from eq: (2.10):

$$L\frac{di_{\alpha\beta}}{dt} = V_{s,\alpha\beta} - V_{c,\alpha\beta} - ri_{\alpha\beta} \tag{2.11}$$

The Park transformation from eq:(2.11) can be applied as:

$$V_{s,\alpha\beta} = V_{s,dq}e^{j\omega t} \tag{2.12}$$

$$V_{c,\alpha\beta} = V_{c,dq}e^{j\omega t} \tag{2.13}$$

$$i_{\alpha\beta} = i_{dq}e^{j\omega t} \tag{2.14}$$

So, substituting values from eq:(2.12)-(2.14) into eq:(2.11) and solving will result into:

$$L\frac{di_{dq}}{dt} = V_{s,dq} - V_{c,dq} - ri_{dq} - j\omega Li_{dq} \tag{2.15}$$

which can be written into matrix form as:

$$L\frac{d}{dt}\begin{bmatrix} i_d \\ i_q \end{bmatrix} = \begin{bmatrix} V_{sd} \\ V_{sq} \end{bmatrix} - \begin{bmatrix} V_{cd} \\ V_{cq} \end{bmatrix} - r\begin{bmatrix} i_d \\ i_q \end{bmatrix} - \omega L\begin{bmatrix} 0 & 1 \\ -1 & 0 \end{bmatrix}\begin{bmatrix} i_d \\ i_q \end{bmatrix} \tag{2.16}$$

Based on eq:(2.16), the inner control of dq-decoupled vector control can be developed. The block diagram of the inner control is shown in **Figure 2:12**.

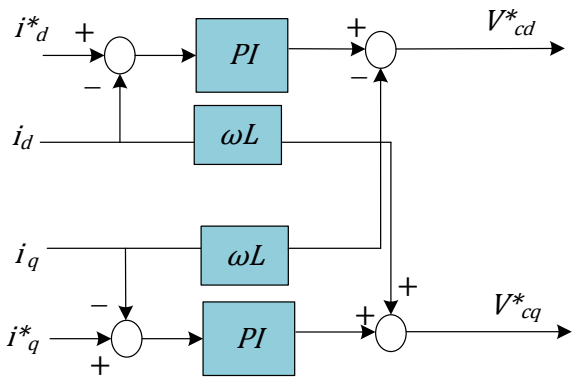

Figure 2:12 *Inner control diagram of dq-axis vector control*

The apparent power at the PCC can be calculated as:

$$S_{dq} = \frac{3}{2} V_{s,dq} i^*_{dq} = \frac{3}{2}\{(V_{sd} + jV_{sq})(i_d - ji_q)\} \tag{2.17}$$

$$S_{dq} = \frac{3}{2}\{(V_{sd} i_d + V_{sq} i_q) + j(V_{sq} i_d - V_{sd} i_q)\} \tag{2.18}$$

In this thesis, the d-axis is related to the active power and the q-axis is related to the reactive power. Further, the d-axis is aligned to the AC grid voltage by the PLL, hence the q-axis voltage becomes zero, so the apparent power will be:

$$S_{dq} = P_s + jQ_s = \frac{3}{2}(V_{sd} i_d - jV_{sd} i_q) \tag{2.19}$$

Hence, active and reactive power at the PCC (node *S*) can be obtained by separating real and imaginary terms:

$$P_s = \frac{3}{2}(V_{sd} i_d) \tag{2.20}$$

$$Q_s = -\frac{3}{2}(V_{sd} i_q) \tag{2.21}$$

2.5.2 Outer Controller of the VSC Station

The basic operation of the outer controller for vector control works similar to the direct control as described in Section 2.5.1.1. The vector control can control either active power (P_S) or DC node voltage (V_{dc}) to provide a reference for the d-axis current (i_d*) depending on the DC side network (HVDC link or MTDC grid) requirements of the VSC station. It can provide a reference for q-axis current (i_q*) either by controlling reactive power (Q_S) or AC grid voltage (V_S) depending on the requirements of the AC side network (AC grid) of the VSC station. The power supplied into the DC grid (rectified) is regarded as positive, and taken out (inverted) is regarded as negative, analogous to generation and load in an AC power system. The advanced control methods that take into account the power balancing phenomena of a MTDC grid are discussed in detail in Section 3.3. In this Section, only basic control of five parameters is covered.

2.5.2.1 Active Power Control

Active power control is implemented in order to control the active power through the VSC station to its desired reference value. It uses a proportional-integral (PI) regulator to eliminate the steady state error as shown in **Figure 2:13**. The output of the active power controller (i_d*) provides a reference to the d-axis of the inner current controller and is limited to keep the current through the VSC station within the rated limits.

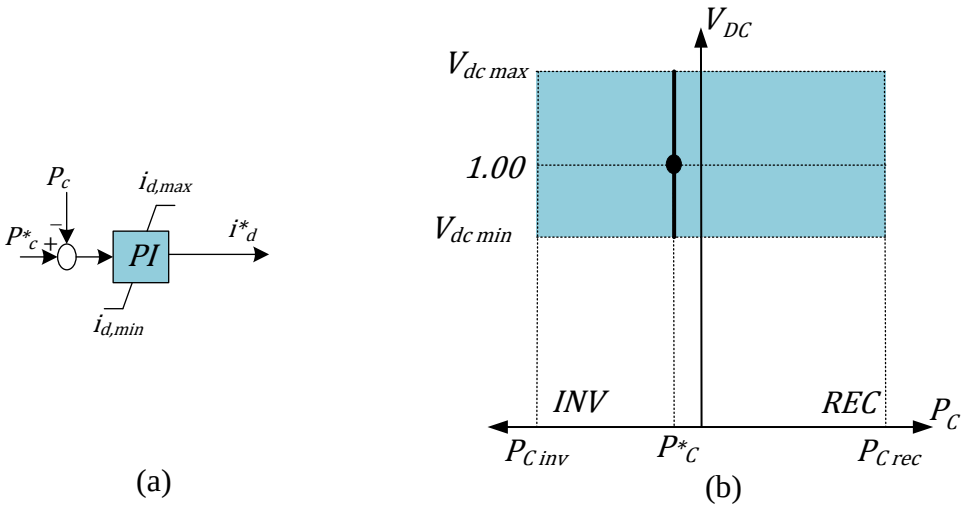

Figure 2:13 *Active power control* (a) *Control block diagram of active power control* (b) *PV characteristics of constant active power control*

2.5.2.2 DC Voltage Control

The DC voltage control of the VSC station is the most important control for stable operation of the VSC transmission, as it ensures the power balance through the DC system. The output of the DC voltage controller (i_d*) also provides a reference to the d-axis of the inner current controller which is why each VSC station can either control active power or DC voltage. DC voltage control uses the PI control to keep the DC voltage constant by making the steady state error zero through the integral gain as shown in **Figure 2:14**.

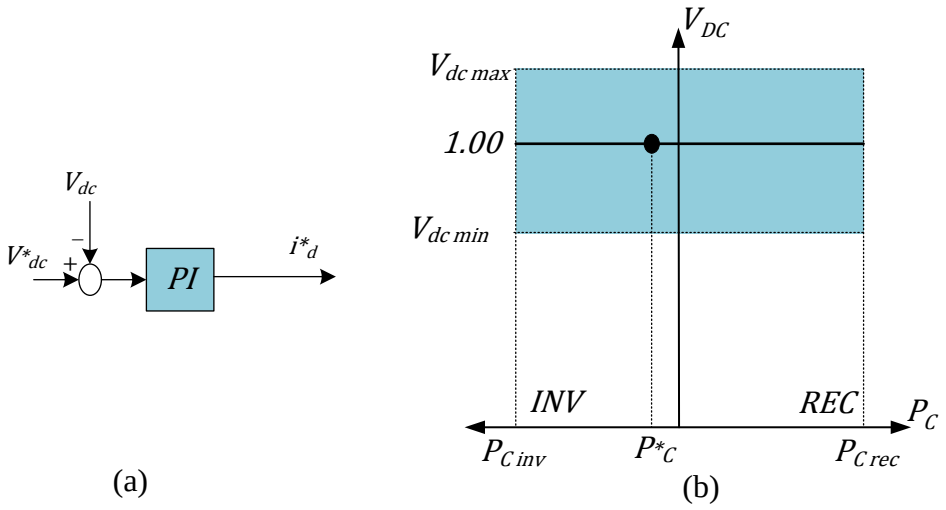

Figure 2:14 *DC voltage control* (a) *Control block diagram of DC voltage control* (b) *PV characteristics of constant DC voltage control*

2.5.2.3 Reactive Power Control

Reactive power control by the VSC station can be achieved by implementing a PI regulator. The output of the DC voltage controller (i_q*) also provides a reference to the q-axis of the inner current controller as shown in **Figure 2:15**. The output of the reactive power controller is also limited to maintain the total current through the VSC station within the rated limits, but with priority given to the active power current control.

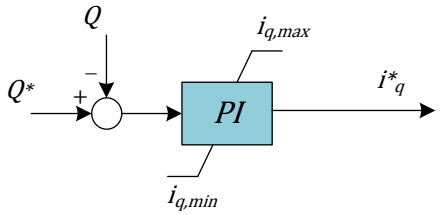

Figure 2:15 *Control block diagram of reactive power control*

2.5.2.4 AC Grid Voltage Control

The VSC station can also control the AC grid voltage in the case of connection to a weak grid. The AC grid voltage controller regulates AC grid voltage using a PI controller which compares the AC grid voltage with a reference voltage and maintains zero steady state error. The output of the PI regulator is used as the reference (i_q*) for the q-axis inner current controller. The control block diagram of the AC voltage control is shown in **Figure 2:16**.

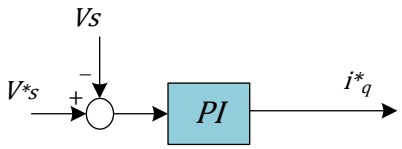

Figure 2:16 *Control block diagram of the AC voltage control*

2.6 Capability Chart of the VSC Station

As discussed in Section 2.3.3, a VSC station can operate at any point within a theoretical PQ diagram. However, actual operation of the VSC station is limited by many factors. The VSC station can be represented as the equivalent of a synchronous generator without inertia in the system, due to its independent active and reactive power controlling capability, and it has certain operational limits similar to those of a synchronous generator. These limits need to be taken into account in order to obtain the realistic behaviour of the VSC station from a power system stability point of view. Three factors that mainly limit the operation range of a VSC station are:

(a) Maximum reactive power which a converter can absorb and inject constrained by DC link voltage and AC grid operating limits.

(b) Maximum active power, or more specifically the current through the converter.

(c) The current in the cable is limited due to thermal ratings and cable is major cost of the MTDC system.

These factors for an individual converter station are also affected by the AC grid stability limits that can be determined by the AC system strength and impedance characteristics quantified as the Short Circuit Ratio (SCR) [65]. SCR is also taken as one of the limiting parameters using a common approach of defining it as the ratio of short-circuit MVA of the AC system to MW rating of the VSC station. A minimum value SCR may be required to obtain the required reactive power from the VSC station. The steady state capability of the VSC station decides the maximum active and reactive power that can be transferred between the VSC station and the AC grid.

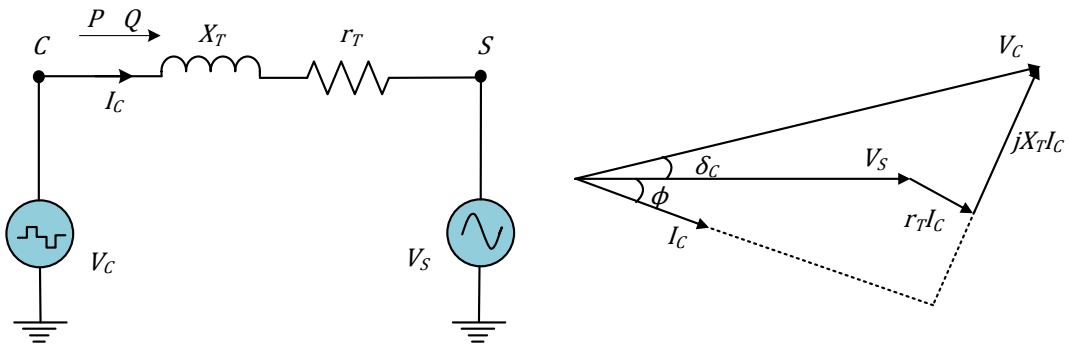

Figure 2:17 *Simplified AC equivalent representation of the VSC terminal*

The bi-quadratic equation for the voltage at the sending end, (node *C*) can be given as [66]:

$$V_c^4 + [2(r_T P_c + X_T Q_c) - V_s^2]V_c^2 + (r_T^2 + X_T^2)(P_c^2 + Q_c^2) = 0 \quad (2.22)$$

where, X_T and r_T represent the combined reactance and resistance respectively of the phase reactor and the transformer. V_C and V_S are the voltages at node *C* (VSC converter) and node *S* (AC grid) respectively, with δ_C as the phase difference between the two node voltages. By solving eq:(2.22) for Q_C, the Maximum Available Power (MAP) curve of a given AC grid voltage (V_S) can obtained by:

$$Q_c = \frac{V_s^2}{4X_T} - \frac{X_T}{V_s^2} P_c^2 \quad (2.23)$$

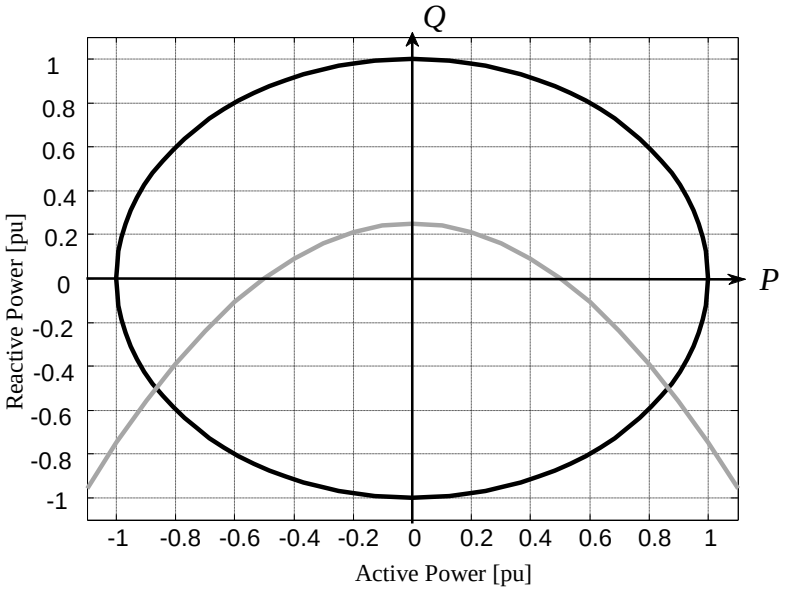

Figure 2:18 *PQ characteristics with reactive power absorbtion limit at SCR=1*

Figure 2:18 shows the PQ characteristics for SCR=1 with (V_C =1). It shows that the amount of reactive power that can be absorbed by the VSC station is limited. Further, the overall operation area of the VSC node is very limited with a low SCR as compared to the theoretical PQ characteristics of the VSC station.

2.6.1 Maximum DC Voltage Limit

The reactive power generated by the VSC station mainly depends on the voltage difference between the VSC terminal voltage V_C and AC grid voltage V_S. The voltage V_C at the converter node *C* is also limited by the DC node voltage as given by:

$$V_{c,max} = m_a \frac{V_{dc,max}}{2} \tag{2.24}$$

where, $V_{c,max}$ is the maximum VSC converter node voltage and $V_{dc,max}$ is the maximum DC node voltage of the VSC station. If the VSC station is equipped with a tap changer transformer, the AC voltage at the filter bus can be regulated [67]. The voltage limit circle can be found by modifying active and reactive power flow equations (2.4) and (2.5) in order to eliminate $cos\delta$ and $sin\delta$:

$$\sin\delta = \frac{P\,X_T}{V_s V_c}, \quad \cos\delta = \left(Q + \frac{V_s^2}{X_T}\right)\frac{X_T}{V_s V_c} \tag{2.25}$$

Putting these in the following equation leads to the equation of a circle with the centre of the circle at $\left(0, \frac{V_s^2}{X_T}\right)$ and a radius of $\frac{V_s V_c}{X_T}$.

$$sin^2\,\delta + \, cos^2\,\delta = 1 = \left(\frac{P\,X_T}{V_s V_c}\right)^2 + \left[\left(Q + \frac{V_s^2}{X_T}\right)\frac{X_T}{V_s V_c}\right]^2 \tag{2.26}$$

$$\left(\frac{V_s V_c}{X_T}\right)^2 = P^2 + \left(Q + \frac{V_s^2}{X_T}\right)^2 \tag{2.27}$$

The radius of the MVA capability circle of the VSC station depends on the AC grid node *S* voltage and the converter node *C* voltage. The reactive power injection limit of the VSC station is shown in **Figure 2:19**.

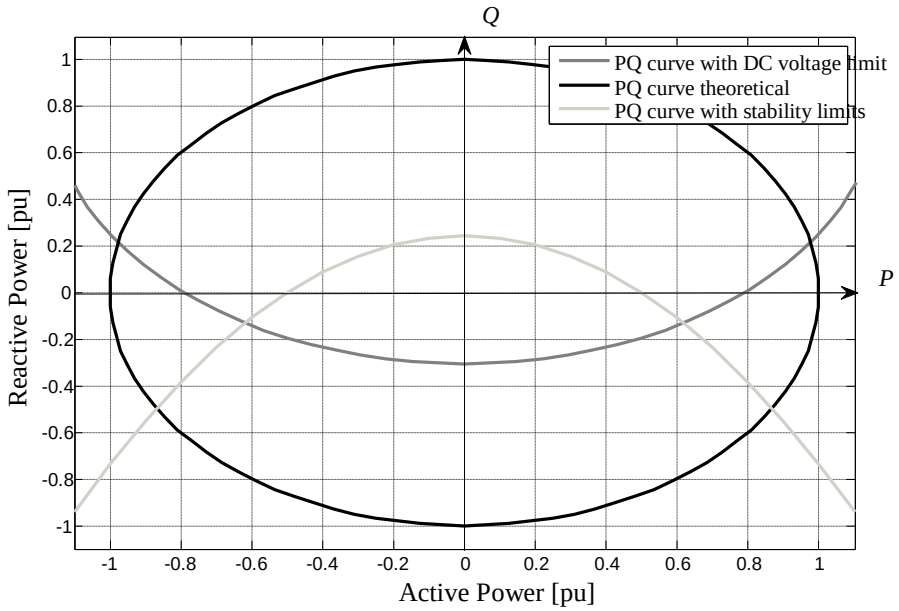

Figure 2:19 *PQ characteristics with reactive power injection limit at SCR=1*

2.6.2 Maximum Current Limit

The PQ diagram covers only active and reactive power limits. However, in the case of the VSC station, the current through the converter must be limited in order to protect the switching devices (IGBTs). In the event of a fault, the switches are switched off for their protection and the diodes conduct the current [68]. The maximum current through the converter multiplied by the actual AC voltage defines the MVA circle of the capability chart. This MVA capability increases and decreases proportionally with the AC grid voltage V_S.

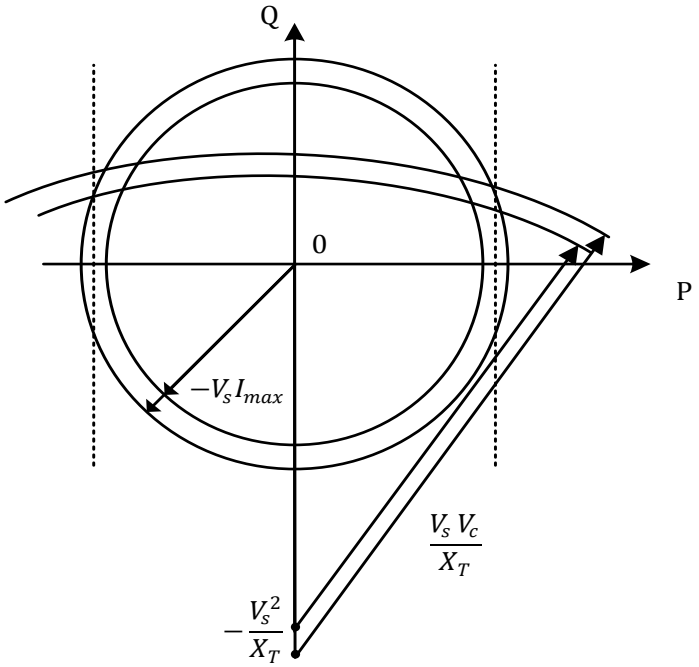

Figure 2:20 *Theoretical MVA capability chart with current limits*

The DC cable power limit at rated DC voltage is indicated by the vertical dotted lines in the PQ diagram shown in **Figure 2:20**. The limitations of the capability chart of the VSC station can be altered by the phase shift transformer in steady state operation. When the voltage at the AC filter bus is increased, the radius of the MVA circle and the AC voltage limit is also increased as shown in **Figure 2:20**. However, in dynamic operation, a tap changer is typically too slow to react to the changing situation of the VSC station, so the capability chart of the VSC station cannot be influenced by the tap changer settings.

2.7 PV Characteristics and Safe Operating Limits of the VSC Station

As discussed in Section 2.6, the operation of the VSC station has different limitations. It is necessary to incorporate these limitations into the PV droop characteristics of the various control configurations for inner and outer control.

Three main limitations that need to be considered for protection of the VSC station and DC cables are:

(a) Maximum power capacity

(b) DC voltage levels

(c) Maximum DC current

The maximum power limit is caused by the current limit rating of the switching devices and cables, which limit the AC current and hence limit maximum power transfer. The maximum power limit can be represented as a straight vertical line in the PV characteristics curve as shown in **Figure 2:21**.

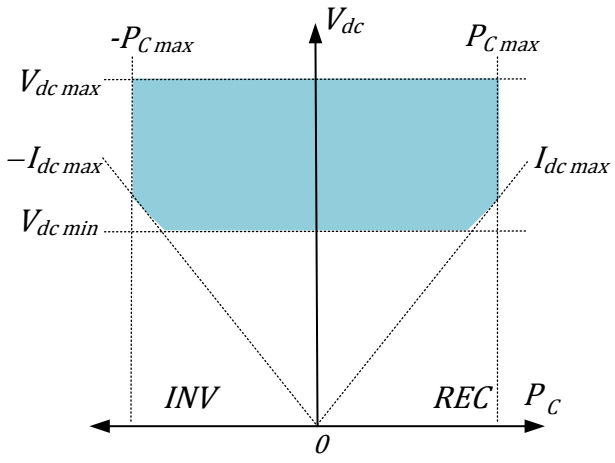

Figure 2:21 *PV characteristics with safe operating region*

The DC voltage has upper and lower limits. The upper limit is mainly defined by the insulation requirements of the switching components. The DC voltage has a lower level limit as the DC link should not be discharged below its lower level to maintain the normal operation of the VSC station. The value of the lower limit depends on the

VSC converter topology and control implementation. For a PWM converter it is typically defined as being in the region of $1.28V_S$, where V_S is the line-line rms AC grid voltage at node *S*. The upper and lower DC voltage limits can be represented as horizontal lines in the PV characteristics curve as shown in **Figure 2:21**.

The maximum DC current limit ensures that the VSC station operates below the maximum limit during all operating conditions. If the operating DC voltage of the VSC station is reduced, then the amount of power transfer should be reduced proportionally in order to keep the DC current below the maximum limit. The DC current limits can be represented by the straight lines that intersect at the origin in the PV characteristics curve.

2.8 Chapter Summary

This chapter presented the systemised three-layered control structure of the integrated AC/MDTC grids operation. The fundamental operation of the VSC station is explained including an overview of different configurations of the VSC converter and terminal voltage and power control of the VSC station. The detailed control of the VSC station for different AC grid requirements is presented, and is followed by an overview of the modelling techniques of VSC transmission. Finally, the PV characteristics and safe operating limits are discussed along with a capability chart of the VSC station, which shows that operating limits and AC grid strength should be considered in the control implementation of the VSC station for stable operation of the VSC station under all conditions.

CHAPTER 3

Power Balancing in MTDC Grid

3.1 Introduction

Power balancing inside the MTDC grid is an essential requirement for the stable operation of MTDC grids. The stored energy in the MTDC grid is very limited i.e. only in capacitors and cables, as compared to inertia and kinetic energy in the rotating machines in an AC system. Hence, a fast and autonomous controller needs to be implemented as a primary control to achieve the power balancing, while maintaining the DC node voltages within the limits.

The goal of this chapter is to compare different DC voltage control methods for the power balancing in an MTDC grid, and identify the appropriate control method for primary control to achieve this objective. To achieve this goal a comparison analysis of various DC voltage control methods is performed against the specified criteria under three different operating conditions.

The organisation of the chapter is given as: Section 3.2 discusses the structure of the MDTC grid. Section 3.3 and 3.4 describe the principle of the power balancing in the MTDC grid and requirements of primary control respectively. The implementation of different methods are described in Section 3.5, followed by a comparison analysis in Section 3.6.

3.2 Structure of the VSC Based MTDC Grid

3.2.1 Radial MTDC Grid

The radial MTDC grid is suitable for small size networks with limited power transmission requirements, where a single HVDC link can be used to transfer power from small offshore installations or feed offshore Oil & Gas platforms. In a radial MTDC grid, all the VSC stations are connected to the grid through a single HVDC link. The power sharing and controllability in the radial MTDC grid is easier than in a meshed MTDC grid. The major drawback of a radial MTDC grid is that an outage of the HVDC link will result in the interruption of the whole MTDC grid.

3.2.2 Meshed MTDC Grid

The meshed MTDC grid can be used to transfer a large amount of power from large offshore stations and AC networks. It is more reliable than the radial MTDC grid, as it can also provide N-1 security operation. However, with the aforementioned advantages, meshed MTDC grids are still at the development stage, so challenges like power flow control, system protection and fault handling need to be overcome [2]. One particular challenge to the meshed MTDC grid operation is power balancing, which is the focus of this chapter. Appropriate primary control is required to maintain the power balance and hence the DC voltage in the meshed MTDC grid.

3.3 Specifications of the Primary Control

The primary control is required to act automatically, without any external communication, in response to the power imbalance in the MTDC grid. The stored

energy in the MTDC grid is very limited (only in capacitors and cables), as compared to inertia and kinetic energy in the rotating machine in an AC system. Therefore, the power-DC voltage characteristics are more sensitive than the power-frequency characteristics of an AC system. Hence, the response of the controller required in the MTDC grid is faster, which leads to smaller time constants for the primary controls of the MTDC grids of only a few milliseconds. Some of the important requirements given in [59] can be summarised as:

- Precise control under normal operation
- Stable operation under disturbance
- Automatic dynamic power sharing
- Operation within permitted limits
- Rescheduling capability

Fast and direct response is required from the primary control. The DC voltage control methods implemented in the outer control loop of the VSC station are considered for primary control of the MTDC grid, similar to frequency droop control for the AC system as shown in **Figure 3:1**.

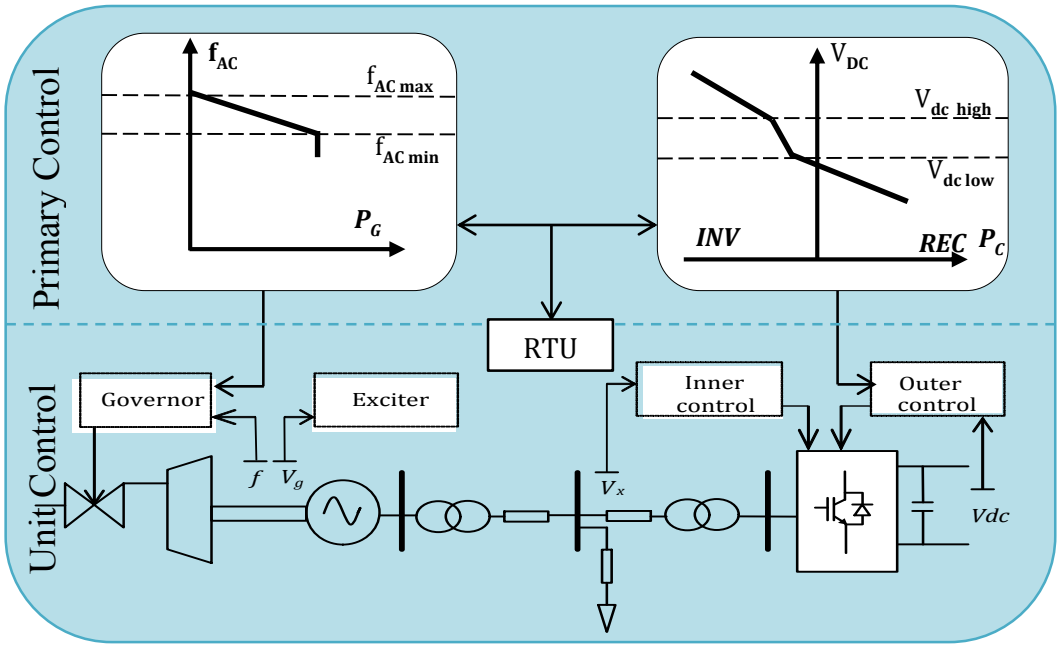

Figure 3:1 *Primary control implementation in the AC/MTDC grid*

3.4 Principle of Power Balancing in the Meshed MTDC Grid

A number of VSC stations are connected together to form the VSC-based MTDC grid system. The voltage of the DC grid is the key indicator for the power balance in the MTDC grid, similar to the frequency for an AC system. If the power into a MTDC grid increases excessively, the DC node voltage can increase beyond the limits and may trigger the protection equipment (damping resistor) [70]. Whereas, if there is shortage of power into the MTDC grid, the DC node voltage may drop to below minimum limits that may lead to unstable operation of the control system and limit the reactive power capability, hence the AC voltage support, of the VSC station [71]. The control of the DC voltage is an essential task for at least one of the VSC stations. The active power flow through all other terminals needs to be balanced to maintain the DC voltage within the operating limits for stable operation of the MTDC grid. The control of the DC node is categorised under two main categories in the literature, centralised voltage control [16], [72], [73] and distributed voltage control [74]–[76].

From the point of the reactive power control, each of the VSC stations in the MTDC grid can operate either in *Q*-control mode to provide constant reactive power or in V_{ac}-control to keep the AC voltage constant at the PCC to support the weak AC system.

3.4.1 Centralised Voltage Control

In centralised voltage control, the DC node voltage is controlled by one VSC station, which acts as the power slack station (known as the master VSC station) in the MTDC grid, while the rest of the VSC stations control the power (regarded as the slave VSC stations). It can provide a control on well-defined operating points for normal operating conditions or small disturbances around the operating point in a large MTDC grid [29]. However, if there is only one slack (DC voltage regulating) VSC station then it may be required to be over-rated, as the maximum rating of the DC node voltage regulating VSC station should be greater than the sum of the power from all of the power/current regulating VSC stations and losses in the MTDC grid [15]. Mathematically, this can be represented as:

$$P_{MAX\ SLACK} \geq \sum_{i=1}^{N-1} P_{DC,i} + \sum_{j=1\ i\neq j}^{M} P_{LOSS,ij} \tag{3.1}$$

where,

$P_{MAX\ SLACK}$ is the maximum active power of the DC voltage regulating N^{th} VSC station;

$P_{DC,i}$ is the active power of i^{th} VSC station operating in the power/current regulating mode;

$P_{LOSS,ij}$ is the line loss of the branch of any two VSC station in the MTDC grid.

From the above constraint, it can be understood that it will be difficult for a single VSC station to regulate the DC node voltage, when the size of the MTDC grid gets larger. Further, it will also not be possible to provide N-1 security for the VSC stations operation in the event of outage of the DC node voltage regulating VSC station. Therefore, for reliable and secure operation of the MTDC grid, a backup mechanism is required to handle large disturbances and N-1 security in the event of an outage in the slack VSC station.

3.4.2 Distributed Voltage Control

Distributed voltage control can be implemented in a MTDC grid by applying linear droop control to the VSC stations required to participate in DC voltage regulation, similar to the implementation of frequency droop control in an AC system. Distributed voltage control can provide a stable operating point during disturbances in a large MTDC grid. Since all the power fluctuations in the MTDC grid are distributed among the several participating VSC stations, no single station is exposed to high stresses and required to be oversized, contrary to centralised voltage control. Further, there is no back-up mechanism necessary to provide N-1 security in distributed voltage control. The power sharing among the DC voltage regulating VSC stations is determined by the relative droop constant values of the VSC stations. The VSC station with the smaller droop constant value will have the higher share of the disturbed power among the particular VSC stations and vice versa.

However, with implementation of simple linear droop control, response of the VSC station varies directly with the amount of disturbance, which may lead to unstable

operation of the MTDC grid. Hence, appropriate primary control is required to control the response of the VSC stations in the stable operating region.

Further, the new operating points following a disturbance under droop control do not track the reference set points and result in deviation from the desired power flow in the MTDC grid. Therefore, establishment of a stable operating point and desired power flow following an outage or disturbance requires an appropriate secondary control for the MTDC grid, which is discussed in the Section 4.2.

3.5 Primary Control Implementation in the MTDC Grid

A number of control methods are proposed in the literature for the DC node voltage control and power balancing of the MTDC grid system. A general overview of the different methods is given in [29]. The control methods that act automatically, without any external communication, in response to normal and disturbed operation are considered for primary control in this study. In order to analyse the performance of these existing and extended DC voltage control methods, a comparison is performed according to the requirements of the primary control discussed in Section 3.3.

The tuning of controllers is performed in accordance with the common approach adopted for power electronics converters i.e. the response time increases towards the outer loop in cascaded control. Following the method described in [77], the Modulus Optimum (MO) technique in applied for tuning of inner loop, as it provides fast response. Whereas, the outer loop is tuned according to the Symmetric Optimum (SO) technique, in order to obtain optimised response. (The tuning parameter calculations are given in Appendix A.2)

3.5.1 DC voltage Margin Control

DC voltage margin control is basically an extension of the centralised master-slave control configuration to handle the N-1 security issue in the centralised control [16][73] [78]. If the master (single DC voltage regulating) VSC station trips out, or it reaches its maximum power limit and starts to operate in power control mode, a slave (power control mode) VSC station with DC voltage margin control in the MTDC grid takes over as master VSC station. This potential master VSC station, that can act as back-up to the master VSC station, has two voltage references $V_{dc\ high}$ and $V_{dc\ low}$ with the difference referred to as "margin". **Figure 3:2** shows the control block diagram and characteristic curve of the voltage margin control method.

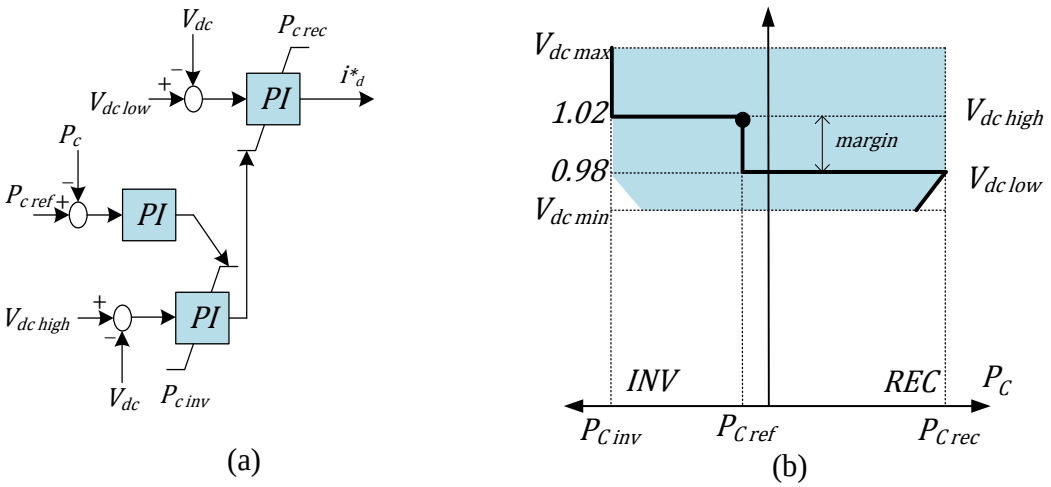

Figure 3:2 *DC voltage margin control:* (a) *control block diagram* (b) *characteristics curve*

The VSC station under voltage margin control operates in power control mode until the MTDC grid is under normal operation with only small disturbances i.e. as long as the DC voltage remains within the margin. However, under large disturbance (voltage deviation beyond the margin) the control can be shifted between the lower DC voltage

level ($V_{dc\ low}$) and higher DC voltage level ($V_{dc\ high}$) depending on the disturbance type in the MTDC grid. In the case of power shortage in the MTDC grid, the control shifts towards the lower level of the potential master VCS station and vice versa.

There can be more than one potential master VSC station in the MTDC grid with DC voltage margin implemented, but their voltage references should be sufficiently different in order to avoid the control hunting between these VSC stations. The priority and power set points of the potential VSC stations can be changed by the value of their voltage level.

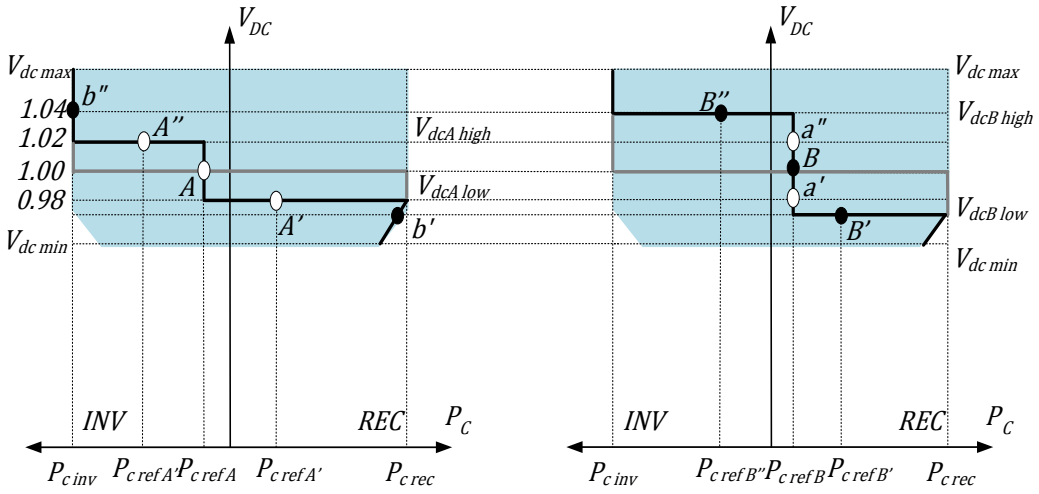

(a) VSC1 (b) VSC2

Figure 3:3 *Operation of two VSC stations in DC voltage margin control*

As an example, VSC-A and VSC-B shown in **Figure 3:3** are two potential master VSC stations. In steady state, the stations operate at operating point A and B respectively. In the event of a large disturbance, VSC-A can switch to a point A'or A'' shown in **Figure 3:3** (a) and let VSC-B operate in power control mode at point a'or a'' respectively shown in **Figure 3:3** (b). Once VSC-A reaches its upper or lower limits, i.e. point b'or b'', VSC-B can switch to the operating point B′or B″.

DC voltage margin control resolves the N-1 security issues in centralised voltage control by providing a backup control strategy. However, it has two major drawback:

(a) It involves complex control of several levels within a limited DC voltage operating range.
(b) Sudden voltage level transition can result in additional stress on the MTDC grid.

3.5.2 DC voltage Droop Control

There are two basic principles of implementing the DC voltage droop control that are most commonly proposed in the literature, current based control and power based control, under the category of distributed DC voltage control for the MTDC grid discussed in Section 3.4.2. The current based droop control uses the I-V characteristic, whereas the power based droop control uses the P-V characteristic to control the DC node voltage as shown in **Figure 3:4**. The current based droop control is regarded as linear because of the linear relationship between the DC node voltage and current in the capacitive MTDC grid, so it is directly linked with the MTDC grid's dynamics [29]. In contrast, the relationship between power and DC node voltage is non-linear, hence power based droop control is regarded as non-linear.

However, power based control is more advantageous where study is focused on power flows rather than stability analysis of the MTDC grid [26]. It also has similarity to the frequency droop control of the AC system, and is easy to implement into vector controlled inner current control of the VSC station [79]. It can represent the direct relationship between the AC side power (P_c) of the VSC station and DC node voltage,

so in this thesis, droop control will be referred to as power based control, since the focus of the study is power flow control in the MTDC system.

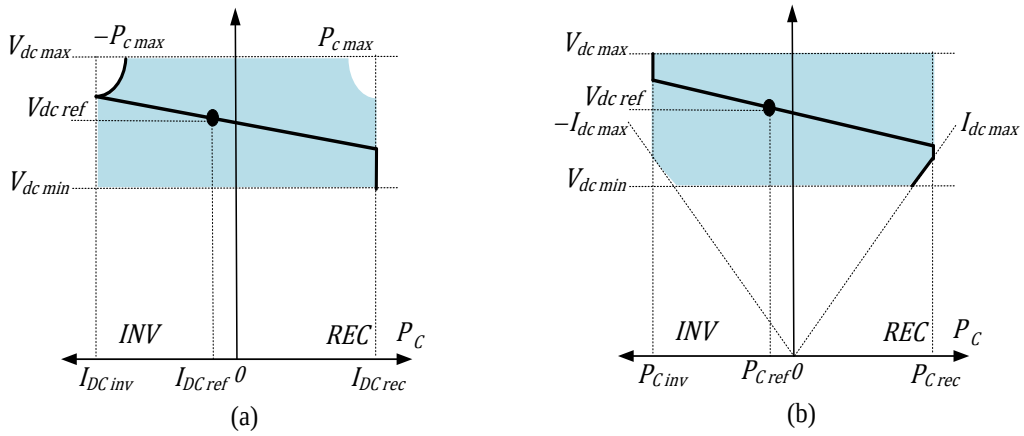

Figure 3:4 *Basic droop characteristic curve* (a) *current based droop curve* (b) *power based droop curve*

Droop control can be simply regarded as proportional control with droop gain (K_{DC}), which is given as:

$$K_{DC} = \frac{\Delta P_c}{\Delta V_{dc}} \tag{3.2}$$

The droop gain (K_{DC}) of the proportional control represents the sensitivity of the change in power (ΔP_c) to the change in the DC voltage (ΔV_{dc}) i.e. the increment or decrement of power exchange (in *MW*) from the MTDC grid in response to the increment or decrement of DC node voltage (per *kV)*. The higher the droop gain (K_{DC}), the more sensitive the controller will be to the change in DC voltage [79]. The characteristic curves of AC frequency droop control and DC voltage droop control can be drawn with the inverse of their respective proportional gain constants [80]. The slope of the DC voltage droop characteristic curve can be defined by the negative

of the droop constant (σ_{DC}), which is equal to the inverse of the droop gain (K_{DC}), given by:

$$\sigma_{DC} = \frac{\Delta V_{dc}}{\Delta P_c} \tag{3.3}$$

Figure 3:5 (a) and (b) shows the control block diagrams of two different ways to implement DC droop control, while (c) is the P-V droop characteristic curve of the DC droop control.

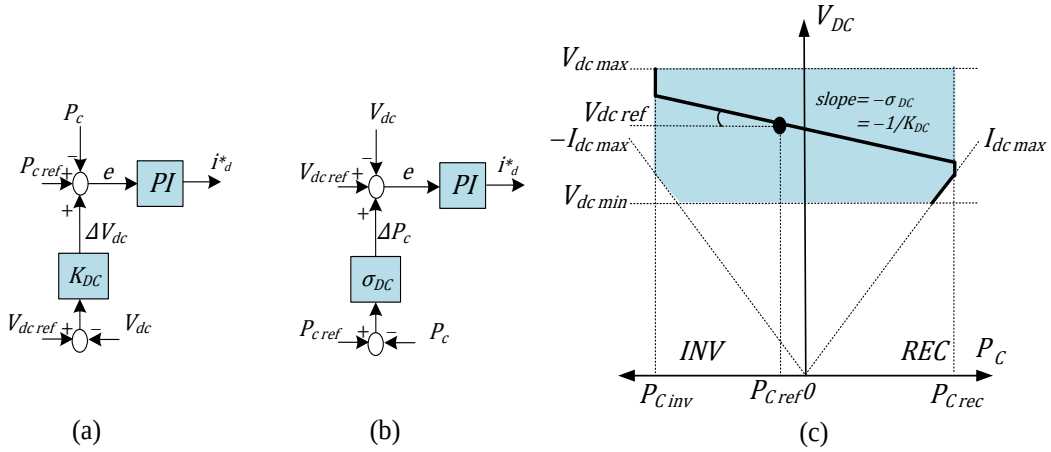

Figure 3:5 *DC voltage droop control* (a) *control block diagram with droop gain* (b) *control block diagram with droop constant* (c) *DC droop characteristics curve*

The steady state behaviour of droop control can be varied from constant power mode all the way to constant voltage mode by varying the droop constant. If droop gain (K_{DC}) is set to be zero in **Figure 3:5** (a), the DC droop control will behave as constant power control and if droop constant (σ_{DC}) is set to zero in **Figure 3:5** (b), it will act as constant voltage control. If steady state error (e) is considered zero with implementation of PI control, then the following equation for DC droop control can be obtained from **Figure 3:5** (a) and (b):

$$P_{c\,ref} - P_c + K_{DC}\left(V_{dc\,ref} - V_{dc}\right) = 0 \tag{3.4}$$

Similarly, an equation of droop can be obtained by using droop constant value, given as:

$$P_{c\,ref} - P_c + \frac{1}{\sigma_{DC}}\left(V_{dc\,ref} - V_{dc}\right) = 0 \tag{3.5}$$

The stability of the droop control depends on the droop constant (σ_{DC}) and hence the droop gain (K_{DC}). As discussed in Section 3.4.2 with regards to distributed control, due to the difference in the DC voltage across the MTDC grid, the desired power flows cannot be obtained with a unique DC voltage reference as in the case of AC grid frequency. In order to obtain the desired power flows under steady state operation, different voltage set points are required for every VSC station participating in droop control.

3.5.3 Autonomous Control

Autonomous control is an extension of voltage margin control by including a droop into the margin area of the voltage margin control. It allows all VSC stations to adjust the DC node voltage following the droop characteristic, within upper and lower voltage limits [25]. The operation point of all the VSC stations is decided by the natural power balance in the MTDC grid, similar to an AC system where load flow changes to balance the generation and demand without any control of energy flow in the network. The P-V droop characteristic curve of the autonomous control is shown in **Figure 3:6**.

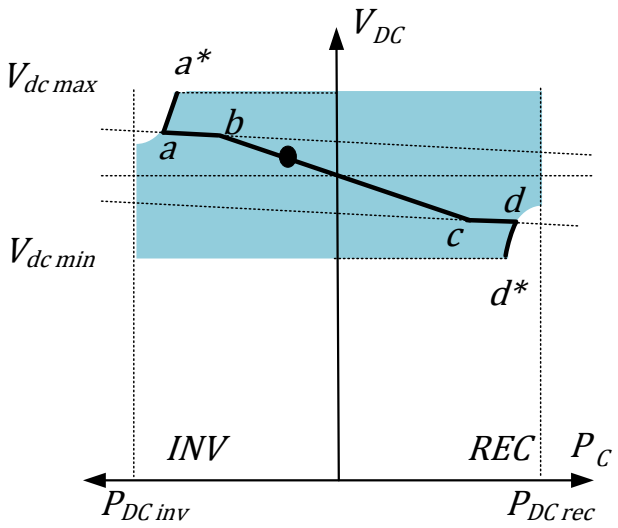

Figure 3:6 *Autonomous droop characteristics curve*

3.5.4 Dead-band Droop Control

Dead-band droop control is an extension of DC droop control, and aims to eliminate the steady state deviation from the reference set points, due to the lack of the PI (Proportional Integral) control in the DC droop control [27]. It is actually a combination of the voltage margin concept with DC droop control, so that all the VSC stations do not regulate the DC node voltage all the time, but instead operate in power control mode to maintain the desired power in normal conditions or with small disturbances i.e. while the DC node voltage remains within a certain margin. **Figure 3:7** shows the block diagram of DC voltage dead-band droop control along with the droop characteristics curve.

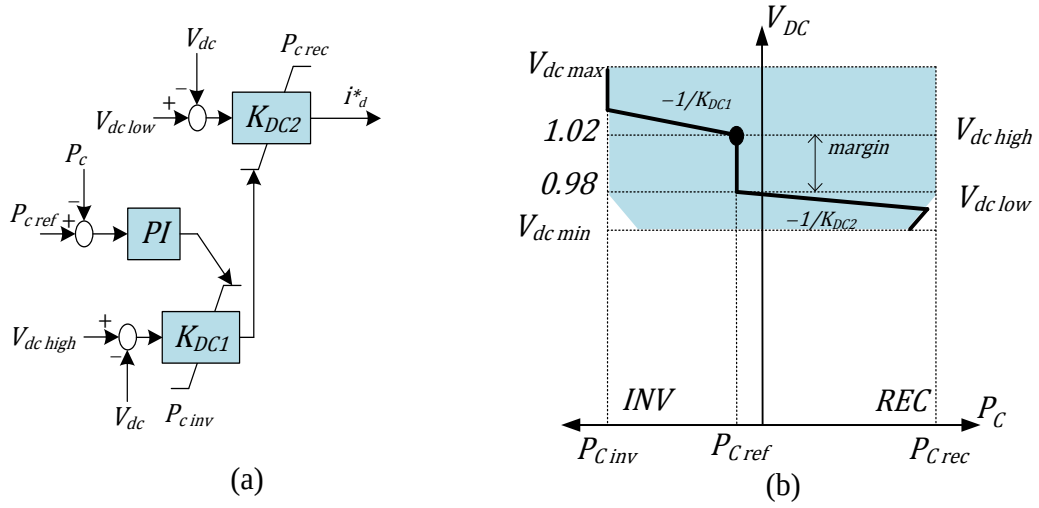

Figure 3:7 *DC voltage dead-band droop control* (a) *control block diagram with DC voltage dead-band droop gain* (b) *DC voltage dead-band droop characteristics curve*

A similar approach can be applied to keep the voltage constant within a power margin. This is called power dead-band droop, where power is not controlled according to reference values within the defined margin or band. **Figure 3:8** shows the block diagram of power dead-band droop control along with its droop characteristics curve.

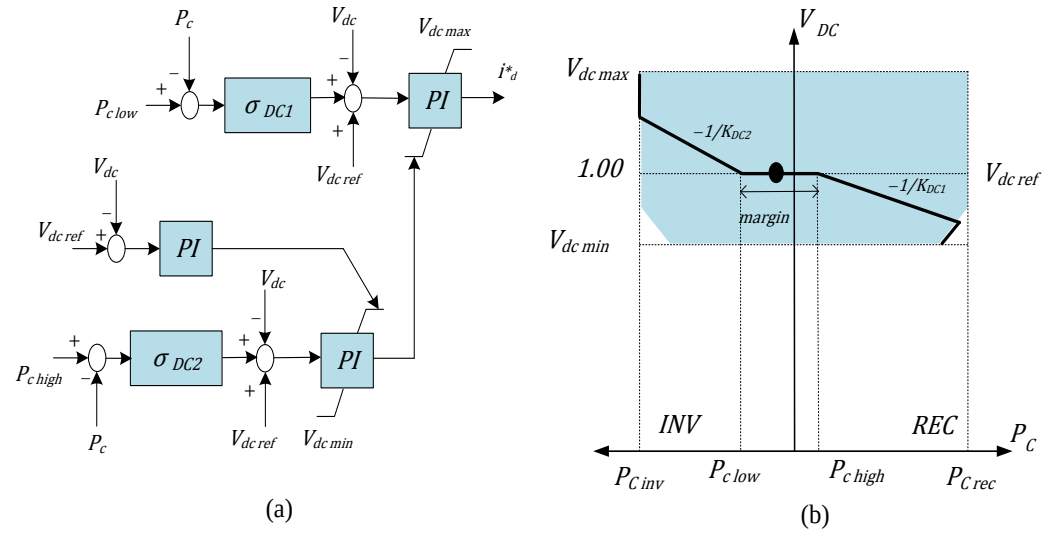

Figure 3:8 *Power dead-band droop* (a) *control block diagram with power dead-band droop gain* (b) *Power dead-band droop characteristics curve*

3.5.5 Active-band Droop Control

Active band droop control is a further extension of DC droop control, suggested in the literature [28] [81]. It is a droop-based control with two different droop constants for normal and disturbed operating conditions in the MTDC grid. Here, the overall control of the MTDC grid can be optimised for normal and disturbance conditions separately by optimising two droop constants. **Figure 3:9** shows the block diagram of active-band droop control along with the droop characteristics curve.

Active-band droop control can be regarded as the generalised control method, as all different controls such as: master-slave, voltage margin, droop and dead-band droop, can be implemented by setting specific droop parameters for the normal and disturbed region of the active band droop control [81]. Power dead-band droop can be obtained by setting infinite droop constant (power control mode) in the normal operation region. Similarly, voltage dead-band can obtained by setting a zero droop constant (voltage control mode) in the normal operating region. The voltage margin can be obtained with an infinite droop constant (power control mode) in the normal operating region and a zero droop constant (voltage control mode) in the disturbance operating region. Regular droop can be obtained with the same droop constant in both (normal and disturbed) operating regions. Further, control is possible with droop control in the normal operating region and zero droop constant in the disturbance operating region.

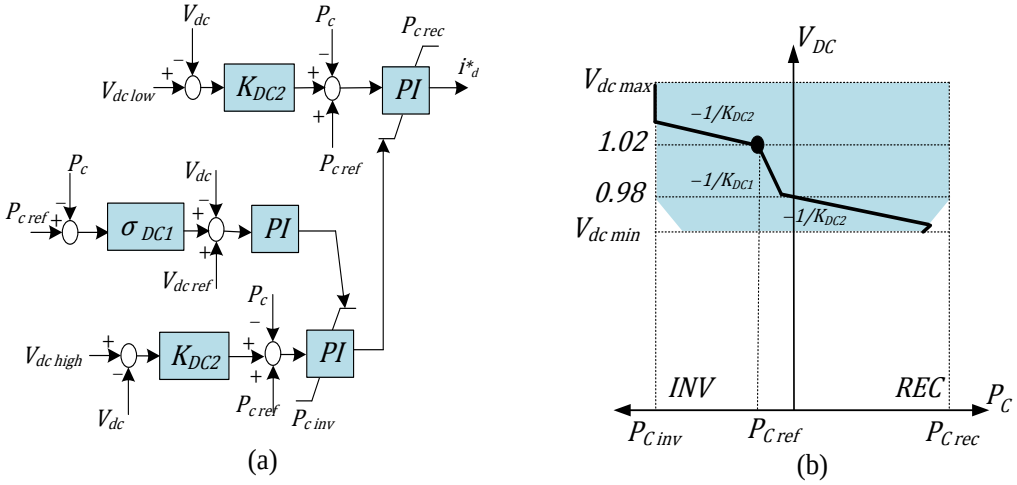

Figure 3:9 *Active-band droop* (a) *control block diagram with droop gain* (b) *Active-band droop characteristics curve*

3.5.6 Tri-band Droop Configuration

In the case of active-band droop control, response to disturbances is the same because of the same droop constants for the lower and upper bands. However, power imbalances in the MTDC grid can be further distinguished as imbalance of the power due to the excessive power, i.e. uncontrolled power from the OWF, and shortage of power due to outages of a major component. Active-band control can be extended to have two different droop constants in the upper and lower band in addition to normal band droop in order to add more flexibility for control of two different disturbances at the primary control level. This allows the operator to change the response for two different disturbances through the secondary control. The implementation of the Tri-band droop control configuration is exactly the same as the Active-band droop, except the difference in the values of the droop constant for the upper and lower bands as shown in **Figure 3:10**.

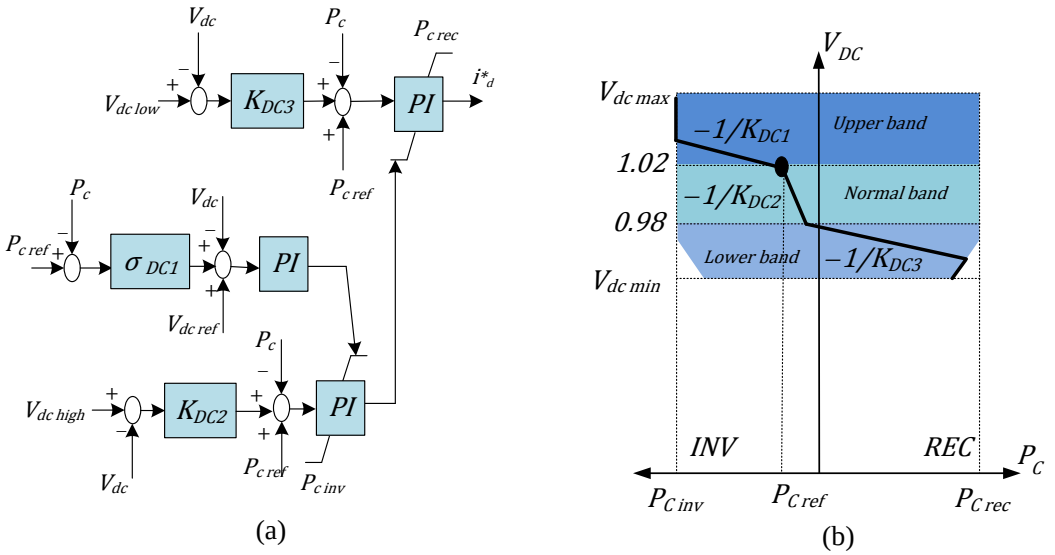

Figure 3:10 *Tri-band droop* (a) *control block diagram with droop gain* (b) *Tri-band droop characteristics curve*

3.6 Comparison of the Primary Control Methods

A five-terminal MTDC grid is simulated as an example to demonstrate transmission of 1GW power among four AC grids connected to VSC1, VSC3, VSC4, VSC5 and an offshore windfarm (OWF) connected to VSC2, to compare the performance of the discussed six control configurations. The AC grids and OWF are modelled as a three-phase AC voltage sources, with zero impedance (i.e. acting as infinite bus). **Figure 3:11** shows the layout of the five-terminal grid and **Table 3-1** shows the rated parameters of the MTDC grid. The initial transient from the control actions are regarded as clear. The system is setup to perform a comparison of the afore-mentioned control methods under three different conditions i.e. normal, small disturbance and large disturbance. In the AC system a small disturbance is defined as incremental changes in the system load, while a system fault, a loss of generation or circuit contingencies are regarded as a large disturbance [82]. In contrast, in the MTDC grid, the uncontrolled generation from the OWF can be considered as a disturbance, along

with incremental load changes and outages, which can be categorised as small or large according to the amount of change in the power generation. Therefore, in this study three disturbance conditions are simulated using the power variation and outage of the offshore windfarm. The power variation from the OWF is given in **Table 3-2**. In the initial steady state condition, the OWF produces 200MW power, and then power is ramped up to 300MW to simulate a small disturbance, followed by an outage as a large disturbance in the MTDC grid. The AC Grid 2 is assumed to export 600MW to the remaining three AC grids connected to the MTDC grid during all the operating conditions.

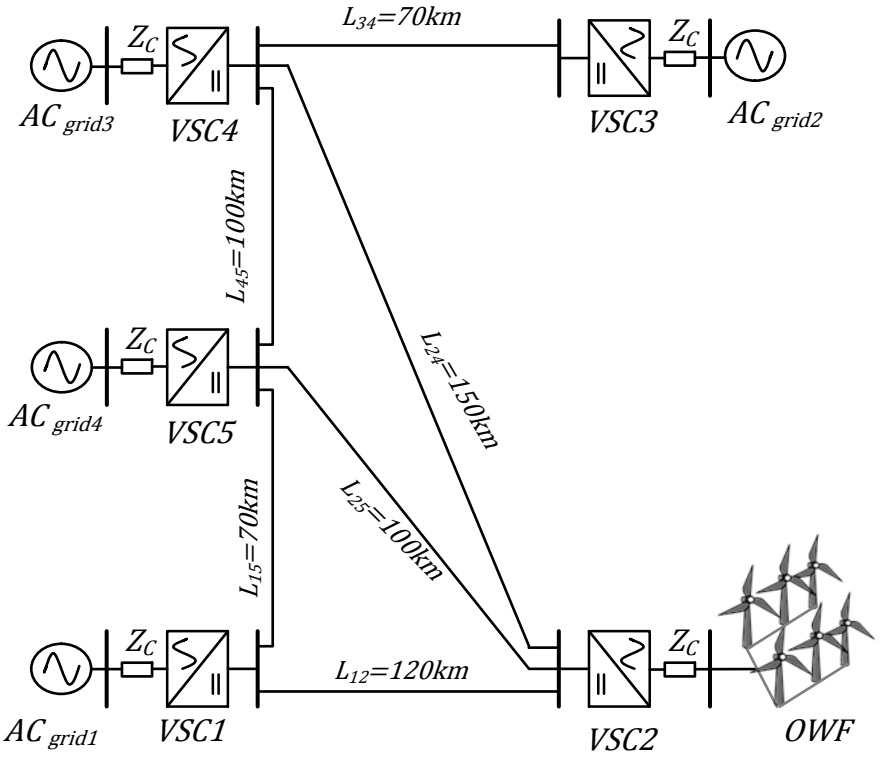

Figure 3:11 *Layout of the five-terminal MTDC grid*

The AC grid is simulated as an ideal voltage source behind a source impedance, while the MTDC grid is simulated in per unit (pu) quantities using 400kV DC base voltage and 1000MVA base power and other rated parameters given in **Table 3-1**. The lengths

of the DC grid cables are taken as: l_{12}=120km, l_{15}=70km, l_{25}=100km, l_{24}=150km, l_{34}=70km and l_{45}=100km (refer Appendix A.1 for details on parameter calculations).

Table 3-1 *Parameters of the MTDC grid used for control performance comparison*

MTDC grid parameters	**ratings**	**AC grid parameters**	**ratings**
VSC Power (S_{VSC})	1000MVA	AC grid power (S_G)	4000MVA
DC node voltage (V_{dc})	400kV	AC grid voltage PCC (V_s)	220kV
OWF Power (P_{owf})	500MW	Filter bus voltage (V_Z)	180kV
Cable resistance (r_{dc})	0.02 Ω/km	Ph: reactor+Tran: Imp (Z_C)	0.008+j0.25pu

In terms of control, the VSC2 (OWF) and VSC3 operate as sources (rectifiers) in power control mode; the remaining three VSC stations (VSC1, VSC4 and VSC5) are implemented with different control configurations to perform the comparison. VSC4 and VSC5 are specified to operate as loads (inverters), whereas VSC1 can act as either a source (rectifier) or load (inverter) according to the specified control configuration. The converter power vs DC node voltage (PV) characteristics curve for each VSC station of the MTDC grid are provided for six different control configurations in order to indicate the operating point of each VSC station in three different operating conditions. The output variation from the OWF is given **Table 3-2**. Point (OP_0) refers to the initial steady state operating condition measured at 1.5s, while (OP_1) and (OP_2) refers to the operation under small disturbance and large disturbance measured at 2.9s and 3.5s respectively.

Table 3-2 *OWF power output variation for three operating conditions*

Steady state operating points	Initial steady state (OP_0)	Small disturbance (OP_1)	Large disturbance (OP_2)	Max: output (400 MW)
Time(s)	1.5-2	2-3	3-4	4-5
OWF Power (P_{owf})	0.2 pu	0.2-0.4pu ramp	Outage	0.4pu

The response of the VSC2 (OWF) and VSC3 (source) is almost the same for all control configurations, as they are assumed to operate in power control mode; i.e. the power (P_c) controlled at reference value ($P_{c\ ref}$) and the DC node voltage (V_{dc}) change according to the DC voltage at different VSC stations in the MTDC grid. **Figure 3:12** (a-top) shows the PV characteristics curve of the VSC2 (OWF) operating as a rectifier in the power control mode with initial steady state operating point (OP_0) and small disturbance operating point (OP_1) at the end of a power ramp, while the outage is shown with characteristics line at large disturbance operating point (OP_2). The dashed lines show the safe operating region, as discussed in Section 2.2. The power (P_c) and DC node voltage (V_{dc}) of the VSC station are shown in **Figure 3:12** (a-middle & bottom). Since, the DC side capacitors modelled for the MTDC grid are not initially charged, so the MTDC gird is energised after one second. The initial transients can be observed for up to half a second after which system stabilise.

The PV characteristics curve for VSC3 is shown in **Figure 3:12**(b-top): its constant power mode operation with respective power (P_c) and DC node voltage (V_{dc}) is shown in **Figure 3:12**(b-middle & bottom). The following Section discusses in detail the response of the remaining three VSC stations under different control methods.

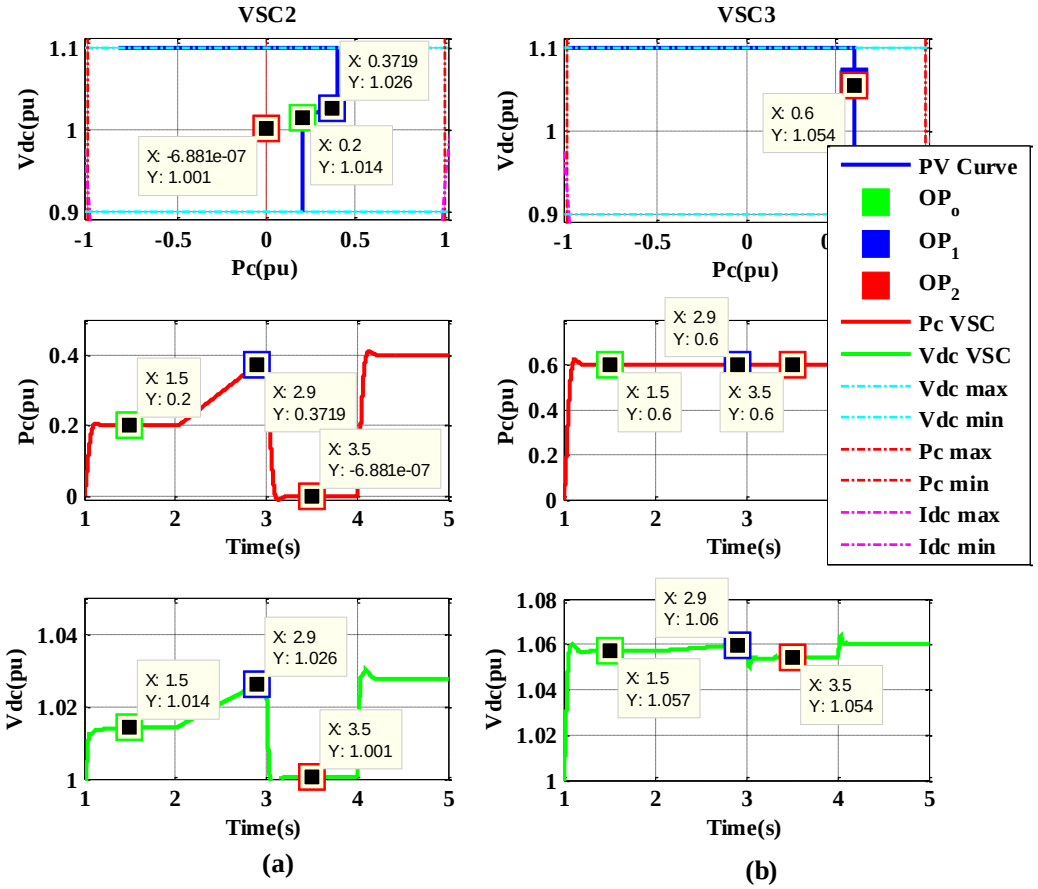

Figure 3:12 *PV characteristics curve of VSC2 & VSC3* (a) *VSC2 response in power control mode* (b) *VSC3 response in power control mode*

3.6.1 DC Voltage Margin Control Response

As discussed in Section 3.5.1, voltage margin control is one of the basic control configurations that can operate a VSC station in two different modes according to the different operating states of the MTDC grid. The converter power and DC voltage response of the VSC1 is shown in the **Figure 3:13**(middle & bottom respectively). The PV characteristics curve of the voltage margin is shown in **Figure 3:13**(top). It

can be seen clearly that VSC1 controls the DC node voltage (V_{dc}) at two different levels, i.e. 0.99-1.02pu, according to the pre-defined DC voltage margin of 0.03pu.

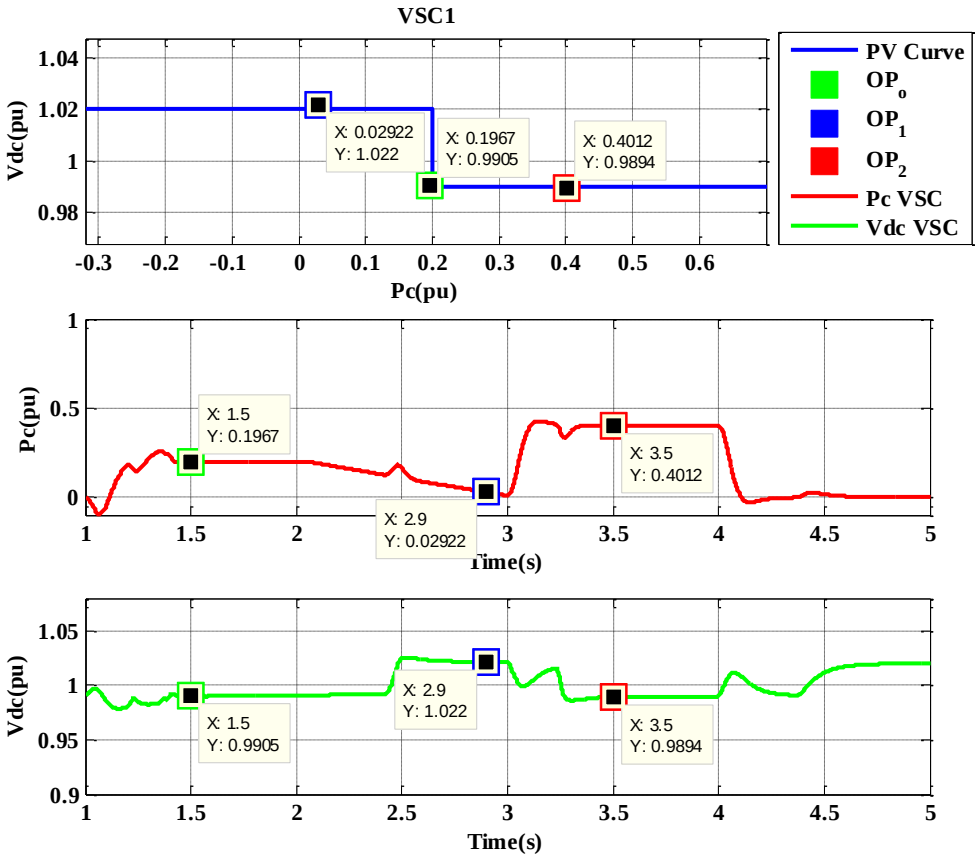

Figure 3:13 *PV characteristic curve and VSC1 response under DC voltage margin control*

In initial steady state operation (OP_0), the VSC1 controls the (V_{dc}) at the lower level 0.99pu until a small disturbance occurs due to the ramping power of the OWF from t=2-3s that exceeds the DC node voltage (V_{dc}) from the DC voltage margin. The VSC1 shifts the DC node voltage control to the upper level 1.02pu of the voltage margin, so the steady state operating point under small disturbance (OP_1) jumps to the upper level. Whereas, in the event of a large disturbance i.e. outage of OWF from t= 3-4s, power in the MTDC grid is reduced. Hence, the VSC1 under voltage margin control reacts to shift the DC voltage control back to the lower level of the margin and increase

power into the MTDC grid. The kink appears in the output power of VSC1 at t=2.3s in **Figure 3:13**(middle) and oscillations in the DC voltage output waveform in **Figure 3:13**(bottom) and **Figure 3:14**(bottom) are due to the sudden shift of the DC voltage level and relatively slow response of the voltage margin control. The steady state operating point (OP_2) can be seen at the lower level.

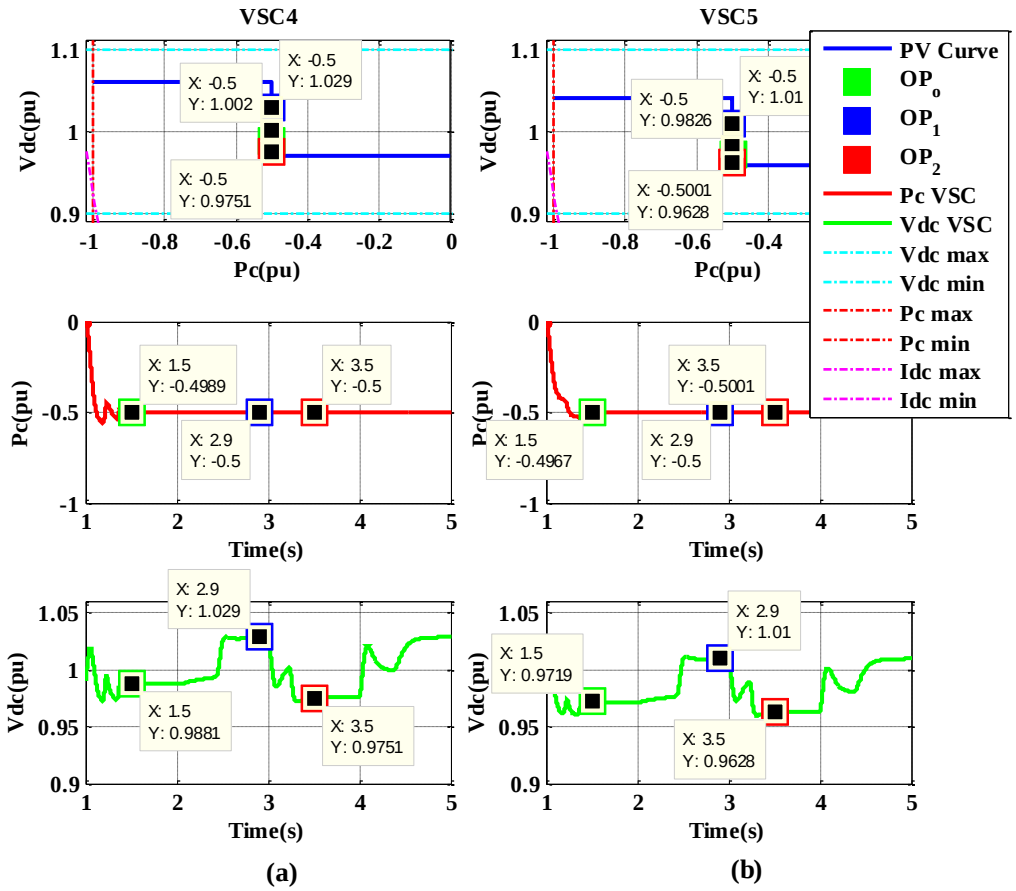

Figure 3:14 *PV characteristics curve of VSC4 & VSC5* (a) *VSC4 response under DC voltage margin control* (b) *VSC5 response under DC voltage margin control*

VSC4 and VSC5 are specified with a DC voltage margin of 0.07 and 0.10pu respectively; hence the margin is not exceeded under all three different operations, so VCS4 and VSC5 operate in power control mode. The **Figure 3:14**(a & b-top) shows the PV characteristics curve for VSC4 and VSC5 respectively. The power and voltage response is shown in **Figure 3:14**(a, b-middle & bottom).

Acting as a primary control, DC voltage margin control responds automatically to small and large disturbances in the MTDC grid along with precise operating points and power sharing. However, the voltage margin needs to be kept sufficiently high to avoid hunting between the converters and a sudden shift in the voltage levels adds to high overshoot and stresses the other converters. Generally, the response of the voltage margin control is not very fast.

3.6.2 DC Voltage Droop Control Response

DC voltage droop control is also a basic control technique that responds proportionally to changes in the DC node voltage (V_{dc}) and converter power (P_c) according to the droop value. DC voltage droop control is implemented at VSC1, VSC3 and VSC5 with the same droop constant (σ_{DC}), i.e. 0.05 at each VSC station. Hence, the converter power (P_c) and DC voltage (V_{dc}) response of the three VSC stations is similar. When the OWF starts to ramp up the power into the MTDC grid at t=2.0s, and the DC node voltage increases, the VSC1 starts to decrease the power input proportionally as it operates as a source, as shown in the **Figure 3:15** (middle & bottom respectively). Whereas, VSC4 and VSC5 increase the power output because they act as load. The converter power (P_c) and DC voltage (V_{dc}) response of both the converters is shown in **Figure 3:16**(a & b middle & bottom respectively). The PV characteristics curves of VSC1, VSC4 and VSC5 under DC voltage droop are shown in **Figure 3:15**(top) and **Figure 3:16**(a & b-top) respectively. The steady state operating points (OP_0), (OP_1) and (OP_2) of the three VSC stations can be seen to follow the respective droop characteristic curves identically.

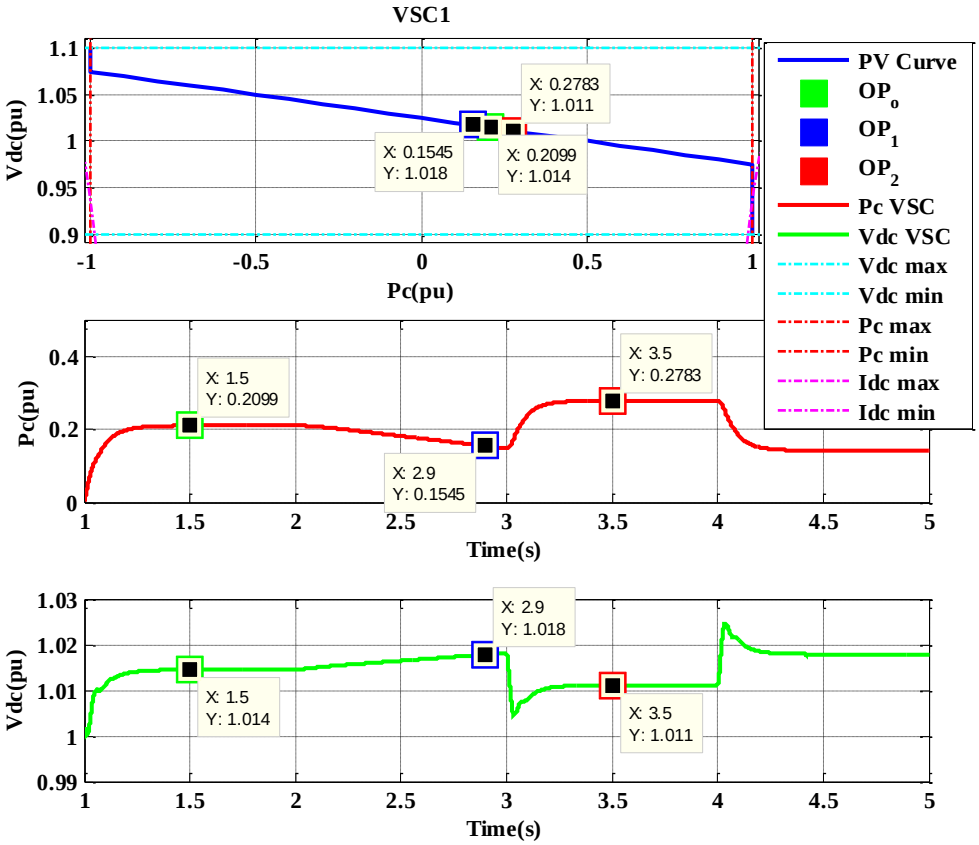

Figure 3:15 *PV characteristic curve and VSC1 response under DC voltage droop control*

Droop control provides stable operation under normal conditions and responds well to disturbances in the MTDC grid. However, it reacts according to the same droop characteristics curve in the event of small or large disturbances without differentiating between a small and large disturbance, resulting in steady state deviation from the references.

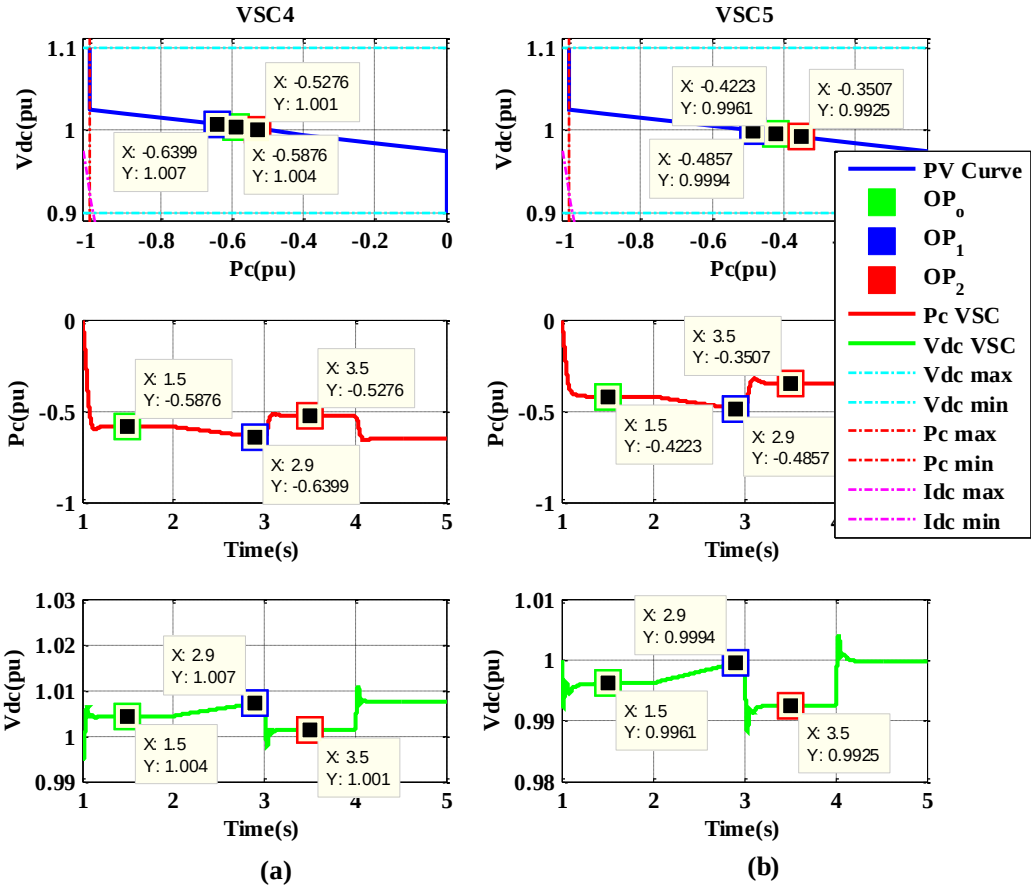

Figure 3:16 *PV characteristics curve of VSC4 & VSC5* (a) *VSC4 response under DC voltage droop control* (b) *VSC5 response under DC voltage droop control*

3.6.3 Autonomous Control Response

Autonomous control is advanced implementation of DC voltage droop control, where droop is implemented in the margin area, with droop characteristics determined by the variation of the upper and lower voltage limits rather than any specified droop constant. The starting point for the DC voltage upper limit (b) of the VSC1 is set to be 1.05pu and the starting point of the DC voltage lower limit (c) is set to be at 0.98pu of the DC voltage, while for both VSC4 and VSC5, (b) is set to be 1.025pu and (c) to be at 0.98pu.

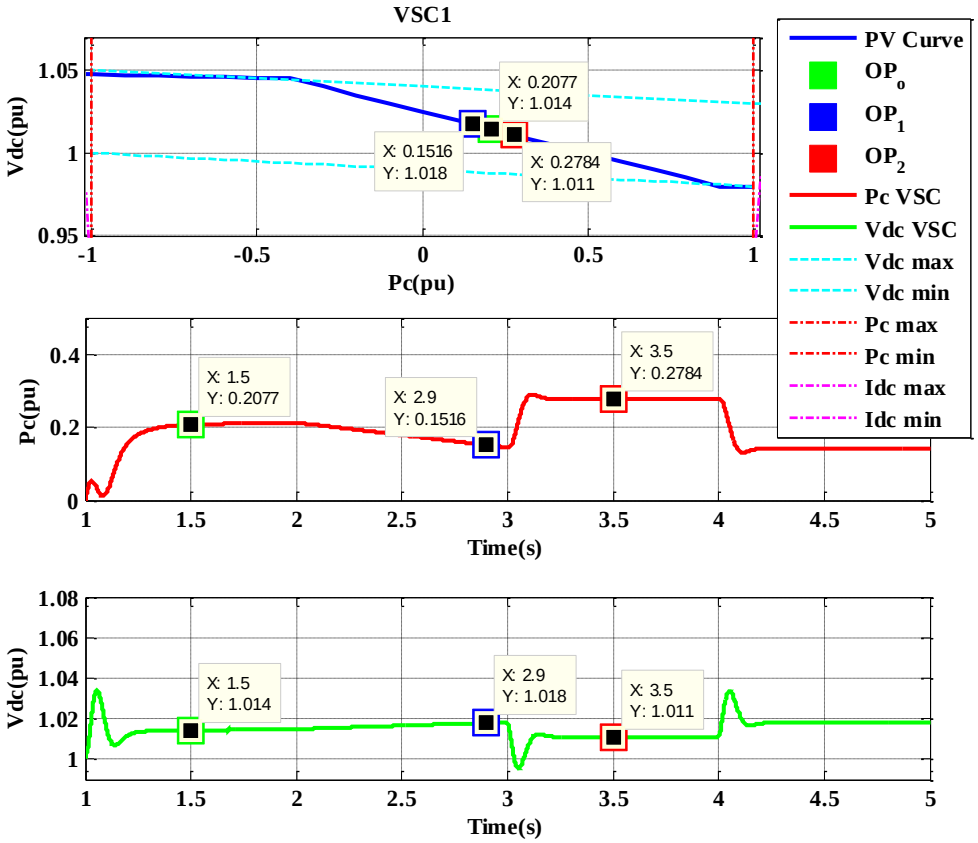

Figure 3:17 *PV characteristic curve and VSC1 response under Autonomous control*

With the given set of upper and lower limits, the converter power (P_c) and DC voltage (V_{dc}) response of the three VSC stations is identical to the response with DC voltage droop control. The PV characteristics curve of VSC1, VSC4 and VSC5 under DC voltage droop are shown in **Figure 3:17**(top) and **Figure 3:18**(a & b-top) respectively. The DC node voltage increases once the OWF starts to ramp up the power into the MTDC grid at t=2.0s, and the VSC1 starts to decrease the power input according to the (bc) droop characteristic, as shown in the **Figure 3:17**(middle & bottom respectively). VSC4 and VSC5 increase the power output following their respective (bc) droops, shown in **Figure 3:18**(a & b-middle & bottom respectively). Acting as a primary control, behaviour of autonomous control is similar to dc voltage droop control. However, unlike droop control each of the VSC station receives the Load

Reference Set Point (LRSP) from the secondary control. The characteristics (bc) can be moved up and down on DC voltage axis to ensure the safe operation of the VSC station at all times. The steady state operating points OP_0, OP_1 and OP_2 of the three VSC stations can be seen to follow the respective droop characteristic curves identically.

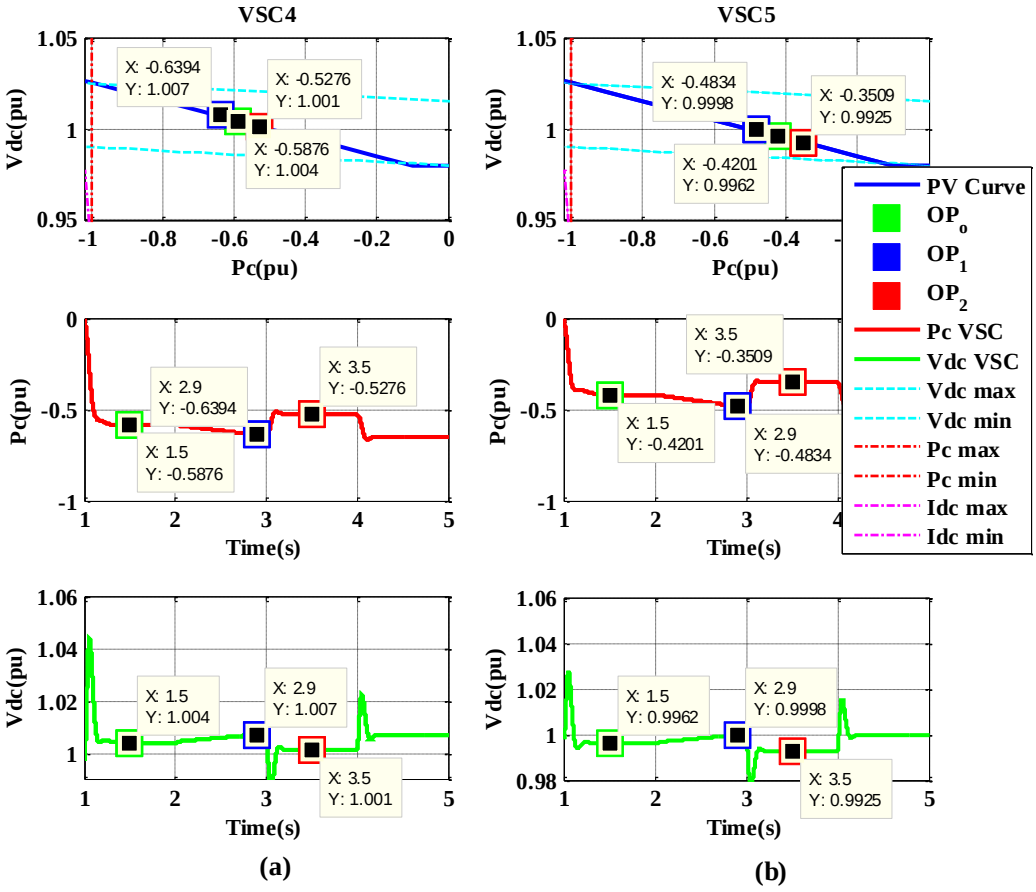

Figure 3:18 *PV characteristics curve of VSC4 & VSC5* (a) *VSC4 response under autonomous control* (b) *VSC5 response under autonomous control*

3.6.4 Dead-band Droop Control Response

Dead-band droop control is implemented with two different configurations; DC voltage dead-band droop and power dead-band droop. VSC1 is implemented with

power dead-band droop control, with DC voltage being controlled at 1.015pu and power dead-band or margin between 0-0.2 pu, as shown in **Figure 3:19**(top).

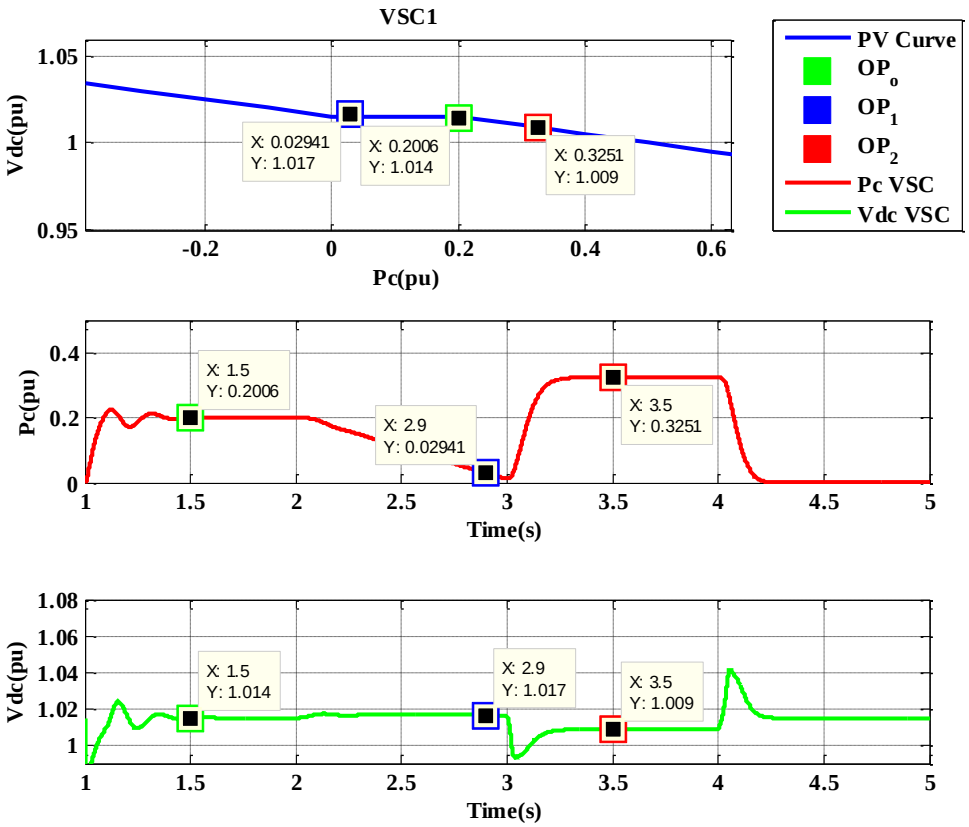

Figure 3:19 *PV characteristic curve and VSC1 response under power dead-band droop control*

The converter power (P_c) and DC voltage (V_{dc}) response of VSC1 in **Figure 3:19** (middle & bottom) show a proportional decrease in (P_c) with constant (V_{dc}) unlike other droop controls discussed earlier. The VSC4 and VSC5 are implemented with DC voltage dead-band droop. In the voltage dead-band case of VSC4, power is controlled at -0.5pu within the voltage dead-band or margin of 1-1.025pu, as shown in the PV characteristics curve **Figure 3:20**(a-top). While in the case of VSC5, the voltage dead-band droop or margin is set between 0.99-1.01pu with power to be

controlled at -0.5pu as shown in the PV characteristics curve **Figure 3:20**(b-top). The upper and lower voltage limits are added with a droop characteristics curve of 0.05 droop constant (σ_{DC}). The converter power (P_c) and DC voltage (V_{dc}) response of VSC4 and VSC5 are shown in **Figure 3:20**(a & b-middle & bottom respectively) and indicate that both VSC stations control power until the DC node voltage is within the defined band or margin.

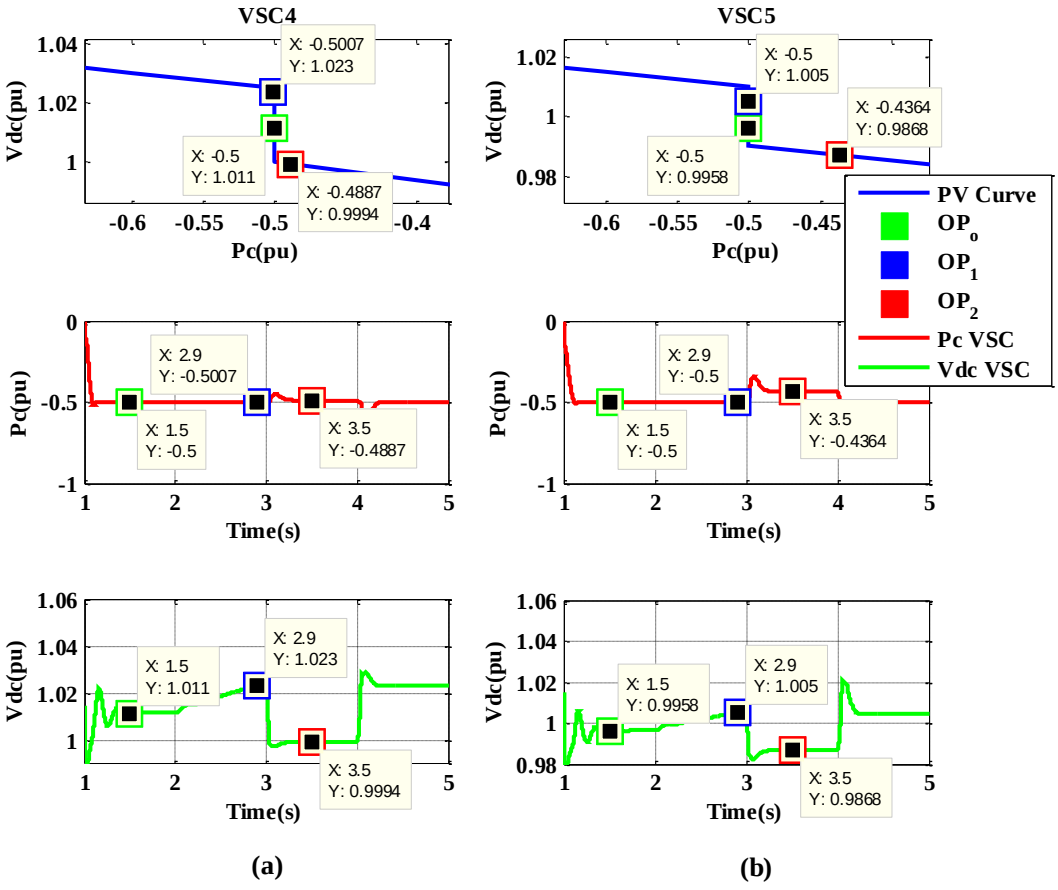

Figure 3:20 *PV characteristics curve of VSC4 & VSC5* (a) *VSC4 response under DC voltage dead-band droop control* (b) *VSC5 response under DC voltage dead-band droop control*

It can be observed that dead-band droop control acts to operate within the respective dead-band region (power dead-band or DC voltage dead band) during the initial steady state operation OP_0 and with small disturbance OP_1. In the event of a large disturbance

OP_2 shifts to follow the droop characteristics curve to share the power imbalance with other VSC stations. As a primary control, dead-band droop control can provide a well-defined operating point and stable operation against small and large disturbances. It enables the VSC stations to sustain the small disturbances without affecting the operation of other VSC stations in the MTDC grid. It also provides power oscillation damping for the VSC station.

3.6.5 Active-band Droop Control Response

Active-band droop control, being the extension of dead-band droop control, provides an additional droop (inner droop) in the voltage margin area. It makes the dead-band an active-band along with droop (outer droop) in the upper and lower voltage limits.

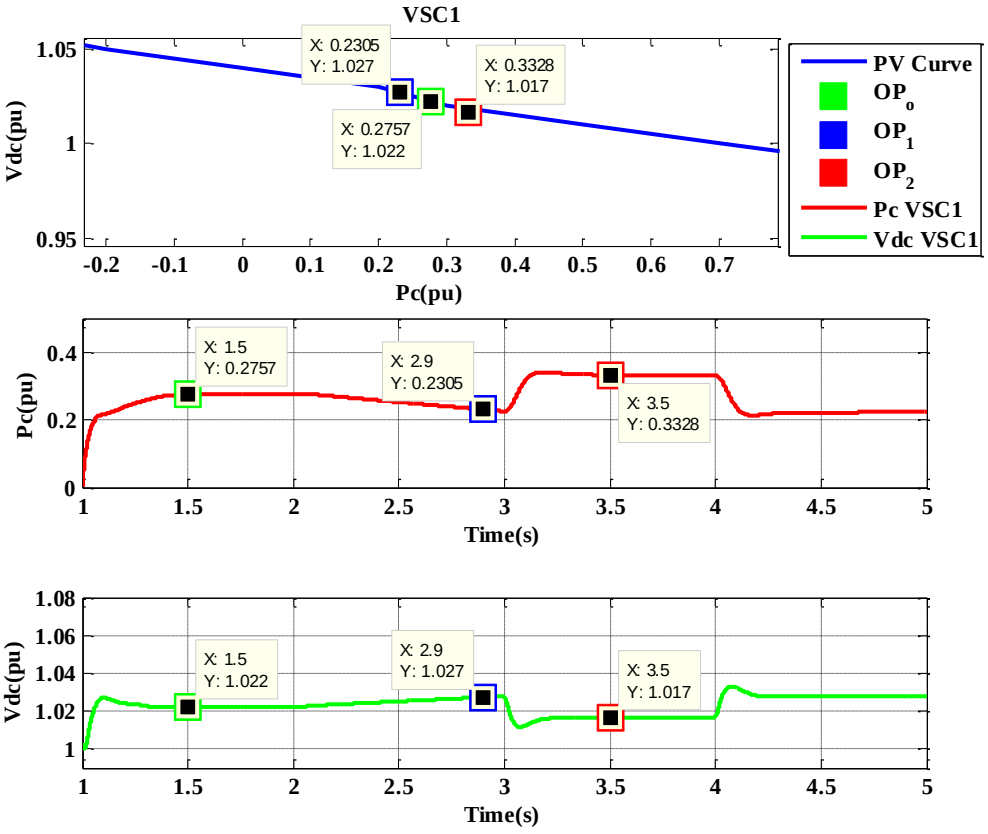

Figure 3:21 *PV characteristic curve and VSC1 response under active-band droop control*

Active-band droop control is implemented here by setting droop in the margin area (σ_{DC1}) as 0.1 and upper and lower limit droop (σ_{DC2}) as 0.05 in all three VSC stations under study. The PV characteristics curve of VSC1, VSC4 and VSC5 under active-band droop are shown in **Figure 3:21**(top) and **Figure 3:22**(a & b-top) respectively.

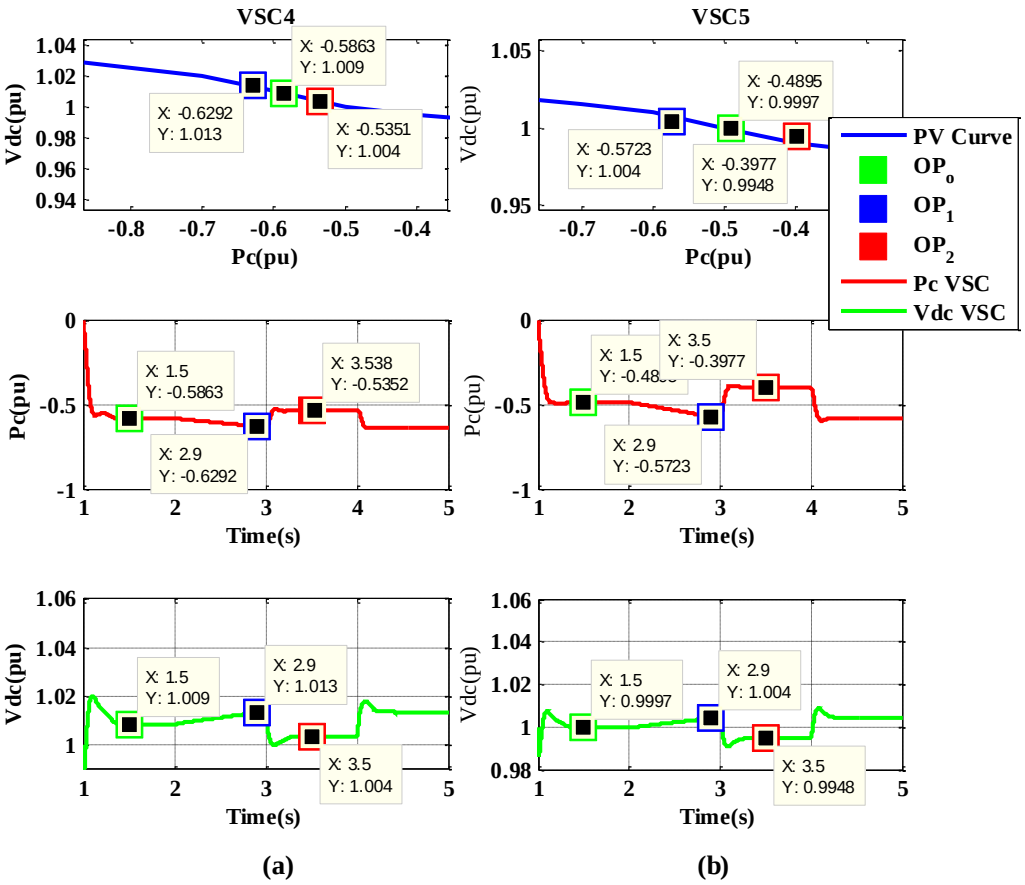

Figure 3:22 *PV characteristics curve of VSC4 & VSC5* (a) *VSC4 response under active-band droop control* (b) *VSC5 response under active-band droop control*

It can be observed that all three VSC stations operate within their respective inner droops during initial steady state operation (OP_0) and with small disturbance (OP_1). However, in the event of a large disturbance (OP_2), their operation shifts to follow the outer droop characteristics curve to share the power imbalance with other VSC stations. The converter power (P_c) and DC voltage (V_{dc}) responses of VSC4 and VSC5

during the three operating states are shown in **Figure 3:22**(a & b-middle & bottom respectively). Active-band droop control provides a well-defined operating point and stable operation against small and large disturbances, as a primary control. It enables the VSC stations to choose the two different optimised droops under normal operation and disturbance band operation in the MTDC grid.

3.6.6 Tri-band Droop Control Response

Tri-band droop control, being a further extension of active-band droop control, decouples the outer droop into two different droops (upper band and lower band) in the upper and lower voltage limits region. It enables a separate response towards excessive power imbalance and reduced power imbalance in the MTDC grid.

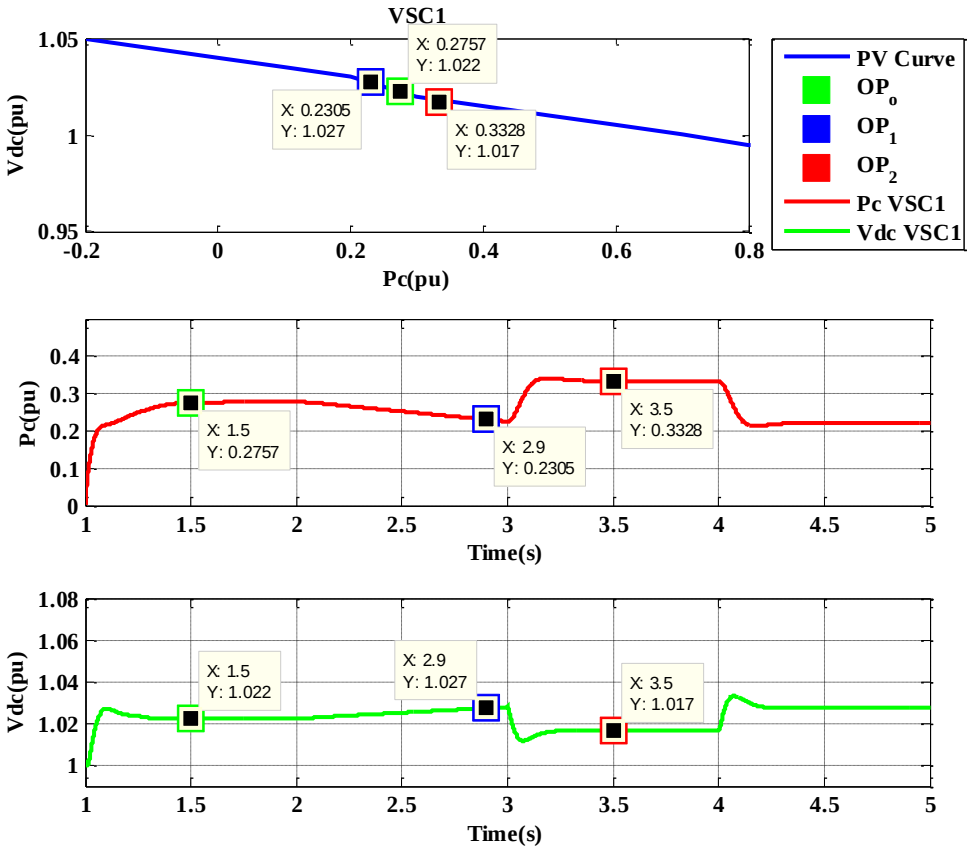

Figure 3:23 *PV characteristic curve and VSC1 response under tri-band droop control*

Tri-band droop control is implemented here by setting the droop in the margin area (σ_{DC1}) as 0.1, the upper band droop (σ_{DC3}) as 0.05 and the lower band droop (σ_{DC3}) as 0.0666 in all three VSC stations under study. The PV characteristics curve of VSC1, VSC4 and VSC5 under active-band droop are shown in **Figure 3:23** (top) and **Figure 3:24**(a & b-top) respectively.

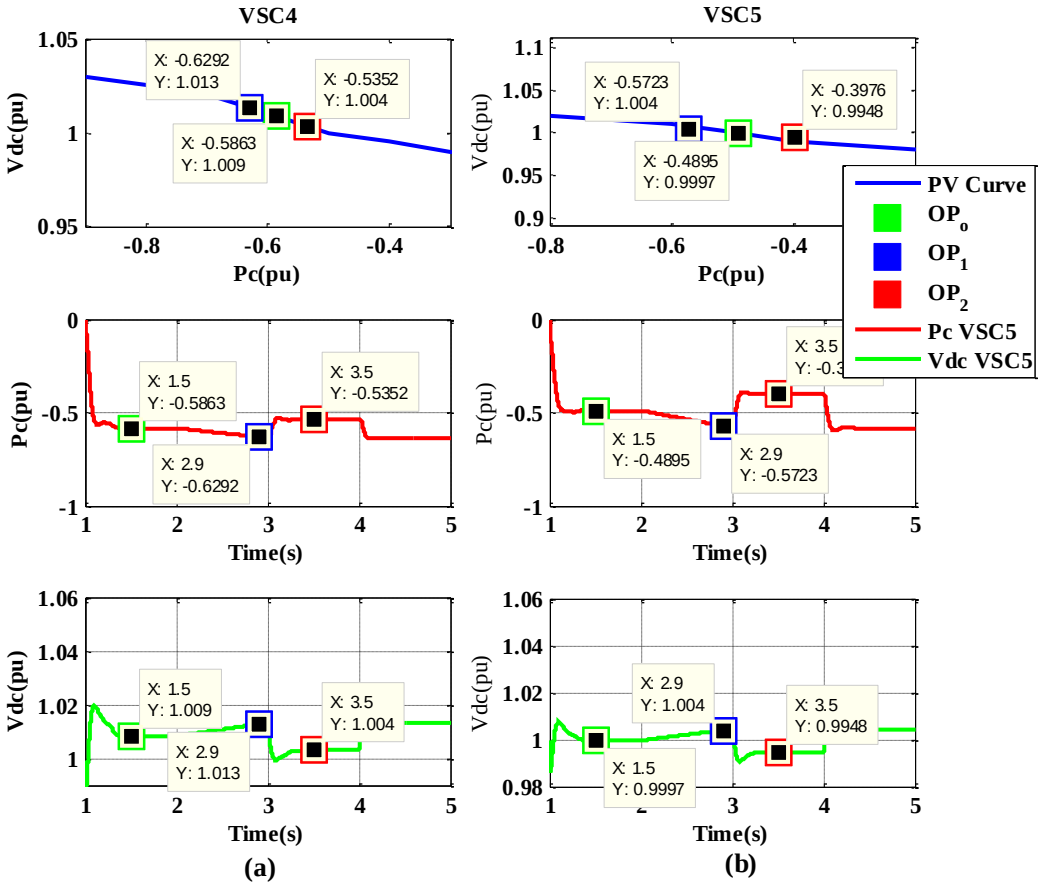

Figure 3:24 *PV characteristics curve of VSC4 & VSC5* (a) *VSC4 response under tri-band droop control* (b) *VSC5 response under tri-band droop control*

The response of the tri-band droop is the same as the active band droop response (as expected) during initial steady state operation (OP_0) and with small disturbance (OP_1). However, in the event of a large disturbance (OP_2), the response of tri-band droop differs slightly to follow the lower band droop to share the power shortage imbalance with other VSC stations in the MTDC grid. This shows decoupling of the droop

response of the lower band from the upper band in tri-band droop control. The converter power (P_c) and DC voltage (V_{dc}) responses of VSC4 and VSC5 during the three operating states are shown in **Figure 3:24**(a & b-middle & bottom respectively). Tri-band droop control provides a well-defined operating point and stable operation against small and large disturbances, as a primary control. Additionally, it enables the VSC stations to choose the three different optimised droops under normal operation and during power imbalances due to excessive or shortage of power in the MTDC grid.

3.6.7 Primary Control Comparison Summary

It is observed that during the power ramping from the OWF, the power into the MTDC grid increases, which results in the power imbalance in it, so each of control configuration responses according to its PV characteristics to balance the power. For example, in the case of voltage margin control, the master acting VSC station controls DC link voltage at lower level from t=2.0s to t=2.5s by reducing its power until the power limit (0.2pu) is reached and shifts to the higher level. Whereas, in all droop control configuration, the power and DC link voltage of each VSC station changes proportionally to their droop constants to maintain power balance in the MTDC grid.

It can be concluded from the comparison of the primary control methods performed for both the normal and disturbed operation of the six different control configurations that some configurations have advantages over others for one criteria and disadvantages for the other criteria. The results show that voltage margin control has the advantage of precise control while it lacks the operational stability and the flexibility of regulating the voltage and power during normal and disturbed band

operation. The dead-band droop control can provide precise power flow with stable operation but still lacks the flexibility of the voltage and power regulation in normal band operation. Whereas, the active-band droop control can provide precise power flow with stable operation and flexibility of the voltage and power regulation in normal band operation, but it has limitations on re-scheduling capability i.e. the droop response against the disturbance is the same for disturbances due to excessive and shortage of the power in the MTDC grid. Finally, the tri-band droop can provide precise power flow with stable operation and flexibility of the voltage and power regulation in normal band operation along with full re-scheduling capability. A generic configuration, tri-band control, can be an attractive control method applied for the primary control, which can be switched to any other control configuration according to operating conditions and requirements by changing the droop constants settings. Tri-band droop control has the added advantage in the rescheduling capability over the active-band droop control.

As indicated by the comparison of the different DC voltage control methods, primary control is able to respond to any power imbalance caused by the disturbances i.e. load/generation changes and outages. The response of primary control to these disturbances is accompanied by steady-state deviations in control parameters (power/ DC voltage). Hence, a secondary control is required to restore the operation of the VSC stations to the desired reference values after the disturbances. The implementation of the secondary control is discussed in Section 4.2.

3.7 Chapter Summary

A primary control for power balancing of the MTDC grid is suggested, similar to primary control of the AC grid, comprising of a fast and autonomous controller integrated into the outer control loop of the VSC station. This enables control of the DC node voltages and power balancing control in the MTDC grid. The implementation and comparison of six different control methods is performed against the requirements. It is observed that some configurations have advantages over others for one criteria and disadvantages for other criteria. Therefore, in actual practice a primary control may comprise of a combination of different control configurations according to the operational requirements of each VSC station. A generic configuration such as tri-band control is found be an attractive control method to be applied for the primary control, which can be switched to any other control configuration according to the operating conditions and requirements by changing the droop constants settings.

Further, it was also observed that the secondary control is required to adjust the power deviations and restore the pre-disturbance conditions. The requirements and implementation of the secondary control to provide updated references to the VSC station of the MTDC grid is discussed in Chapter 4.

CHAPTER 4

Power Flow Control of combined AC/DC systems

4.1 Introduction

The power sharing control between the combined AC and DC grid is one of main challenges for integrated operation of two grids. As discussed in Section 3.4, DC voltage in the MTDC grid varies with power exchange variation following disturbances or events. The VSC stations with droop control adjust their power with respect to voltage according to their droop settings, so that MTDC grid operation is stable and within the limits. However, the VSC system is not able to regain the post disturbance operation by itself, so a secondary control is required from the system operator to reschedule the VSC set point to maintain the desired flow.

In this chapter, a co-ordinated control is suggested as a secondary control strategy for re-scheduling of the references of the AC and DC grids in order to obtain the planned power injections along with maintaining DC voltage within the required profile. A combined AC/DC power flow algorithm with generic tri-band configuration is proposed for calculating updated references for the co-ordinated control. The first Section discusses the requirement of the secondary control for combined AC/DC grid operation. The second Section provides the description of the power flow model. In the third Section, detailed modelling is presented. The fourth Section presents an overview of the general power flow solution technique followed by the proposed combined algorithm for combined AC/DC grid power flow solutions. Finally, case

studies are performed with co-ordinated control after the validation of the proposed algorithm to show the outcomes of the co-ordinated control implementation.

4.2 Specifications of the Secondary Control

The secondary control is required to achieve the desired power flow sharing between AC and DC grids following a disturbance in the AC/MTDC grid. It acts as a co-ordination control among all the VSC stations in the MTDC grid in order to provide the updated power and DC voltage references. The secondary control actions under the co-ordinated control provide the updated references that decide the overall steady-state power flows in the MTDC grid in order to restore the voltages within the required profile and obtained planned operation [59].

A centralised co-ordinated control system can be implemented as a secondary control to communicate the updated settings of the VSC and generator units in order to maintain the desired power flows from both MTDC and AC grids, which may include:

- Power and DC voltage references (P_{REF} and V_{REF}) for each VSC station and AC generator unit;
- Droop gains for individual droop bands (K_{DC1}, K_{DC2} *and* K_{DC3}) of each VSC station;
- Band limits settings i.e. ($V_{DC\ HIGH}$ and $V_{DC\ LOW}$).

The centralised co-ordinating controller requires the actual measurement from Remote Terminal Units (RTU) of all the VSC stations to determine the actual operation of the MTDC grid. This includes the actual converter power and DC node voltages with their limit settings such as: maximum and minimum DC voltage and power limits, including any individual assigned band DC voltage limits for specific control

configurations, e.g. voltage margin and Tri-band droop control. The implementation of the co-ordinated control is shown in **Figure 4:1**. In this thesis, the communication system used for co-ordinated control is assumed to be reliable. Since primary control is suggested to be autonomous, so in the case of loss of communication system operation will still be stable, but without the desired power flow sharing between AC and DC grids. The rescheduling from the co-ordinated control can be set to event based or cyclic in time span of a few minutes.

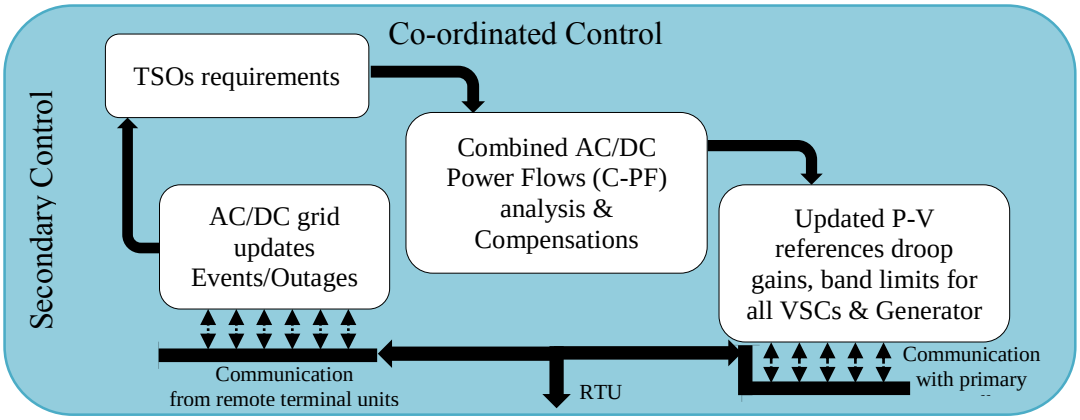

Figure 4:1 *Co-ordination Control system implementation*

Further, tertiary control can be implemented in order to obtain the optimised reference set points of planned operation for the primary and secondary control, which is be discussed in Chapter 5.

4.3 Combined AC/MTDC Grid Power Flow Models and Calculations

The Combined AC/DC Power Flow (C-PF) provides the steady state operating point for the integrated AC/DC power system. It can be used in secondary control for re-scheduling the power and voltage references of the VSC stations, wind integration analysis and N-1 security assessments. However, the power vs voltage relationships

in a DC grid are very different from that of an AC grid; the solution of two different sets of numerical equations is required to obtain the C-PF. The implementation of the different DC voltage control modes of the VSC stations in the MTDC system makes it further complicated.

The operational flexibility of distributed control makes it more advantageous, as more than one VSC station controls the DC link voltage of the MTDC system. Different distributed control methods and their comparison have already been discussed in Section 3.5.2. There has been a lot of research to explore the steady state and the dynamic behaviour of MTDC systems in the literature [3,4,5]. The focus of previous work has been only on the MTDC network, while considering the integrated AC network as an infinite node or single AC network with several nodes. However, it is necessary to have complete C-PF models of the MTDC grids along with interconnected large AC grids, to obtain the steady state operating point including the droop control effects after a disturbance, without the need of building a full detailed dynamic model of the entire AC/DC system. Further, it facilitates the computation of the updated references of the co-ordinated control. The loads are modelled as constant PQ load in the AC grid.

4.3.1 Solution Methods

There are two main approaches used for the C-PF solutions in the literature, which are classified as the unified and the sequential methods. A detailed and general model of the VSC based MTDC system with full power flow equations including VSC converter loss, transformer and filters is presented in [86] for sequential power flow calculation. In the unified method, the power flow of the entire AC/DC system is

solved simultaneously using a modified Jacobi technique [35][38], where all the AC and DC variables are available after each iteration. In contrast, in the sequential method, the AC and DC networks are solved sequentially, one after another [34]. However, the work has mainly focused on AC grids with an embedded multi-terminal HVDC network. A multi-option power flow approach is proposed in [87], where a multi-terminal HVDC system with asynchronous AC grids is solved without considering the DC droop control mode of the VSC stations. A DC power flow algorithm with generic droop lines implementation with a method to specify mean voltage instead of a single slack bus in the MTDC grid is proposed in [38]. Since the MTDC grid is expected to interconnect the large AC grids, this raises an issue of solving more than one AC or DC grids in the C-PF algorithm. A combined solution of an AC/DC system with more than one AC and DC grid requires a greater number of variables to be included.

In this thesis, the unified approach similar to [87] is adopted, to develop a generalised C-PF algorithm, for the solution of a combined AC/DC network, along with the implementation of the generic droop control in order to indicate the effects of the various power balancing controls. The issue of more than one AC grid solution is dealt with by categorising the interconnected AC grids into integrated and non-integrated AC grids. Where, the AC and DC grid are considered to be integrated, and can be solved simultaneously, if the slack bus of the DC grid is connected to the AC grid. All the non-integrated asynchronous AC grids can be solved separately and their outputs added into the integrated AC/DC grid solution in the C-PF algorithm. Further, this C-PF algorithm can also be integrated to the existing AC power flow models.

4.4 Steady State Modelling for VSC Based MTDC System

Three main aspects are included for the steady state model representation of the VSC based MTDC system.

(a) VSC converter station, which forms a link between the AC and DC system.

(b) Control modes of the VSC station that decide the operation state of the VSC station.

(c) Losses in the VSC station due to converter switching losses, conduction losses, and line losses of the AC side filters and transformers.

4.4.1 VSC Converter Station Representation and Calculations

The VSC converter station forms a link between the DC and AC grids. **Figure 4:2** shows that DC grid node D connects to the AC grid node S through the converter-switching component, phase reactor, filter and coupling transformer. The steady state model includes the impedance Z_T of the coupling transformer, the susceptance B_F of the filter and phase reactor impedance Z_C, while only losses represents the switching components of the VSC station. The phase reactor impedance Z_C is connected between node C and node *F*, and the shunt susceptance B_F of the low pass filter is connected to node *F*, which further connects to the AC grid node S through the coupling transformer impedance Z_T.

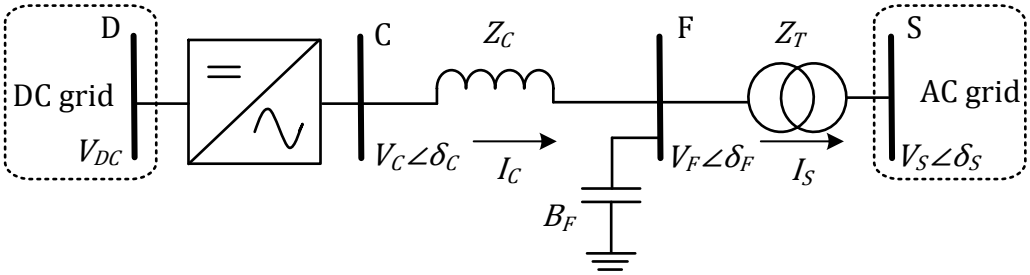

Figure 4:2 *Two node representation between AC and DC grid*

Thus, power flow equations from the AC node of the converter station can be given as [86]:

$$P_c = V_c^2 G_c - V_c V_F [G_c \cos(\delta_F - \delta_c) - B_c \sin(\delta_F - \delta_c)] \tag{4.1}$$

$$Q_c = -V_c^2 B_c + V_c V_F [G_c \sin(\delta_F - \delta_c) + B_c \cos(\delta_F - \delta_c)] \tag{4.2}$$

while the power flow equations from the filter node to the converter node can be given as:

$$P_{FC} = -V_F^2 G_c + V_F V_c [G_c \cos(\delta_F - \delta_c) + B_c \sin(\delta_F - \delta_c)] \tag{4.3}$$

$$Q_{FC} = V_F^2 B_c + V_F V_c [G_c \sin(\delta_F - \delta_c) - B_c \cos(\delta_F - \delta_c)] \tag{4.4}$$

The expression for the power flow from the filter node to the AC grid can be given as:

$$P_{FS} = V_F^2 G_T + V_F V_s [G_T \cos(\delta_F - \delta_s) - B_T \sin(\delta_T - \delta_s)] \tag{4.5}$$

$$Q_{FS} = -V_F^2 B_T + V_F V_s [G_T \sin(\delta_F - \delta_s) + B_T \cos(\delta_F - \delta_s)] \tag{4.6}$$

Similarly, the expression for the power flow from the AC grid PCC node to the filter node can be given as:

$$P_s = -V_s^2 G_T - V_s V_F [G_T \cos(\delta_s - \delta_F) + B_T \sin(\delta_s - \delta_T)] \quad (4.7)$$

$$Q_s = V_s^2 B_c + V_s V_F [G_T \sin(\delta_s - \delta_F) - B_T \cos(\delta_s - \delta_T)] \quad (4.8)$$

However, the calculation of the AC grid power injection from each converter station, through eq :(4.1)-(4.8), requires a separate internal iterative loop. To avoid the additional loop, an alternative method of calculating the AC grid active power $P_{S,i}$ is given as [35]:

$$P_{s,i} = P_{c,i} - P_{Loss\ L,i} \quad (4.9)$$

where, $P_{C,i}$ represents the active power from the VSC station and $P_{LOSS\ L,i}$ represents the total line losses from the node C side to the node S (PCC) of the AC grid, as explained in Section 4.4.3. The calculation of power from the node C to node S depends upon the control type of node S (PCC). If it is PQ type, then both active power *Ps* and reactive power *Qs* are known, whereas if PCC is assigned as PV type, calculation of Qs can be determined by:

$$Q_{S,i} = Q_{G,ACi} - Q_{L,ACi} - Q_{inj,ACi} \quad (4.10)$$

Then the current injection at PCC can be given as:

$$I_{S,i} = \frac{(P_{S,i} + jQ_{S,i})}{V_S \angle \delta_S} \quad (4.11)$$

Once $I_{S,i}$ is determined, the voltage at filter node $V_{F,i}$ can be calculated as:

$$V_{F,i} = V_{S,i} + I_{S,i}Z_{T,i} \tag{4.12}$$

Complex power at filter node F can be calculated as:

$$S_{F,i} = V_{F,i}I_{S,i}^{*} - V_{F,i}^{2}B_{F,i} \tag{4.13}$$

The current through the phase reactor $I_{C,i}$ can be calculated as:

$$I_{C,i} = \frac{S_{S,i}^{*}}{V_{F,i}^{*}} \tag{4.14}$$

Hence, the converter voltage $V_{C,i}$ at node C can be given as:

$$V_{C,i} = V_{F,i} + I_{C,i}Z_{C,i} \tag{4.15}$$

Finally, the complex power at node C can be calculated as:

$$S_{C,i} = V_{C,i}I_{C,i}^{*} \tag{4.16}$$

4.4.2 VSC Converter Station Control Modes

As discussed in Section 3.3, the main challenge of the VSC based MTDC system is control of the DC link voltage i.e. the active power balancing in the MTDC grid. The comparison performed in Section 3.6 suggested that power balancing can be ensured by a mix of different control methods implemented together in the MTDC grid, and suggested Tri-band droop control as the most generic for the primary control. For reactive power control, each of the VSC stations in the MTDC grid can operate either in *Q*-control mode to provide constant reactive power or V_{ac}-control to keep AC voltage constant at the PCC to support a weak AC system. Therefore, the PCC of

each VSC station can be assigned as a PV- or PQ node, according to its operation mode, as shown in **Figure 4:3**.

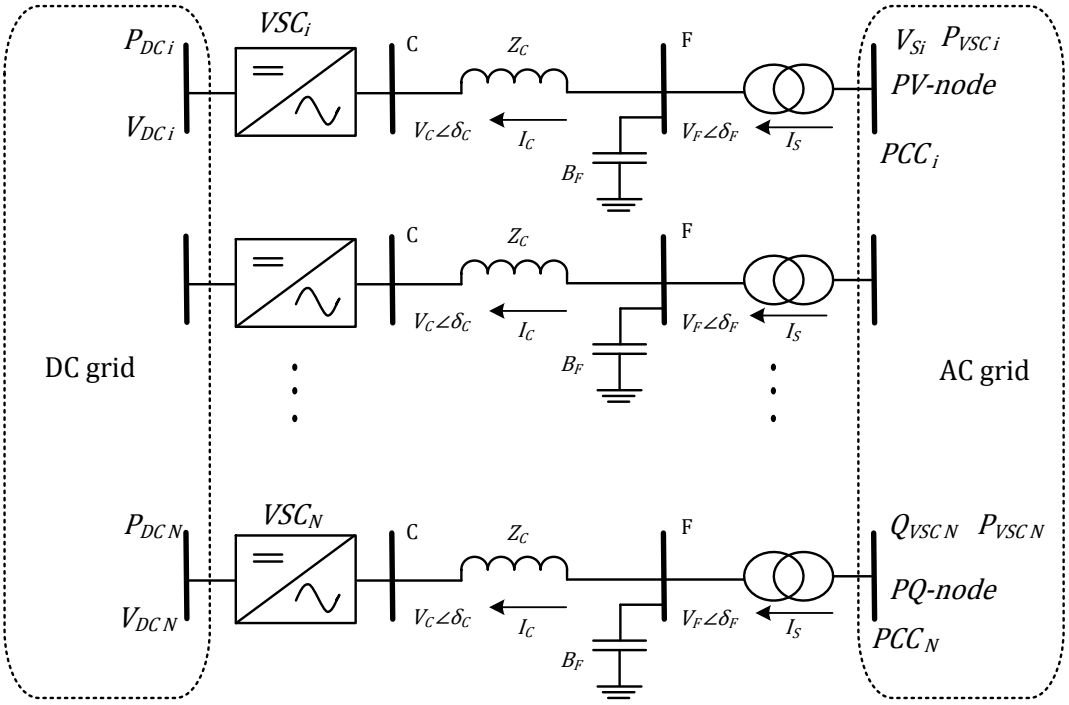

Figure 4:3 *VSC model for AC/DC grid integration*

The steady state model for the combined AC/DC power flow calculation needs to take into account the steady state behaviour of the active power versus the DC link voltage represented by the PV characteristics of the VSC station. The various DC voltage control methods implemented show that the PV characteristic can be a combination of more than one linear or nonlinear function of the DC voltage. The expression for a single linear PV-droop characteristic of the i^{th} VSC of the MTDC grid can be expressed as:

$$\Delta P_{DC,i} = K_{DC,i}\,(\Delta\, V_{DC,i}) \tag{4.17}$$

$$P_{DC,i} = P_{DC,REF\,i} - K_{DC,i}\,(V_{DC,i} - V_{DC,REF\,i}) \tag{4.18}$$

where,

$P_{DC,i}$ is actual power at the DC node (*node i*) of the VSC station,

$P_{DC,REF\,i}$ is the desired reference power,

$K_{DC\,i}$ is the droop gain of the DC droop voltage controller,

$V_{DC,i}$ is the actual DC link voltage at the VSC station,

$V_{DC,REF\,i}$ is the reference DC voltage normally taken as the rated DC link voltage for the VSC station.

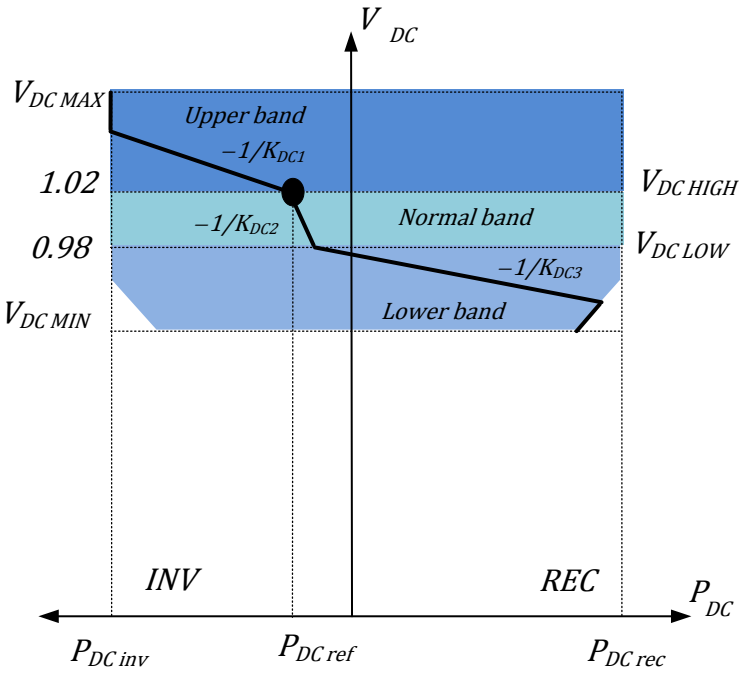

Figure 4:4 *PV characteristics of Tri-band control*

The most generic, tri-band control shown in **Figure 4:4** is implemented in the combined AC/DC power flow algorithm. This comprises of three droop bands depending on DC link voltage levels: upper band, normal band and lower band. The upper band is categorised as the region between $V_{DC,MAX}$ and $V_{DC,HIGH}$. The normal

band region is between $V_{DC,HIGH}$ and $V_{DC,LOW}$. And the lower band region is between $V_{DC,LOW}$ and $V_{DC,MIN}$.

$V_{DC,MAX}$ and $V_{DC,MIN}$ is usually set to be ±5% of the reference DC link voltage ($V_{DC,REF}$) and $V_{DC,HIGH}$ and $V_{DC,LOW}$ can be set to ±2% of the reference DC link voltage ($V_{DC,REF}$). So, the generic form of the Tri-band (non-linear PV-droop) characteristics for the i^{th} VSC station of the MTDC grid is expressed as:

$$P_{DC,i}(V_{DC,i}) = \begin{cases} P_{DC,REF\,i} - K_{DC1,i}(V_{DC,i} - V_{DC,HIGH\,i}) \quad if \;\; V_{DC,HIGH\,i} < V_{DC,i} < V_{DC,MAX} \\ P_{DC,REF\,i} - K_{DC2,i}(V_{DC,i} - V_{DC,HIGH\,i}) \quad if \;\; V_{DC,LOW\,i} < V_{DC,i} < V_{DC,HIGH\,i} \\ P_{DC,REF\,i} - K_{DC3,i}(V_{DC,i} - V_{DC,LOW\,i}) - K_{DC2,i}(\Delta V_{K2,i}) \; if V_{DC,MIN} < V_{DC,i} < V_{DC,LOW\,i} \end{cases} \quad (4.19)$$

where,

$P_{DC,i}$ is actual power at the DC side of the VSC station,

$P_{DC,REF\,i}$ is the desired reference power,

$V_{DC,i}$ is the actual DC link voltage at the VSC station,

$K_{DC1\,i}$, $K_{DC2\,i}$ and $K_{DC3\,i}$ are the droop gains of the DC droop voltage controller for the normal, upper and lower band respectively,

$V_{DC,HIGH\,i}$ and $V_{DC,LOW\,i}$ are the upper and lower DC link voltages for the normal band operation references of the i^{th} VSC station,

$\Delta V_{K2,i} = V_{DC,HIGHi} - V_{DC,LOW\,i}$,

$V_{DC,MAX}$ is the upper limit of the DC link voltage mainly defined by the insulation requirements of the switching components.

$V_{DC,MIN}$ is the lower limit. The DC link should not be discharge below its lower level to maintain the normal operation of the VSC station.

Implementation of almost all other control configurations is also possible by changing the value of the droop gains. For example, by setting the normal band droop gain K_{DC2} to zero, an infinite (very high) droop gain for upper band (K_{DC1}) and the lower band (K_{DC3}) will lead it to behave as the DC voltage margin control. While setting all three band droop gains equal will result in simple linear DC voltage droop mode of distributed control. In the dynamic simulations a Proportional-Integral (PI) controller is used to implement the constant DC voltage control, but theoretically it can be represented with an infinite (very high) value of droop gain.

4.4.3 Converter Losses and Operating Limits

The VSC converter losses are taken into account using a generalised VSC station loss model [88], in which losses are written as a function of the magnitude of the converter current $I_{C,i}$ and given by:

$$P_{Loss,C\,i} = a_i \times \left|I_{C,i}\right|^2 + b_i \times \left|I_{C,i}\right| + c_i \qquad (4.20)$$

As given in the equation, overall losses are divided into three categories; a_i and b_i indicate the quadratic and linear relation to the VSC station current $I_{C,i}$ respectively, and *c* represents no load losses, where $I_{C,i}$ can be given as:

$$I_{C,i} = \frac{\sqrt{P_{C,i}^2 + Q_{C,i}^2}}{\sqrt{3}(V_{C,i})} \tag{4.21}$$

Active power losses in the phase reactor and transformer can be calculated as:

$$P_{Loss,L\,i} = \; R_{X,i} \times \left| I_{C,i} \right|^2 + R_{C,i} \times \left| I_{C,i} \right|^2 \tag{4.22}$$

where $R_{X,i}$ and $R_{C,i}$ are the resistances of the coupling transformer and phase reactor respectively. The total losses from the DC side of the i^{th} VSC station up to the PCC_i of the AC grid can be given as:

$$P_{Loss,i} = \; P_{Loss,C\,i} + P_{Loss,L\,i} \tag{4.23}$$

4.5 General Power Flow Solution

The purpose of solving the power flow is to obtain the values for the state variables under given specified parameters for a power network. The state variables X comprised of the unknown node voltages and angles of the power network, while actual parameters P_{act} comprise of the load, generation and control modes at different nodes. The estimated parameters P_{es} are obtained from the updated state variables and can be represented as the parametric estimation function of the state variables $f(X)$. The mismatches between the actual parameters P_{act} and estimated parameters P_{es} are represented as mismatch vector $\mathbf{g}(X)$. The power flow problem involves the solution of the nonlinear equations, so an iterative numerical method is required; most commonly the Newton Raphson (NR) method is proposed for the power flow solution

[89][90]. A generalised flow chart of the NR iterative process for the power flow solution is shown in **Figure 4:5**. The generalised form of the power flow solution solved by the iterative process can be given as:

$$X^{(k)} = X^{(k+1)} + \Delta X^{(k)} \tag{4.24}$$

$$\Delta X^{(k)} = (\mathbf{J}^{(k)})^{-1}.\mathbf{g}(X^{(k)}) \tag{4.25}$$

where, X is the state variable vector with $X^{(k)}$ and $X^{(k+1)}$ as k^{th} and $(k+1)^{\text{th}}$ estimates respectively. The Jacobian matrix represents the linearization of the parametric estimation function $f(X)$ with respect to the state variable X over an operating point described by the actual parameters P_{act} and estimated variables [31].

$$\mathbf{J} = \frac{\partial P_{es}}{\partial X} = \frac{\partial f(X)}{\partial X} \tag{4.26}$$

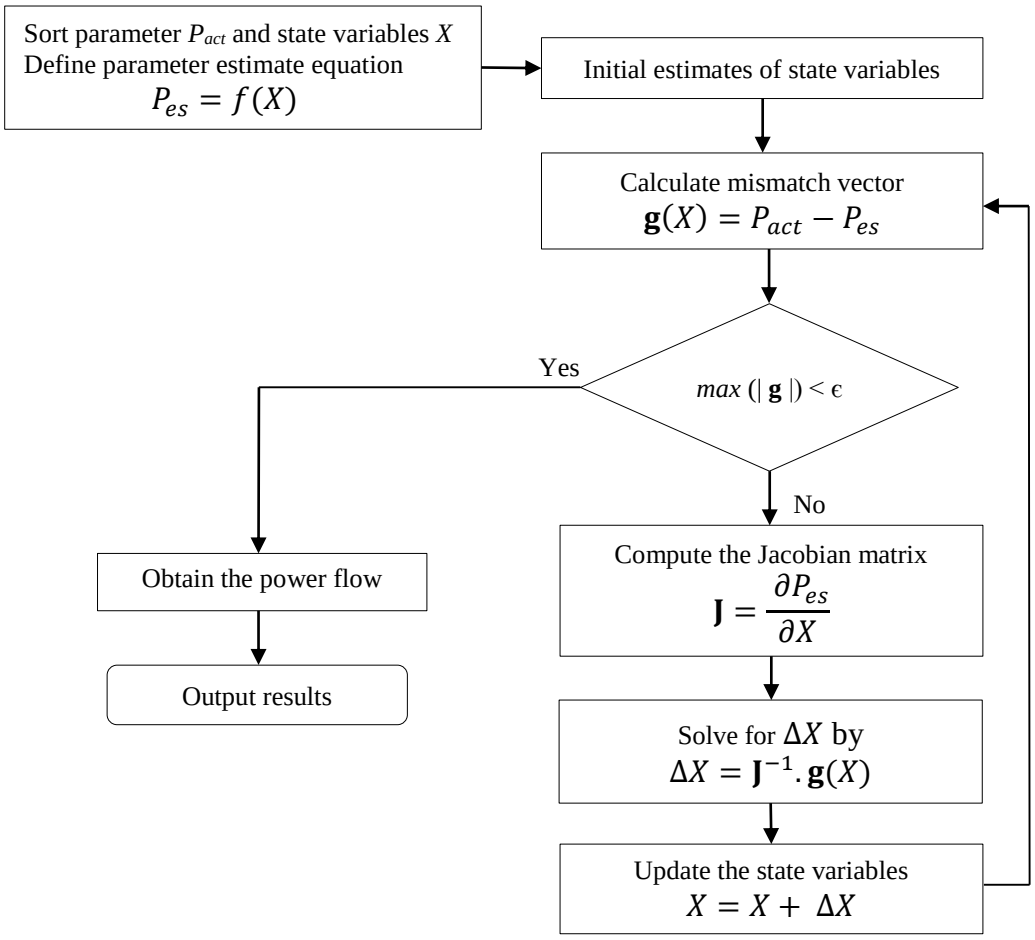

Figure 4:5 *Newton-Raphson method flow chart for generalised power flow*

4.5.1.1 AC Grid Power Flow Equations

The power flow problem of an AC grid of *M* nodes usually involves *2(M-1)* state variables. The state variables for the AC power flow are the node voltages and angles that can be given as: $X_{AC} = [V_i, \dots V_{M-1}, \delta_i, \dots \delta_{M-1}]^T$. The estimated parameter P_{es} can be represented as the parametric estimation function of the AC state variables $f(X_{AC})$ and can be calculated as the AC power flow injection for all the nodes in the AC grid (excluding the slack node) given by:

$$f(X_{AC}) = P_{inj,ACi} = \sum_{j=1}^{M} V_i V_j Y_{ij} \cos(\delta_i - \delta_j - \theta_{ij}) \quad (4.27)$$

$$f(X_{AC}) = Q_{inj,ACi} = \sum_{j=1}^{M} V_i V_j Y_{ij} \sin(\delta_i - \delta_j - \theta_{ij}) \quad (4.28)$$

where M is the total number of the AC nodes, V_i, V_j, δ_i and δ_j are the node voltage magnitudes and angles of the i^{th} and j^{th} AC nodes respectively, and θ_{ij} is the angle between the respective nodes voltages. Y_{ij} is the node admittance matrix of the AC grid.

The mismatch vector is given as $\mathbf{g}(X_{AC}) = [\, \mathrm{g}P_{AC1}, \ldots \mathrm{g}P_{AC\,M-1}, \mathrm{g}Q_{AC1}, \ldots \mathrm{g}Q_{AC\,M-1}]^T$. The power injections of a VSC station can be added as a negative load to extend the mismatch equations for the AC nodes including the PCC, and are given as:

$$\mathbf{g}P_{ACi} = P_{G,ACi} - P_{L,ACi} - P_{inj,ACi} - P_{vsc,i} \quad (4.29)$$

$$\mathbf{g}Q_{ACi} = Q_{G,ACi} - Q_{L,ACi} - Q_{inj,ACi} - Q_{vsc,i} \quad (4.30)$$

where,

$\mathbf{g}P_{ACi}$ and $\mathbf{g}Q_{ACi}$ are the AC active and reactive power mismatches at each node (i),

$P_{G,ACi}$, $P_{L,ACi}$, $Q_{G,ACi}$ and $Q_{L,ACi}$ are the AC active and reactive power generation and load respectively at each node (i),

$P_{inj,ACi}$and $Q_{inj,ACi}$ are the net power injection at each node, which can be obtained from eq:(4.27) and eq:(4.28),

$P_{vsc,i}$ and $Q_{vsc,i}$ are the VSC station active and reactive power injections at the PCC for the DC grid connected nodes only.

The Jacobian matric $\mathbf{J}_{AC}$ of the AC grid shows the variation of the AC estimated parametric function $f(X_{AC})$ with respective AC state variables X_{AC}. The generalised form is given as:

$$\mathbf{J}_{AC} = \frac{\partial f(X_{AC})}{\partial X_{AC}} = \begin{bmatrix} \frac{\partial P_{AC}}{\partial \delta_{AC}} & \frac{\partial P_{AC}}{\partial V_{AC}} \\ \frac{\partial Q_{AC}}{\partial \delta_{AC}} & \frac{\partial Q_{AC}}{\partial V_{AC}} \end{bmatrix} \tag{4.31}$$

4.5.1.2 DC Grid Power Flow Equations

In the case of the DC grid, since there are no angles involved in the DC power flow, the power flow problem of the DC grid with *N* nodes involve only *N-1* state variables that are only the DC node voltages and can be given as: $X_{DC} = [V_{DCi}, \dots V_{DC\,N-1}]^T$. Similar to the AC grid, the estimated parameter P_{es} can be represented as the parametric function of the DC state variables $f(X_{DC})$ and can be calculated as the DC power flow injection for all the nodes in the DC grid (excluding the slack node) given by:

$$f(X_{DC}) = P_{inj,DCi} = V_{DC,i} \sum_{j=1}^{N} V_{DC,j}\, Y_{DC,ij} \tag{4.32}$$

where, *N* is the total number of nodes in the DC grid, $V_{DC,i}$ is the i^{th} DC node voltage and Y_{DC} is the DC node admittance matrix. With the linear PV-droop control implementation, the parametric function can be extended as:

$$f(X_{DC}) = P_{inj,DCi} = V_{DC,i}(\sum_{j=1}^{N} V_{DC,j}\, Y_{DC,ij}) + K_{DC,i}(V_{DC,i} - V_{DC,REF\,i}) \quad (4.33)$$

In the case of PV droop control with a combination of multiple linear and non-linear PV droop characteristics, the parametric expression can be extended as suggested in [38]:

$$f(X_{DC}) = P_{inj,DCi} = V_{DC,i}(\sum_{j=1}^{N} V_{DC,j}\, Y_{DC,ij}) + P_{DC,i}(V_{DC,i}) \quad (4.34)$$

where, $P_{DC,i}(V_{DC,i})$ is defined by eq: (4.19).

The mismatch vector only comprises of the active power given as:

$\mathbf{g}(X_{DC}) = [\, \mathrm{g}P_{DC1}, \ldots \mathrm{g}P_{DC\,N-1}]^T$. The power mismatch equations for the DC power flow can be given as:

$$\mathbf{g}P_{DCi} = P_{DCi} - P_{inj,DCi} \quad (4.35)$$

$$P_{DC,i} = P_{S,i} - P_{Loss,i} \quad (4.36)$$

where,

$\mathbf{g}P_{DCi}$ is the DC active power mismatches at each node (*i*),

$P_{inj,DCi}$ are the net power injection at each node given by eq:(4.32),

$P_{DC,i}$ is the active power at the DC side of the converter, which can be calculated from eq: (4.36),

$P_{S,i}$ is the power at the Point of Common Coupling (PCC*i*) of the VSC station,

$P_{Loss,i}$ is the total losses at the VSC station.

The Jacobian matric of the DC grid $\mathbf{J}_{DC}$ shows the variation of the DC estimated parametric function $f(X_{DC})$ with respective DC state variables X_{DC}. The generalised form is given as:

$$\mathbf{J}_{DC} = \frac{\partial f(X_{DC})}{\partial X_{DC}} = \begin{bmatrix} \frac{\partial P_{inj,DC1}}{\partial V_{DC1}} & \cdots & \frac{\partial P_{inj,DC1}}{\partial V_{DC\,N-1}} \\ \vdots & \ddots & \vdots \\ \frac{\partial P_{inj,DC\,N-1}}{\partial V_{DC1}} & \cdots & \frac{\partial P_{inj,DC\,N-1}}{\partial V_{DC\,N-1}} \end{bmatrix} \tag{4.37}$$

Thus, Jacobian elements for linear PV-droop can be obtained as:

$$\frac{\partial P_{DCi}}{\partial V_{DCi}} = 2V_{DCi}Y_{DC,ii} + \sum_{\substack{j=1 \\ j\neq i}}^{N} Y_{DC,ij}\,V_{DC,j} + K_{DC,i} \tag{4.38}$$

$$\frac{\partial P_{DCi}}{\partial V_{DCj}}_{j\neq i} = V_{DCi}Y_{DC,ij} \tag{4.39}$$

However, in the case of the PV droop control with a combination of multiple linear and non-linear PV droop characteristics, the Jacobian elements need to be modified for each band of the PV droop by:

$$\frac{\partial P_{DCi}}{\partial V_{DCi}} = 2V_{DCi}Y_{DC,ii} + \sum_{\substack{j=1 \\ j\neq i}}^{N} Y_{DC,ij}\,V_{DC,j} + \frac{\partial P_{DCi}(V_{DCi})}{\partial V_{DCi}} \tag{4.40}$$

$$\frac{\partial P_{DCi}}{\partial V_{DCj}}_{j\neq i} = V_{DCi}Y_{DC,ij} \tag{4.41}$$

where, $\frac{\partial P_{DCi}(V_{DCi})}{\partial V_{DCi}}$ can be defined according to the estimated DC voltage $V_{DC,i}$ at each iteration as:

$$\frac{\partial P_{DCi}(V_{DCi})}{\partial V_{DCi}} = \begin{cases} K_{DC1,i} & if\ V_{DC,HIGH\ i} < V_{DC,i} < V_{DC,MAX} \\ K_{DC2,i} & if\ V_{DC,LOW\ i} < V_{DC,i} < V_{DC,HIGH\ i} \\ K_{DC3,i} & if\ V_{DC,MIN} < V_{DC,i} < V_{DC,LOW\ i} \end{cases} \quad (4.42)$$

4.5.1.3 Slack Converter Losses Equations

The power at the PCC of the slack VSC station is calculated as:

$$P_{S,slack} = V_{DC,slack} \sum_{j=1}^{N} V_{DC,j}\, Y_{DC,slack} - P_{Loss,slack} \quad (4.43)$$

where, $P_{Loss,slack}$ are DC slack node losses needed to calculate the DC slack node power. In the unified approach [87], the slack station losses are considered as a separate state variable X_s. The additional mismatch equation is given as:

$$0 = X_s - P_{Loss,slack} \quad (4.44)$$

where, $P_{Loss,slack}$ can be obtained from eq:(4.23).

4.6 Proposed Combined AC/DC Power Flow Algorithm

The proposed generalised combined AC/DC power flow approach aims to benefit from most of the advantages of both the techniques, unified and sequential, while avoiding their drawbacks. The unified combined power flow approach enables the AC and DC network equations to be solved simultaneously in the same iteration, resulting in merging all internal and external loops into a single iterative loop. However,

solution of *N* independent DC networks requires adding *N* more variables in the single iterative loop. In the sequential combined power approach, the AC and DC network equations need to be solved sequentially in separate iterations. The AC grid power flows change after the slack node power is updated by the DC network iteration, thus external iteration is required to ensure the overall convergence of the combined system, which not only complicates the power flow but also takes more time to solve. Its main advantage is the easy integration of the DC network equations with the AC load flow equation without changing the existing AC load flow models. In the combined power flow approach the AC and DC network equations of the integrated AC grid are solved simultaneously in a single loop iteration, while non-integrated AC grids can be solved separately. This enables it to be integrated with the AC power flow model for solution of the combined AC/DC grid by regarding the large AC system as non-integrated AC grids similar to [87], without changing the existing AC load flow model. The flow chart of the proposed algorithm is shown in the **Figure 4:6**. Further generic droop control characteristics are implemented to demonstrate the possibility of handling any control modes of the VSC station in the C-PF algorithm.

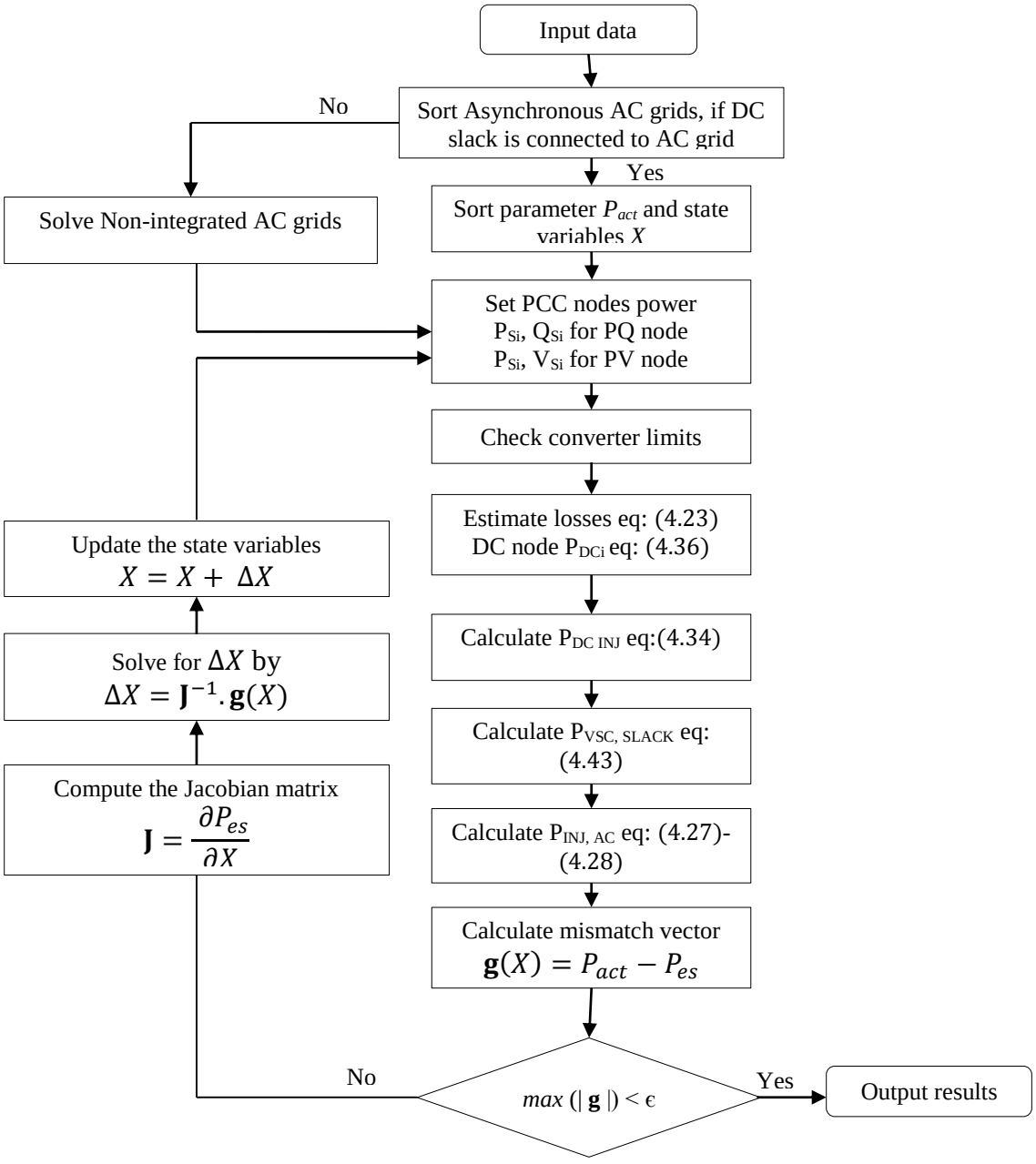

Figure 4:6 *Flow chart for Combined power flow algorithm*

4.7 MTDC Grid AC/DC combined Power Flow analysis and Model Validation

4.7.1 Test case System

The original IEEE14 bus network represents a portion of American power system with 14 buses, 20 branches, 5 generators and 11 loads. Three generators act as a synchronous condensers for providing reactive power compensation. It is also equipped with 1 two winding and three winding transformer. A test case system of AC/DC integrated grids is suggested to perform the combined AC/DC power flow analysis using the proposed combined algorithm. The first seven AC branches of the IEEE 14 bus AC network are converted to DC branches connected to the AC grid via VSC stations to model a DC grid comprising of a five-terminal MTDC system described in Section 3.6. This produces the test case system of an integrated AC/DC14 bus network, as shown in **Figure 4:7**. The values for the line impedances and loads of the AC network are the same as in the original IEEE14 bus data (refer to Appendix A.3 for input data of modified IEEE14 bus network). Two synchronous condensers are changed to synchronous generators. One synchronous generator and two transformers are neglected. The loads are modelled as constant PQ loads and generator at *node 8* as *PV-node* with *node1* as slack bus. The OWF at *node2* and asynchronous AC grid at *node3* are modelled slack buses. The converter station *VSC1* (slack node of the DC network) is connected to *node1* of the AC system. The converter stations *VSC2* and *VSC3* are in power control mode in order to model the power variations from the offshore windfarm and the interconnection to an asynchronous infinite AC grid at *node2* and *node3* of the AC system respectively. The other two converter stations *VSC4* and *VSC5* also operate in the power control mode to provide constant

power to the AC grid and they are connected to *node6* and *node7* of the AC system respectively. The detailed operation modes and converter ratings are given in **Table 4-1**.

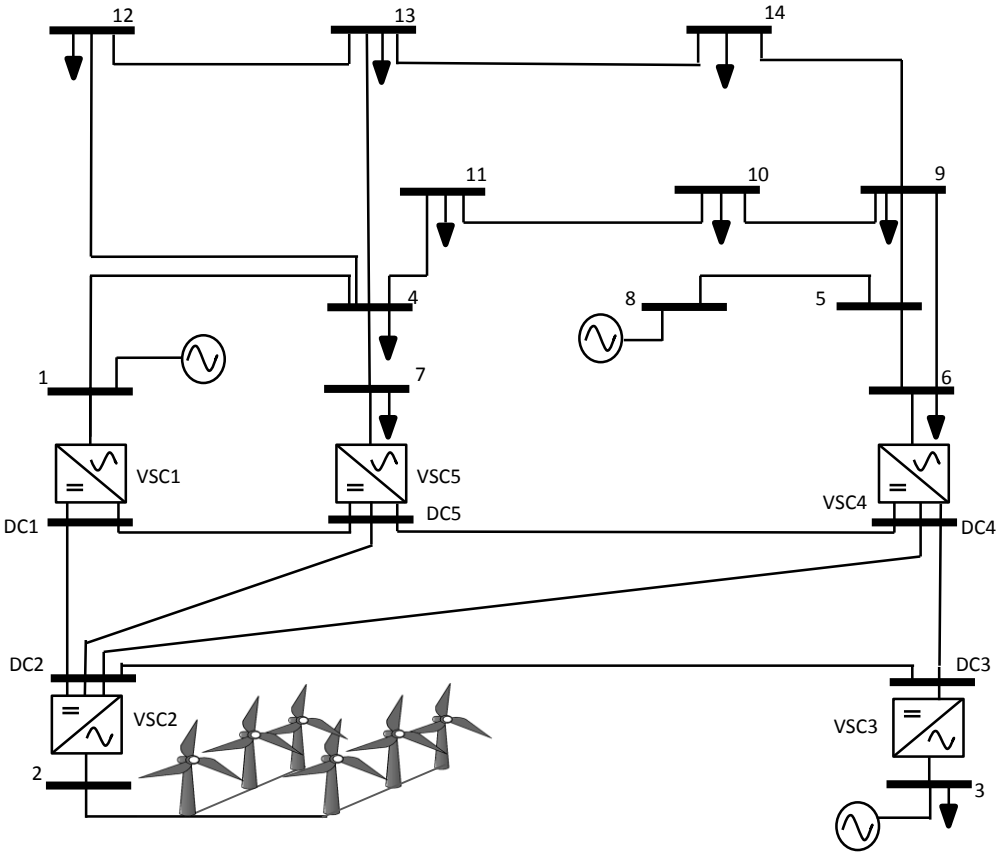

Figure 4:7: *Modified IEEE14 network with five-terminal MTDC system*

Table 4-1 *VSC Operation mode and PCC types*

VSC stations	**P_{VSC} *(MW)***	**V_{DC} *(kV)***	**VSC control**	**PCC Type**	**AC grid node**
VSC1	*slack*	±200	V_{DC}-control	PQ	Bus1
VSC2	-200	±200	P-control	PQ	Bus2
VSC3	-50	±200	P-control	PQ	Bus3
VSC4	60	±200	P-control	PV	Bus6
VSC5	60	±200	P-control	PV	Bus7

In the five-terminal MTDC system, *VSC1* (slack node) regulates the DC link voltage of the MTDC system at ±200kV (1pu). The rest of the VSC stations are set to control power measured at the PCC of each station. P_{VSC2} and P_{VSC3} are set to inject 200MW and 50MW into the MTDC system respectively, while P_{VSC4} and P_{VSC5} are set to supply 60MW to the AC system. The important parameters considered for the AC/DC combined power flow analysis are shown in **Table 4-2**. The lengths of the DC grid cables are taken as: l_{12}=120km, l_{15}=70km, l_{25}=100km, l_{24}=150km, l_{23}=150km, l_{34}=70km and l_{45}=100km.

Table 4-2 *AC/DC grid parameters for combined power flow*

AC/DC grid parameters	**ratings**	**Converter parameters**	**Value**
AC Power base ($S_{AC,base}$)	100MVA	Ph: reactor impedance (Z_C)	0.006+j0.20 pu
DC Power base ($S_{DC,base}$)	100MVA	Transformer Impedance (Z_X)	0.002+j0.05 pu
AC Voltage base ($V_{AC,base}$)	400kV	Filter Susceptance (B_F)	0.01 pu
DC Voltage base ($V_{DC,base}$)	±200kV	Cable resistance (R_{DC})	0.02 Ω/km

4.7.2 Model Validation and Comparison

The validation of proposed C-PF algorithm is required in order to ascertain that model can represent the steady state behaviour of the combined AC/DC grid with MTDC grid controls in similar way as complete dynamic model in time domain simulations. If C-PF algorithm can represent the response of the combined AC/DC systems accurately, then it can used in secondary control to estimate the updated references of

the VSC station for the re-scheduling without running complete dynamics simulations. A power flow analysis is performed on the test case system using the proposed C-PF algorithm implemented in open source Matlab toolbox, MATPOWER [91]. In order to validate the results from the combined AC/DC power flow algorithm, the same test case has been simulated in PSCAD/EMTDC [92] using average VSC models as discussed in Section 2.4. In this validation study, converter switching and conduction losses are neglected, to match VSC representation with the average VSC model. Further, *VSC2* is off due to a windfarm outage, in order to simplify the expected power variation from the windfarms.

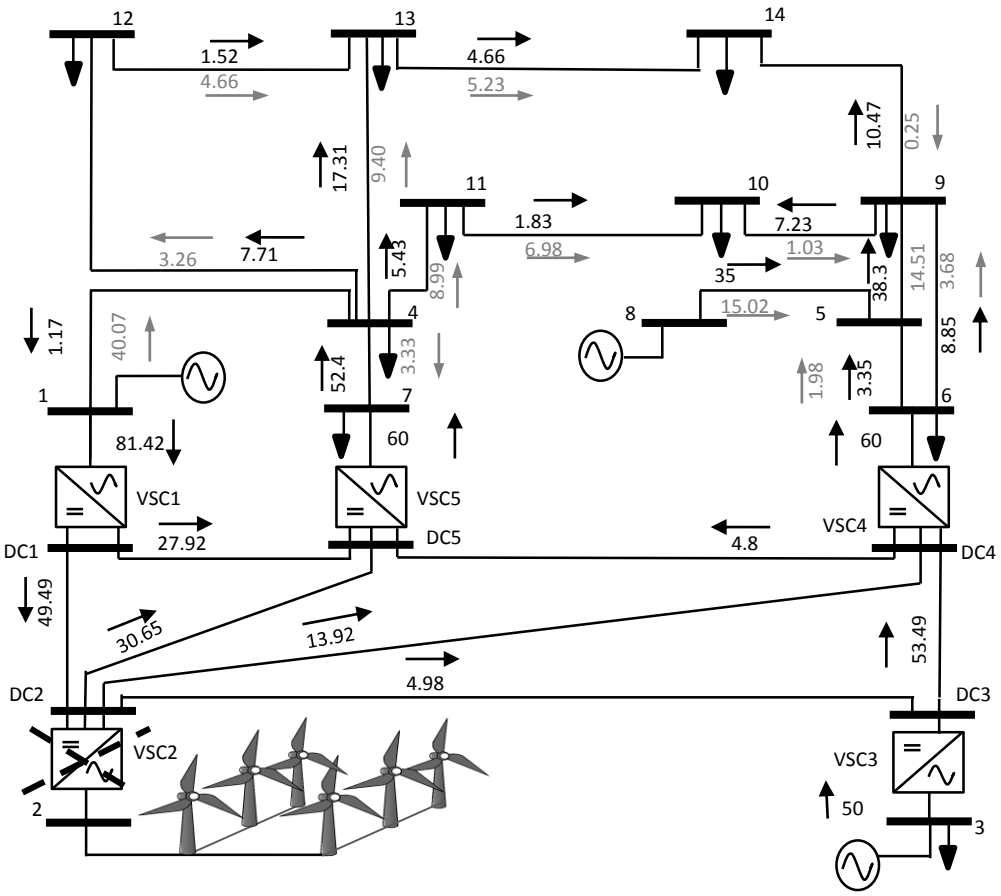

Figure 4:8 *Branch flows in AC/DC integrated 14 bus test case system*

Legends: → *represents active power in MW*

→ *represents reactive power in MVar*

The arrows in **Figure 4:8** show the branch flows obtained from the power flow analysis of the test case system by the proposed algorithm. The combined power flow algorithm is found to converge in 0.21s and six iterations with good accuracy. The comparisons of the results are shown in **Figure 4:9-Figure 4:12**. The voltage magnitude of AC *node6* and *node7* can be observed as fixed to 1pu in **Figure 4:9**, as the PCC of their VSC stations (*VSC4* and *VSC5*) are assigned to PV mode. The voltage at the DC *node1* can also be observed as fixed to 1pu in **Figure 4:10**, as it is assigned as the slack node for the DC grid. The percentage error in AC node voltages due to the line losses of two different models is found to be less than 0.1%.

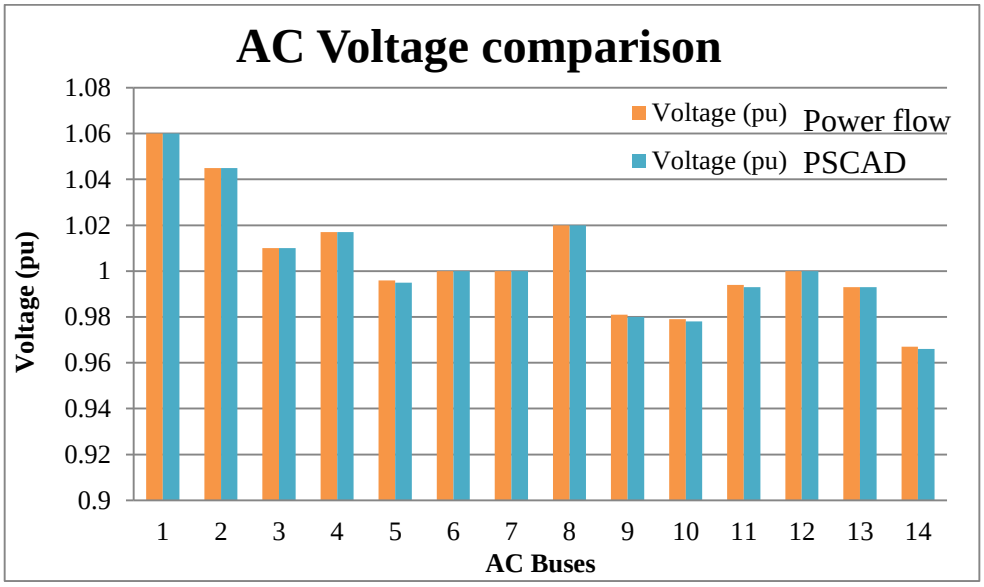

Figure 4:9 *AC nodes voltage magnitude comparison*

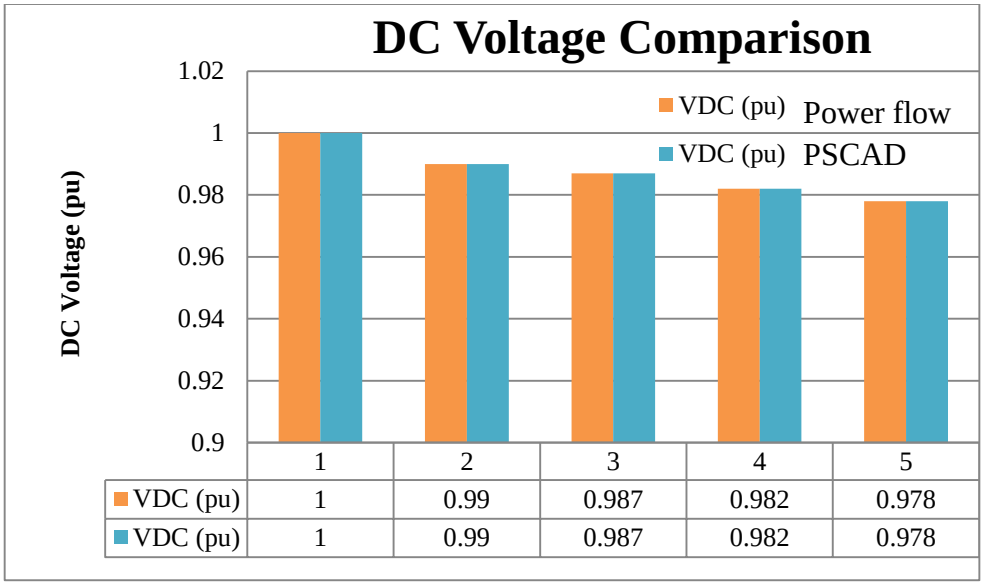

	1	2	3	4	5
VDC (pu)	1	0.99	0.987	0.982	0.978
VDC (pu)	1	0.99	0.987	0.982	0.978

Figure 4:10 *DC node voltage comparison*

The active power of the AC grid shows good match in **Figure 4:11**, except for the AC slack node (*node1*) that shows a slight difference, which can be due to the line losses of the two different models. The DC voltage at *node1* is highest, since it injects the highest active power into the DC grid during the outage of offshore windfarm, while *node4* and *node5* have the lowest voltages, as they absorb active power from the DC grid in **Figure 4:12**.

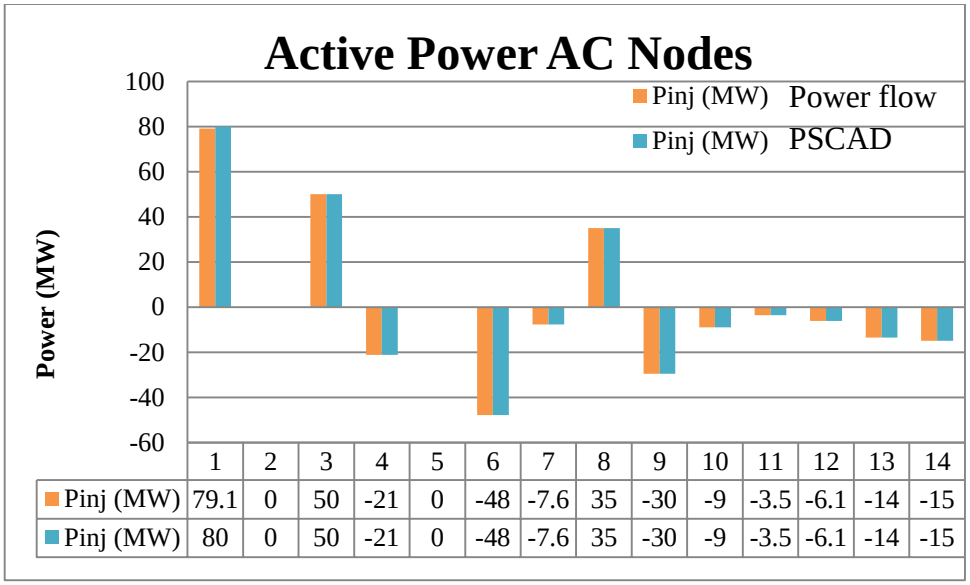

	1	2	3	4	5	6	7	8	9	10	11	12	13	14
Pinj (MW)	79.1	0	50	-21	0	-48	-7.6	35	-30	-9	-3.5	-6.1	-14	-15
Pinj (MW)	80	0	50	-21	0	-48	-7.6	35	-30	-9	-3.5	-6.1	-14	-15

Figure 4:11 *Active power comparison of AC nodes*

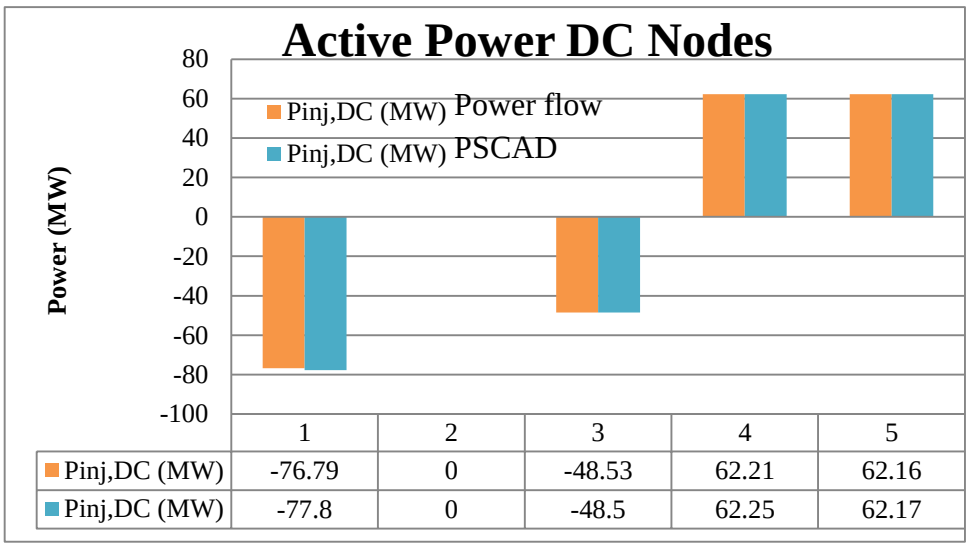

	1	2	3	4	5
Pinj,DC (MW)	-76.79	0	-48.53	62.21	62.16
Pinj,DC (MW)	-77.8	0	-48.5	62.25	62.17

Figure 4:12 *Active power comparison of DC nodes*

4.8 Co-ordinated Control Implementation with Generic Tri-band Droop

The detailed implementations of generic Tri-band droop control in the combined power flow algorithm was discussed in Section 4.4.2. In this Section, four cases of different droop control are implemented under different scenarios with and without

rescheduling from the co-ordinated control. The test case system is assumed to be over dependent on Offshore Windfarm (OWF) power generation. Three scenarios are simulated using the power variation and outage of the offshore windfarm. In the first scenario, the OWF produces very high power of 200MW. In the second scenario, the OWF goes into outage and in the third scenario the OWF produces a nominal power of 80MW. The converter switching and conduction losses are taken into account using the generalised converter model discussed in Section 4.4.3 with eq: (4.20) co-efficient $a = 2.88(\Omega)$, $b = 0.88(kV)$ and $c = 1.1\ (MW)$.

The re-scheduling is required through the co-ordination control in response to an event or disturbance, such as the second scenario (outage of OWF), in order to maintain pre-disturbance or desired power flow from the MTDC grid. Depending on the preferences of TSOs, the co-ordinated control can setup new references: for example, TSOs may prefer to compensate power from a generator (*Gen3*) through *VSC3* in the event of OWF outage. The co-ordinated control can calculate the compensated power reference for *Gen3* and *VSC3* by applying (C-PF) with the actual operating condition of the combined AC/DC grid. The criteria for compensation can also be decided as exact compensation (if available) for taking the system back to pre-disturbance conditions, or it could be approximate to keep the voltage just within the required profile. With pre-defined band limits in the generic Tri-band droop control implemented in C-PF, the approximate compensation can be indicated easily, and appropriate droop gains can also be determined for re-scheduling in co-ordinated control. In this study power compensation of 90MW is chosen from *Gen3* for rescheduling from the co-coordinated control.

VSC4 and *VSC5* are considered for generic Tri-band droop control implementation with three droop bands i.e. upper droop band, normal droop band and lower droop band. All other VSC stations and the AC grid operate under the same conditions as described in Section 4.7.1, and actual reference conditions are given in **Table 4-3**.

Table 4-3 *Actual operating references with rescheduling form the co-ordinated controller*

AC grid *node*	**Gen:**	**V_{AC} (p.u)**	**P_G (MW)**	**PCC type**	**VSC *stations***	**P_{VSC} (MW)**	**VSC control**
Bus1	Gen1	1.06	*slack*	PQ	VSC1	*slack*	V_{DC}-control
Bus2	OWF	1.045	200	PQ	VSC2	-200	P-control
Bus3	Gen3	1.01	34.2	PQ	VSC3	-10	P-control
Bus6	-	1.0	-	PV	VSC4	50	PV-droop
Bus7	-	1.0	-	PV	VSC5	50	PV-droop
Bus8	Gen8	1.02	35	-	-	-	-

The DC voltage levels of the VSC stations determine their droop bands, such that if the DC voltage at a particular VSC station is between high and maximum then the VSC station will operate in the upper droop band, in the normal droop band if between high and low and in the lower droop band if between low and minimum. The voltage levels for upper, normal and lower droop band for *VSC4* and *VSC5* are specified minor differences in order to highlight the different band operation. The higher voltage limit $V_{DC\,HIGH}$ of the normal band is set equal to DC voltage reference $V_{DC\,REF}$ and the lower voltage limit $V_{DC\,LOW}$ are set to –0.5% of $V_{DC\,REF}$, while the maximum and minimum voltage limits ($V_{DC\,MAX}$ and $V_{DC\,MIN}$) for the upper and lower droop band is ±2% of $V_{DC\,REF}$ respectively. The values of DC voltage for the droop bands are given in **Table 4-4**.

Table 4-4 *Voltage levels for droop bands*

VSC stations	V_{MAX} *(pu)*	V_{HIGH} *(pu)*	V_{LOW} *(pu)*	V_{MIN} *(pu)*
VSC4	1.02	1	0.995	0.98
VSC5	1.02	1	0.995	0.98

In the case studies (a)-(d), only voltage and power outputs of *VSC4* and *VSC5* are presented for simplification under three scenarios. The values for droop gains for four cases are given in **Table 4-5**.

Table 4-5 *Droop gain values of VSC4 and VSC5 for four cases*

Cases	K_{DC1}	K_{DC2}	K_{DC3}
Case(a) Droop control	20	20	20
Case(b) Dead band droop	20	0	20
Case(c) Active band droop	20	10	20
Case(d) Voltage Margin	∞ (1e10)	0	∞ (1e10)

Case (a) DC droop control:

As shown in **Table 4-5**, the droop gains (K_{DC}) are equal for all three droop bands in case (a), so the PV droop characteristics of DC droop control is linear. The PV droop characteristic of *VSC4* and *VSC5* are shown in **Figure 4:13**(a) and (b) respectively, with three different linear droop lines in the three bands according to the specified voltage levels. The DC node voltages and active powers of *VSC4* and *VSC5* in the three scenarios are shown in **Figure 4:13**(c) and (d), represented as OP_0 for the first scenario, OP_1 for the second and OP_2 for the third. In the first scenario, since there is very high power penetration from the OWF into the MTDC grid, voltages and powers at the DC *node4* and *node5* are high, so both VSC stations can be seen to operate in the upper bands of their respective PV droop characteristics. However, once there is an OWF outage in the second scenario, the voltages and powers in both VSC station drop: *VSC4* starts to operate in the lower droop band, and *VSC5* operation goes into the normal droop band of the PV droop characteristics as shown by OP_1 in **Figure 4:13**(a) and (b) respectively. In the third scenario, the OWF produces nominal power, so, as expected, the voltages and powers of both VSC stations return to the nominal values and operate in the normal droop band of the PV characteristics, shown by OP_2 in **Figure 4:13** (a) and (b).

Figure 4:14 shows the voltages and power of *VSC4* and *VSC5* under linear droop control with re-scheduling from the co-ordinated control during the second scenario i.e. OWF outage. It can be observed from **Figure 4:14** (a) and (b) that voltage profiles of both VSC station can be maintained in the upper and normal bands respectively through power compensation by the co-ordinated control.

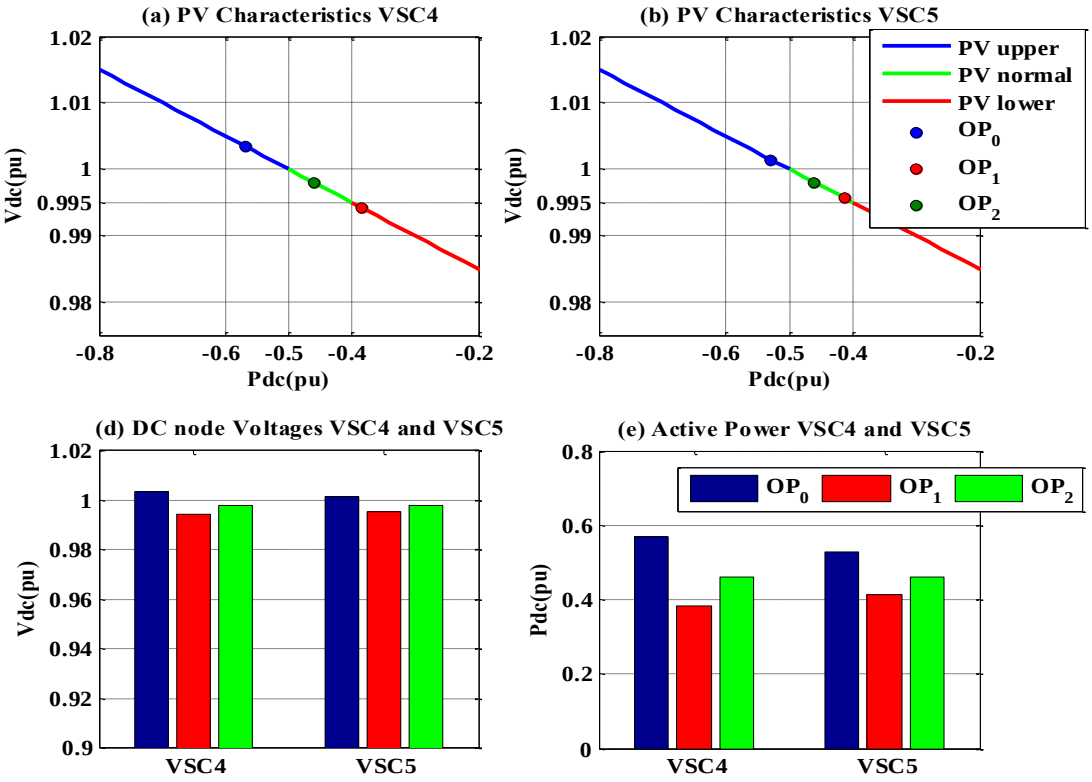

Figure 4:13 *DC Droop control operation without co-ordinated control*

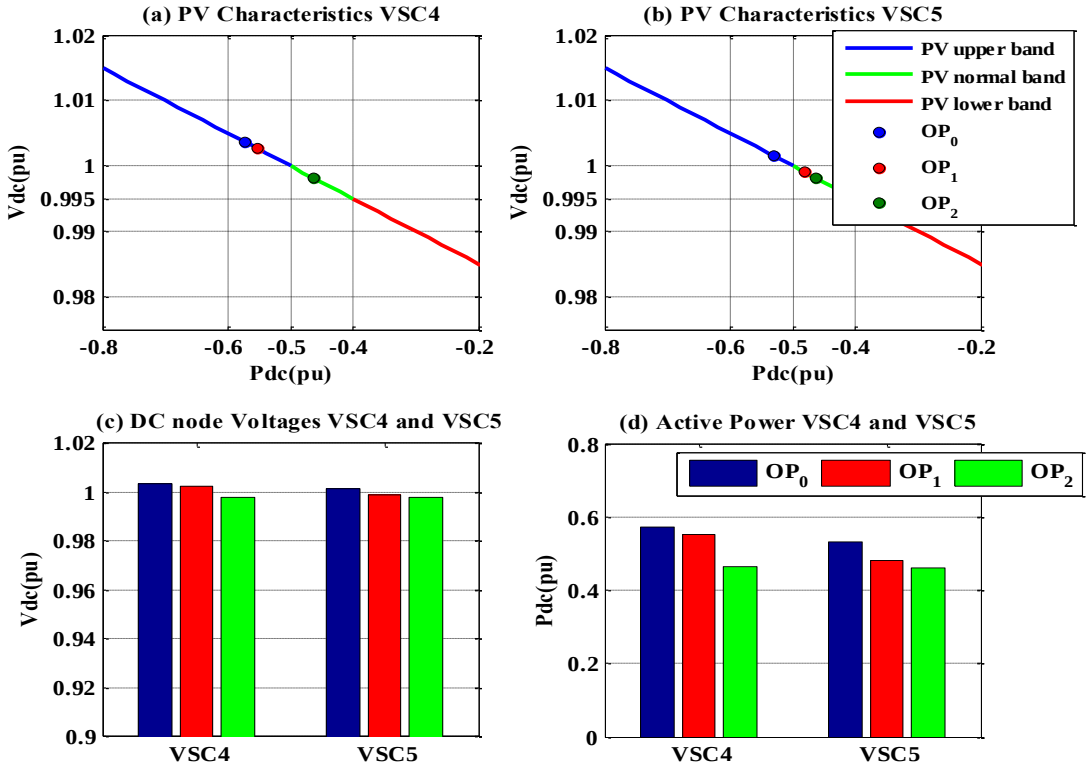

Figure 4:14 *DC Droop control operation with power compensation from co-ordinated control*

Case (b) Dead band droop control:

In case (b), the normal band droop gain (K_{DC2}) is set to zero, so the overall PV droop characteristic is non-linear. The VSC station in the normal droop band operates in constant power control. In the first scenario and second scenario, both VSC stations can be seen to operate in the upper band and lower band of their respective PV droop characteristics, similar to case(a) shown by OP_0 and OP_1 in **Figure 4:15**(a) and (b) respectively. However, in the third scenario, when the voltages of both VSC stations are in the range of the normal band, *VSC4* and *VSC5* start to operate in constant power control shown by OP_2 in **Figure 4:15**(a) and (b) respectively.

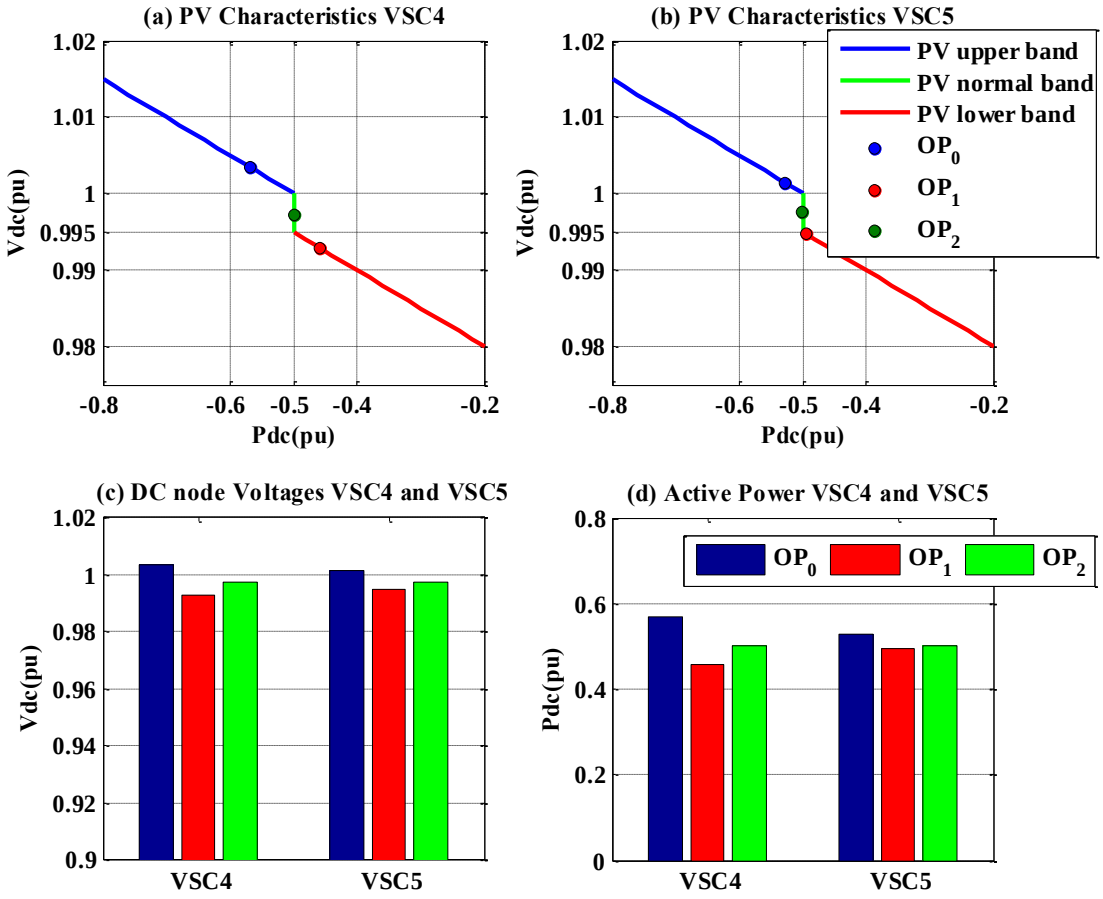

Figure 4:15 *Dead-band Droop control operation without co-ordinated control*

The voltage and power outputs after the power compensation by the co-ordinated control is shown in **Figure 4:16**. As expected, the voltage profiles of both VSC station can be improved from the lower band to the upper and normal bands under the second scenario through the power compensation by the co-ordinated control as can be seen in **Figure 4:16**(a) and (b).

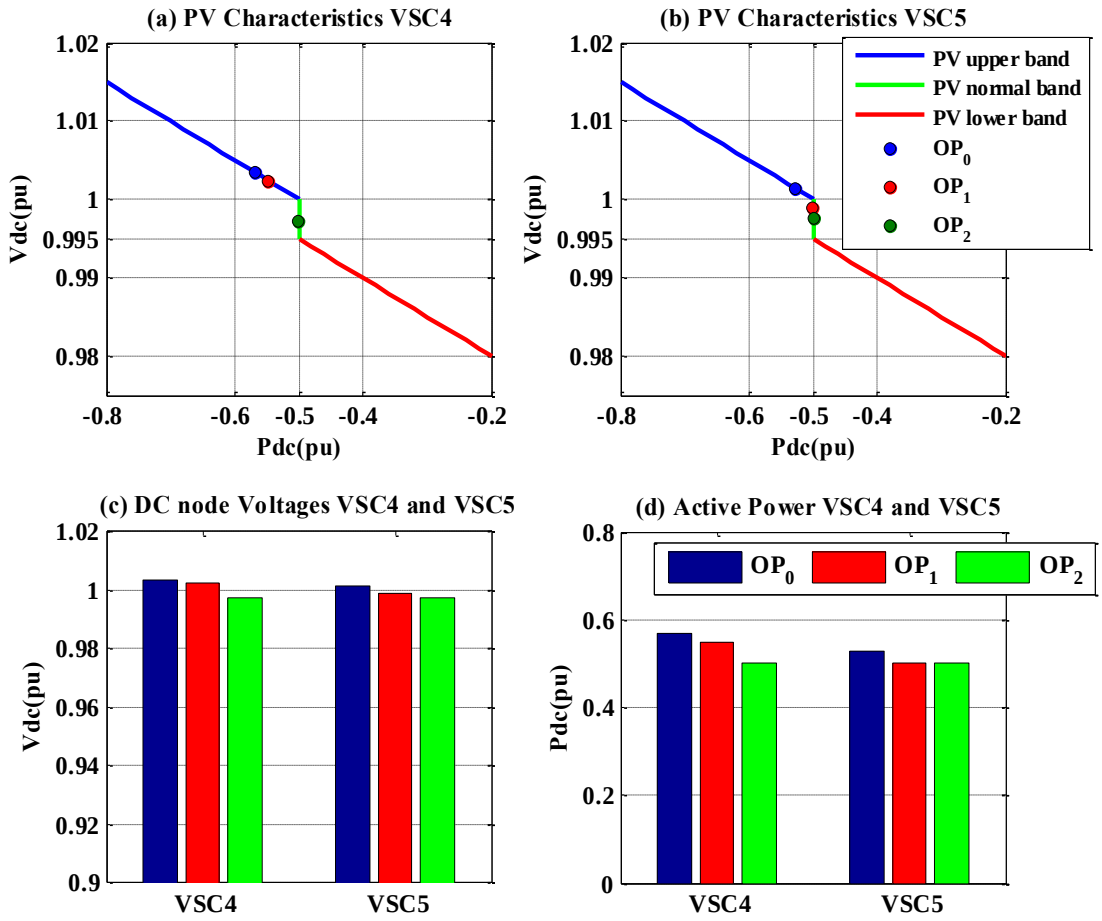

Figure 4:16 *Dead-band Droop control operation with co-ordinated control*

Case (c) Active band droop control:

In case (c), the normal band droop gain (K_{DC2}) is set to a lower value than the upper band droop gain (K_{DC1}) and the lower band droop gain (K_{DC3}), so the overall PV droop

characteristic is non-linear. The VSC station in the normal droop band operates with a smaller droop until the DC voltages are in the range of the normal band. In the first scenario and second scenario, both VSC stations can be seen to operate in the upper band and lower band of their respective PV droop characteristics, similar to case (a) and case (b) shown by OP_0 and OP_1 in **Figure 4:17**(a) and (b) respectively. However, in the third scenario, when the voltages of both VSC stations are in the range of the normal band, *VSC4* and *VSC5* start to operate with a smaller droop shown by OP_2 in **Figure 4:17**(a) and (b) respectively.

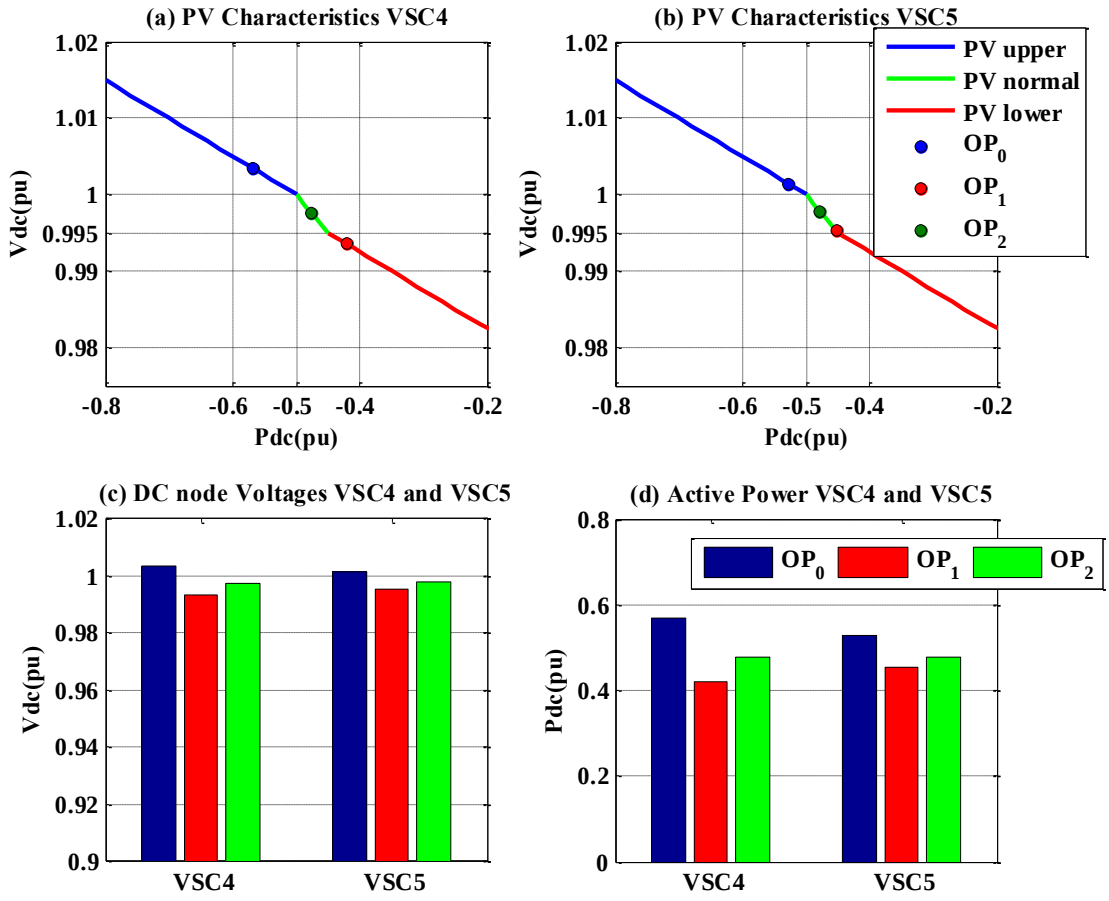

Figure 4:17 *Active band Droop control operation without co-ordinated control*

The voltage and power outputs after the re-scheduling by the co-ordinated control is shown in **Figure 4:18**. As expected, the voltage profiles of both VSC stations can be improved from the lower band to the upper and normal bands under the second scenario through the re-scheduling by the co-ordinated control as shown in **Figure 4:18** (a) and (b).

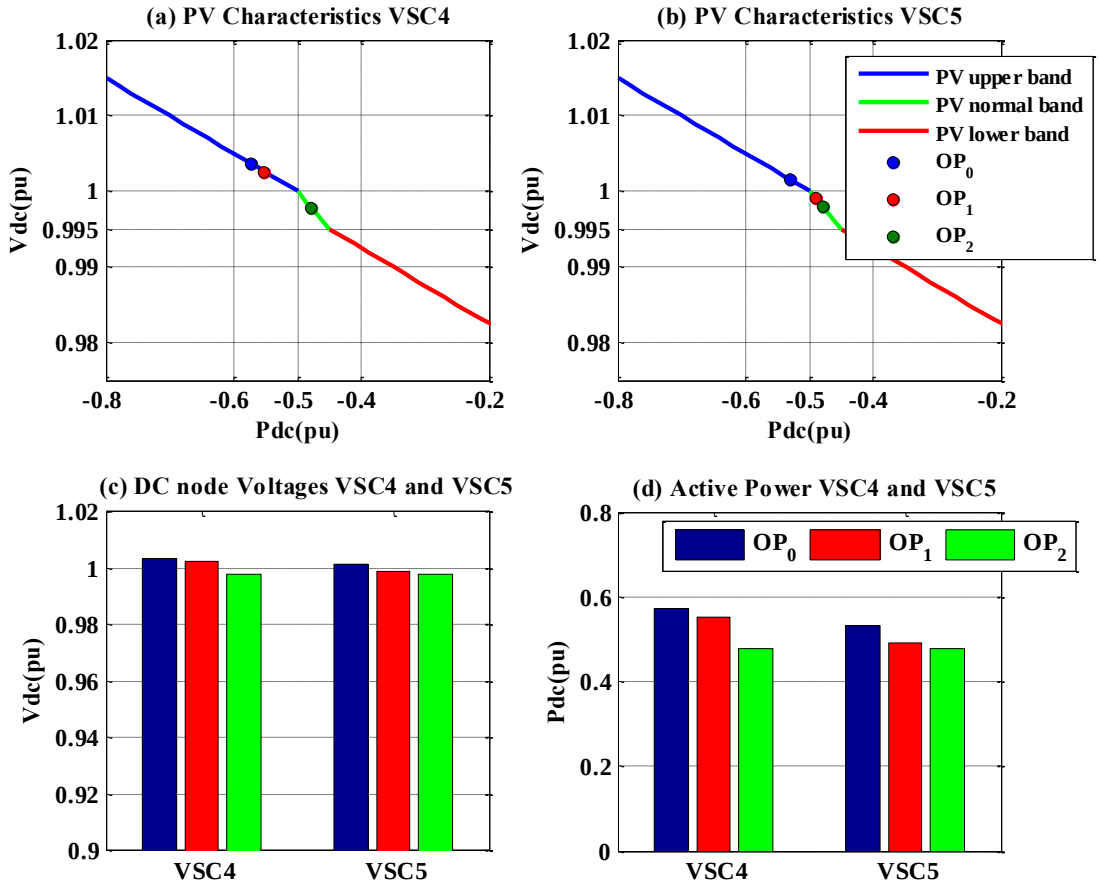

Figure 4:18 *Active band Droop control operation with co-ordinated control*

Case (d) Voltage margin control:

In case (d), the voltage margin control is implemented in two different methods. In both methods, the upper and lower band droop gains (K_{DC1} and K_{DC3}) are set to a very

high value e.g. (1×10^{10}), while the normal band droop gain (K_{DC2}) is set to zero for method1 and 10 for method 2. Method 1 is implemented in *VSC4* and method 2 in *VSC5*.

The overall PV droop characteristics for both methods is non-linear. Both the VSC stations in the upper and lower bands are set to operate in constant voltage control at high and low voltage levels respectively, while in the normal band *VSC4* is set to operate with constant power control and *VSC5* is set to operate under droop control. The **Figure 4:19**(a) shows that, in the first scenario and second scenario, *VSC4* operates in constant voltage control in the upper and lower bands of its PV characteristics, indicated by OP_0 and OP_1, while it operates in constant power control in the third scenario indicated by OP_2. The higher voltage limit of the normal band of *VSC5* is set to 0.4% of $V_{DC\ REF}$ (DC reference voltage) and the lower voltage limit of *VSC5* is set to –0.8% of $V_{DC\ REF}$ in order to avoid the hunting between the voltage controlling VSC stations. The voltages of *VSC5* remains in the range of the normal band during all three scenarios, therefore it operates under droop control shown by OP_0, OP_1 and OP_2 in **Figure 4:19**(b) without any re-scheduling from the co-ordinated controller.

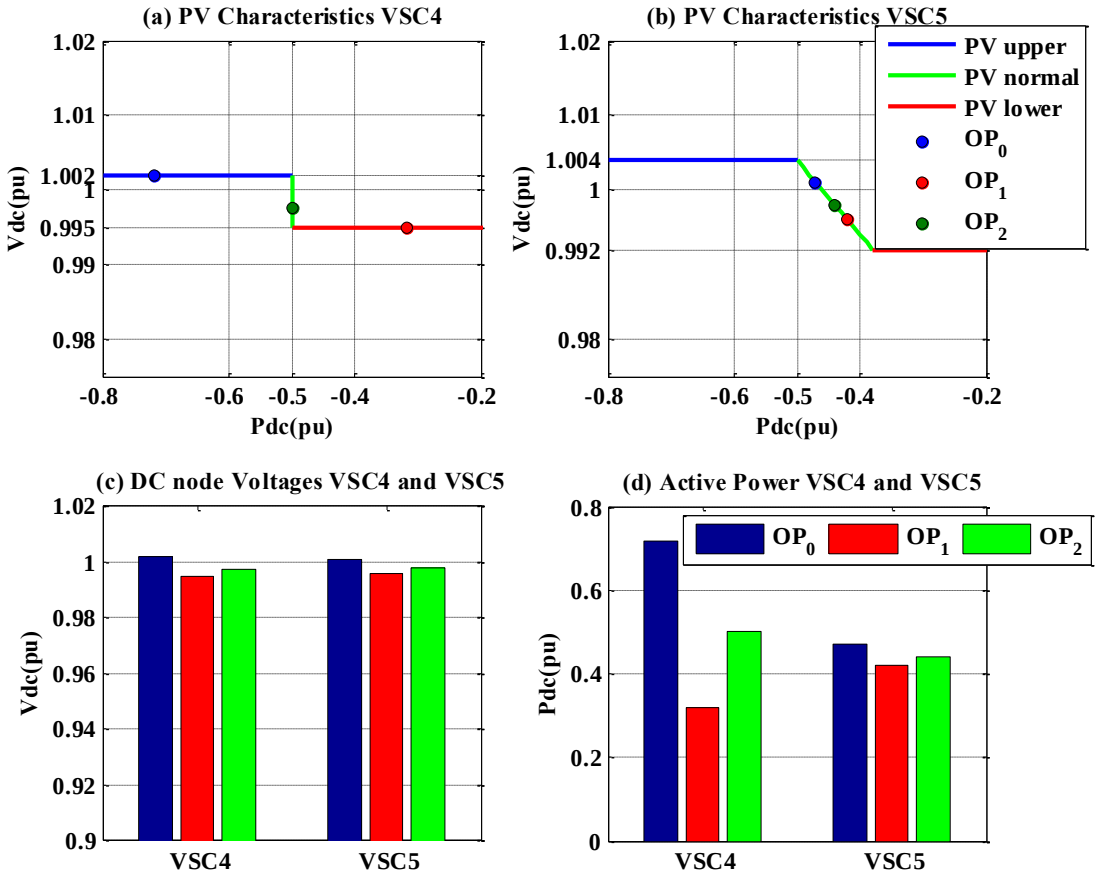

Figure 4:19 *Voltage margin control operation without co-ordinated control*

Figure 4:20 shown the voltages and power of *VSC4* and *VSC5* under voltage margin control with re-scheduling from the co-ordinated control during the second scenario. It can be observed from **Figure 4:20** (a) that the voltage of *VSC4* shifts to the upper level during second scenario (OP_1) through the power compensation by the co-ordinated control. *VSC5* maintains its operation in the normal band even after re-scheduling as shown in **Figure 4:20**(b).

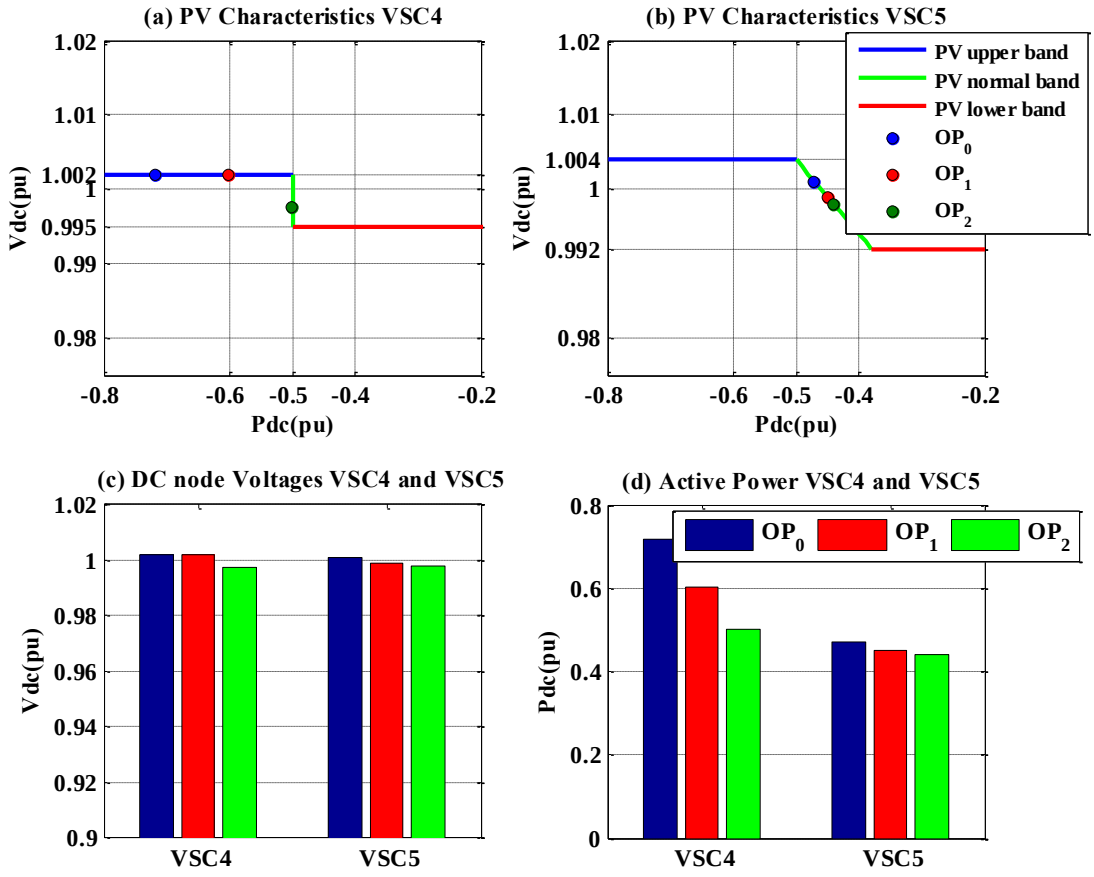

Figure 4:20 *Voltage margin control operation with co-ordinated control*

4.9 Chapter Summary

This chapter presented a co-ordinated control as a secondary control strategy for the power flow control of combined AC/DC grid operation. A combined AC/DC power flow algorithm for the solution of the combined AC/DC network is implemented in the co-ordinated control in order to obtain updated references for the VSC stations and generator units after a disturbance, without need of building a full detailed dynamic model of the combined AC/DC system. The combined power flow validation performed shows a good accuracy. The generic tri-band configuration can apply separated droop for imbalance due to the power excess and deficit in addition to the dedicated droop for normal operation, and it can adopt all major droop control

methods into the combined AC/DC power flow analysis to allow maximum flexibility for the co-ordination control.

The case studies performed show that the proposed combined power flow indicates the effects of the DC droop control on the power sharing between the combined AC and DC grids in the steady state, following a VSC station outage or other disturbance conditions, without needing to use its complete dynamic analysis. The case study results confirms that planned power flows and power deviations can be maintained by providing the updated references to the VSC station and generator units by the implementation of the proposed co-ordinated control.

CHAPTER 5

Optimal and Secure Operation of combined AC/DC system

5.1 Introduction

The rescheduling performed by the secondary control to provide the updated references to restore the DC grid to pre-disturbance conditions was discussed in Section 4.2. However, this may not be the optimal and most secure operating point for the overall integrated AC/MTDC grid. In order to ensure the optimal operating references a tertiary control system based on Combined AC/DC Optimal Power Flow (C-OPF) analysis is required. Also, the necessary security analysis needs to be performed to ensure that the optimal operating points are secure during N-1 contingencies.

The objective of this chapter is to suggest a method for the C-OPF and a Security Assessment (SA) method for the tertiary control of the combined AC/DC grid. Section 5.2 discusses the requirement of tertiary control for combined AC/DC grid operation. Section 5.3 suggests a method for the combined optimisation of the AC/DC grid, followed by Section 5.4 on a security analysis method that is suggested to determine secure and optimal operating points through tertiary control. Section 5.5 discusses the power transfer capability analysis of the MTDC grid though the proposed iterative security analysis method.

5.2 Specifications of Tertiary Control

Tertiary control is the upper layer control that enables the Security Constrained Economic Dispatch (SCED) by providing a secure and operational plan for the integrated AC/MTDC grid. This takes into account technical aspects and includes their economic constraints, according to the given objective function. It provides the optimal and secure references to both VSC stations and AC generators. The time horizon for SCED can be in the range of 20-30 minutes. The references for the VSC stations include:

- Optimal active power and DC voltage references;
- Optimal reactive power or AC voltage references.

Additionally, tertiary control may reduce and increase the DC voltage limits for the normal operating band of the Tri-band voltage control.

The tertiary control involves Optimal Power Flow (OPF) algorithms to obtain the optimal operating references according to the given objective function. Conventional OPF is essential for power system planning and operation and is applied mainly to minimise the cost of operation and losses. However, in the case of an integrated AC/MTDC grid, the security of the power system is equally as important as cost and loss minimisation, due to the fast acting power electronics devices in the MTDC grid. Consequently, in this study an iterative process for security analysis based on Optimal Power Flow (C-OPF) is suggested, which enables the achievement of an optimal operation plan along with sufficient security margin for the secure operation of the integrated system under N-1 contingency. Further, the power generation in the MTDC

grid is mainly from Offshore Windfarms (OWF), so tertiary control also needs to include stochastics of wind forecast along with load forecasts for the AC grid.

5.3 Optimal Power Flow (OPF) of AC/MTDC Grid

Combined OPF of AC/DC grid (referred as C-OPF from here onwards in this thesis) is required to evaluate the potential effects of the MTDC grid on the steady state operation of the integrated AC/DC grid. It is essential to evaluate the benefit of the MTDC grid during the planning process, and the optimal operation of the combined grid. The conventional AC OPF needs to be extended to include MTDC grid state variables and power flow equations, so this Section describes the formulation of the C-OPF for the combined AC/DC grids and Section 5.4 presents the iterative process of security analysis based on C-OPF.

5.3.1 Optimisation Modelling for Combined AC/DC System

As described in Section 4.3, there are two different approaches for the solution of combined AC/DC power flow. Similarly, C-OPF can also be solved by sequential or unified approaches. However, in combined AC/DC power flow calculations, the active and reactive power injections from the AC generators and VSC stations are taken as specified quantities in order to calculate the unknown state variables (AC node angles, AC and DC node voltages). In the C-OPF calculations, these specified quantities are regarded as the control variables to be optimised in order to achieve certain goals defined in the objective function.

In the sequential approach C-OPF solution, the control variables i.e. P_{VSC} and Q_{VSC} of the VSC stations are defined at the PCC node, and additional steps are required to

calculate the converter node power (P_C) based on the PCC injection, before the DC power flow can be solved. This increases the computational complexity of the C-OPF model. In contrast, in the unified approach the control variables can be defined at converter node C shown in **Figure 5:1**, instead of the PCC node, so that an additional step of power calculation from the converter node to the PCC node is not required.

In previous studies, OPF of combined AC/DC grids has been considered in [39]–[42], [93]–[95]. In [93] the VSC based HVDC system considered was limited to point to point connection without considering the VSC losses. In [41] C-OPF problem is converted into a convex problem by reformulating it using Second Order Cone Programing (SOCP), while [39] uses nonlinear power flow equations and proposes a unified approach to solve C-OPF taking into account a generalised loss model of the VSC station. Additional constraints and distributed DC voltage control have been considered in [94] for loss minimisation. In [40], [42] C-OPF has been considered for several different objectives. A cost benefit analysis based on C-OPF has been proposed in [95].

For the C-OPF model in this study, the steady state modelling of the VSC is the same as used for the Combined AC/DC Power Flow (C-PF) calculations covered in Section 4.4.1. The equivalent VSC representation for C-OPF is shown **Figure 5:1**. The VSC on the AC side is represented as an equivalent AC generator and on the DC side as a controlled DC voltage source. The power injections from both sources are limited by the minimum voltage limit and maximum switching current limit constraints. The AC side of the VSC has independent control of active and reactive power. The AC and

DC grids are coupled by active power exchange represented by the power flow equations, which are solved by the C-OPF model.

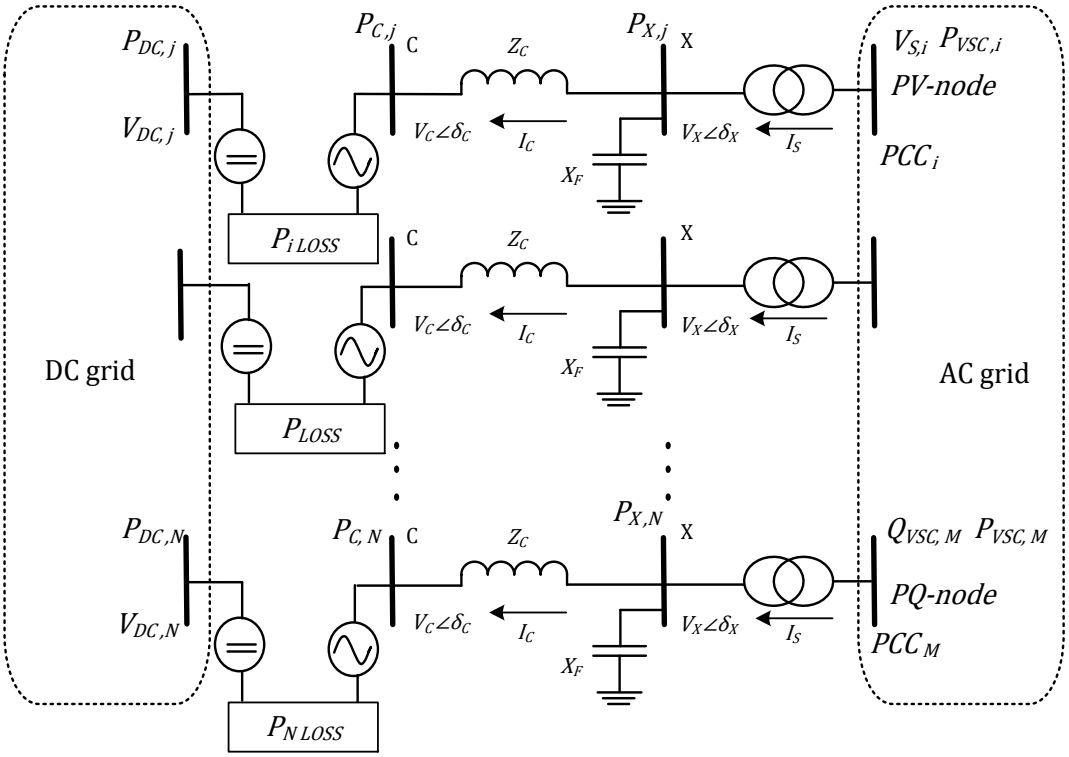

Figure 5:1 *Equivalent representation of the VSC, as a link between the AC and DC grids*

However, some additional constraints have to be considered in the C-OPF model of the MTDC system:

1) Operational constraints

The active power through all the converters should be balanced taking into account the VSC station losses. The VSC power balance equation can be given as:

$$P_{C,j} - P_{DC,j} - P_{VSC\ loss,j} = 0 \tag{5.1}$$

where,

$P_{C,j}$ is the active power at the converter node

$P_{DC,j}$ is the DC node injection

$P_{VSC\ loss,j}$ is the VSC station loss that can be calculated with the generalised quadratic polynomial loss equation as covered in Section 4.4.3 as:

$$P_{VSC\ loss,j} = a + b(I_{C,j}) + c(I_{C,j})^2 \text{ and } I_{C,j} = \frac{\sqrt{P_{c\,j}^2 + Q_{c\,j}^2}}{V_{c\,j}}.$$

2) VSC capacity constraints

The steady state operating point of the VSC must be constrained within the PQ capacity limits of the converter determined by the maximum current through the VSC switches ($I_{C,j}$) and the maximum DC voltage V_{DC} as described in Section 2.6.

$$-I_{C,jmax}V_{C,j} \leq S_{C,j} \leq I_{C,jmax}V_{C,j} \tag{5.2}$$

The DC voltage constraints of the VSC can be given as:

$$V_{DC,j\ min} \leq V_{DC,j} \leq V_{DC,j\ max} \tag{5.3}$$

Similarly, the DC current constraints through the DC cables can be given as:

$$-I_{DC,max} \leq I_{DC,jk} \leq I_{DC,j\ max} \tag{5.4}$$

5.3.2 Optimisation Formulation for Combined AC/DC System

The classical AC OPF can be written as a minimisation of a general objective function $f(x)$, with the equality constraints $g(x)$ and inequality constraints $h(x)$. The complete optimisation case can be written as:

$$min_x\, f(x) \tag{5.5}$$

$$g(x) = 0 \tag{5.6}$$

$$h(x) \leq 0 \tag{5.7}$$

$$x_{i\,min} \leq x_i \leq x_{i\,max} \tag{5.8}$$

where, x is the optimisation vector containing state variables and control variables. The state variables determine the state of the system and comprise of AC grid node angles and AC/DC grid node voltage magnitudes given by $z = \left[\delta_i,\ V_i, V_{DC,j}\right]^T$. The, control variables control the system state and include the active and reactive power injections from the generators and the VSC converters, given by $u = \left[P_{Gi}, P_{VSCj}, Q_{Gi}, Q_{VSCj}, I_{DC,j}\right]^T$. They may include ratios and phase angles of tap-changers or phase shifters or any other controlling device in the system, but they are not taken into account here in this study. If the AC grid comprises of M number of nodes and the DC grid has N numbers of nodes then $1 \leq i \leq M$ and $1 \leq j \leq N$. So the complete optimisation vector can be given as:

$$x = \left[\delta_i,\ V_i, P_{Gi}, P_{VSCj}, Q_{Gi}, Q_{VSCj}, V_{DC,j}, I_{DC,j}\right]^T.$$

As in the conventional AC OPF state vector, δ_i and V_i are the voltages and angles at each AC bus node respectively. P_{Gi} and Q_{Gi} are the power injections from the AC generators. In addition to these, the C-OPF state vector includes $P_{VSC,j}$ and $Q_{VSC,j}$

which are the AC side active and reactive power injection of the VSC along with the nodal voltages ($V_{DC,j}$) and branch currents ($I_{DC,j}$) of the DC grid.

5.3.2.1 Equality Constraints

The equality constraints take into account the non-linear active and reactive power equalities at each node of the AC and DC network. With M as the number of the AC network buses, N as the number of DC network buses, G_{AC} as the conductance matrix for the AC grid, B_{AC} as the susceptance matrix for the AC grid and G_{DC} as the conductance matrix for the DC grid, the equality constraints can be described as follows:

a) AC Equality constraints

The AC grid active power flow equations can be modified to incorporate the active power injection from the VSC:

$$P_{Gi} - P_{Li} - P_{INJ,ACi} - P_{C,j} = 0 \tag{5.9}$$

where,

$$P_{INJ,ACi} = V_i \sum_{k=1}^{M} V_k [G_{ik} \cos(\delta_i - \delta_k) + B_{ik} \sin(\delta_i - \delta_k)]$$

Similarly, the AC grid reactive power flow equations can be modified to incorporate the reactive power injection from the VSC:

$$Q_{Gi} - Q_{Li} - Q_{INJ,ACi} - Q_{C,j} = 0 \tag{5.10}$$

where,

$$Q_{INJ,ACi} = V_i \sum_{k=1}^{M} V_k [G_{ik} \sin(\delta_i - \delta_k) - B_{ik} \cos(\delta_i - \delta_k)]$$

b) DC Equality constraints

The power balance in the DC grid can be given in either linear form with current injection of each node as in eq :(5.11), or in non-linear form with active power injection at each node given by eq :(5.12).

$$I_{DC,j} - G_{DC} V_{DC,j} = 0 \tag{5.11}$$

$$P_{INJ,DCj} - \sum_{j=1}^{N} V_{DC,j} I_{DC,j} = 0 \tag{5.12}$$

5.3.2.2 Inequality Constraints

The inequality constraints for the C-OPF includes the linear and nonlinear inequalities of the AC and DC grids.

a) AC Inequality constraints

The linear inequalities constraints of the AC grid include the upper and lower bounds of the AC node angles, voltages, active power and reactive power of the generators. The non-linear inequalities includes the limits on the AC branch flow given as a function of node angles and voltages that can be written as eq:(5.13).

$$-S_{ik,max} \leq S_{ik}(\delta, V) \leq S_{ik,max} \tag{5.13}$$

b) DC Inequality constraints

The DC inequality constraints comprise of upper and lower limits of DC voltage as linear inequalities. The non-linear inequalities includes the apparent power through the VSC as given by eq:(5.14) and DC branch flows given as a function of the DC node voltages given in eq:(5.15).

$$-S_{vscj,max} \leq S_{vsc\ j} \leq S_{vscj,max} \tag{5.14}$$

$$-P_{jl\ DC,max} \leq P_{jl\ DC}(V_{DC}) \leq P_{jk\ DC,max} \tag{5.15}$$

5.3.1 Solution Method for C-OPF

The optimisation problem can be solved either by their simplified linear formulations or with full non-linear formulations as mentioned in Section 5.3.1. The solution of the simplified formulation is much faster and reduces the computational burden, however the accuracy of the results may reduce significantly and it may not be able to calculate the reactive power and voltage levels or losses in the system. The choice of optimisation solver mainly depends on the formulation of the problem, and a specific solver may be required to solve non-linear and non-convex problems, such as the interior-point method used in [40] and the second order cone method proposed in [96].

In this thesis, non-linear formulation for the C-OPF is proposed in order to obtain as accurate references as possible for optimal scheduling from the tertiary control. The *fmincon* solver in combination with the interior-point algorithm has been used to solve non-linear formulation of the C-OPF problem in this thesis. However, while using *fmincon*, a global optimal solution cannot be guaranteed, i.e. a better solution might exist. The aim here is to formulate an optimisation algorithm for the combined AC/DC grids: global optimisation is very time consuming, and is a separate field of study. A more stable optimum can be ensured if required, by running *fmincon* several times with different initial conditions.

5.3.2 Verification of the C-OPF Method

A Combined Optimal Power Flow (C-OPF) analysis is performed on the modified IEEE test network described in Section 4.7.1, using the *fmincon* solver in combination with the interior-point algorithm implemented in MATLAB. There are many objective functions that can be chosen in eq:(5.5) of the C-OPF algorithm, including minimisation of losses, cost and voltage deviations. In this study most common application of cost minimisation is applied that can be given as:

$$min_x\, f(x) = \sum_{i=1}^{ng} f_P^i\left(p_g^i\right) \tag{5.16}$$

where, $f_P^i(p_g^i)$ are the polynomials of the cost function of each generator which cab given as.

$$f_P^i\left(p_g^i\right) = Cn\, p^n + \cdots C1p + C0 \tag{5.17}$$

In order to validate the proposed procedure, the C-OPF is performed on the same test network with the upper and lower bounds of the control variables locked to the values obtained from the C-PF through the combined AC/DC algorithm in Section 4.7.2 given in **Table 5-1**. The assumptions for the modified IEEE14 bus network are kept same as described in Section 4.7.1 and *VSC2* is also assumed to be off due to a windfarm outage, in order to simplify the expected power variation from the windfarms. The arrows in **Figure 5:2** show the branch flows obtained from the power flow analysis of the test case system by the proposed procedure of the C-OPF. The C-OPF results are found to converge in 0.30s and are an almost exact match with C-PF results by only around 0.01% error. The voltage at the DC *node1* is fixed to 1pu, as it is assigned as the slack node for the DC grid (refer to Appendix A.3 for input data of modified IEEE14 bus network).

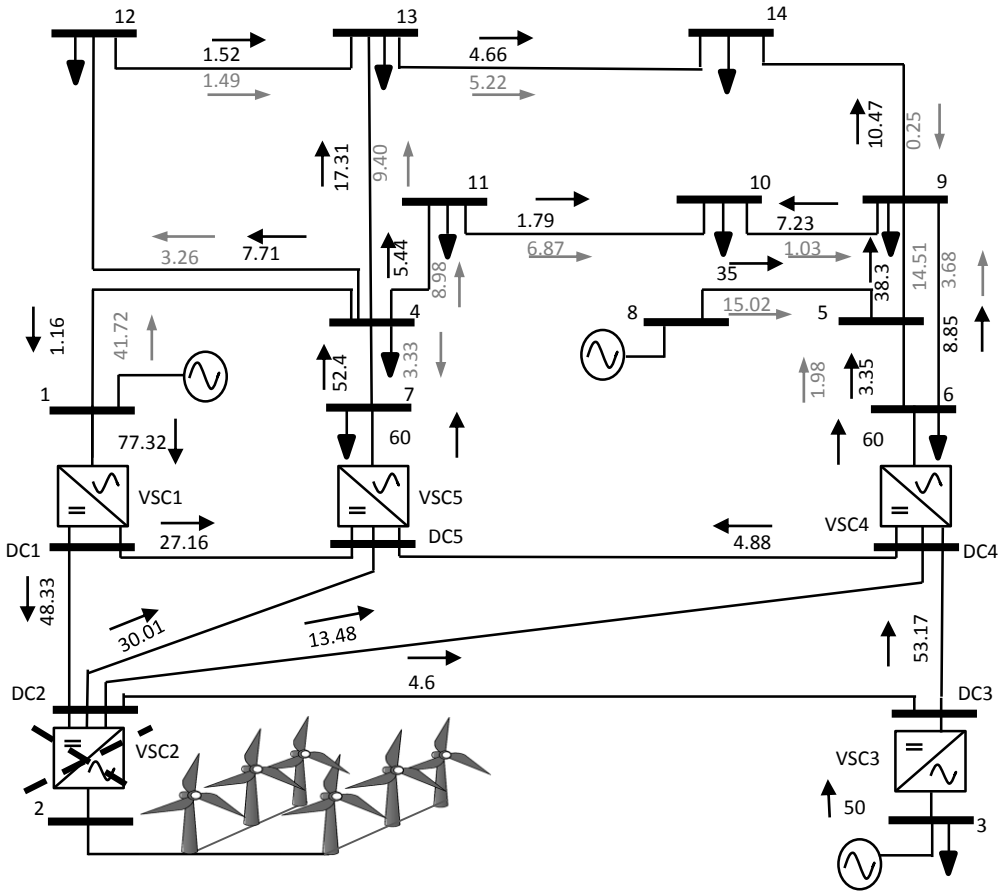

Figure 5:2 *C-OPF branch flows in modified IEEE14 test case system*

Legends: → *represents active power in MW*

→ *represents reactive power in MVar*

Table 5-1 *Fixed parameters of modified IEEE Network for C-OPF*

AC grid *node*	**Genera -tion**	**P_G (MW)**	**Q_G (MVAr)**	**VSC *stations***	**P_{VSC} (MW)**	**VSC control *PCC type***
Bus1	Gen1	*slack*	-	VSC1	*slack*	V_{DC}-Q
Bus2	OWF	0.0	0.0	VSC2	0.0	P-Q
Bus3	Gen3	74.2	19	VSC3	-50	P-Q
Bus6	-	-	-	VSC4	60	P-V
Bus7	-	-	-	VSC5	60	P-V
Bus8	Gen8	35	15.02	-	-	P-V

Further, a comparison of the optimised cost operation in the two cases i.e. base case of the locked variables and without locked variables is also performed to evaluate the effect of optimisation. The **Table 5-2** shows the cost of generation can be reduced by 221 $/h by performing the optimisation of combined AC/DC grid with the proposed C-OPF algorithm.

Table 5-2 *Comparison of the cost of generation*

C-OPF	Cost function ($/h)	Cost difference ($/h)
Base case	3966.8	221.0
Optimised case	3745.8	

5.4 Operational Security Analysis of Combined AC/DC System

Security of the combined AC/DC system operation is equally important as cost minimisation or loss reduction. Due to involvement of fast reacting VSCs and the stochastic energy generation from the offshore windfarms (OWF), security analysis of combined AC/DC grid operation has become indispensable. The security has a cost, and higher security levels usually have higher costs. Finding a secure and optimal operating point is a new challenge for tertiary control instead of considering only minimal cost dispatch. The security criterion for an AC grid is usually N-1 i.e. the system should be able to operate safely without overloading any equipment in the event of failure of any component in the power system. When combined operation of the AC/DC grid is planned, it is necessary to take into account the contingencies on both AC and DC systems. However, it is not clear that the N-1 criterion is to be considered for both AC and DC grids separately or as a meshed single system. Since the purpose of this study is to implement tertiary control for a combined AC/DC grid, the N-1 security criterion is considered for the complete integrated system.

The main limitation of the C-OPF when applied to tertiary control is that it focuses on the optimisation of a single configuration of the combined system, while the Transmission System Operator (TSO) has to identify, how robust the system is against the credible (N-1) contingencies. A significant amount of the equipment for an offshore DC grid may have high risk of failure, which can lead to instability if not taken into account during the operational planning of the integrated system. An iterative process of security analysis based on C-OPF is suggested, that enables a TSO

to achieve the optimal operation plan along with sufficient security margin for the secure operation of the integrated system under credible contingencies.

5.4.1 Security Control and Optimisation Method for Combined AC/DC System

Security control is a very important task for the TSO in order to ensure the optimal and secure operation of the power system. For an AC grid, Security Constrained Optimal Power Flow (here onwards referred as SCOPF) is usually used for SCED. SCOPF is an extension of OPF that guarantees the secure operation of the system with minimal generation cost under normal operation but also in the case of any contingency state due to any equipment failure. Two major approaches, preventive and corrective, have been suggested for implementation of SCOPF in the literature.

The detailed execution of SCOPF for an AC grid is proposed in [97], [98] presents its present day applications, while a detailed explanation of its state-of-art, challenges and forth-coming trends are given in [99]. In [100] SCOPF is extended to obtain the least cost of security by post-contingency control of VSC based HVDC line extensions. The studies of Combined AC/DC grid Security Constrained Optimal Power Flows (C-SCOPF) are also presented in [101]–[104]. The author in [101] presents preventive and corrective formulation for C-SCOPF using a linearised model of the AC/DC grid and the same author has extended it to probabilistic C-SCOPF with stochastic infeed to consider wind power variations in [103]. In [102] a linear current distribution method is proposed for correction control lines. A full C-SCOPF using a nonlinear model of AC/DC lines, including the DC-DC converter, is proposed in [104]. Reliability assessment of the combined AC/DC grid has been performed in

[105] considering high wind penetration and spinning reserves, and a tool for C-SCOPF study is also suggested. A new method of Risk Based Security Constrained Optimal Power Flow (RB-SCOPF) is suggested for the AC grid in [106].

However, as described in [99], SCOPF problem formulation in the general form is a non-linear, non-convex, large-scale static optimisation problem. The challenge for SCOPF is the size of the problem when large networks are considered with many contingencies. The direct solution of the SCOPF for a large network is non-linear and requires unrealistically huge computing power when considering all possible contingencies simultaneously. Different size reduction techniques to solve this problem have been proposed such as:

- Iterative contingency selection scheme,
- Bender decomposition,
- Linearisation of post contingencies,
- Network compression.

In this study, an iterative procedure for security analysis is proposed to overcome the computation complexity of the full non-linear model by combining the C-OPF with the Steady State Security Assessment (SSSA) method. The purpose of this study is to highlight the importance of considering security constraints for the optimisation at tertiary control rather than proposing an accurate tool for the C-SCOPF to determine the cost of security. The proposed security analysis process is used for Security Constrained Economic Dispatch (SCED) and secure transfer capacity computation of the MTDC grid, since its role has become even more important in dealing with uncertainties during operational planning by the TSOs.

5.4.2 Proposed Security Assessment Process for Combined AC/DC System

In the iterative process of security assessment, first of all a base case scenario is optimised by applying the C-OPF algorithm suggested in Section 5.3 to obtain an optimised plan, and then all feasible contingencies are applied one-by one instead of adding a number of constraints to the actual OPF formulations. A C-PF suggested in Section 4.6 is applied to check for any limit violation after each contingency. If any limits are violated, decision based rules can be initiated and C-PF is repeated to that particular contingency. The major constraint violations include the transmission line overloads, bus voltage limit violations and real and reactive generation limit violations. The decision based rules can be formulated according to the type of constraints violation, such as controlling the reactive power form nearest available source to remove the voltage drop violation at specific bus. The security constrained analysis is performed at tertiary control only, primary and secondary control are not involved. The tertiary control performs security assessment process to check the constraint violations and take corrective action, for example, if voltages at some buses are under the minimum limit then tertiary control can change the AC grid voltage point of the nearest VSC station in PV control to add reactive compensation. Once all feasible contingencies are applied, the optimal plan obtained will be secure and it can be implemented for SCED in the tertiary control. The new reference set points are sent to secondary and primary control. However, the limiting side of this process is that cost of security cannot be obtained. The flow chart of the proposed security assessment is shown in **Figure 5:3** and the basic steps for the iterative process can be given as:

Step 1) Develop a base case scenario with forecast OWF connected through the MTDC grid, generation and load demand of the combined AC/DC system.

Step 2) Solve the C-OPF for the base case to obtain the optimal operating plan of the system with the algorithm proposed in Section 5.3 for any defined objective, i.e. cost minimisation, loss minimisation etc.

Step 3) Prepare a list of feasible contingencies and start applying them one-by-one. Set counter $i=1$. Here, feasible contingencies refer to those contingencies that do not result in isolation of any generators or loads in the combined AC/DC system.

Step 4) Solve the C-PF and check if the optimal operating condition is secure for the contingency *i.* If it is, then increase counter. If it is not, then apply some decision based rule to mitigate the contingency. For example, if voltages at some buses are under the minimum limit then add reactive compensation by nearest PV controlled converters.

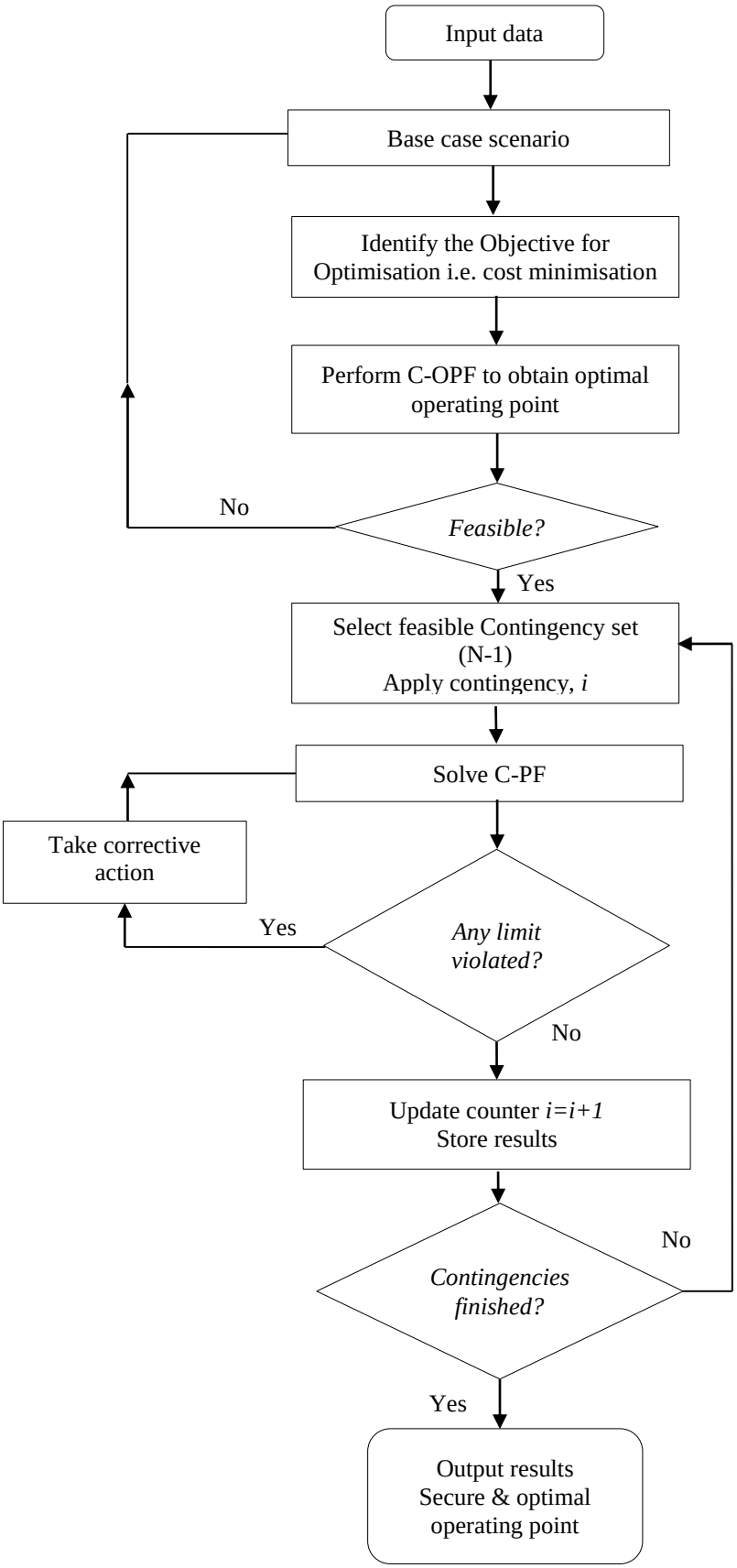

Figure 5:3 *Flow chart for proposed iterative security assessment method*

5.4.3 Comparison of Optimal Plan With and Without Security Assessment

A case study was performed on the modified IEEE test network described in Section 4.7.1 to show the importance of considering security constraints for the optimisation of the tertiary control. The test network was solved for minimised cost of generation with 50 MW of generation from the OWF. A feasible optimal plan obtained from the C-OPF could be used for the operation planning at tertiary control level to provide optimal references to generators units of the AC grid and converter stations of the DC grid shown in **Table 5-3**.

Table 5-3 *Optimal reference for operational planning in tertiary control*

AC grid ***node***	**Genera -tion**	**V_{AC} (p.u)**	**P_G (MW)**	**Q_G (MVAr)**	**VSC** ***stations***	**P_{VSC} (MW)**	**Q_{VSC} (MVAr)**	**V_{DC} (p.u)**
Bus1	Gen1	1.025	16.71	9.74	VSC1	22.09	6.89	1.00
Bus2	OWF	1.06	50	-1.75	VSC2	-50	1.75	1.0025
Bus3	Gen3	1.06	49.82	11.91	VSC3	-25	7.09	1.0017
Bus6	-	1.034	-	-	VSC4	30.10	15.47	1.0004
Bus7	-	1.023	-	-	VSC5	17.04	7.50	0.9995
Bus8	Gen8	1.06	67.71	25.4	-	-	-	-

Further, a security assessment was performed against all feasible contingencies without any corrective actions made to the optimal plan. **Figure 5:4** shows the voltage profile of six critical buses under six credible contingencies. It can be observed that voltages at the critical buses fall well below the ±6% voltage regulation limits (supposed for this test network) during four contingencies.

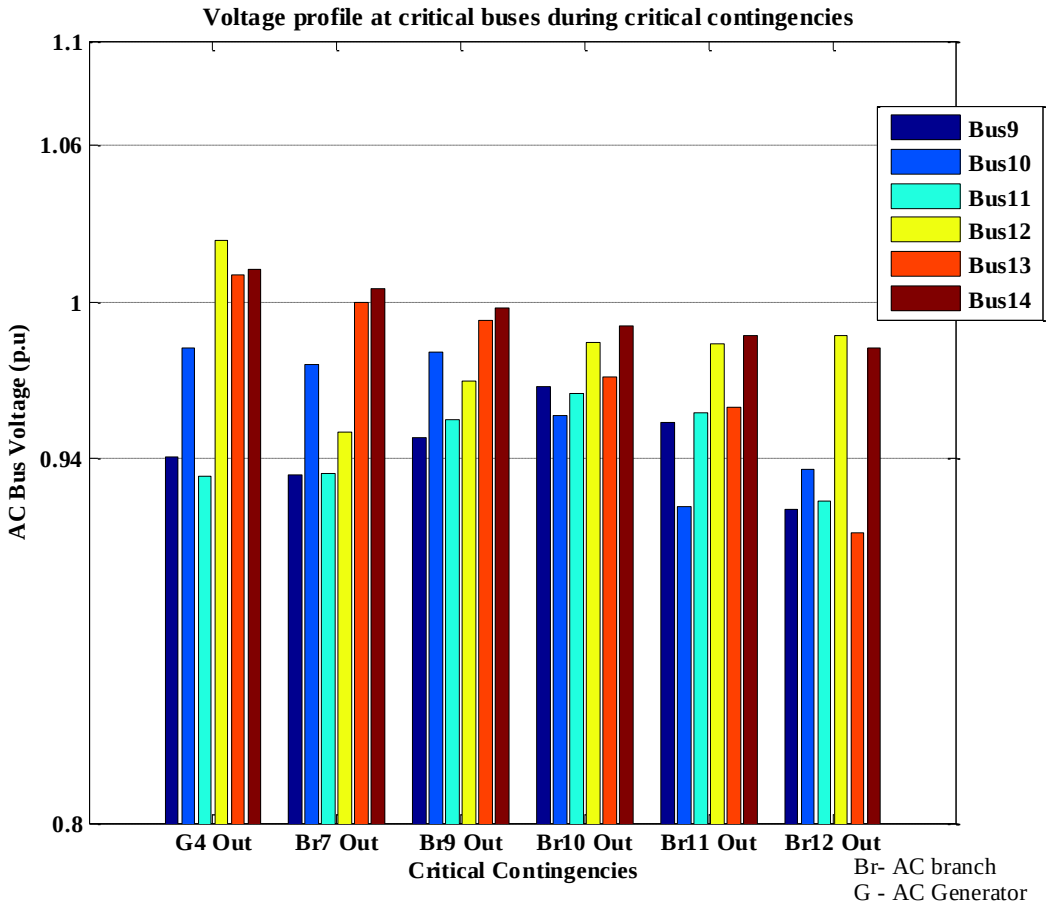

Figure 5:4 *Voltage profile of critical buses under critical contingencies without corrective actions during proposed security assessment*

It is assumed, in the decision-based rules that, if there is a drop in the voltage, then the set point of the PV controlled VSC stations can be increased to provide reactive power compensation. A secure optimal reference plan for tertiary control is given in **Table 5-4**, when the complete iterative process of security assessments proposed in Section 5.4.2 is applied with the required corrective actions. **Figure 5:5** shows the voltage profiles at the same buses under the same contingencies. It can be clearly observed that by increasing reactive power from *VSC4* and *VSC5* during the contingencies the voltage profile at all the critical buses can be maintained within the prescribed constraints of ±6% voltage regulation by the proposed iterative security assessment method.

Table 5-4 *Secure and Optimal reference for operational planning in tertiary control*

AC grid *node*	**Genera -tion**	**V_{AC} (p.u)**	**P_G (MW)**	**Q_G (MVAr)**	**VSC *stations***	**P_{VSC} (MW)**	**Q_{VSC} (MVAr)**	**V_{DC} (p.u)**
Bus1	Gen1	1.04	16.71	7.32	VSC1	22.09	6.89	1.00
Bus2	OWF	1.06	50	-1.75	VSC2	-50	1.75	1.0025
Bus3	Gen3	1.06	49.82	11.91	VSC3	-25	7.09	1.0017
Bus6	-	1.05	-	-	VSC4	30.10	19.13	1.0004
Bus7	-	1.05	-	-	VSC5	17.04	11.75	0.9995
Bus8	Gen8	1.06	67.71	19.46	-	-	-	-

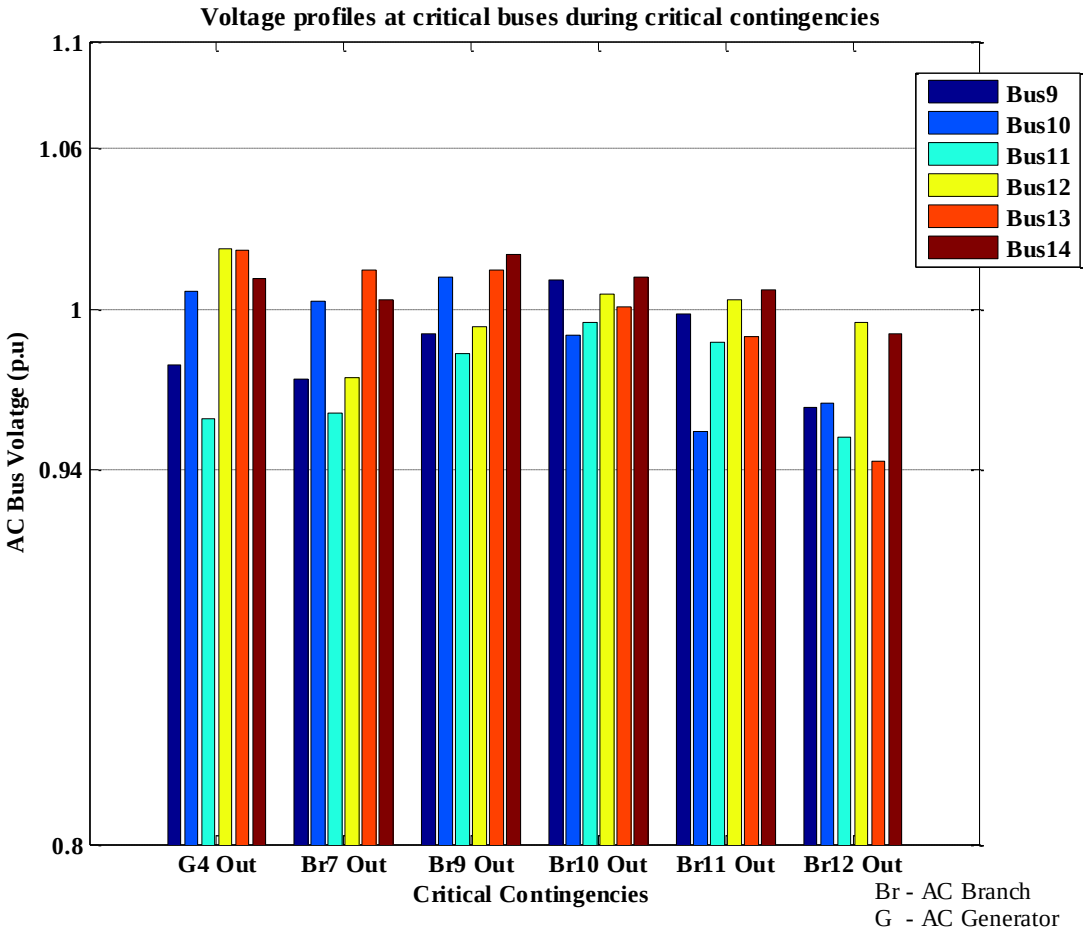

Figure 5:5 *Voltage profile of critical buses under critical contingencies with corrective actions during proposed security assessments*

Table 5-5 shows the cost of security by comparing the cost function values before and after security assessments. It can be observed that cost of security is almost negligible in this case, as optimisation is performed taking into account active power cost only which in this case accounts for only losses due to reactive power flow.

Table 5-5 *Generation cost comparison before and after security assesments*

C-OPF	Cost function ($/h)	Cost difference ($/h)
Optimised case without Security Assessments	3766.3	0.1
Optimised case with Security Assessments	3766.4	

5.5 Power Transfer Capacity Analysis of Combined AC/DC System

Power transfer capacity is another important quantity for the operational planning of the combined AC/DC system concerning system security. It indicates the amount of power that can be transmitted from one point to another point in a transmission network. The ability of the system to accommodate more inter-area power transfers can be a rough indicator of system security, especially concerning to the DC grid, which has been proposed for capturing primary power from the OWF and interconnecting different AC grids. Another benefit of knowledge regarding the power transfer capacity of the integrated DC grid could be the indication of its reliability and economic efficiency when considering alternative transmission expansion.

5.5.1 Power Transfer Capacity Analysis of MTDC Grid

One of the major benefits of integrating OWFs and interconnecting different AC grids through a MTDC grid is the potential for improved reliability. For example, the power output variations from OWF or loss of generation at any interconnected AC grid can be replaced by the generation from other AC grids. Overall, an interconnected system can endure the contingencies that isolated systems cannot survive.

A power transfer capacity analysis is performed using the proposed iterative process suggested in Section 5.4.2 on the modified IEEE test network (described in Section (4.7.1)) with parameters defined in **Table 5-4** for secure and optimal operation of the combined AC/DC grid. Within the DC grid, *VSC2* and *VSC3* are selected as sources and *VSC4* and *VSC5* are regarded as sinks, whereas *VSC1* can be either source or sink depending on whether it is acting as a source or a load. Therefore, if *VSC1* acts as a load the total power transfer from sources to sinks can be given as:

$$P_{MTDC} = P_{21} + P_{25} + P_{24} + P_{34} \tag{5.18}$$

Similarly, if *VSC1* is acting as a source the total power transfer from source to sinks can be given as:

$$P_{MTDC} = P_{15} + P_{25} + P_{24} + P_{34} \tag{5.19}$$

The power transfer capability is calculated after each possible contingency to determine whether the DC grid can survive the contingencies and is capable of transferring the required power in the event of possible outages without violating the security constraints. The power transfer through the MTDC grid without any outage

is found to be 73 MW. The power transfer corresponding to each outage is shown in **Figure 5:6** and **Figure 5:7**. The power transfer is reduced as shown in **Figure 5:6**(a) during the outages of G2 (integrated OWF) and G3, which is acting as an interconnected AC grid. Similarly, with the converters VSC1, VSC2 and VSC3 being source converters their respective outages reduce the power transfer through the MTDC grid as shown in **Figure 5:7**(b). However, due to both AC and DC grids being meshed systems, the outage of any single branch does not cause power transfer reduction through the MTDC grid as shown in **Figure 5:6**(b) and **Figure 5:7**(b) respectively.

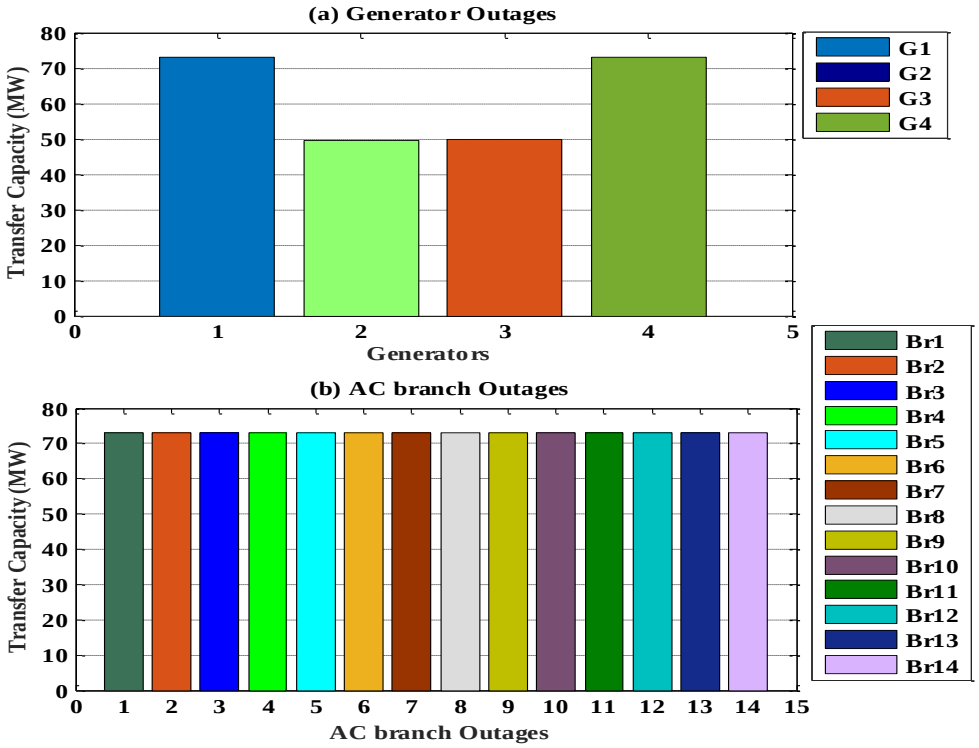

Figure 5:6 *Power transfer through the MTDC grid during outages of generators and AC branches*

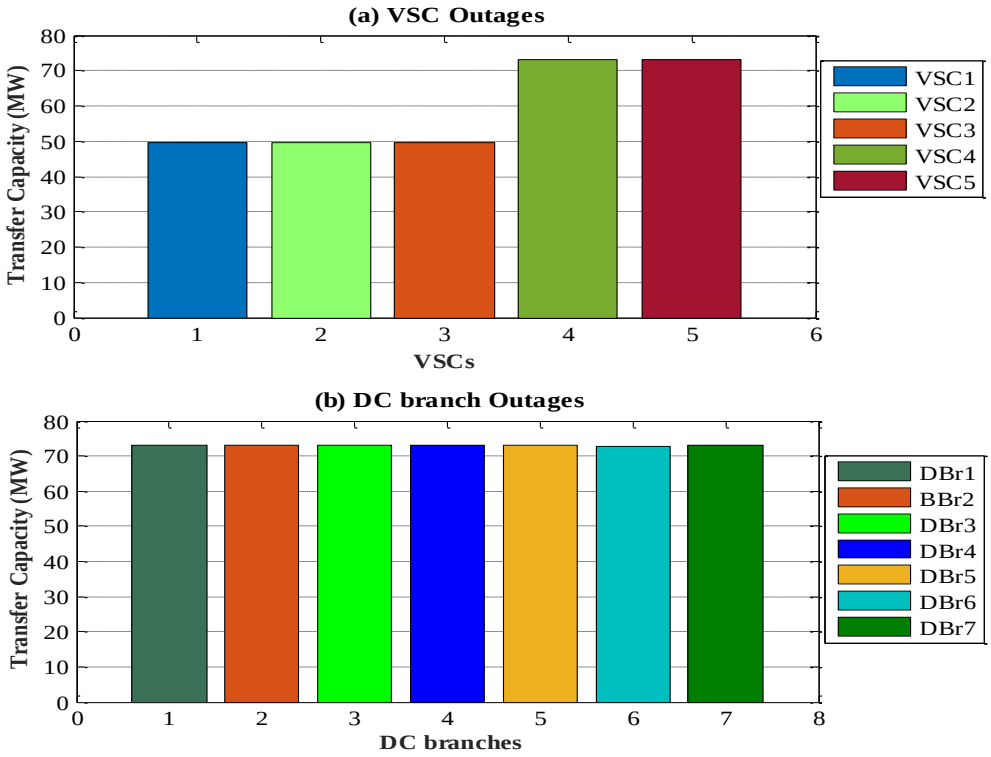

Figure 5:7 *Power transfer through the MTDC grid during outages of VSCs and DC branches*

5.5.2 Security Margin of the MTDC Grid

The power transfer capability analysis performed in Section 5.5.1 can be extended to determine the security margin of the MTDC grid that can be used for the real time security analysis of the combined AC/DC grid. Security margin is the measure of how much additional power a system can transfer without compromising the security of the system. Thus, an operator can determine that in certain circumstances preventive or corrective measure would be effective or not. A secure transfer capability can be determined based on the output from the OWF and generation schedules.

In order to measures the security margin the proposed iterative security analysis process flow chart shown in **Figure 5:3** is repeated by increasing the OWF output until any of the constraints formulated in C-OPF are violated. **Figure 5:8**(a) shows

the transfer capability estimation of two states of the network under all possible credible contingencies, whereas **Figure 5:8**(b) shows the difference of power between the two states, called the security margin.

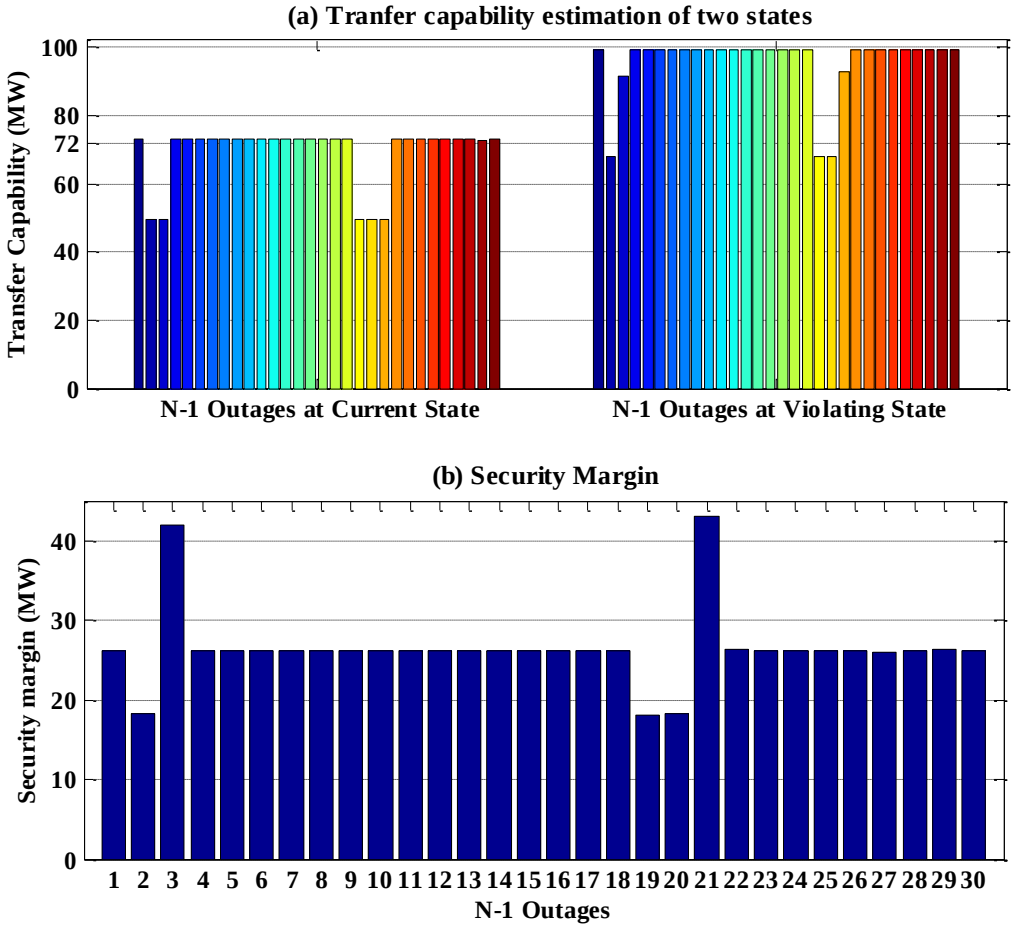

Figure 5:8 *Security margin estimation*

5.6 Chapter Summary

In this chapter, the requirement for tertiary control acting as the upper level control to provide an operational plan for integrated AC/MTDC grid operation is discussed. An optimisation method for C-OPF is proposed to obtain the optimal operating references according to the given objective function. Further, it is observed that the security of the combined AC/DC grid operation is equally important as economical operation.

Therefore a simplified iterative process for security assessment based on C-OPF is suggested, which enables the achievement of the optimal operation plan along with sufficient security margin for the secure operation of the integrated system under credible contingencies. The comparison of the optimal plans with and without security assessment shows that if tertiary control provides an optimal plan on which security assessments with corrective measure is performed, then secure operation of the combined system can be maintained during the contingencies.

Finally, a power transfer capability analysis of the MTDC grid is performed with the proposed security assessment method to determine the potential improved reliability of the combined AC/DC grid. Different contingencies performed in the case study shows that the MTDC grid can transfer the required power and the system can survive through credible (N-1) contingencies. Transfer capability analysis is extended to estimate security margins.

CHAPTER 6

Conclusions and Future work

6.1 Conclusions

The research work of this thesis started with the objective of developing an operational strategy for the secure and optimal operation of integrated AC/MTDC meshed grids, citing the plans for a large offshore MTDC grid as proposed for the North Sea and the Scotland-Shetland offshore hub. The basic principles of the well-established three-layered AC grid control is employed to identify the power balancing, coordination and dispatch requirements of the DC grid. Appropriate control methods are proposed for primary, secondary and tertiary control layers in order to accomplish the identified requirements for the secure and optimal operation of combined AC/MTDC grids.

Firstly, a comparison study was performed on different power balancing controls to find the most suitable control method for the primary control of the meshed DC grid. Secondly, the combined AC/DC grid power flow method is proposed to provide updated references for the VSC station in order to maintain coordinated power flow control under the secondary control layers. Finally, a security constraint optimisation method for the combined AC/DC grid is proposed for economic dispatch under the tertiary control layer of the three-layered hierarchal control.

A number of case studies were performed to implement the proposed control methods on a combined AC/DC test case network. The performance of the proposed control methods is validated in a hierarchical control structure for the secure and optimal

operation of integrated AC/MTDC grids. The conclusions obtained from this research work can be grouped into the following three main areas:

1) MTDC grid control
    - It can be concluded from the comparison of six different DC voltage control configurations for both normal and disturbed operation that some configurations have advantages over others for one criteria and disadvantages for the other criteria. A mix of different control configurations may need to be implemented for the MTDC grid according to the actual operating condition or the preferred operation of each VSC station. The most generic control configuration, tri-band droop control, is found to be attractive for the Primary control of the AC/MTDC grids.
2) Combined AC/MTDC modelling
    - An Analytical expression has been implemented that enables a generic tri-band droop application in the C-PF algorithm which can adopt any other control configuration.
    - The C-PF algorithm with tri-band droop implementation can provide an indication of the exact operating point of each VSC station under any voltage control configuration for the co-ordination control, without running the full dynamic model of the combined system.
    - A simplified iterative process for security analysis based on Optimisation Power Flow (C-OPF) has been formulated, which enables the optimal operation plan to be achieved with sufficient security margin for the secure operation of the integrated system under all credible contingencies.
3) Combined AC/MTDC Operation

- The Primary control with various DC droop controls is able to respond to any power imbalance caused by disturbances i.e. load/generation changes or outages.
- The case study results confirm that planned power flows and power deviations can be managed by providing the re-scheduling (updated references) to the VSC station and generator units by the implementation of the proposed co-ordinated control.
- Co-ordination control enables the Independent System Operator (ISO) or Transmission System Operator (TSO) to choose the percentage limits of the voltage and power regulation for the normal operation of each VSC station.
- It is observed that security of the combined AC/DC grid operation is as equally important as economical operation. The comparison of the optimal plan with and without security assessment shows that security assessments performed on the optimal plan in the tertiary control provides the optimal references for dispatch, which is secure under all credible contingencies.
- Finally, a power transfer capability analysis of the MTDC grid is performed with the proposed security assessment method to determine the potential improved reliability of the combined AC/DC grid. Different contingencies performed in the case study show that the MTDC grid can transfer the required power and the system can survive through the major contingencies. Transfer capability analysis can be extended to estimate security margins.

6.2 Future Work Emerging from This Research

- The tertiary control could be employed with more advanced C-OPF techniques based on a global optimisation method such as Evolutionary Algorithms (EA) to avoid the risk of selecting local optima at tertiary control level.
- The iterative security assessment can be further developed with some fast computation methods for the security constrained optimisation based on decomposition algorithms. Further, contingencies can also be ranked with risk indices according to their severity and likelihood to provide the Risk-Based Security Constrainted Dispatch (RB-SCED) at tertiary control level. However, this requires suitable impact definitions and contingency probability, which is usually obtained from previous operation experience. Consequently, it may requires more maturity in the operation of the MTDC grids.
- The application of various power control devices such as DC-DC converters into MTDC grids is being suggested in some references. The C-PF algorithm can be extended to include the mathematical model of these devices, in order to include their effects and control for the co-ordinated control.
- The C-OPF algorithm can be extended to include the generic tri-band droop as implemented in the C-PF, in order to include the effects of the droop control at the tertiary control. Similarly, the models of the power control devices should also be included into the C-OPF algorithm.
- The application of energy storage devices in the MTDC grid can offer a number of benefits for the stable operation and reliability of the grid. The appropriate representation of these devices in the C-PF and C-OPF algorithms

can enable the secondary and tertiary control to include the short-term response of the energy storage devices for the corrective rescheduling.

- The ownership of the MTDC grid can have an impact on the integrated AC/MTDC grid operation. The combined AC/MTDC operation may be managed by various interconnected TSOs. It is also possible that an Independent System Operator (ISO) can own and operate the MTDC grid in co-ordination with interconnected TSOs. The various operational and planning issues need to be considered for the ownership decision of MTDC grid.

References

[1] NSTG, "North Sea Transnational Grid project." [Online]. Available: http://www.nstg-project.nl/project/introduction/. [Accessed: 20-May-2015].

[2] Gov.scot, "North Sea Grid Development." [Online]. Available: http://www.gov.scot/Topics/Business-Industry/Energy/Infrastructure/north-sea-grid. [Accessed: 20-May-2015].

[3] FOSG, "Friends of the Supergrid." [Online]. Available: http://www.friendsofthesupergrid.eu/. [Accessed: 20-May-2015].

[4] EWEA, "European Wind Energy Association." [Online]. Available: http://www.ewea.org/. [Accessed: 20-May-2015].

[5] Airtricity, "European Offshore Supergrid Proposal: Vision and Executive Summary," 2010.

[6] Windpoweroffshore, "Tennet sells stake in DolWin3 grid connection." [Online]. Available: http://www.windpoweroffshore.com/article/1281084/tennet-sells-stake-dolwin3-grid-connection. [Accessed: 20-May-2015].

[7] CORE, "Centre for Offshore Renewable Engineering." [Online]. Available: http://www.nce.co.uk/Pictures/web/n/e/p/Round_3_sites.jpg. [Accessed: 20-May-2015].

[8] T. McNichol, *AC/DC: The Savage Tale of the First Standards War*. Jossey-Bass A Wiley Imprint, 2006.

[9] J. Reeve, "Multiterminal HVDC Power Systems," *IEEE Trans. Power Appar. Syst.*, vol. PAS-99, no. 2, pp. 729–737, 1980.

[10] F. Mazzoldi, J. P. Taisne, C. J. B. Martin, and B. A. Rowe, "Adoption of the Control Equipment to Permit 3-Terminal Operation of the HVDC link between Sardinia, Corsica and Mainland Italy," *IEEE Trans. Power Deliv.*, vol. 4, no. 2, pp. 1269–1275, 1989.

[11] W. F. Long, J. Reeve, J. R. McNichol, M. S. Holland, J. P. Taisne, J. LeMay, and D. J. Lorden, "Application Aspects of Multiterminal DC power Transmission," *IEEE Trans. Power Deliv.*, vol. 5, no. 4, pp. 2084–2098, 1990.

[12] "ABB:Quebec-New-England." [Online]. Available: http://new.abb.com/systems/hvdc/references/quebec-new-england. [Accessed: 20-May-2015].

[13] M. Barnes and A. Beddard, "Voltage Source Converter HVDC Links – The State of the Art and Issues Going Forward," *Energy Procedia*, vol. 24, no. January, pp. 108–122, Jan. 2012.

[14] N. R. Chaudhuri, B. Chaudhuri, R. Majumder, and A. Yazdani, *Multi-terminal Direct-Current Grids: Modeling, Analysis, and Control*. JohnWiley & Sons, Inc, 2014.

[15] R. T. PINTO, "Multi-Terminal DC Networks, System Integration and Dynamics Control," PhD thesis, Technische Universiteit Delft, 2014.

[16] T. Nakajima and S. Irokawa, "A Control System for HVDC Transmission by Voltage Sourced Converters," in *Power Engineering Society Summer Meeting*, 1999, pp. 1113–1119.

[17] "Wikipedia:list of HVSC projects." [Online]. Available: https://en.wikipedia.org/wiki/List_of_HVDC_projects. [Accessed: 20-May-2015].

[18] ABB.com, "HVDC light (VSC)." [Online]. Available: http://new.abb.com/systems/hvdc/hvdc- light. [Accessed: 20-May-2015].

[19] H. Rao, "Architecture of Nan ' ao Multi-terminal VSC-HVDC System and Its Multi-functional Control," *CSEE J. POWER ENERGY Syst.*, vol. I, no. I, 2015.

[20] Jin Zhong and Q. Duan, "Implementing Smart Grid Technologies in China : Experiences and Future Approach Smart Grid in China," in *IEEE Power and Energy Society Seminar Presentation*, 2015.

[21] NR Electric, "World First Five-Terminal VSC-HVDC Transmission Project," 2014.

[22] EE.Publishers, "Hierarchical control in a 5-terminal VSC-HVDC project." [Online]. Available: http://www.ee.co.za/article/hierarchical-control-5-terminal-vsc-hvdc-project.html. [Accessed: 20-May-2015].

[23] T. H. M. S. Rashid and R. Islam, "Prospects of Renewable Energy Resources and Regional Grid Integration for Future Energy Security & Development in SAARC Countries," *Int. J. Res. Eng. Technol.*, pp. 43–51, 2013.

[24] F. D. Bianchi and O. Gomis-Bellmunt, "Droop Control Design for Multi-terminal VSC-HVDC Grids based on LMI Optimization," *IEEE Conf. Decis. Control Eur. Control Conf.*, pp. 4823–4828, Dec. 2011.

[25] C. Barker and R. Whitehouse, "Autonomous Converter Control in a Multi-terminal HVDC System," *Int. Conf. AC DC Power Transm.*, pp. 1–5, 2010.

[26] W. Wang, M. Barnes, and O. Marjanovic, "Droop Control Modelling and Analysis of Multi-terminal HVDC for Offshore Wind Farms," *10th IET Int. Conf. AC DC Power Transm. (ACDC 2012)*, pp. 1–6, 2012.

[27] C. Dierckxsens, K. Srivastava, M. Reza, S. Cole, J. Beerten, and R. Belmans,

"A Distributed DC Voltage Control Method for VSC MTDC Systems," *Electr. Power Syst. Res.*, vol. 82, no. 1, pp. 54–58, 2012.

[28] T. K. Vrana, L. Zeni, and O. B. Fosso, "Active Power Control with Undeadband Voltage & Frequency Droop Applied to a Meshed DC Grid Test System," in *Energy Conference and Exhibition (ENERGYCON), IEEE International*, 2012, pp. 612–616.

[29] T. K. Vrana, J. Beerten, R. Belmans, and O. B. Fosso, "A Classification of DC Node Voltage Control Methods for HVDC Grids," *Electr. Power Syst. Res.*, vol. 103, pp. 137–144, 2013.

[30] E. Veilleux and B. Ooi, "Power Flow Analysis in Multi-Terminal HVDC Grid," in *Power Systems Conference and Exposition (PSCE)*, 2011, pp. 1–7.

[31] T. M. Haileselassie and K. Uhlen, "Power Flow Analysis of Multi-terminal HVDC Networks," *2011 IEEE Trondheim PowerTech*, no. 4, pp. 1–6, Jun. 2011.

[32] R. Pinto, S. Rodrigues, E. Wiggelinkhuizen, R. Scherrer, P. Bauer, and J. Pierik, "Operation and Power Flow Control of Multi-Terminal DC Networks for Grid Integration of Offshore Wind Farms Using Genetic Algorithms," *Energies*, vol. 6, no. 1, pp. 1–26, Dec. 2012.

[33] F. Gonzalez-Longatt, J. Roldan, and C. A. Charalambous, "Power Flow Solution on Multi-Terminal HVDC Systems : Supergrid Case," in *International Conference on Renewable Energies and Power Quality (ICREPQ'12)*, 2012.

[34] J. Beerten, D. Van Hertem, and R. Belmans, "VSC MTDC Systems with a Distributed DC Voltage Control – A Power Flow Approach," in *IEEE Trondheim PowerTech*, 2011, pp. 1–6.

[35] M. Baradar, M. Ghandhari, and D. Van Hertem, "The Modeling Multi-terminal VSC-HVDC in Power Flow Calculation using Unified Methodology," *2011 2nd IEEE PES Int. Conf. Exhib. Innov. Smart Grid Technol.*, pp. 1–6, Dec. 2011.

[36] R. Z. Chai, B. H. Zhang, Z. Q. Bo, and J. M. Dou, "A Generalized Unified Power Flow Algorithm for AC / DC Networks Containing VSC-Based Multiterminal DC Grid," in *International Conference on Power System Technology (POWERCON 2014)*, 2014, pp. 20–22.

[37] F. Gonzalez-Longatt, J. M. Roldan, E. S. De Ingenieros, and C. A. Charalambous, "Solution of AC / DC Power Flow on a Multi- Terminal HVDC System : Illustrative Case Supergrid Phase I," in *47th International Universities Power Engineering Conference*, 2012, pp. 1–7.

[38] W. Wang and M. Barnes, "Power Flow Algorithms for Multi-terminal VSC-

HVDC with Droop Control," *IEEE Trans. Power Syst.*, vol. 29, no. 4, pp. 1721–1730, 2014.

[39] R. Wiget and G. Andersson, "Optimal Power Flow for Combined AC and Multi-terminal HVDC Grids based on VSC Converters," *2012 IEEE Power Energy Soc. Gen. Meet.*, pp. 1–8, Jul. 2012.

[40] J. Rimez, "A Combined AC/DC Optimal Power Flow Algorithm for Meshed AC and DC Networks Linked by VSC Converters," *Electr. Power Syst. Res.*, vol. 20, no. 2, pp. 1–6, 2009.

[41] M. Baradar and M. R. Hesamzadeh, "Modelling of Multi-Terminal HVDC Systems in Optimal Power Flow Formulation," *IEEE Electr. Power Energy Conf.*, pp. 170–175, 2012.

[42] M. Aragüés-Peñalba, J. Beerten, J. Rimez, D. Van Hertem, and O. Gomis-bellmunt, "Optimal Power Flow Tool for Hybrid AC/DC Systems," in *11th IET Int. Conf. AC DC Power Transm.*, 2015.

[43] F. Akhter, D. E. Macpherson, and G. P. Harrison, "Enhanced Multi-terminal HVDC Grid Management for Reliable AC Network Integration," *7th IET Int. Conf. Power Electron. Mach. Drives (PEMD 2014)*, pp. 0495–0495, 2014.

[44] M. Aragüés-Peñalba, A. Egea-Àlvarez, O. Gomis-Bellmunt, and A. Sumper, "Optimum Voltage Control for Loss Minimization in HVDC Multi-terminal Transmission Systems for Large Offshore Wind Farms," *Electr. Power Syst. Res.*, vol. 89, pp. 54–63, Aug. 2012.

[45] J. Beerten and D. Van Hertem, "Primary and Secondary Power Control of Multiterminal HVDC Grids," *AC DC Power Transm. (ACDC 2012), 10th IET Int. Conf.*, pp. 1–7, 2012.

[46] J. Dragon, L. F. Beites, M. Callavik, D. E. J. Hanson, a Marten, and a Morales, "Development of Functional Specifications for HVDC Grid Systems," no. 1, pp. 1–8, 2015.

[47] B4-WG.37, "VSC Transmission," *Int. Conf. Large High-Volatge Electr. Syst.*, vol. CIGRE, 2005.

[48] N. Flourentzou, V. G. Agelidis, and G. D. Demetriades, "VSC-Based HVDC Power Transmission Systems : An Overview," *IEEE Trans. POWER Electron.*, vol. 24, no. 3, pp. 592–602, 2009.

[49] S. Kouro, M. Malinowski, K. Gopakumar, J. Pou, L. G. Franquelo, B. Wu, J. Rodriguez, M. A. Pérez, and J. I. Leon, "Recent Advances and Industrial Applications of Multilevel Converters," *IEEE Trans. Ind. Electron.*, no. August, pp. 2553–2580, 2010.

[50] J. Rodríguez and J. Lai, "Multilevel Inverters : A Survey of Topologies , Controls , and Applications," *IEEE Trans. Ind. Electron.*, pp. 724–738, 2002.

[51] A. M. Abbas and P. W. Lehn, "PWM based VSC-HVDC systems — A review," *2009 IEEE Power Energy Soc. Gen. Meet.*, pp. 1–9, Jul. 2009.

[52] S. K. Chaudharyt, A. M. Gole, and R. Teodorescut, "Modular Multi-level Converter based HVDC System for Grid Connection of Offshore Wind Power Plant," in *9th IET International Conference on AC and DC Power Transmission*, 2010.

[53] A. Lindberg and T. Larsson, "PWM and Control of Three Level Voltage Source Converters In An HVDC Back-To-Back Station," in *6th International Conference on AC and DC Power Transmission*, 1996, no. 297–302.

[54] M. A. Boost and P. D. Ziogas, "State-of-the-art Carrier PWM Techniques: a Critical Evaluation," *IEEE Trans. Ind. Appl.*, vol. 24, no. 2, pp. 271–280, 1988.

[55] M. a. Perez, S. Bernet, J. Rodriguez, S. Kouro, and R. Lizana, "Circuit Topologies, Modelling, Control Schemes and Applications of Modular Multilevel Converters," *IEEE Trans. Power Electron.*, vol. PP, no. 99, pp. 1–1, 2014.

[56] M. R. Haddioui, "Control and Modulation Strategies for MMC - based HVDC," Master thesis,Department of Energy Technology, Aalborg Univeristy, 2015.

[57] J. Liang, O. Gomis-Bellmunt, J. Ekanayake, N. Jenkins, and W. An, "A Multi-terminal HVDC Transmission System for Offshore Wind Farms with Induction Generators," *Int. J. Electr. Power Energy Syst.*, vol. 43, no. 1, pp. 54–62, Dec. 2012.

[58] L. Livermore, J. Liang, and J. Ekanayake, "MTDC VSC Technology and Its Applications for Wind Power," in *45th International Universities Power Engineering Conference*, 2010.

[59] CIGRE Working Group B4.52, "HVDC Grid Feasibility Study," 2013.

[60] J. Peralta, H. Saad, S. Dennetière, and Jean Mahseredjian, "Dynamic Performance of Average-Value Models for Multi-terminal VSC-HVDC Systems," in *IEEE Power and Energy Society General Meeting*, 2012, pp. 1–8.

[61] M. M. Z. Moustafa, "Operating Limits and Dynamic Average-Value Modelling of VSC-HVDC Systems," University of Manitoba, 2011.

[62] L. Malesani and P. Tomasin, "PWM Current Control Techniques of Voltage Source Converters - A Survey," in *19th Annual Conference of IEEE Industrial Electronics*, 1993, pp. 670–675.

[63] B. T. Ooi and X. Wang, "Voltage Angle Lock Loop Control of the Boost type PWM Converter for HVDC Application," *IEEE Trans. Power Electron.*, vol. 5, no. 2, pp. 229–235, Apr. 1990.

[64] J. Machowski, J. W. Bialek, and J. R. Bumby, *Power System Dynamics and Control*, Second Edi. JohnWiley & Sons, Ltd., 2008.

[65] J. Z. Zhou and A. M. Gole, "VSC Transmission Limitations Imposed by AC system Strength and AC Impedance Characteristics," in *11th IET Int. Conf. AC DC Power Transmission*, 2015.

[66] A. B. Morton, "A Guide to ' Steady-State ' Voltage Stability Analysis," no. November, pp. 1–26, 2007.

[67] S. G. Johansson, G. Asplund, E. Jansson, and R. Rudervall, "Power System Stability Benefits with VSC DC-Transmission Systems," in *Cigré Conference Session*, 2004, pp. 1–8.

[68] S. Cole, "Steady-State and Dynamic Modelling of VSC HVDC Systems for Power System Simulation," PhD thesis, Katholieke Universiteit Leuven, 2010.

[69] T. K. Vrana and O. B. Fosso, "Technical Aspects of the North Sea Supergrid," *ELECTRA 15 CIGRE J.*, pp. 6–19, 2011.

[70] S. K. Chaudhary, R. Teodorescu, P. Rodriguez, and P. C. Kjær, "Chopper Controlled Resistors in VSC-HVDC Transmission for WPP with Full-scale Converters," in *IEEE PES/IAS Conference on Sustainable Alternative*, 2009, pp. 1–8.

[71] L. Zhang, L. Harnefors, and H. P. Nee, "Interconnection of Two Very Weak AC systems by VSC-HVDC Links using Power-Synchronization Control," *IEEE Trans. Power Syst.*, vol. 26, no. 1, pp. 344–355, 2011.

[72] W. Lu and B.-T. Ooi, "Optimal Acquisition and Aggregation of Offshore Wind Power by Multiterminal Voltage-Source HVDC," *IEEE Trans. POWER Deliv.*, vol. 18, no. 1, pp. 201–206, 2003.

[73] J. Zhu and C. Booth, "Future Multi-Terminal HVDC Transmission Systems using Voltage Source Converters," in *45th International Universities Power Engineering Conference*, 2010, pp. 1–6.

[74] W. Lu and B.-T. Ooi, "Premium Quality Power Park Based on Multi-Terminal HVDC," *IEEE Trans. Power Deliv.*, vol. 20, no. 2, pp. 978–983, Apr. 2005.

[75] R. L. Hendriks, G. C. Paap, and W. L. Kling, "Control of a Multi-terminal VSC Transmission Scheme for Connecting Offshore Wind Farms," in *European Wind Energy Conference*, 2007.

[76] L. Xu, B. W. Williams, and L. Yao, "Multi-Terminal DC Transmission Systems for Connecting Large Offshore Wind Farms," in *Power and Energy Society General Meeting - Conversion and Delivery of Electrical Energy in the 21st Century*, 2008, pp. 1–7.

[77] C. Bajracharya, M. Molinas, M. Ieee, J. A. Suul, T. M. Undeland, and F. Ieee, "Understanding of tuning techniques of converter controllers for VSC-HVDC," 2008.

[78] V. Mier, P. G. Casielles, J. Coto, and L. Zeni, "Voltage Margin Control for Offshore Multi-use Platform integration Key Words," in *International Conference on Renewable Energies and Power Quality*, 2012.

[79] T. M. Haileselassie and K. Uhlen, "Primary Frequency Control of Remote Grids Connected by Multi-terminal HVDC," *IEEE PES Gen. Meet.*, pp. 1–6, Jul. 2010.

[80] P. Kundur, *Power System Stability and Control*. McGraw-Hill, Inc., 1994.

[81] O. B. Fosso, L. Zeni, and T. K. Vrana, "Dynamic Active Power Control with Improved Undead-band Droop for HVDC Grids," *10th IET Int. Conf. AC DC Power Transm. (ACDC 2012)*, pp. 52–52, 2012.

[82] P. Kundur, J. Paserba, V. Ajjarapu, G. Andersson, A. Bose, C. Canizares, N. Hatziargyriou, D. Hill, A. Stankovic, C. Taylor, T. Van Cutsem, and V. Vittal, "Definition and Classification of Power System Stability," *IEEE Trans. Power Syst.*, vol. 19, no. 3, pp. 1387–1401, 2004.

[83] S. Cole, J. Beerten, and R. Belmans, "Generalized Dynamic VSC MTDC Model for Power System Stability Studies," *IEEE Trans. POWER Syst.*, vol. 25, no. 3, pp. 1655–1662, 2010.

[84] R. T. Pinto, "Comparison of Direct Voltage Control Methods of Multi-Terminal DC (MTDC) Networks through Modular Dynamic Models," in *4th European Conference Proceedings on Power Electronics and Applications*, 2011, pp. 1–10.

[85] T. M. Haileselassie and K. Uhlen, "Precise Control of Power Flow in Multiterminal VSC-HVDCs using DC Voltage Droop Control," *2012 IEEE Power Energy Soc. Gen. Meet.*, pp. 1–9, Jul. 2012.

[86] J. Beerten, S. Cole, and R. Belmans, "Generalized Steady-State VSC MTDC Model for Sequential AC / DC Power Flow Algorithms," *IEEE Trans. POWER Syst.*, vol. 27, no. 2, pp. 821–829, 2012.

[87] M. Baradar and M. Ghandhari, "A Multi-Option Uni fi ed Power Flow Approach for Hybrid AC /DC Grids Incorporating Multi-terminal VSC-HVDC," *IEEE Trans. POWER Syst.*, vol. 28, no. 3, pp. 2376–2383, 2013.

[88] G. Daelemans, K. Srivastava, M. Reza, S. Cole, and R. Belmans, "Minimization of Steady-State Losses in Meshed Networks using VSC HVDC," in *Power & Energy Society General Meeting,, 2009. PES '09. IEEE*, 2009, pp. 1–5.

[89] J. Arrillaga and B. Smith, *AC-DC Power System analysis*. The Institution of Electrical Engineers, London, UK, 1998.

[90] J. Arrillaga and C. P. Arnold, *Computer analysis of Power Systems*. JOHN WILEY & SONS, 1990.

[91] R. D. Zimmerman, C. E. Murillo Sánchez, and R. J. Thomas, "MATPOWER: Steady-State Operations, Planning, and Analysis Tools for Power Systems Research and Education," *Power Syst. IEEE Trans.*, vol. 26, no. 1, pp. 12–19, 2011.

[92] "User's guide (PSCAD) Power System Computer Aided Design." Manitoba HVDC Research Centre, Winnipeg, Manitoba, 2010.

[93] A. Pizano-Martinez, C. R. Fuerte-Esquivel, H. Ambriz-Pérez, and E. Acha, "Modeling of VSC-based HVDC systems for a Newton-Raphson OPF algorithm," *IEEE Trans. Power Syst.*, vol. 22, no. 4, pp. 1794–1803, 2007.

[94] J. Cao, W. Du, H. F. Wang, and S. Q. Bu, "Minimization of Transmission Loss in Meshed AC / DC Grids With VSC-MTDC Networks," vol. 28, no. 3, pp. 3047–3055, 2013.

[95] W. Feng, A. Le Tuan, L. B. Tjernberg, A. Mannikoff, and A. Bergman, "A New Approach for Benefit Evaluation of Multiterminal VSC-HVDC using a Proposed Mixed AC/DC Optimal Power Flow," *IEEE Trans. Power Deliv.*, vol. 29, no. 1, pp. 432–443, 2014.

[96] M. Baradar, M. R. Hesamzadeh, and M. Ghandhari, "Second-order Cone Programming for Optimal Power Flow in VSC-Type AC-DC Grids," *IEEE Trans. Power Syst.*, vol. 28, no. 4, pp. 4282–4291, 2013.

[97] O. Alsac and B. Stott, "Optimal Load Flow with Steady-State Security," *IEEE Trans. Power Appar. Syst.*, vol. PAS-93, no. 3, pp. 745–751, 1974.

[98] F. Capitanescu, M. Glavic, D. Ernst, and L. Wehenkel, "Applications of Security-Constrained Optimal Power Flows," *Mod. Electr. Power Syst. Symp. MEPS06*, p. 7, 2006.

[99] F. Capitanescu, J. L. Martinez Ramos, P. Panciatici, D. Kirschen, A. Marano Marcolini, L. Platbrood, and L. Wehenkel, "State-of-the-art, Challenges, and Future Trends in Security Constrained Optimal Power Flow," *Electr. Power Syst. Res.*, vol. 81, no. 8, pp. 1731–1741, 2011.

[100] G. A. S. Chatzivasileiadis, T. Krause, "Security-Constrained Optimal Power Flow including Post-Contingency Control of VSC-HVDC lines," in *XII symposium of specialists in electrical operation and expansion planning*, 2012.

[101] R. Wiget and E. Iggland, "Security Constrained Optimal Power Flow for HVAC and HVDC Grids," *Power Syst. Comput. Conf.*, 2014.

[102] S. Chatzivasileiadis, "Security Constrained OPF Incorporating Corrective Control of HVDC," in *Power Systems Computation Conference (PSCC)*, 2014.

[103] R. Wiget and M. Vrakopoulou, "Probabilistic Security Constrained Optimal Power Flow for a Mixed HVAC and HVDC Grid with Stochastic Infeed," in *Power Systems Computation Conference (PSCC)*, 2014.

[104] G. Saplamidis, Vasileios, Roger Wiget and O. Andersson, "Security Constrained Optimal Power Flow for Mixed AC and Multi-Terminal HVDC Grids," in *Power Systems Computation Conference (PSCC)*, 2014.

[105] M. Aragüés-Peñalba, J. Rimez, J. Beerten, D. Van Hertem, and O. Gomis-bellmunt, "Secure and Optimal Operation of Hybrid AC/DC Grids with Large Penetration of Offshore Wind," in *11th IET International Conference on AC and DC Power Transmission*, 2015, pp. 1–9.

[106] Q. Wang, "Risk-based Security-Constrained Optimal Power Flow: Mathematical Fundamentals, Computational Strategies, Validation, and use within Electricity Markets," PhD thesis, Iowa State University, 2013.

Appendix

Appendix A.1 Parameters Calculations

The following Matlab code is used to calculate the parameters of the VSC stations and MTDC grid.

```
%% programme for calculating VSC converter
%% and MTDC grid parameters
clear all
clc
%% Convereter rated parameters
r = 0.36;
L = 0.0048;
Xl = (2*pi*50*L);
Vdc=400;                % +/- 200kV

% Line ditance Km
l12 = 120;
l15 = 70;
l25 = 100;
l24 = 150;
l23 = 150;
l34 = 70;
l45 = 100;
Rdc = 0.02;               % ohm/km
Sr  = 1000;               % rated MVA
Vr  = 180;                %kV

% capcitor values
Ti = 0.005;              % 100ms tao
Cdc= (2*Ti*Sr)/Vdc^2

% So phase quantities wil be
S_r = (2/3)*(Sr)
V_r = sqrt(2/3)*(Vr)     % Vd_base = Vq_base (Vn peak phase)
I_r = (S_r/V_r)          %kA
Z_r = (V_r/I_r)          %ohms

%% claculate DQ base ( per phase base)
%% All base values are equal to rated value
Sbase=Sr;                % Sn MVA base
Vbase=Vr;                % Vn LL rms kV base
                         % Vn Phase rms = Vn/sqrt(3)
                         % Vn Phase peak = sqart(2/3) Vn
S_b = (2/3)*(Sbase);    % S_b=3*(Vn phase rms*In phase rms)
                        % S_b=2/3*(Vn phase peak*In phase peak)
                        % Vdq_b*Idq_b = (2*sqrt(3)/3)* Vn*In
Vs_b = sqrt(2/3)*(Vbase)  % Vd_base = Vq_base (Vn peak phase)

Is_b = (S_b/Vs_b);       %kA
Zs_b = (Vs_b/Is_b)       %ohms

```

```
%% DC system base values
Sdc_b =(3/2)*S_b
Vdc_b = Vdc
Idc_b = Sdc_b/Vdc_b
Rdc_b = Vdc_b/Idc_b

Edc_b = Sdc_b*1;          % Enery stored in capactor in 1s
Cdc_b = (2*Edc_b)/Vdc^2   % since Edc_b= 1/2*Cdc*Vdc^2

% pu values are
r_pu = r/Zs_b          % typically 0.01= 1% drop at rated Vac
Xl_pu= Xl/Zs_b
L_pu = Xl_pu/(100*pi) % typically 0.06 = 6% drop at rated Vac
Cdc_pu=Cdc/Cdc_b      % typically 0.1=at 100ms and rated power

Vs_pu = V_r/Vs_b
Is_pu = I_r/Is_b
Vdc_pu= Vdc/Vdc_b
Rdc_pu= Rdc/Rdc_b
%% droop pu conversion
go = 0.05;
Ki = 1/go
Ki_b = Vdc_b/Sdc_b
Ki_pu = Ki/ Ki_b
%% each line +/- for PSCAD
r12_pu = Rdc_pu*l12/2
r15_pu = Rdc_pu*l15/2
r25_pu = Rdc_pu*l25/2
r23_pu = Rdc_pu*l23/2
r24_pu = Rdc_pu*l24/2
r34_pu = Rdc_pu*l34/2
r45_pu = Rdc_pu*l45/2
%% each line for Powerflow in Matlab
r12_pu1 = Rdc_pu*l12
r15_pu1 = Rdc_pu*l15
r25_pu1 = Rdc_pu*l25
r23_pu1 = Rdc_pu*l23
r24_pu1 = Rdc_pu*l24
r34_pu1 = Rdc_pu*l34
r45_pu1 = Rdc_pu*l45
%% Converter voltage at Inverter end

Vs_r = Vs_pu;    Vs_i=0;

[Z_a, Z_m] = cart2pol(r_pu,Xl_pu);

```

```
Vz_a = Z_a,      Vz_m = Is_pu*(Z_m)


[Vz_r, Vz_i] = pol2cart(Vz_a, Vz_m);

Vcon_r = Vs_r + Vz_r;
Vcon_i = Vs_i + Vz_i
Vcon = (Vcon_r)+ j*(Vcon_i);

[Vcon_a, Vcon_m] = cart2pol(Vcon_r, Vcon_i)

%% modulation index
m_b = (2*Vs_b)/Vdc_b
m_a = (2*Vcon_m*Vs_b)/(Vdc_pu*Vdc)
m = (m_a/m_b)
m_pu = (2*Vcon_m)/(Vdc_pu)

```

Appendix A.2 Tuning Controller Parameters:

The tuning of the controllers of all control configuration is done by using Modulus Optimum and Symmetrical Optimum criteria implemented in following Matlab code.

```
%% programme for tuning parameters of controller

clear all
clc
%% Convereter rated parameters
r_pu = 0.0111;    % per unit resistance
L_pu = 0.000148; % per unit inductance
Wb = 2*pi*50;    % base frequency
Ta = 100e-6;     % average coverter time delay

%% Inner control tuning parameters for all
%% control cofigurations using Modulus optimum criteria
Wc_c = 5000*pi;     % cut-off frequency of inner current loop

% Intergral time constant
Ti_c = L_pu/r_pu;  % tao

% Proportional gain
Kp_c = Ti_c*r_pu/(2*Ta);

%% Outer control tuning parameters for all
%% control cofigurations using Symetrical optimum criteria

%% Active and reactive power controller
Wc_pq = 10*pi;  % cut-off frequency for outer control loop

% Integral time constant
Ti_pq = 2*Ti_c; % equal to equivelent delay of inner loop

% Proportional gain
Kp_pq = 2*(Ti_pq*Wc_pq)/3*sqrt(1+(Ti_pq*Wc_pq));


%% DC volatge controller
% The DC volatge controller was tunned using trial and error
% with following values giving the optimal response

% Integral time constant
Ti_dc = 0.01;

% Proportional gain
Kp_dc = 2;

%% AC grid voltage controller
% The PI regulator of AC grid volatge was tunned
% to following values
```

```
% to following values

% Integral time constant
Ti_ac = -0.308;

% Proportional gain
Kp_ac = 0.175;

```

Table A.2-1 *Table of tuning parameters used in all control configurations*

Controller	**Proportional gains**	**Integral Time constants**
Inner Current Controller	*Kp_c*	*Ti_c*
	1	0.0133
Active and Reactive Power Controller	*Kp_pq*	*Ti_pq*
	0.7571	0.0267
AC grid Voltage Controller	*Kp_ac*	*Ti_ac*
	0.1750	-0.308*
DC Voltage Controller	*Kp_dc*	*Ti_dc*
	2	0.01

* T_{i_ac} is negative shows that the quantity decreases with the time.

Appendix A.3 Modified IEEE14 Network Data:

Table A.3-2 *Modified IEEE14 bus data*

AC grid *node*	Bus type	P_G (p.u)	Q_G (p.u)	P_L (p.u)	Q_L (p.u)	Q_{max} (p.u)	Q_{min} (p.u)
Bus1	3	-	-	-	-	1.0	-1.0
Bus2	3	0.0	0.0	-	-	1.5	-1.5
Bus3	3	74.2	19	24.2	19	1.4	-1.2
Bus4	1	-	-	21.2	7.5	-	-
Bus5	1	-	-	-	-	-	-
Bus6	1	-	-	47.8	1.6	-	-
Bus7	1	-	-	-	-	-	-
Bus8	2	35	15.02	-	-	1.24	1.24
Bus9	1	-	-	29.5	16.6	-	-
Bus10	1	-	-	9	5.8	-	-
Bus11	1	-	-	3.5	1.8	-	-
Bus12	1	-	-	6.1	1.6	-	-
Bus13	1	-	-	13.5	5.8	-	-
Bus14	1	-	-	14.9	5.0	-	-

Table A.3-3 *Modified IEEE14 branch data*

From ***node***	**To** ***node***	**Resistance (p.u)**	**Reactance (p.u)**	**Line charging (p.u)**	**Tap ratio (p.u)**
6	5	0.0	0.2091	0.0	1.0
6	9	0.0	0.5561	0.0	1.0
1	4	0.0	0.1091	0.0	1.0
7	4	0.0	0.2520	0.0	1.0
4	11	0.0949	0.1989	0.0	1.0
4	12	0.1229	0.2558	0.0	1.0
4	13	0.0661	0.1302	0.0	1.0
5	8	0.0	0.1761	0.0	1.0
5	9	0.0	0.1100	0.0	1.0
9	10	0.3181	0.0845	0.0	1.0
9	14	0.1271	0.2703	0.0	1.0
10	11	0.0820	0.1920	0.0	1.0
12	13	0.2209	0.1998	0.0	1.0
13	14	0.1709	0.3480	0.0	1.0

Table A.3-4 *Generator const data*

Generator	***NCOST***	***f*** **($/h)**	**P (MW)**
1	3	0.04	20
2	3	0.0	20
3	3	0.01	20
8	3	0.01	20

Appendix B. Publications

Enhanced multi-terminal HVDC grid management for reliable AC network integration

F. Akhter†, D.E. Macpherson*, G.P. Harrison**

**Institute for Energy System, School of Engineering*
University of Edinburgh, Kings Building, Edinburgh EH9 3JL, UK
† F.Akhter@ed.ac.uk

Keywords: Multi-Terminal High Voltage Direct Current (MTDC) grid, Voltage Source Converter (VSC), power flow control, droop control, secondary control.

Abstract

This paper presents a secondary control for MTDC systems to update the DC voltage and converter power references of the VSC stations operating under droop control, in order to eliminate the large power deviation from their desired reference power. The rated values of the VSC station used as reference does not take into account the power losses in the converter, DC line and the voltage drops in the DC transmission lines. This creates a constant difference between rated DC voltage reference and actual DC voltage value of the VSC station. This difference is multiplied by the droop gain of the VSC station, hence causing power deviations in the MTDC grid system. In this paper a secondary control is implemented for a four-terminal HVDC system modelled in EMTDC/PSCAD, to demonstrate the reduction in power deviation by the proposed secondary control.

1 Introduction

Offshore wind energy is seen as the most promising source of electricity generation for achieving the European renewable energy targets. A number of wind farms are under installation in the North Sea, and more are planned, to collect the huge potential of wind energy at significant distances from land. This will be extended to include the interconnection between the countries to form a MTDC grid [1].

The Voltage Source Converter (VSC) technology's capabilities of multi-directional power flow and control flexibility are fundamental to a MTDC grid system. With the systematic control of the VSCs and MTDC grid system, the integration of wind farms and interconnections between countries can be made more reliable to support the AC network. The VSC-based MTDC grid system is connected to shore by a common DC link. The active power flow through all the terminals need to be balanced to keep the DC link voltage constant, similar to the constant system frequency requirement of an AC system, for the stable operation of VSC stations. A combination of primary control strategies proposed for the DC link voltage control and power flow dispatch of the MTDC grid system including Master-Slave, Voltage Margin and Voltage Droop control are suggested in [2]–[5].

The main drawback of the Master-Slave control strategy with the Voltage Margin method is that only one VSC station controls the DC link voltage of the MTDC grid system. An outage in the DC link voltage controlling VSC station leads to failure of the whole MTDC grid system. In the case of the Voltage Droop control more than one VSC station share responsibility for the DC link voltage control, therefore, outage of any single VSC station cannot cause failure of the complete MTDC grid system. Hence, the Voltage Droop control is regarded as most suitable, because of the flexible control operation of the MTDC grid system, similar to the frequency droop control of an AC system.

Although, various advantages of the DC Voltage Droop control implementation in an MTDC grid system have been explored in the literature, little has been discussed on the issue of the power deviation from the desired reference power of the VSC station operating under the Droop Control, due to the difference in the DC voltage of the VSC stations. In [6], the impact of the DC line voltage drop on the power flow under Voltage Droop control is discussed in detail and an analytical expression is proposed to deal with this issue, but the references cannot be updated instantaneously.

Power balancing and maintaining the required power flows from the MTDC grid system is fundamental to its reliable integration with the AC network. Therefore, a secondary control of the MTDC grid system as proposed in [7], analogous to that in an AC grid system, needs to be implemented to compensate for this power deviation and instantaneously update the power and voltage references of the primary control of the VSC stations, in order to maintain the scheduled power flow dispatch from the MTDC grid system.

In this paper, a secondary control is proposed for the instantaneous update of the DC voltage reference to avoid the power deviation caused by the difference in DC voltage of the VSC stations due to the voltage drop in the DC lines. A comparison of two four-terminal HVDC grid systems modelled in EMTDC/PSCAD is presented, one without the proposed secondary control and another with the proposed secondary control. The results show that secondary control can update instantaneously the DC voltage references and hence the power deviations are reduced eliminated from the MTDC grid system.

2 Control Structure of MTDC grid

The MTDC grid control is reduced to the control of a single VSC station (as a fundamental unit of the MTDC grid system); similarly, the control of the AC grid is represented by the control of a synchronous generator. The similarities between the MTDC grid control structure and AC grid control structure is shown in Figure 1. The primary control of the MTDC grid system comprises an inner and an outer controller, analogous to the exciter and governor control of the AC grid system. The secondary control is introduced to supply updated references for primary control to avoid the power deviation and obtain scheduled power flow dispatch from the MTDC grid system.

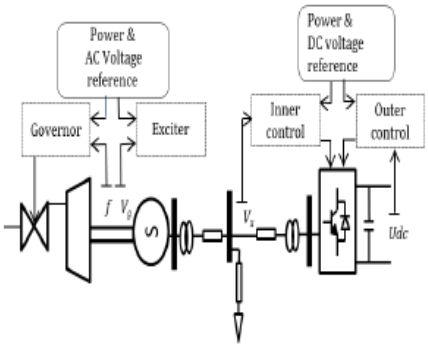

Figure 1: AC and MTDC grid control structure comparison

2.1 Primary Control

The primary control maintains the basic VSC station operation by the inner controller, and ensures the co-ordinated balance operation of the MTDC grid system as a whole through the outer controller. The detailed primary control structure of the MTDC grid system is shown in Figure 3.

The inner controller uses synchronously rotating *dq* reference control, explained in [8] [9], which decouples active and reactive power control to provide independent active and reactive power control at each VSC station, similar to how the governor and the exciter provide independent control in the AC grid system.

The outer controller can be operated under various modes of operation according to the requirements of the MTDC grid system. The operation modes include: constant active power or constant DC link voltage; constant reactive power or constant AC voltage. The control mode that most closely resembles the frequency droop control of the AC grid system is DC voltage droop control [10] as shown in Figure 2.

The implementation of the DC droop controller is given by:

$$P_c = P_{c\,ref} + R\,(U_{dc\,ref} - U_{dc}) \qquad (1)$$

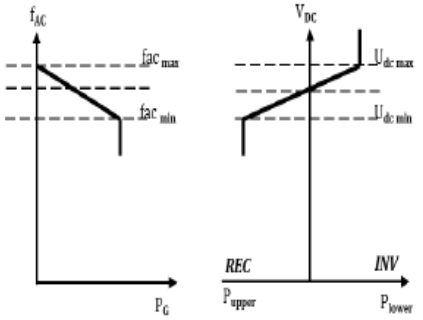

Figure 2: Primary droop control comparison of AC and MTDC grid

where, P_c is actual power at the Point of Common Coupling (PCC) of the VSC station, $P_{c\,ref}$ is desired reference power, R is the droop gain of the DC voltage controller, U_{dc} is the actual DC link voltage at the VSC station and $U_{dc\,ref}$ is the rated DC link voltage for the VSC station.

However, when rated DC link voltage values are used for $U_{dc\,ref}$ this does not take into account the voltage drops in the transmission line. The difference, when multiplied by the droop gain of the DC voltage controller, produces a large deviation in the actual power P_c of the converter station. To avoid this power deviation a power flow analysis can be performed to produce an appropriate DC voltage reference by keeping one VSC station as voltage regulator as suggested in [10], whereas, with the proposed secondary control described in this paper, it can be achieved instantaneously without the need for power flow analysis.

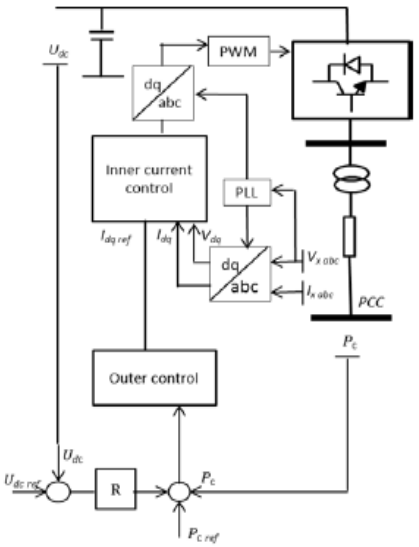

Figure 3: Detailed primary control structure of the MTDC grid system

2.2 Secondary Control

The secondary control is implemented to update the reference to the desired value, which will eliminate the difference between the actual and rated reference DC link voltage, so that actual power at the VSC station can be maintained near to the reference value. Since, in steady state the actual measured values of the DC link (U_{dc}) account for the voltage drop in the transmission and represent the true DC link voltage reference, so the relationship between rated reference and updated reference can be given as:

$$U_{dc\ updated} = U_{dc\ ref} + \Delta U_{dc} \quad (2)$$

where,

$$\Delta U_{dc} = U_{dc\ ref} - U_{dc} \quad (3)$$

The difference (ΔU_{dc}) between rated $U_{dc\ ref}$ and actual U_{dc} is added to the rated $U_{dc\ ref}$ to acquire the updated DC link voltage reference ($U_{dc\ updated}$). This will eliminate the steady state power deviation due to the DC voltage drops in the transmission line.

Similarly, the power references ($P_{c\ ref}$) can be changed to produce the updated power reference ($P_{c\ updated}$), in order to account for the power losses in the VSC station. In steady state, when the DC link voltage references are updated to the $U_{dc\ updated}$, the power deviation at the VSC station represents power losses in the VSC station and DC transmission line.

$$P_{c\ updated} = P_{c\ ref} + \Delta P_c \quad (4)$$

where,

$$\Delta P_c = P_{c\ ref} - P_c \quad (5)$$

Once the difference (ΔP_c) between the desired $P_{c\ ref}$ and actual P_c is added to the desired $P_{c\ ref}$, the updated power reference ($P_{c\ updated}$) will take into account the losses of the VSC station and DC line; hence steady state power deviation due to the VSC station and DC line losses will be reduced. Figure 4, shows implementation for secondary control.

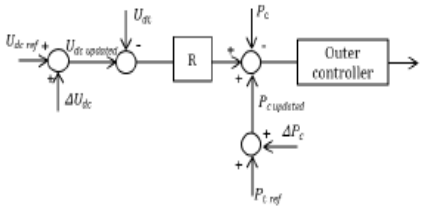

Figure 4: Secondary control implementation

3 System configuration

The hypothetical four-terminal HVDC model with every terminal connected to each other shown in Figure 5 has been simulated (to get a simple representation of a meshed network) in EMTDC/PSCAD simulation software to verify the proposed secondary control. The VSC station1 (terminal-1) is set on Power Control mode, whereas the other three VSC stations (VSC2, VSC3 and VSC4) are set to DC voltage Droop Control.

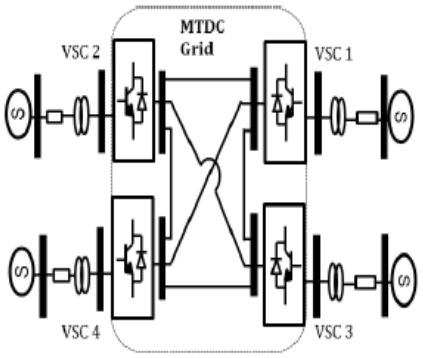

Figure 5: Four terminal HVDC system

Two different scenarios have been simulated; one without secondary control and the other with, secondary control implemented to demonstrate the reduction in the steady state power deviation with the proposed secondary control. Further, a change in power flow pattern can be simulated to show the balance distribution of power in the MTDC grid system under disturbance conditions. The AC grids are represented by their aggregated models.

The parameters used have been inspired from [10], R_{cable}=0.01Ω/km, C=5 μF/km, R_{DC}=40 MW/kV, $P_{c\ Rated}$= 100MW each and $U_{dc\ Rated}$= 50kV each. The lengths of the cables are given as; l_{12}=150km, l_{14}=170km, l_{13}=100km, l_{23}=150km, l_{24}=120km and l_{34}=100km.

Table 1 shows the set reference taken for the four VSC stations in the steady state operation condition.

Table 1: Reference values used for simulation

VSC stations	VSC1	VSC2	VSC3	VSC4
$P_{C\ ref}$ (MW)	-90	10	30	50
$U_{dc\ ref}$ (kV)	–	50	50	50
R_{DC} (MW/kV)	–	40	40	40

4 Simulation results

4.1 MTDC system under droop with no secondary control

The first simulation is performed with set reference from Table 1; here the DC voltage reference for the three VSC stations under DC Droop control is the rated DC link voltage. It can be observed from Figures 6 and 7 that power deviations are proportional to the difference between the reference DC voltage (i.e. $U_{dc\ ref}$ =50kV) and the actual DC voltage (U_{dc}). Table 2 shows the deviations in power caused by the difference of the DC voltages in the DC link at each VSC station.

Table 2: Power deviations and DC voltage difference

VSC Station	VSC1	VSC2	VSC3	VSC4
P_c (MW)	-90	8.76	50.126	31.34
U_{dc} (kV)	_	49.625	50.002	49.973
ΔP(MW)	0.0	-1.24	0.126	1.34
ΔU(kV)	_	-0.375	0.002	-0.027

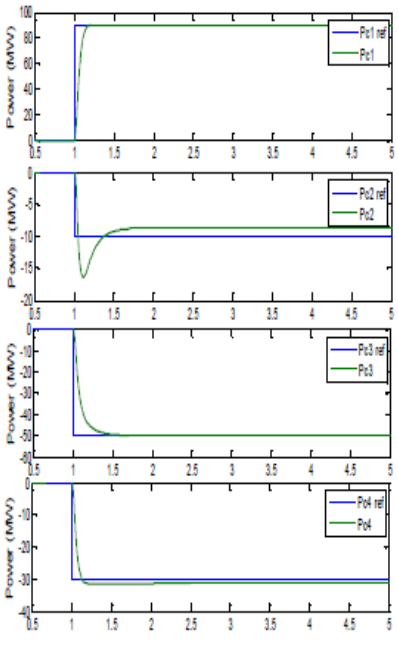

Figure 6: Actual and reference power without secondary control

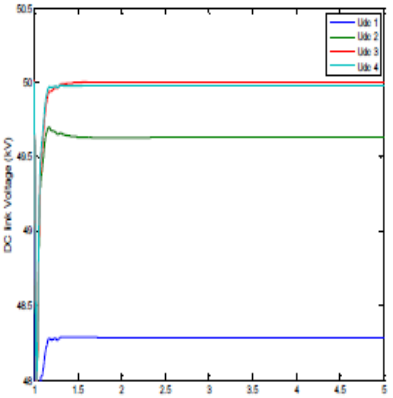

Figure 7: DC link voltages without secondary control

4.2 MTDC system under droop with secondary control

In the second simulation, the secondary control is applied and the DC link voltage references for the three VSC stations (VSC2, VSC3, VSC4) are updated according to the voltage drops in the DC transmission line. Figures 8 and 9 show that power deviation of the VSC station is reduced and precise power flow can be obtained from the MTDC grid system without need of references being updated through the DC power flow analysis.

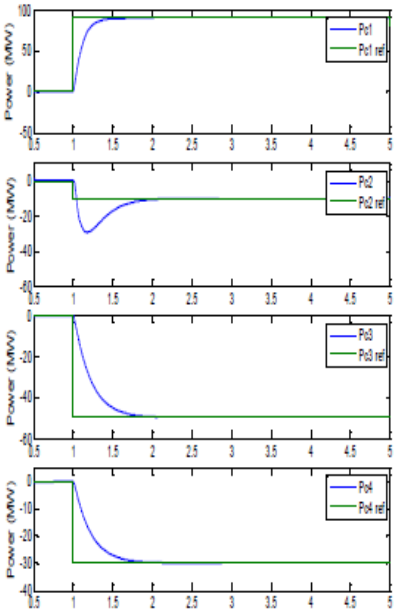

Figure 8: Actual and reference power with secondary control

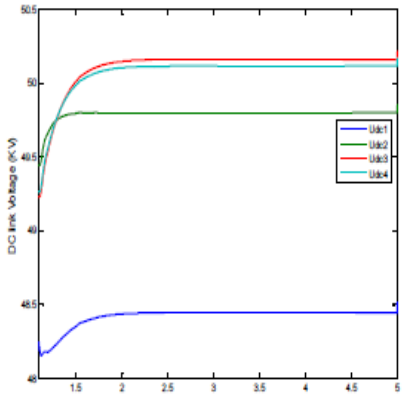

Figure 9: DC link voltages with secondary control

5 Conclusion

In this paper a secondary control has been proposed to update the DC voltage and converter power references of the VSC stations operating under droop control, in order to reduce the large power deviation from their desired reference power. It is observed that DC voltage rated values of the VSC station used as reference causes power deviation in the MTDC grid system. The proposed secondary control can provide updated references for primary control to avoid the power deviation and obtain scheduled power flow dispatch from the MTDC grid system.

Acknowledgement

The author would like to acknowledge the affiliation and funding resources for this research from Sukkur Institute of Business Administration, Sukkur, Pakistan

References

[1] E. Summary, "Eueopean Offshore Suppergrid Proposal," 2010.

[2] J. Zhu and C. Booth, "Future Multi-Terminal HVDC Transmission Systems using Voltage Source Converters," pp. 1–6, 2010.

[3] R. T. Pinto, "Comparison of Direct Voltage Control Methods of Multi-Terminal DC (MTDC) Networks through Modular Dynamic Models," pp. 1–10.

[4] L. Xu and L. Yao, "DC voltage control and power dispatch of a multi-terminal HVDC system for integrating large offshore wind farms," *IET Renew. Power Gener.*, vol. 5, no. 3, p. 223, 2011.

[5] R. Silva, R. Teodorescu, S. Member, and P. Rodriguez, "Power Delivery in Multiterminal VSC-HVDC Transmission System for Offshore Wind Power Applications," pp. 1–8.

[6] T. M. Haileselassie and K. Uhlen, "Impact of DC Line Voltage Drops on Power Flow of MTDC Using Droop Control," *IEEE Trans. Power Syst.*, vol. 27, no. 3, pp. 1441–1449, Aug. 2012.

[7] J. Beerten and D. Van Hertem, "PRIMARY AND SECONDARY POWER CONTROL OF MULTITERMINAL HVADC GRID."

[8] T. Nakajima, S. Irokawa, and T. Corporation, "A Control System for HVDC Transmission by Voltage Sourced Converters," pp. 1113–1119, 1999.

[9] C. Bajracharya, M. Molinas, M. Ieee, J. A. Suul, T. M. Undeland, and F. Ieee, "Understanding of tuning techniques of converter controllers for VSC-HVDC," 2008.

[10] T. M. Haileselassie and K. Uhlen, "Precise control of power flow in multiterminal VSC-HVDCs using DC voltage droop control," *2012 IEEE Power Energy Soc. Gen. Meet.*, pp. 1–9, Jul. 2012.

DC Voltage Droop Control Implementation in the AC/DC Power Flow Algorithm: Combinational Approach

F. Akhter[1†], D.E. Macpherson[1], G.P. Harrison[1], W.A. Bukhsh[2]

[1]Institute for Energy System, School of Engineering
University of Edinburgh, Kings Building, Edinburgh EH9 3JL, UK
† F.Akhter@ed.ac.uk

[2]Center for Electric Power and Energy
Technical University of Denmark, Denmark

Keywords: Multi-Terminal High Voltage Direct Current (MTDC) grid, Voltage Source Converter (VSC), AC/DC combined power flow analysis, DC droop control.

Abstract

In this paper, a combinational AC/DC power flow approach is proposed for the solution of the combined AC/DC network. The unified power flow approach is extended to include DC voltage droop control. In the VSC based MTDC grids, DC droop control is regarded as more advantageous in terms of operational flexibility, as more than one VSC station controls the DC link voltage of the MTDC system. This model enables the study of the effects of DC droop control on the power flows of the combined AC/DC system for steady state studies after VSC station outages or transient conditions without needing to use its complete dynamic model. Further, the proposed approach can be extended to include multiple AC and DC grids for combined AC/DC power flow analysis. The algorithm is implemented by modifying the MATPOWER based MATACDC program and the results shows that the algorithm works efficiently.

1 Introduction

Offshore wind energy is seen as the most promising source of electricity generation for achieving the European renewable energy targets. A number of wind farms are planned and under installation to collect the huge potential of wind energy at farther distances in the North Sea. This has been extended to a wider concept of a DC 'Supergrid' for the interconnection of European countries with a MTDC grid [1], due to the technical advantages of VSC based MTDC systems.

The Voltage Source Converter (VSC) technology's capabilities of multi-directional power flow and independent power control capability are fundamental to a MTDC grid system. With the systematic control of the VSCs and the MTDC grid system, the integration of wind farms and interconnections between countries can be made more reliable to support the AC network. The VSC-based MTDC grid system is connected to shore by a common DC link. The active power flows through all the terminals need to be balanced to keep the DC link voltage constant for the stable operation of the VSC stations, similar to the constant system frequency requirement of an AC system.

The integration of the proposed European DC 'Supergrid' to the existing AC transmission system has produced many challenges. A major challenge is to obtain the steady state operating point for the combined AC/DC power system. The power vs voltage relationships in DC are very different than in an AC grid; two different sets of numerical equations are required to be solved to obtain the combined AC/DC power flows. This is further complicated by the implementation of the different DC voltage control modes of the VSC stations in the MTDC system. The DC droop control is regarded as more advantageous in terms of the operational flexibility, as more than one VSC station controls the DC link voltage of the MTDC system. However, this produces issues such as power deviation due to DC droop control, discussed in detail in [2]. There has been a great deal of research to explore the steady state and the dynamic behaviour of MTDC systems in the literature [3,4,5]. The main focus of previous work has been only on the MTDC network, while considering the integrated AC network as an infinite bus or a network with several buses. However, it is necessary to have combined AC/DC power flow models to obtain the steady state operating point after a disturbance without need of building full a detailed dynamic model of the entire AC/DC system. There are two main approaches used for the combined AC/DC power flow solutions in the literature, which are classified as the unified and the sequential methods. A detailed and general model of the VSC MTDC system with full power flow equations including VSC converter loss, transformer and filters is presented in [6] for sequential power flow calculation. In the unified method, the power flow of the entire AC/DC system is solved simultaneously using a modified Jacobi technique [7], where all the AC and DC variables are available after each iteration. Whereas, in the sequential method, AC and DC networks are solved sequentially, one after another [8]. However, the work has mainly focused on AC grids with an embedded multi-terminal HVDC network. A multi-option power flow approach is proposed in [9], where a multi-terminal HVDC system with asynchronous AC grids is solved without considering the DC droop control mode of the VSC stations. A combined AC/DC system with more than one DC grid requires a greater number of variables to be included.

The major contribution of this paper is the extension of the unified power flow approach to include the DC voltage droop control. A general combinational AC/DC power flow approach is proposed, which combines the unified and sequential approaches for the solution of a combined AC/DC

network, along with the implementation of the DC voltage droop control. Further, this approach can be extended to study multiple AC and DC grids for the combined AC/DC power flow analysis. A modified IEEE14 bus network with five-terminal MTDC network and three asynchronous AC zones is used to test the combinational AC/DC power flow algorithm. The results obtained shows that the proposed combinational AC/DC algorithm can solve the combined AC/DC system robustly to produce a feasible power flow solution.

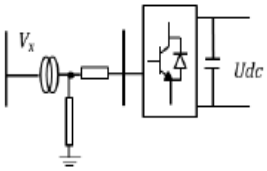

Figure 2: Steady state VSC station model

2 Steady state modelling for VSC based MTDC system

In this study three main aspects are included for the steady state model representation of the VSC based MTDC system. First is the VSC converter station, which forms a link between the AC and DC system. The second one is the VSC converter station control modes that decide the operation state of the VSC station. The third is the loss in the VSC station that accounts for the power losses due to AC side filters and transformers.

2.1 VSC converter station representation

The converter station model considered for this study is similar to the general and detailed steady state model used in [6], as shown in Figure 2. It can be represented by a controllable voltage source behind a complex impedance. The phase voltages are assumed to be symmetric and harmonic free with balanced converter operation. As shown in Figure 1, the controllable voltage source V_C represents the converter. It is connected to the phase reactor impedance Z_C, which is connected to susceptance B_F of the low pass filter, which further connects to the AC grid through the coupling transformer Z_T. Thus power flow equations from the AC bus of the converter station can be given as:

$$P_c = V_c^2 G_c - V_c V_F [G_c \cos(\delta_F - \delta_c) - B_c \sin(\delta_F - \delta_c)] \quad (1)$$

$$Q_c = -V_c^2 B_c + V_c V_F [G_c \sin(\delta_F - \delta_c) + B_c \cos(\delta_F - \delta_c)] \quad (2)$$

While the power flow equations from the filter bus to the converter bus can be given as:

$$P_{FC} = -V_F^2 G_c + V_F V_c [G_c \cos(\delta_F - \delta_c) + B_c \sin(\delta_F - \delta_c)] \quad (3)$$

$$Q_{FC} = V_F^2 B_c + V_F V_c [G_c \sin(\delta_F - \delta_c) - B_c \cos(\delta_F - \delta_c)] \quad (4)$$

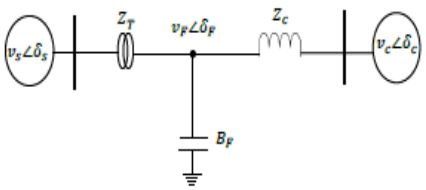

Figure 1: VSC station representation for power flow study

The expression for the power flow from the filter bus to the AC grid can be given as:

$$P_{FS} = V_F^2 G_T + V_F V_s [G_T \cos(\delta_F - \delta_s) - B_T \sin(\delta_T - \delta_s)] \quad (5)$$

$$Q_{FS} = -V_F^2 B_T + V_F V_s [G_T \sin(\delta_F - \delta_s) + B_T \cos(\delta_F - \delta_s)] \quad (6)$$

Similarly, the expression for the power flow from the AC grid bus to the filter bus can be given as:

$$P_S = -V_s^2 G_T - V_s V_F [G_T \cos(\delta_s - \delta_F) + B_T \sin(\delta_s - \delta_T)] \quad (7)$$

$$Q_S = V_s^2 B_c + V_s V_F [G_T \sin(\delta_s - \delta_F) - B_T \cos(\delta_s - \delta_T)] \quad (8)$$

However, the calculation of the AC grid power injection from each converter station, through eq:(1-8) requires a separate internal iterative loop. To avoid the addition loop, an alternate method of the AC grid active power calculation $P_{S,i}$ is given as [7]:

$$P_{s,i} = P_{c,i} - P_{Loss,i} \quad (9)$$

where $P_{C,i}$ represents the active power from the VSC station and $P_{LOSS,I}$ represents the total losses from DC side of converter station to the PCC of the AC grid, explained in section (2.3).

2.2 VSC converter station control modes

The basic VSC station has two different control loops, the inner loop and the outer loop. The inner controller uses synchronously rotating *dq* reference control to control the converter currents independently, which decouples active and reactive power control to provide independent active and reactive power control at each VSC station, similar to the governor and the exciter of the synchronous generator, which provide active and reactive power control in the AC grid system. The outer controller can be operated under various modes of operation according to the requirements of the MTDC grid system. For the purpose of power flow calculation only steady state behaviour of the outer controller is considered.

The active power operation modes include:

a) Constant active power (P-control)
b) Constant DC link voltage (U_{dc}-control)

The reactive power operation modes include:

a) Constant reactive power (Q-control)
b) Constant AC voltage (V_{ac}-control)

The DC voltage droop control is implemented that most closely resembles the frequency droop control of the AC grid system, where more than one VSC station share responsibility for the DC link voltage control, therefore, outage of any single VSC station cannot cause failure of the complete MTDC grid system [5]. The DC voltage droop control is shown in Figure 3.

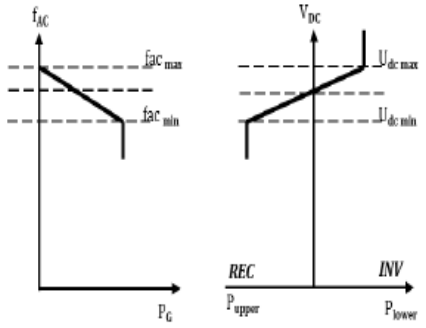

Figure 3: Droop control comparison of AC and DC grid

The implementation of the DC droop controller is given by:

$$P_c = P_{c\,ref} + R_D\,(U_{dc\,ref} - U_{dc}) \quad (10)$$

where, P_c is actual power at the Point of Common Coupling (PCC) of the VSC station, $P_{c\,ref}$ is the desired reference power, R_D is the droop gain of the DC voltage controller, U_{dc} is the actual DC link voltage at the VSC station and $U_{dc\,ref}$ is the rated DC link voltage for the VSC station. However, to ensure the co-ordinated balanced operation of the MTDC system with N number of VSC stations, one station is considered as the DC slack station to regulate the DC link voltage near the reference value. Each VSC station is modelled as a PV-node or PQ-node bus at the PCC, according to its operation mode, as shown in Figure 4.

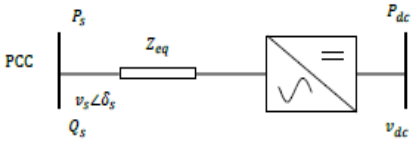

Figure 4: Control mode representation of the VSC station

2.3 VSC converter station losses

The VSC converter losses are taken into account using a generalised VSC station loss model [10], in which losses are written as a function of the magnitude of the converter current I_c and given by:

$$P_{Loss,C} = a + b \times |I_c| + c \times |I_c|^2 \quad (11)$$

As given in the equation, overall losses are divided into three categories, a represents no load losses, b and c indicate the linear and quadratic relation to the VSC station current I_c respectively, where I_c can be given as:

$$Ic = \frac{\sqrt{P_c^2 + Q_c^2}}{\sqrt{3}(V_c)} \quad (12)$$

Whereas, active power losses in the phase reactor and transformer can be calculated as:

$$P_{Loss,L} = R_T \times |I_c|^2 + R_c \times |I_c|^2 \quad (13)$$

Where, R_T and R_C are the resistances of the coupling transformer and phase reactor respectively. The total losses from DC side of the VSC station up to the PCC of the AC grid can be given as:

$$P_{Loss} = P_{Loss,C} + P_{Loss,L} \quad (14)$$

3 General AC/DC grids power flows

In this section, general power flow equations for the combined AC/DC grids are presented.

3.1 AC power flow equations

The AC power flow injection for all the buses in the AC grid excluding the slack bus can be given as:

$$P_{inj,ACi} = V_i \sum_{j=1}^{M} V_j \left[G_{ij}\cos(\delta_i - \delta_j) + B_{ij}\sin(\delta_i - \delta_j)\right] \quad (15)$$

$$Q_{inj,ACi} = V_i \sum_{j=1}^{M} V_j \left[G_{ij}\cos(\delta_i - \delta_j) - B_{ij}\sin(\delta_i - \delta_j)\right] \quad (16)$$

where M is the total number of the AC buses, V_i, V_j, δ_i and δ_j are the bus voltage magnitude and angle of the ith and jth AC buses respectively. $Y_{ac} = G+jB$ is the bus admittance matrix of the AC grid. The VSC station injections can be added as a negative load to extend the mismatch equations for the AC buses including the PCC, and are given as:

$$0 = P_{GDi} - P_{inj,ACi} - P_{s,i} \quad (17)$$

$$0 = Q_{GDi} - Q_{inj,ACi} - Q_{s,i} \quad (18)$$

where, P_{GDi} and Q_{GDi} are the net power generation at each bus, while $P_{inj,ACi}$ and $Q_{inj,ACi}$ are the net power injection at each bus, which can be obtained from eq(15) and eq(16). $P_{s,i}$ and $Q_{s,i}$ are the VSC station reference power at the PCC for VSC station connected buses only.

3.2 DC power flow equations

The DC power flow injection for all the buses in the DC grid excluding the slack bus can be given as:

$$P_{Inj,DCi} = -V_{DC,i} \sum_{j=1}^{N} V_{DC,j}\, Y_{DC,ij} \quad (19)$$

where, N is the number of the total buses in the DC grid, V_{DCi} is the ith DC bus voltage and Y_{DC} is the DC bus admittance matrix. The power mismatch equations for the DC power flow equation can be given as:

$$0 = P_{inj,DCi} - P_{DC,i} \qquad (20)$$

where, $P_{DC,i}$ is the reference power at the DC side of the converter, which can be calculated as:

$$P_{DC,i} = P_{s,i} - P_{Loss,i} \qquad (21)$$

3.3 Slack converter losses equations

The power at the PCC of the slack VSC station is calculated as:

$$P_{s,slack} = V_{DC,slack} \sum_{j=1}^{N} V_{DC,j} Y_{DC,slack} - P_{Loss,slack} \qquad (22)$$

where, $P_{Loss,slack}$ are DC slack bus losses needed to calculate the DC slack bus power. In the unified approach [9], the slack station losses are considered as a separate variable X_s. The additional mismatch equation is given as:

$$0 = X_s - P_{Loss,slack} \qquad (23)$$

where, $P_{Loss,slack}$ can be obtained from eq(14).

4 Combinational AC/DC power flow algorithm

The combinational AC/DC power flow approach is proposed to benefit from most of the advantages of both the techniques, unified and sequential, while avoiding their drawbacks. The unified combined power flow approach enables the AC and DC network equations to be solved simultaneously in the same iteration, resulting in merging all internal and external loops in a single iterative loop. However, solution of N independent DC networks requires adding N more variables in the single iterative loop, which makes it more complex.

In the sequential combined power approach the AC and DC network equations need to be solved sequentially in separate iterations. The AC network power flow changes after the slack bus power is updated by the DC network iteration, thus external iteration is required to ensure the overall convergence of the combined system, which not only complicates the power flow but also takes more time to solve. Its main advantage is the easy integration of the DC network equations with the AC load flow equation without changing the existing AC load flow models.

In the combinational power flow approach the AC and DC network equations are solved simultaneously in a single loop iteration but the iteration runs N times for N independent networks rather than increasing to N additional variables. It can also be integrated with the AC power flow model by regarding a large AC system as an external system similar to [9], without changing the existing AC load flow model. The flow chart of the proposed algorithm is shown in the Figure 5. Further droop control characteristics are implemented to demonstrate the possibility of handling any control modes of the VSC station in the algorithm.

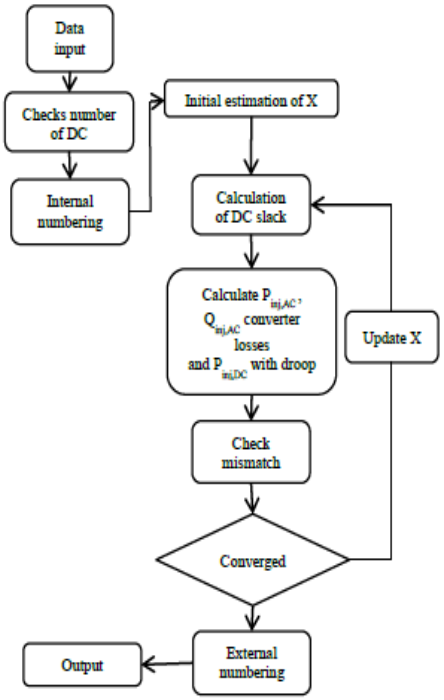

Figure 5: Flow chart for the combinational power flow

5 Test system

In this study, the combinational AC/DC power flow algorithm is implemented on a modified IEEE14 bus test network, which is shown as a single line diagram in Figure 6. A five-terminal MTDC system is integrated with a modified IEEE14 bus AC network. The converter station *VSC1* (slack bus of the DC network) is connected to *bus1* of the AC system. The converter station *VSC2* and *VSC3* are in P-control mode in order to capture maximum power from the offshore windfarms (modelled as asynchronous generator buses) *bus2* and *bus3* of the AC system. The remaining two converter stations *VSC4* and *VSC5* operate in the DC droop control mode and are connected to the *bus6* and *bus7* of the AC system respectively.

The *VSC1* regulates the DC link voltage of the MTDC system at 250kV. Amongst the rest of the VSC stations the *Pcon2* and *Pcon3* are set to inject 50MW each into the MTDC system, while *Pcon3* and *Pcon4* are set to inject 60MW each under droop control in to the AC system. The DC voltage droop gain R_D is set to be 20(MW/kV) for each of the two droop controlled VSC station. The detailed operation modes and converter station parameters are given in Table (1) and Table (2) respectively.

Table 1: Operation mode of VSC station

VSC stations	P_{DC} *(MW)*	V_{DC} *(kV)*	*Type*	*PCC AC bus*
VSC1	*slack*	±250	PV	Bus1
VSC2	50	±250	PV	Bus2
VSC3	50	±250	PV	Bus3
VSC4	-60	±250	PV	Bus6
VSC5	-60	±250	PV	Bus7

Table 2: VSC station parameters

Parameters	*Values*
X_C *(pu)*	0.018
R_C *(pu)*	0.001
X_T *(pu)*	0.112
R_T *(pu)*	0.001
B_F *(pu)*	0.088
a (MW)	1.103
b (kV)	0.887
c (Ω)	2.88

6 Results and discussions

The power flows obtained from the proposed algorithm applied to the modified IEEE14 bus system interconnected with a five-terminal MTDC system are shown by arrow in Figure 6. The results of power injections, voltages and phase angles before and after the outage of a *VSC2* are given in the Table (3) and Table (4) respectively. The (*) represents the asynchronised zones in the AC system.

Table 3: Power injections, voltage and angle of the AC buses before outage

AC BUS	*Voltage (pu)*	*Angle (deg)*	P_{inj} *(MW)*	Q_{inj} *(MVar)*
1*	1.06	0.0	1.54	52.13
2*	1.045	-4.980	0.0	0.0
3*	1.01	-12.72	0.0	0.0
4	1.031	-0.10	10.85	-41.9
5	0.999	2.251	50.98	-14.58
6	0.968	2.546	-21.20	-7.5
7	0.919	7.753	0.0	0.0
8	1.010	5.753	35	7.14
9	1.00	-0.111	-29.5	-16.6
10	0.998	-0.415	-9.0	-5.8
11	1.011	-0.386	-3.5	-1.80
12	1.015	-0.983	-6.1	-1.6
13	1.009	-1.00	-13.5	-5.8
14	0.985	-1.601	-14.9	5.0
DC BUS	*Voltage (pu)*	–	$P_{inj,DC}$ *(MW)*	–
VSC1	1.000	–	21.73	–
VSC2	0.999	–	49.87	–
VSC3	0.998	–	48.75	–
VSC4	0.996	–	-59.91	–
VSC5	0.993	–	-59.85	–

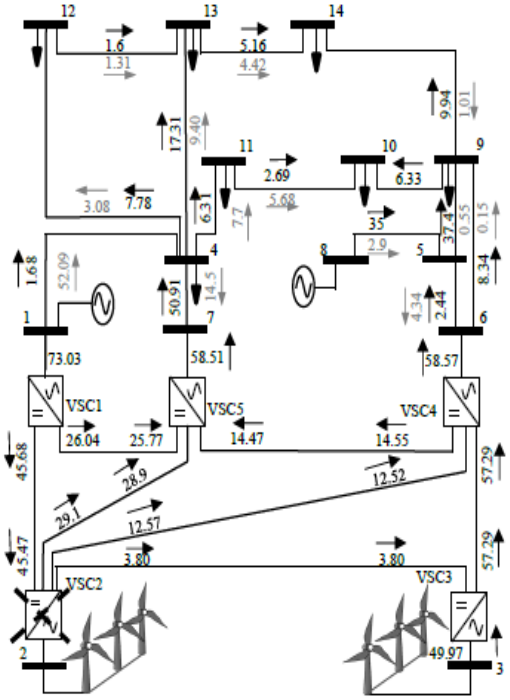

Figure 6: Modified IEEE14 network with five-terminal MTDC system
→ represents active power in *MW*
→ represents reactive power in *MVar*

Table 4: Power injections, voltage and angle of the AC buses after outage

AC BUS	*Voltage (pu)*	*Angle (deg)*	P_{inj} *(MW)*	Q_{inj} *(MVar)*
1*	1.06	0.0	1.68	52.09
2*	1.045	-4.980	0.0	0.0
3*	1.01	-12.72	0.0	0.0
4	1.031	-0.10	10.77	-41.9
5	0.999	2.251	50.91	-14.58
6	0.968	2.546	-21.20	-7.5
7	0.919	7.753	0.0	0.0
8	1.010	5.753	35	7.15
9	1.00	-0.111	-29.5	-16.6
10	0.998	-0.415	-9.0	-5.8
11	1.011	-0.386	-3.5	-1.80
12	1.015	-0.983	-6.1	-1.6
13	1.009	-1.00	-13.5	-5.8
14	0.985	-1.601	-14.9	5.0
DC BUS	*Voltage (pu)*	–	$P_{inj,DC}$ *(MW)*	–
VSC1	1.000	–	71.72	–
VSC2	0.994	–	0.0	–
VSC3	0.994	–	48.75	–
VSC4	0.991	–	-59.83	–
VSC5	0.985	–	-59.79	–

As expected, after the outage of the converter station *VSC2* the power output from the *VSC4* and *VSC5* reduces in accordance to the DC droop characteristics. The results obtained from the combinational AC/DC power flow shows that this proposed approach enables the study of the effects of DC droop control on the power flows of the combined AC/DC system for steady state studies after VSC station outages or transient conditions without needing to use its complete dynamic model.

7 Conclusion

In this paper, a combinational AC/DC power flow approach has been proposed for the solution of the combined AC/DC network. The extended model has been presented to include the DC voltage droop characteristics into the combined AC/DC power flows. This enables the study of the effects of the DC droop control on the power flows of the combined AC/DC system for steady state studies after VSC station outages or transient conditions without needing to use its complete dynamic model. In future work, the proposed approach will be applied to solve combine AC/DC systems with multiple independent AC and DC grids to validate the proposed approach for the AC/DC power flow analysis of a generalised form of combined AC/DC networks.

Acknowledgements

The author would like to acknowledge the affiliation and funding resources for this research from Sukkur Institute of Business Administration, Sukkur, Pakistan.

References

[1] E. Summary, "Eueopean Offshore Suppergrid Proposal," 2010.

[2] F. Akhter, D. E. Macpherson, and G. P. Harrison, "Enhanced multi-terminal HVDC grid management for reliable AC network integration," *7th IET Int. Conf. Power Electron. Mach. Drives (PEMD 2014)*, pp. 0495–0495, 2014.

[3] S. Cole, S. Member, J. Beerten, and R. Belmans, "Generalized Dynamic VSC MTDC Model for Power System Stability Studies," vol. 25, no. 3, pp. 1655–1662, 2010.

[4] R. T. Pinto, "Comparison of Direct Voltage Control Methods of Multi-Terminal DC (MTDC) Networks through Modular Dynamic Models," pp. 1–10.

[5] T. M. Haileselassie and K. Uhlen, "Precise control of power flow in multiterminal VSC-HVDCs using DC voltage droop control," *2012 IEEE Power Energy Soc. Gen. Meet.*, pp. 1–9, Jul. 2012.

[6] J. Beerten, S. Member, S. Cole, and R. Belmans, "Generalized Steady-State VSC MTDC Model for Sequential AC / DC Power Flow Algorithms," vol. 27, no. 2, pp. 821–829, 2012.

[7] M. Baradar, M. Ghandhari, and D. Van Hertem, "The modeling multi-terminal VSC-HVDC in power flow calculation using unified methodology," *2011 2nd IEEE PES Int. Conf. Exhib. Innov. Smart Grid Technol.*, pp. 1–6, Dec. 2011.

[8] J. Beerten, S. Member, D. Van Hertem, S. Member, and R. Belmans, "VSC MTDC Systems with a Distributed DC Voltage Control – A Power Flow Approach," pp. 1–6, 2011.

[9] M. Baradar and M. Ghandhari, "A Multi-Option Uni fi ed Power Flow Approach for Hybrid AC /DC Grids Incorporating Multi-terminal VSC-HVDC," no. August, pp. 2376–2383, 2013.

[10] G. Daelemans, K. Srivastava, S. Member, M. Reza, S. Cole, and R. Belmans, "Minimization of Steady-State Losses in Meshed Networks using VSC HVDC," pp. 1–5, 2009.

Impact of Wind Integration on National Transmission Network

Faheem Akhter[1,2(✉)], D. Ewen Macpherson[1], and Naeem Shahzad[3]

[1] Institute for Energy Systems, University of Edinburgh, Edinburgh, UK
{f.akhter, e.macpherson}@ed.ac.uk
[2] Department of Electrical Engineering, Sukkur Institute of Business Administration, Sukkur, Pakistan
[3] Department of Electronic Engineering, International Islamic University, Islamabad, Pakistan
naeem.chachar@gmail.com

Abstract. Due to the scarcity of fossil fuels and their increasing prices, adoption of renewable resources has become inevitable. Wind energy is being recognized as a potential renewable source of bulk power generation in Pakistan, just as across the world. The wind corridor located from Hyderabad to Keti Bandar has an immense potential for power generation, with two windfarms already in operation and many more planned. A stability analysis of installed and potential Wind Turbines Generators (WTG) type needs to be performed, to analyse the impact of power injection from wind turbines on the voltage level and grid stability of the power network. This analysis can further help to identify appropriate integration location and suitable wind turbine generator for AC network support. This paper presents the analysis of network strength at the point of wind the turbine generator's connection and a comparison of wind turbine generators to support the AC network, which will be useful for identification of suitable type of WTG for reliable operation of integrated system.

Keywords: Wind power integration · Network strength · Wind turbine generators · Stability analysis

1 Introduction

The generation deficit in Pakistan has peaked to 6000 MW in recent years, mainly due to over relaying on conventional resources of energy generation. The installed capacity of the country at the end of 2010 was 21,455 MW of which 31 % was hydro, 67 % thermal (gas & oil), 2 % nuclear and 0.1 % coal. However, due to seasonal variation of water flow it further decreases to 15,254 MW in winter [1]. Presently, this seasonal variation put a large burden on thermal generation due to the absence of renewable generation. This gap can be well filled by harnessing the vast wind resources located across different parts of the country.

According to the wind resource studies carried out by National Renewable Energy Laboratories (NREL) [2], Pakistan has a potential of more than 131,800 MW of wind energy across the country. The Alternative Energy Development Board (AEDB) has so

F.K. Shaikh et al. (Eds.): IMTIC 2013, CCIS 414, pp. 13–23, 2014.
DOI: 10.1007/978-3-319-10987-9_2

Table 1. Least cost generation plan [1]

	2010–11		2029–30	
	(MW)	(%)	(MW)	(%)
Hydro	6,555	31	41,546	37
Thermal-gas	6,571	31	12,015	11
Thermal-oil	7,838	37	6,855	6
Thermal-coal	30	0.1	37,774	34
Bagasse & Bio Waste Plant	0	0	100	0.1
Nuclear	461	2	6,947	6
Wind	0	0	5,400	5
Import	0	0	2,000	2
Total	21,455	100	112,639	100

far allocated land to more than eighteen (18) Independent Power Producers (IPPS) for wind power generation projects of 50 MW each. Twelve 50 MW wind power projects have completed feasibility studies. The plans are to achieve up to 1,800 MW from wind energy by the end of 2020 and a total of 5,400 MW from wind energy sources by 2030, shown in Table 1.

2 Related Work

Comprehensive studies have been performed for the integration of wind power into existing transmission network throughout the world, namely National Renewable Energy Laboratory in United States, Hydro-Quebec in Canada and Risø DTU National Laboratory for Sustainable Energy, in Denmark, Europe, considering both the technological and regional implementation aspects of the topic. Very few studies have been performed in the context of Pakistan. A regional study has been performed in [3], showing the need of regional interconnection for renewable energy integration and future energy security in SAARC countries. [4] presents the statistics of energy mix of sustainable energy option available for Pakistan. The evaluation of wind energy potentials at Keti Bander in particular is presented in [5]. The energy management from the renewable resources in energy deficit network is discussed in [6]. A co-ordination study of wind power and hydro power generation is performed in [7], mainly considering the loading capacity of transmission lines. However, no study has been performed to analyze the dynamic stability analysis of wind power integration into the power system network.

This study presents the stability analysis of the installed and potential Wind Turbine Generator (WTG) types, to analyze the impact of the power injection from wind turbines regarding the voltage level and grid stability of the power network. The existing transmission system has been designed for conventional power generation which is composed of synchronous generators, which can support the stability of the transmission system by providing inertia responses, oscillation damping, synchronizing

power, short-circuit capability and voltage backup during faults. In contrast, wind turbine generators (WTGs) are characterized mainly as fixed speed and variable speed induction generators, doubly fed induction generators and full scale synchronous generators, which are very different from those of conventional generators. This paper presents a comparison of the grid support provided by different WTGs types to identify the most suitable type WTG at each location. A stability analysis of the 50 MW planned wind power project (WPP) is performed on the high wind potential site Jhampir, using PSCAD/EMTDC simulation software [8]. Different WTG concepts are simulated with given grid strength and wind speed at the location to determine the impact of wind turbine generators on the integrated grid. Dynamic analysis is performed to evaluate performance in accordance with the grid code description. Geospatial Toolkit map from NREL [9] shown in Fig. 1 is used to analyze the predicted average monthly wind speed in m/s at the location and the HOMER utility is used to obtain the frequency distribution at the locations.

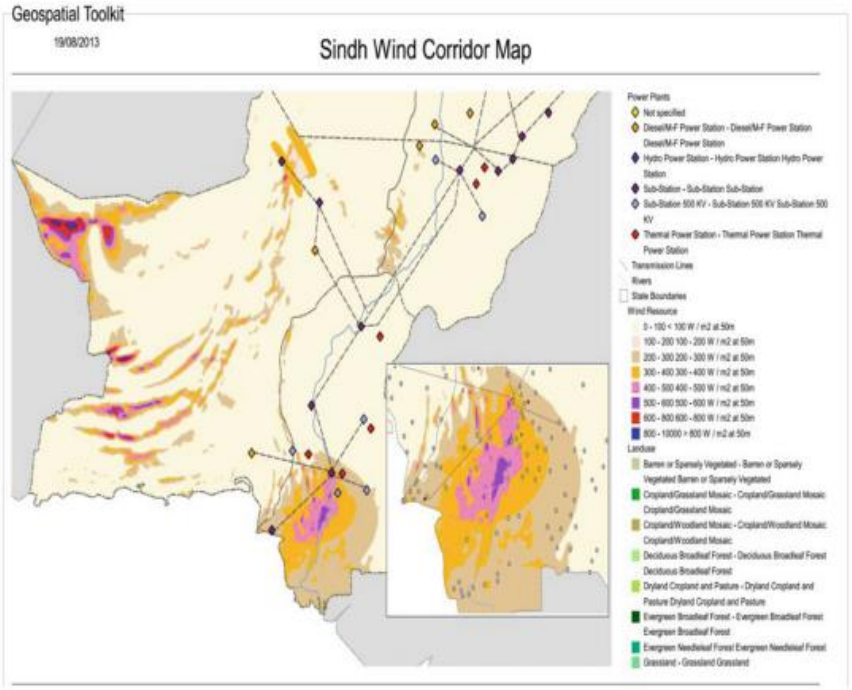

Fig. 1. Sindh wind corridor map (NREL) [9]

3 System Modelling

3.1 Wind Turbine Generator (WTG) Technologies

A wind turbine generator system is typically comprised of the turbine blades and rotor hub assembly to capture power from the wind, a drive-train to step-up the speed from low spinning turbine shaft to the high speed generator, and a generator as an

electromechanical energy converter. WTGs are classified mainly into four types [10], according to their speed control characteristics, i.e., Type 1: Fixed speed wind turbines (SCIG), Type 2: Variable slip wind turbines (OSIG), Type 3: Double feed induction generator (DFIG) wind turbines, and Type 4: Full converter wind turbines (PMSG).

The fixed speed wind turbine is the most basic type turbine employed in wind energy market. It consists of a squirrel-cage induction machine (SCIG) directly connected to the grid and operates with very little variability in turbine rotor speed. It is very robust and reliable in operation but inefficient power capture capability and high reactive power consumption are its main disadvantages. Some of them do not even have pitch control capability. The remaining three types come under the broad category of variable speed turbines, as they are designed to operate over a wide range of rotor speed. Most of them also have the pitching controllability. Pitch and speed controllability enables them to capture more energy over a wide range of wind speed than fixed speed wind turbines. Type 2 wind turbines, the Opti-slip Induction Generator, employs dynamic rotor resistance to control the rotor resistance of the machine and provides variable slip operation up to 10 %. However, power is lost in the resistance. To overcome this disadvantage, the Type 3 wind turbine Double-Fed Induction Generator (DFIG) is designed with a back-to-back AC/DC/AC converter in the rotor circuit to recover the slip energy. As the converter only handles power in the rotor circuit, it does not have to be rated at machine full output power, which makes it more economical. Flux vector control employed in the converter enables decoupled control of active and reactive power, which also helps in maximizing power extraction and support to the grid. The type 4 wind turbine employs a fully rated AC/DC/AC converter to connect the generator to the grid. As there is no direct connection to the grid, so an induction or synchronous generator can be used to obtain variable speed operation with independent real and reactive power control. The most common configuration is the permanent magnet synchronous generator (PMSG). The details of universal manufacture-independent models recommended for wind power interconnection studies of all four types is described in [11].

3.2 Aggregated Wind Power Plant Model

In practice wind power plant (WPP) is comprised of a number of wind turbine generators (WTGs) of the same type. A WTG is usually rated at low voltage output (690 V). Voltage is stepped up to the medium voltage collector system (22 kV) by a transformer located at each WTG. Many closely located WTGs are connected in parallel in a group. Several of these groups are connected to the mains feeder, and several feeders are connected to a substation where the voltage is stepped up to transmission level (132 kV).

In many cases, it is desire able to model the WPP close to the actual implementation, but it may not be practical to model in detail each WTG and collector system for the WPP's power system integration studies. However, when the response to grid disturbances is required, dynamic models of the generator and related controls need to be implemented to know the turbine response. In this study an aggregated single turbine representation is taken to represent a 50 MW WPP comprising 33 units of 1.5 MW WTGs and low voltage pad-mounted transformers in a simplified manner, shown in Fig. 2.

Fig. 2. Single turbine representation of WPP

3.3 Power System Representation

For WPP integration studies, detailed representation of the whole network may not be practical and would involve excessive computational cost and time. So the actual system of the NTDC 132 kV grid shown in Fig. 3 is represented as an infinite bus connected to the PCC through equivalent impedance (Z_{grid}) of the system as shown in Fig. 2. This can be the most important parameter the network strength of the system. An important characteristic of determining the strength of the network is the short circuit ratio (SCR), connected with WPP of rated power $S_{N\ WT}$, can be defined as [10, 12]:

$$SCR = \frac{SCC}{S_{NWT}} = \frac{V_G^2}{Z_{grid}.S_{NWT}} \tag{1}$$

The SSC is the short circuit capacity which depends on voltage levels (V_G) and total power capability at the PCC. The SSC of the power grid is given in the National Power System Expansion Plan (NPSEP) [1]. Hence, the equivalent impedance of the grid (Z_{grid}) can be determined at the PCC as:

$$Z_{grid} = \frac{V_G^2}{SCC} \tag{2}$$

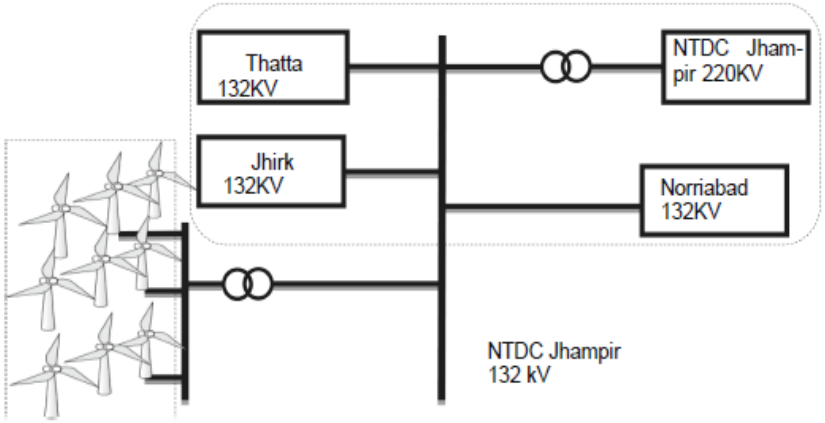

Fig. 3. Single line diagram of 132 kV Jhampir grid

4 Dynamic Simulation Results

4.1 Fixed Speed Wind Turbines

Figure 4 shows the dynamic behavior of the 50 MW WPP comprising fixed speed wind turbine (SCIG) following a rigid three phase fault for 200 ms at the PCC (132 kV) bus. The average wind speed is taken as 10 m/s at the location. The terminal and phase voltage of the wind turbine falls to zero during the fault and resumes to normal after the fault clearance Fig. 4(c) and (e). The electrical power and torque reduces to zero for the duration of the fault Fig. 4(b) and (g), while generator speed increases Fig. 4(d). When the fault is cleared at t = 10.20 s huge reactive power is drawn for excitation of the SCIG, along with the inrush current shown in Fig. 4(e) and (i). The wind turbine recovers to its normal condition 200 ms after fault clearance.

4.2 Variable-Slip Wind Turbines

Figure 5 shows the dynamic performance of the 50 MW WPP comprising variable slip wind turbines (OSIG) during rigid three phase fault at the PCC (132 kV) for 200 ms at average wind speed of 10 m/s. The dynamic behavior of the OSIG wind turbine appears to be the same as for the fixed speed turbine, except that power can be regulated to rated values in the event of higher wind speeds. The wind turbine system draws high reactive power for excitation of the induction generator, Fig. 5(f), after fault clearance and starts to supply active power, Fig. 5(a). The terminal voltage builds up, Fig. 5(c) and speed reduces down to the pre-fault value, Fig. 5(e).

4.3 Double-Feed Induction Generator Wind Turbines

Figure 6 shows the dynamic performance of the 50 MW WPP comprising double-fed induction generators (DFIG) during three phase rigid fault at the PCC (132 kV) bus. The average speed of 10 m/s is assumed with a fault of 200 ms. The wind turbine supplies active power to the grid from both stator and rotor sides. A low voltage protection is applied to avoid the very high rotor current during the fault, which blocks the rotor side converter. This compares the rms line voltage with a pre-set value of voltage dip and blocks the rotor side converter. The DFIG behaves as a squirrel cage induction generator and starts to draw huge reactive power, Fig. 6(g). After the fault clearance terminal voltage builds up and the rotor side converter is unblocked.

4.4 Permanent Magnet Synchronous Generator Wind Turbines

Figure 7 shows the dynamic performance of the 50 MW WPP comprising permanent magnet synchronous generators (PMSG) during a three phase rigid fault at the PCC (132 kV) bus. The fault is simulated for 100 ms and average wind speed is taken as 10 m/s. As observed previously in the dynamic behaviour of Type 1, 2 and 3 systems in Figs. 4, 5 and 6 respectively, the grid voltage drops significantly because of high

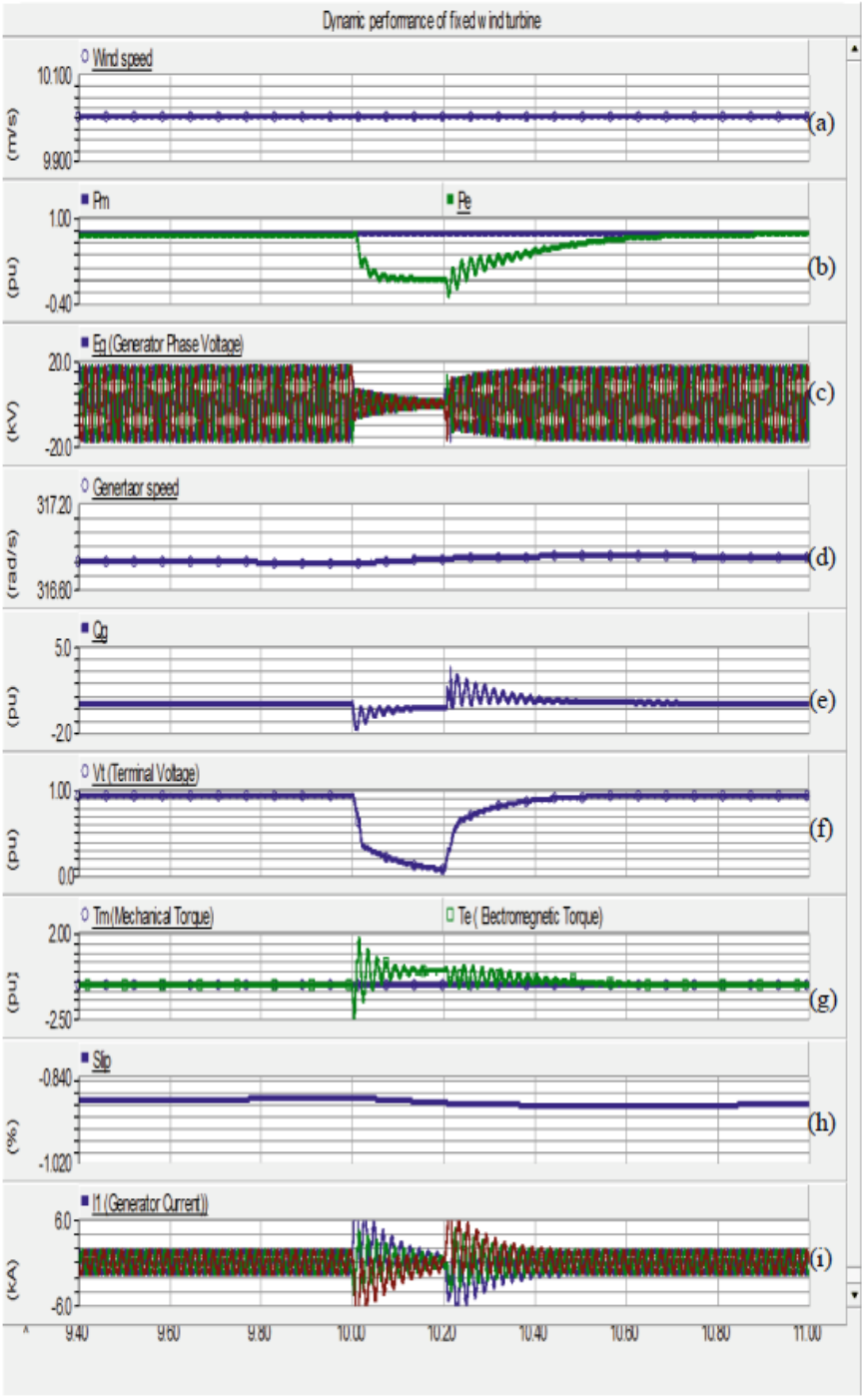

Fig. 4. Dynamic behavior of fixed speed wind turbine WPP

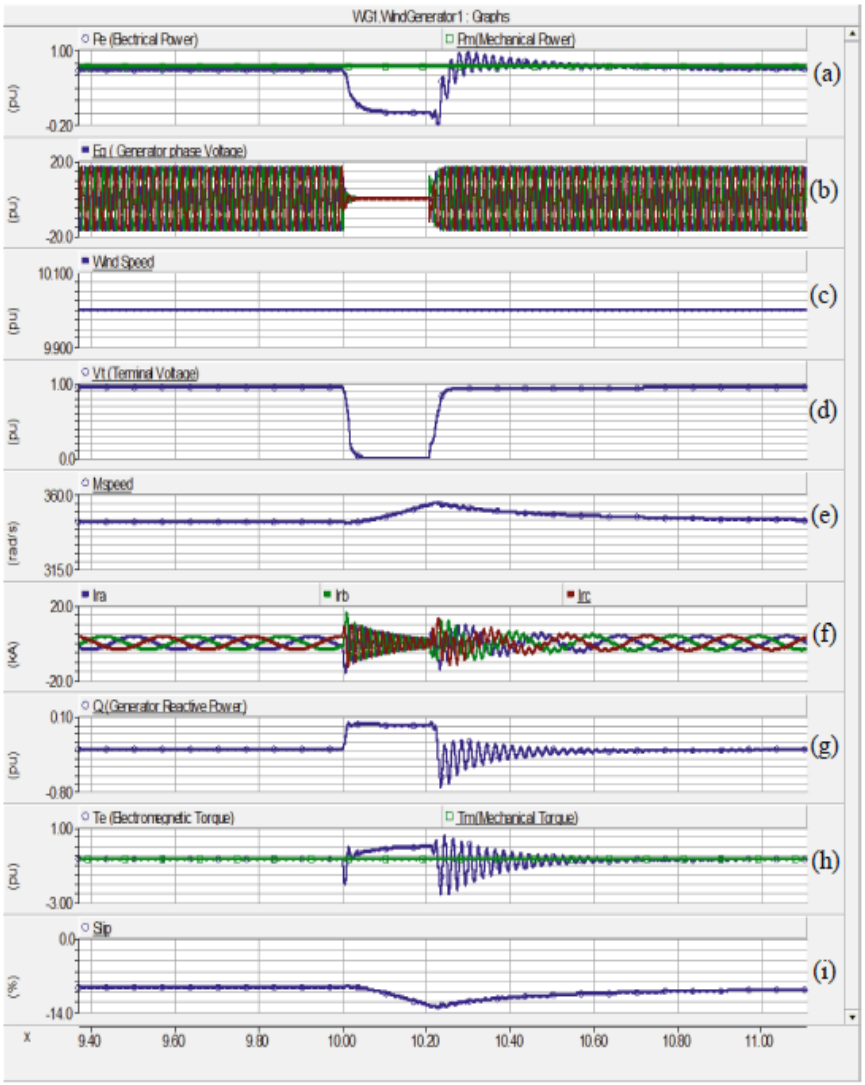

Fig. 5. Dynamic performance of variable slip wind turbine WPP

reactive power consumption by the induction generator. They have limited capability to inject reactive power into the PCC for supporting the voltage and cannot provide the necessary reactive power to raise voltage, whereas the PMSG control system attempts to raise the voltage by producing maximum available reactive power Fig. 7(d).

5 Low Voltage Ride Through (LVRT) Characteristics

One of the most important aspects of grid code compliance of WPP is Low Voltage Ride Through (LVRT) capability characterises. The Fig. 8 shows the LVRT requirement in

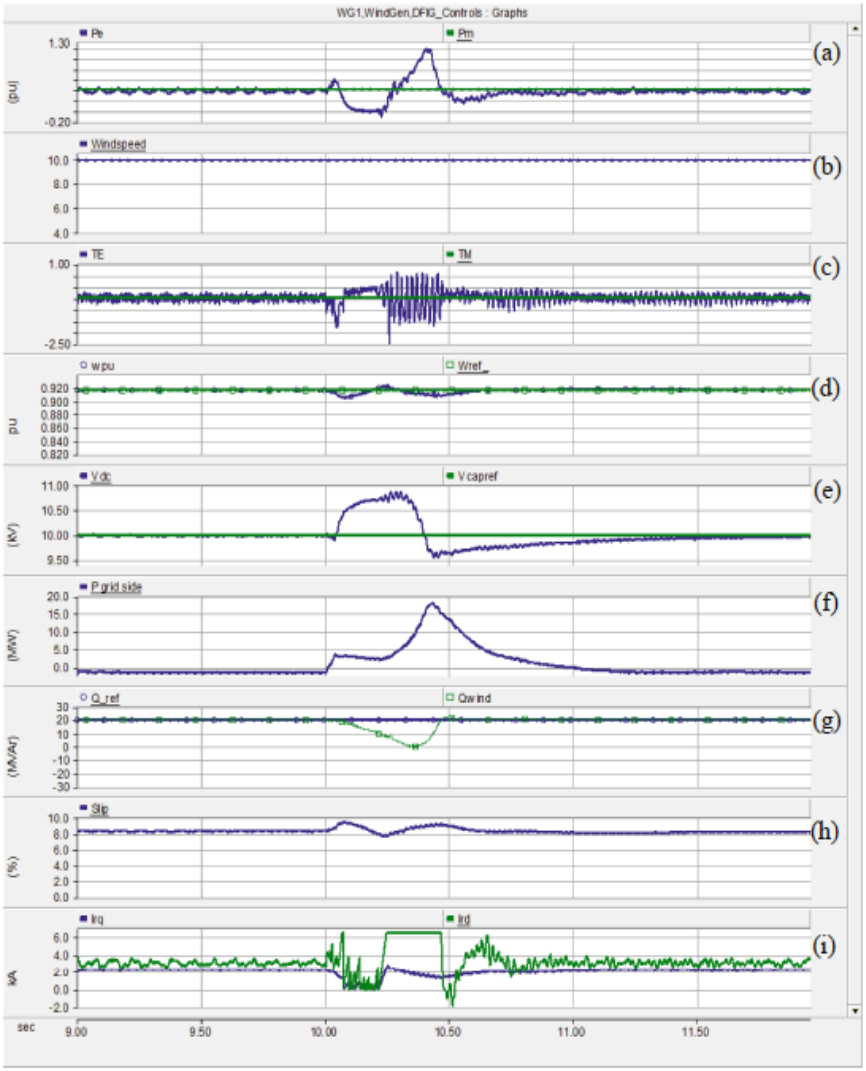

Fig. 6. Dynamic performance of DFIG WPP

German grid code. With the performance of further dynamic response analysis by varying voltage dip level at the PCC and fault duration, LVRT characteristics of each WPP type can be obtained, which can further confirm the grid code compliance of each type.

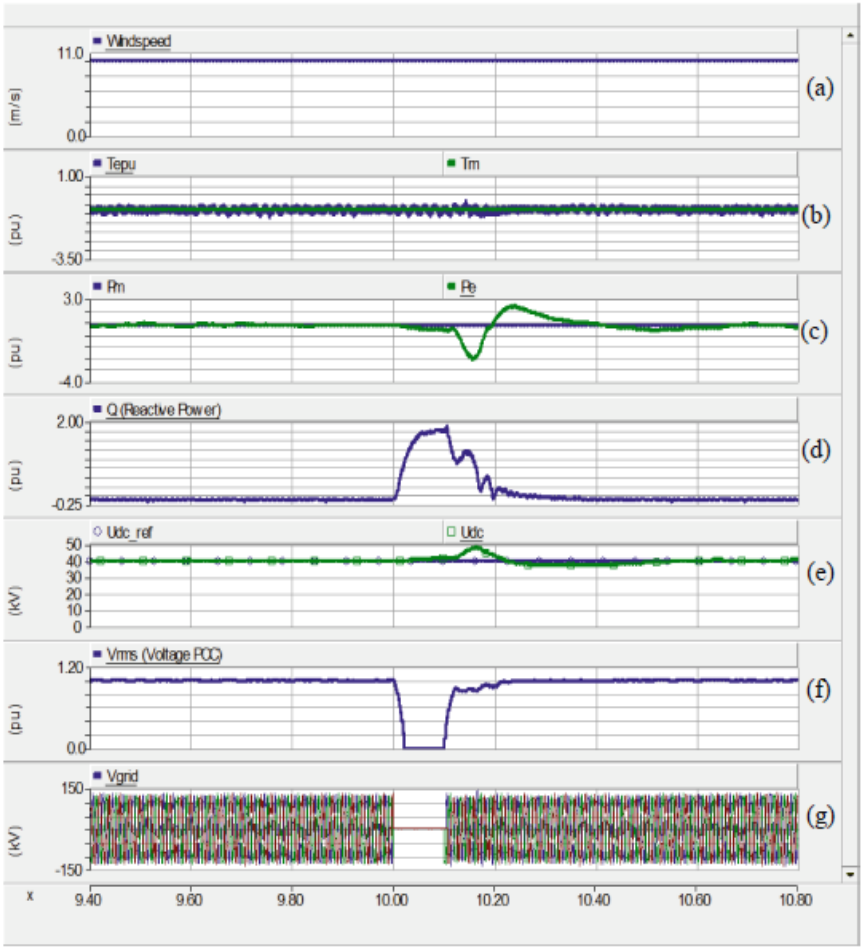

Fig. 7. Dynamic performance of PMSG WP

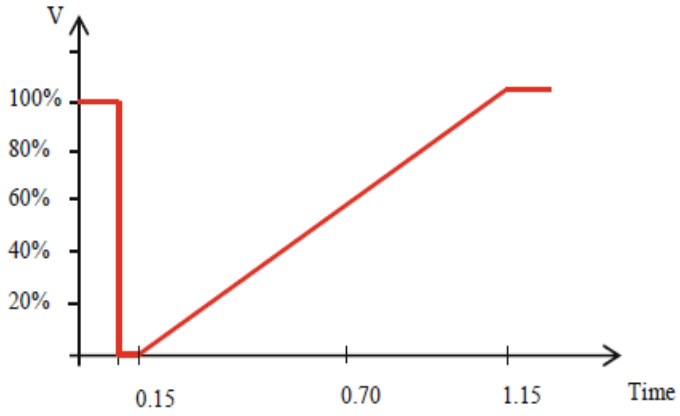

Fig. 8. VRT requirement in German grid code [13]

6 Conclusion

This paper presents the comparison of grid supportability of different WTGs types at the actual strength of the grid to identify the suitable type of WTG for the proposed location of Hyderabad-Keti Bander wind corridor. The active and reactive power controllability analysis of different WTGs types is performed to obtain the comparison of voltage and frequency maintaining capability within the prescribed range of rated values at the point of common coupling (PCC) in normal operation. The simulation result obtained shows that, Type 1, 2 and 3 systems, the grid voltage drops significantly because of high reactive power consumption by the induction generator. They have limited capability to inject reactive power into the PCC for supporting the voltage and cannot provide the necessary reactive power to raise voltage without addition protection and control. Whereas Type 4 (PMSG) wind turbines attempt to raise the voltage by producing maximum available reactive power. To further confirm with grid code compliance LVRT characteristic analysis is suggested to be performed.

Acknowledgement. The author would like to acknowledge the affiliation and funding resources for this research from Sukkur Institute of Business Administration, Sukkur.

References

1. Inc, S.-L.I.: National power system expansion plan. National Transmission and Despatch Company Limited. Final report 32 (2011)
2. Elliott, D.: Wind resource assessment and mapping for Afghanistan and Pakistan. National Renewable Energy Laboratory. Golden, Color, USA (2011)
3. Rashid, T.H.M.S., Islam, R.: Prospects of renewable energy resources and regional grid integration for future energy security & development in SAARC countries. IJRET **2**(1), 43–51 (2013)
4. Asif, M.: Sustainable energy options for Pakistan. Renew. Sustain. Energy Rev. **13**, 903–909 (2009)
5. Ullah, I., Chaudhry, Q.-Z., Chipperfield, A.J.: An evaluation of wind energy potential at Kati Bandar. Pakistan. Renew. Sustain. Energy Rev. **14**, 856–861 (2010)
6. Aamir, M., Poncela, J.: Impact analysis of renewable energy in national grids for energy deficit countries. Commun. Comput. Inf. Sci. Second IMT, **218**, 1–9 (2012)
7. Awan, S.: Hydro and wind power integration: a case study of Dargai station in Pakistan. Energy Power Eng. **4**, 203–209 (2012)
8. User's guide (PSCAD) Power System Computer Aided Design (2010)
9. User manual Geospatial Toolkit (2010). www.nrel.gov/international/geospatial_toolkits
10. Ackermann, T.: Wind Power in Power Systems. Wiley, Chichester (2005)
11. Singh, M., Surya, S.: Dynamic models for wind turbines and wind power plants. National Renewable Energy Laboratory (2011)
12. Grunau, S., Fuchs, F.: Effect of wind-energy power injection into weak grids. In: Proceedings of EWEA Conference (2012)
13. Altın, M., Goksu, O.: Overview of recent grid codes for wind power integration. In: 12th International Conference Optimization of Electrical and Electronic Equipment, OPTIM, pp. 1152–1160 (2010)